

BIBLIOGRAPHIC INFORMATION

PB95-184008

Report Nos:

Title: Effects of Soft Soil and Hysteresis Model on Seismic Demands.

Date: Jul 93

Authors: M. Rahnama and H. Krawinkler.

Performing Organization: Stanford Univ., CA. John A. Blume Earthquake Engineering Center.

Sponsoring Organization: *National Science Foundation, Arlington, VA.*Kajima Corp., Tokyo (Japan).

Contract Nos: NSF-BCS-8901665

Supplemental Notes: Also pub. as Stanford Univ., CA. John A. Blume Earthquake Engineering Center rept. no. REPT-108.

NTIS Field/Group Codes: 89D (Structural Analyses), 50D (Soil & Rock Mechanics)

Price: PC A11/MF A03

Availability: Available from the National Technical Information Service, Springfield, VA. 22161

Number of Pages: 247p.

Keywords: *Soil mechanics, *Dynamic response, *Structural analysis, *Hysteresis, *Soil structure interactions, Displacement, Earthquake engineering, Nonlinear systems, Stiffness, Mathematical models, Strain hardening, Ductility, Ground motion, Earthquake resistant structures, Structural design.

Abstract: The main objective of this research is to develop procedures that will permit an explicit incorporation of the effects of deterioration of structural properties and site surface geology on the seismic demands imposed on structures by strong ground motions. This implies consideration of the influence of stiffness degradation and strength deterioration, including P-delta effects, and of the effects of site soil conditions on those demand parameters that can be used directly for design of structures. Thus, the research combines ground motion and structure response issues, with an emphasis on parameters that incorporate both relevant ground motion as well as structural response characteristics. The first part of this study focuses on the effects of negative strain hardening (P-delta) and strength deterioration on the demand imposed by ground motions on the strength of inelastic SDOF systems. Strength demand is defined here as the strength that needs to be provided in order to limit the ductility of the SDOF system to predefined target value.



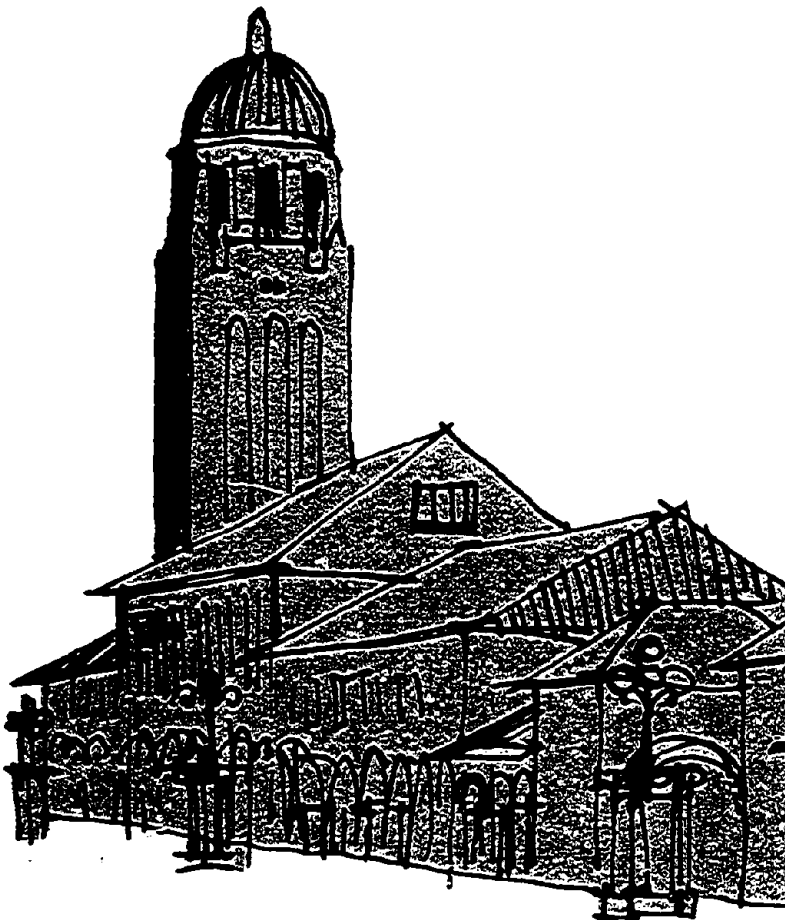
PB95-184008

The John A. Blume Earthquake Engineering Center

Department of Civil Engineering
Stanford University

EFFECTS OF SOFT SOIL AND HYSTERESIS MODEL ON SEISMIC DEMANDS


by
Mohsen Rahnama
and
Helmut Krawinkler



A report on research
sponsored in part by
CUREe-Kajima
and the
National Science Foundation
Grant BCS-8901665

Report No. 108

July 1993

REPRODUCED BY: 
U.S. Department of Commerce
National Technical Information Service
Springfield, Virginia 22161

The John A. Blume Earthquake Engineering Center was established to promote research and education in earthquake engineering. Through its activities our understanding of earthquakes and their effects on mankind's facilities and structures is improving. The Center conducts research, provides instruction, publishes reports and articles, conducts seminars and conferences, and provides financial support for students. The Center is named for Dr. John A. Blume, a well-known consulting engineer and Stanford alumnus.

Address

The John A. Blume Earthquake Engineering Center
Department of Civil Engineering
Stanford University
Stanford, California 94305



PB95-184008

EFFECTS OF SOFT SOIL AND HYSTERESIS MODEL ON SEISMIC DEMANDS

by
Mohsen Rahnama
and
Helmut Krawinkler

**The John A. Blume Earthquake Engineering Center
Department of Civil Engineering
Stanford University
Stanford, CA 94305-4020**

**A report on research sponsored in part by
CUREe-Kajima and the
National Science Foundation, Grant BCS-8901665**

Report No. 108

July 1993

ABSTRACT



PB95-184008

The main objective of this research is to develop procedures that will permit an explicit incorporation of the effects of deterioration of structural properties and site surface geology on the seismic demands imposed on structures by strong ground motions. This implies consideration of the influence of stiffness degradation and strength deterioration, including *P-delta* effects, and of the effects of site soil conditions on those demand parameters that can be used directly for design of structures. Thus, the research combines ground motion and structure response issues, with an emphasis on parameters that incorporate both relevant ground motion as well as structural response characteristics.

The first part of this study focuses on the effects of negative strain hardening (*P-delta*) and strength deterioration on the demand imposed by ground motions on the strength of inelastic *SDOF* systems. Strength demand is defined here as the strength that needs to be provided in order to limit the ductility of the *SDOF* system to predefined target value. ←

P-delta effects, which may cause a negative lateral stiffness (negative "hardening" stiffness) in a structure once a mechanism has formed, will increase the drift (displacement) of the system and may lead to incremental collapse if the structure has insufficient strength. Thus, if a predefined target ductility ratio is to be maintained, more strength must be provided for the structural system. A parameter study is performed to evaluate the effects of strain hardening/softening on seismic response. Bilinear hysteresis systems with a negative hardening stiffness drift significantly and their strength, compared to hardening systems, needs to be increased considerably in order to limit the inelastic deformations to the same ductility ratio. Stiffness degrading systems behave similar to bilinear systems if a positive hardening stiffness exists, but are clearly superior when the hardening stiffness becomes negative.

This study is concerned also with the effects of strength and stiffness deterioration on inelastic strength and displacement demands. Since deterioration is a history dependent problem, a general hysteresis model with energy based deterioration is developed. The

Abstract

hysteretic energy dissipation in each excursion is used to update a deterioration parameter. The results are presented in terms of the ratios of seismic demands of deteriorating systems over undeteriorated systems. The study shows that strength deterioration may greatly affect the response of *SDOF* systems if the hysteretic energy demand approaches the hysteretic energy capacity of the structural system. The response is sensitive to the deterioration parameter that identifies the rate at which strength deterioration occurs. Stiffness degradation is a problem of much less consequence than strength deterioration.

The research related to the study of soft soil effects on seismic demands is carried out in two parts. In the first part advantage is taken of the extensive set of ground motions recorded during the Loma Prieta earthquake and the availability of data on local soil conditions at recording stations. These data sets are utilized to improve the basic understanding of the phenomena involved, identify the most relevant parameters, develop analytical models, and calibrate these models. In the second part of the study simplified models of soil columns are employed for an extensive parameter study on the effects of site soil conditions on seismic demands. A comprehensive set of recorded and generated soft soil ground motions are utilized to obtain phenomenological information on the effects of site soil conditions on *PGA*, *PGD*, and elastic and inelastic displacement and strength demands spectra. In order to generate soft soil motions, a total 25 rock records are used as input for linear and nonlinear ground response analyses of soil columns of different periods. In the nonlinear ground response analysis the top layer of the soil is modeled as a nonlinear medium represented by a bilinear hysteresis model.

The motions obtained at the top of the soil columns are used to derive strength and displacement demand spectra for elastic and inelastic *SDOF* structural systems. The so derived spectra as well as the soft soil *PGA* and *PGD* values are evaluated in the context of seismic design, and a methodology is suggested that permits a more realistic incorporation of soft soil effects in the seismic design process. The study shows that the effects of soft soil on elastic and inelastic strength demands can be represented in a consistent manner through soil modification functions expressing the ratio of strength demands of soft soil motions to rock motions versus the ratio of structure period to soil column period. The elastic and inelastic displacement demand spectra for structures located on soft soils can be derived directly from the strength demands of the motions in the rock underlying the soft soil and the soil modification function, which is a function of soil period and structure ductility.

ACKNOWLEDGMENTS

This report is a reproduction of the senior author's Ph.D. dissertation. The research reported herein is part of a continuing study on the damage potential of ground motions and its implication for design. This study is supported by a research grant provided by Kajima Corporation and administered by CUREe (California Universities for Research in Earthquake Engineering), by the National Science Foundation Grant BCS-8901665, and by the John A. Blume Earthquake Engineering Center. The support provided by these organizations is gratefully acknowledged. The conclusions and opinions expressed in this report are solely those of the authors and do not necessarily represent those of the sponsors.

Several researchers of the John A. Blume Earthquake Engineering Center have provided input to this work. Many thanks are due to all of them, especially to Dr. Aladdin Nassar who has done much fundamental research in this area and has developed software that was used extensively in the data analysis and reduction. Thanks are due also to Professor V.V. Bertero of U.C. Berkeley who has provided much helpful advise and feedback to this research.



TABLE OF CONTENTS

Abstract	i
Acknowledgments	iii
Chapter 1 Introduction	1
1.1 Motivation for this Study	1
1.2 Objective and Scope	2
Chapter 2 Inelastic Consideration in Seismic Design	6
2.1 Introduction	6
2.2 Issues in Present Code Design Approach	7
2.3 Proposed Design Approach (Demand / Capacity)	10
2.3.1 Seismic Demand Parameters and Cumulative Damage Models	14
2.4 Hysteresis Model Issues	16
2.5 <i>SDOF</i> Seismic Demands for Motions in Rock and Stiff Soils	18
2.6 Soil Amplification Issues	20
Chapter 2 Figures	22
Chapter 3 Effects of Hysteresis Models on SDOF Response	34
3.1 Introduction	34
3.2 Classification of Hysteresis Models	35
3.2.1 Nondeteriorating Models	35
3.2.2 Stiffness Degradation Models with Limited Memory	36
3.2.3 History Dependent Strength Deterioration and Stiffness Degradation Models	37
3.3 Hysteresis Rules for Strength Deterioration and Stiffness Degradation Models	37
3.3.1 Strength Deterioration	39
3.3.2 Degradation of Unloading Stiffness	40
3.3.3 Accelerated Degradation of Loading Stiffness	40

3.4 Nonlinear Dynamic Analysis of <i>SDOF</i> Systems	42
3.4.1 Method of Analysis	42
3.4.2 Response Parameters	44
3.4.3 A Damage Indicator for Deteriorating Hysteresis Models	45
3.4.4 Parametric Study of Seismic Demands for <i>SDOF</i> Systems	47
3.5 Effects of Negative Strain "Hardening" (P-Delta) on Seismic Demand Parameters	48
3.5.1 Observations from Time History Analyses	50
3.5.2 Effects of Strain Hardening/Softening on the Strength Reduction Factor <i>R</i>	51
3.5.3 Effects of Strong Motion Duration on Seismic Demands for Systems with Negative Strain Hardening	54
3.6 Effects of Strength Deterioration and Stiffness Degradation on Seismic Demand Parameters	56
Chapter 3 Tables	59
Chapter 3 Figures	61

Chapter 4 Effects of Soil Condition on Seismic Demand of Loma Prieta Ground Motions

Prieta Ground Motions	109
4.1 Introduction	109
4.2 Loma Prieta Ground Motion Records Used in This Study	112
4.3 Attenuation Characteristics for Motions in Rock and Alluvium	114
4.3.1 Attenuation of <i>PGA</i> and <i>PGV</i>	114
4.3.2 Attenuation of Strength Demand Spectra	116
4.4 Seismic Demands for Ground Motion on Soft Soil Sites	118
4.4.1 Strength Demands and <i>R</i> -factor	118
4.4.2 Elastic and Inelastic Displacement Demands	121
4.5 Factors Effecting Soil Amplification	123
4.5.1 Predominant Soil Period	123
4.5.2 Directivity Effects	125
4.5.3 Attenuation Characteristics of Rock Motions	126
4.6 Damage Potential of Soft Soil Ground Motions	126
4.7 Summary	128
Chapter 4 Tables	130
Chapter 4 Figures	133

Chapter 5 Analytical Study of Soft Soil Amplification	160
5.1 Introduction	160
5.2 Soft Soil Consideration in the Seismic Design	162
5.3 Methods of Ground Response Analysis	164
5.3.1 Equivalent Linear Method	165
5.3.2 Linear <i>MDOF</i> Lumped Mass Model	165
5.4 Ground Response Analysis of Selected Soft Soil Sites	167
5.4.1 Evaluation of Site Response at Treasure Island	168
5.4.2 Evaluation of Site Response at APL2, SFA and OAKW Sites	170
5.4.3 Validity of One-Dimensional Soil Column Model	171
5.5 Linear Ground Response Analysis Using <i>MDOF</i> Lumped Mass Models	171
5.5.1 Amplification of Strength Demands	173
5.5.2 Amplification of Displacement Demands	176
5.5.3 Amplification of Input Energy	177
5.5.4 Amplification of Ground Motion Parameters	177
5.6 Ground Response Analysis with Nonlinear Soil Layer	178
5.6.1 Hyperbolic Backbone Curve	179
5.6.2 Ramberg-Osgood Model	180
5.6.3 Method of Analysis and Discussion of Results of Nonlinear Ground Response Analyses	181
5.7 Implications for Seismic Design.....	185
Chapter 5 Figures	187
 Chapter 6 Summary and Conclusions	 227
Bibliography	233

CHAPTER 1

INTRODUCTION

1.1 Motivation for this Study

Seismic design is an attempt to assure that strength and deformation capacities of structures exceed the *demands* imposed by severe earthquakes with an adequate margin of safety. This simple statement is difficult to implement because both demands and capacities are inherently uncertain and dependent on a great number of variables. A desirable long-range objective for research in earthquake engineering is to provide the basic knowledge needed to permit a simple but explicit incorporation of relevant demand and capacity parameters in the design process. The basic capacity parameters of structures are the strength and ductility (maximum deformation over yield deformation) of individual elements, which when assembled into structural configurations, define the strength and ductility capacities of complete structures. At this time, strength capacities of elements and structures can be evaluated with reasonable confidence, and ductility capacities can be estimated from experimental studies and empirical damage models.

A demand parameter is defined here as a quantity that relates seismic input (ground motion) to structural response. Thus, it is a response quantity, obtained by filtering the ground motion through a linear or nonlinear structural filter. A simple example of a demand parameter is the spectral acceleration S_a , which identifies the strength demand for an elastic *SDOF* (single degree of freedom) system. Considering that most structures behave inelastically in a major earthquake, it is evident that this parameter alone is insufficient to describe seismic demands. Relevant demand parameters include, but are not limited to, ductility demand, inelastic strength demand (i.e., the strength required of an inelastic system in order to limit the ductility ratio to a target value), and cumulative

damage parameters such as the hysteretic energy. A discussion on capacity / demand issues related to current seismic practice and a proposed design approach are presented in Chapter two.

The basic design quantities for relating seismic input to structural behavior are the *SDOF* inelastic strength and deformation demands. These demands and other seismic demand parameters strongly depend on the characteristics of input motions as well as the characteristics of the load-deformation behavior of the structure. This study addresses specific issues of a design approach that advocates the explicit incorporation of inelastic seismic demand parameters in the design process. In particular, the evaluation of the effects of the type of hysteresis model and of soft soil amplification on these seismic demand parameters is the focus of this research. For instance, there is a need for a more explicit and realistic representation of soil site effects in the design process. Elastic site specific spectra, which are more and more becoming the basis for deriving seismic design forces for major structures, are inadequate and in many cases misleading vehicles for representing these effects. They are appropriate for design for damage control (serviceability), which is based on essentially elastic behavior, but inappropriate for design for collapse safety where significant inelastic deformations have to be tolerated. For this case inelastic seismic demand parameters should form the basis for design.

1.2 Objective and Scope

There are two main objectives in this research. The first one is to evaluate important seismic demand parameters considering the influence of the deterioration of structural properties (strength and stiffness) during earthquakes. The second objective is to investigate the effects of soft soil amplification of ground motion on the seismic demands. In the following paragraphs these objectives are briefly addressed; a detailed discussion is presented in Chapter two.

During strong ground motion most structures will undergo inelastic load reversals and experience permanent damage. Using a realistic hysteresis model to represent the behavior of structural elements during cyclic loading is important for accurate prediction of the damage a structure may sustain during severe earthquakes. The seismic behavior of a structure subjected to a strong earthquake can be viewed as a process during which the mechanical properties of the structure (stiffness, strength) are continuously modified during inelastic excursions. These modifications may significantly affect the response to

ground motions. The sensitivity of the inelastic seismic demand parameters to characteristics of the hysteresis models and the importance of deterioration in strength and stiffness in seismic response are addressed in this study.

Current seismic codes take into account the effects of soft soil by using a period independent soil factor together with regional zone factors, smoothed elastic response spectra, and period independent reduction factors to identify the seismic demands for design. There are three problems with this approach. First, the regional zone factors, which are measures of "effective" peak ground acceleration, do not account for the often observed amplification of *PGA* at soft soil sites. Second, the smoothed elastic response spectra together with code soil factors, account inadequately for the amplification of response ordinates at soft soil sites. Third, the code approach of scaling the elastic response spectra values by period and soil-type independent reduction factors (*R*-factors) to derive design force demands can easily be shown to be inconsistent and obscures the strength and ductility demand imposed by severe earthquakes.

The first two problems can be overcome by the use of site-specific elastic response spectra, as is permitted and sometimes encouraged in many seismic codes. But the third problem remains. It is not at all clear or well established what a design engineer is supposed to do with a site-specific elastic response spectrum. Use it together with code *R*-factors to derive design force levels? Use it together with elastic analysis to tune the design to acceptable inelastic demand ratios (*IDRs*)? Both approaches have many pitfalls, particularly in view of the fact that site-specific elastic response spectra cannot be established with confidence. The last problem is often circumvented by enveloping site dependent elastic response spectra over a very wide period range, which unduly penalizes structures whose natural periods are not in the range of periods affected by soil amplification. Thus, a consistent approach, that accounts for all these problems in a rational and transparent manner, is needed.

A review of issues related to the present code design approach and a proposed demand / capacity approach for design of structures is presented in Chapter 2. A discussion on the soil amplification and hysteresis models issues is also presented Chapter 2 together with a summary on seismic demands for motions in rock and firm soil.

In Chapter 3 different hysteresis models and the development of a general hysteresis model are presented. Hysteresis models that are capable of representing the deterioration

of structural properties during dynamic loading are introduced. The hysteretic energy is used to define deterioration parameters. These parameters are used to modify the stiffness and strength of *SDOF* systems after each excursion. The effect of negative inelastic stiffness (*P*- δ effects) on the inelastic strength demand and *R*-factor is evaluated. A set of 15 ground motions representative of near-source rock and firm soil motions recorded in Western U.S earthquakes is utilized in order to provide statistical information on demand parameters.

In Chapter 4 an extensive set of ground motions recorded during the Loma Prieta earthquake is utilized to illustrate fundamental issues in ground motion attenuation in stiff and soft soils and the effects different soil conditions have on important seismic demand parameters. A set of 51 ground motions recorded during this earthquake is used for a global evaluation of strength and ductility demands for bilinear *SDOF* systems, with due consideration given to attenuation characteristics and local soil conditions. Regression analysis is employed to evaluate the attenuation characteristics of *PGA* and *PGV* as well as the elastic and inelastic strength demands imposed by rock and alluvium ground motions on bilinear *SDOF* systems. Several records are used to illustrate the large seismic demands generated by soft soil ground motions. For the stations for which soil data are available, the soil profile is modeled as a multi-degree of freedom (*MDOF*) lumped mass system and nearby rock motions are used as input to the soil column model. The elastic response spectra of predicted surface motions are compared with the spectra of recorded motions. In most cases the response spectra of recorded and predicted surface motions are in good agreement. This comparison provides guidance for a general parameter study on the effects of soft soils on seismic demands.

In Chapter 5 analytical studies with recorded and generated soft soil motions are discussed. These studies are concerned with an evaluation of soft soil effects on elastic and inelastic seismic demand parameters. Quantitative information on soft soil effects is presented, using *SDOF* soil column models whose properties are varied to cover a soil period range from 0.5 to 4.0 seconds. In most of the analyses the soil column is modeled as a linear elastic medium with 10% damping. Several analyses cases incorporate nonlinear behavior for the top 30 ft. of soil deposit that represents very soft soil with low shear wave velocity. The soil nonlinearity is represented using a bilinear hysteresis model. Strength demand spectra are developed and a methodology which permits explicit incorporation of soft soil effects in the design process is presented.

Chapter 6 provides a summary of the work completed, as well as conclusions and recommendations for future research.

CHAPTER 2

INELASTIC CONSIDERATION IN SEISMIC DESIGN

2.1 Introduction

Safety and structural damage during strong earthquakes are dependent mainly upon the characteristics of ground motions and the energy absorption and dissipation capacity of structures. A systematic study of those parameters that influence both ground motion and structural response characteristics is needed in order to improve current seismic design practice.

The ability of structures to dissipate the seismic input energy is related to the inelastic behavior of structures. The inelastic response is affected by global dynamic characteristics (e.g., periods, damping) as well as the materials properties, yield strength, ductility capacity, and detailing of the elements of structures. Usually, *SDOF* models are used to represent global response characteristic of structures. Such models should be able to represent the degree of damage sustained by a structure during cyclic loading by adopting an appropriate hysteresis model. Current seismic design codes consider the effects of energy dissipation through inelastic deformation by using an empirical reduction factor to modify the base shear force.

The characteristics of earthquake ground motions are influenced by source mechanism, source-site distance and orientation, travel path, and local geological and soil conditions. Subsoil characteristics have an influence on the amplitude, the frequency content, and the duration of shaking. The seismic waves are modified as they pass from the underlying rock formation through the soil medium. The effects of soil can be seen in

various ground motion characteristics such as peak ground acceleration, peak ground velocity, and the shape of the response spectrum.

Most seismic codes account for the effects of soft soil by increasing the seismic base shear coefficient. Present seismic codes include procedures that account for soil site effects, but in an empirical and non transparent manner that does not represent the physical phenomena that occur when a structure, which is expected to respond *inelastically* in a severe earthquake, is subjected to soft soil ground motions. As a consequence, presently employed design procedures, which are probably adequate in most cases, cannot provide a consistent level of protection and may be overly conservative in some cases and unconservative in others.

2.2 Issues in Present Code Design Approach

Most structures, even though they are expected to behave inelastically during strong ground shaking, are designed based on seismic codes that require no explicit consideration of inelastic response characteristics.

The present UBC regulations (UBC, 1991) provide two methods for earthquake resistant design, the equivalent static lateral force method and the dynamic method. In the static method the structure is to be designed at the allowable stress level for a base shear given by the following formula:

$$V = \frac{ZIC}{R_w} W \quad (2.1)$$

in which

$$C = \frac{1.25S}{T^{2/3}} \leq 2.75 \quad (2.2)$$

In these equations Z is the seismic zone factor, I is the importance factor, S is the site coefficient that depends on the characteristics of the soil and varies from 1.0 for rock to a maximum of 2.0 for soft soil, R_w is an empirical factor that depends on type of structure, and W is the effective seismic weight.

In the dynamic method elastic response spectra are used together with elastic modal analysis and the same R_w factors to estimate the design forces.

The present *UBC* regulation are based on a methodology developed first in the *ATC-03* (Applied Technology Council) project. The primary difference between *UBC* 1991 and *ATC-03* is the use of R_w factors instead of the R factors originally proposed in *ATC-03*. The *ATC-03* R -factors are strength reduction factors that define the design strength demand at the *member strength level*, whereas the *UBC* R_w factors identify the design strength demand at the *allowable stress level*. In this dissertation the term *R-factor* will also be used, but it will define the design strength at the *structure strength level*.

Since a major aspect of this research is to study the soft soil amplification and its effects on the strength demands it is worthwhile to trace the history of the S factor employed in the code.

The great effects of local soil conditions on the surface ground motion and the resulting damage to structures have been demonstrated by several major earthquakes in the past. For the first time in 1974 a soil factor S was introduced into the base shear equation by the Seismology Committee of the Structural Engineers Association of California (*SEAOC*).

In 1976 this S factor was adopted by the Uniform Building Code. The value of S was selected to be in the range of 1.0 to 1.5 depending on the ratio of soil period to structure period. In the absence of information on the site period, S was assumed to be 1.5.

In the 1985 *UBC* Code the soil period dependent S factor was replaced by three period independent S factors for three types of soil profiles. i.e., S_1 for rock and shallow stiff soils, S_2 for deep dense or stiff soils, and S_3 for soft to medium stiff clay and sand. The value of the soil factor for these three types of soil profiles is 1.0, 1.2 and 1.5, respectively. It is interesting to note that these "design" soil factors are different from the soil factors published for the corresponding ground motion spectra, which are 1.0, 1.5, and 2.25, respectively. The differences can only be explained as engineering judgment. An additional soil type, S_4 , identifying soil profiles containing more than 40 feet of soft

clay, was introduced in the *UBC 1988* as a consequence of the large soil amplification observed in 1985 Mexico City earthquake. The S factor for this soil type is 2.0.

The 1989 Loma Prieta earthquake again demonstrated the sensitivity of ground motions and localized patterns of damage to site conditions. For many soft soil sites the code prescribed S factor for S_4 soil profiles is deemed to be too low to account for the soil effects in the period range in which soil characteristics magnify the spectral response. This holds true particularly in regions of lower seismicity where rock motions are relatively small and the soil response is nearly elastic.

There are conceptual problems with the two methods of design (equivalent static and dynamic procedures) suggested in present codes. These procedures rely too much on elastic response spectra and empirical reduction factors, which makes it impossible to relate design to ground motion characteristics, particularly for motions in soft soils. In the equivalent static force procedure a soil factor (S_2, S_3, S_4) is used to account for site amplification of the elastic response spectra, and period independent R_w factors are employed to estimate design forces. These R_w factors are supposed to be a measure of the capacity of the structural system to dissipate energy through inelastic deformations (ductility). It has long been known and confirmed in a recent study by Nassar and Krawinkler (1991) that the relationship between system ductilities and R -factors is period dependent, particularly for short period structures, and is also a function of structural characteristics such as strain hardening and type of hysteretic response. Moreover, R -factors are greatly affected by soft soil effects as will be discussed later.

The energy absorption and dissipation capacity of a structure depends on the strength and ductility, and on the ability of the structure to resist repeated cyclic loading. During cyclic loading the properties of elements of a structure will change. Structural characteristics such as deterioration in strength and degradation in stiffness may significantly affect the response to ground motion. These issues are not considered in present seismic codes.

Inelastic response of structures depends on the real strength of the structural system. Structures have more strength than is required by code design criteria. Overstrength, which is defined here as the difference between the real strength of a structure and the required code design strength, comes from many sources (Osteraas and Krawinkler, 1990). Because of variable overstrength, present designs will result in lateral strengths

that vary widely, dependent on the type of structural system and the number of stories (natural period). As a consequence, the ductility demands that code designed structures may experience in a severe earthquake have little relation to the relative R -factors and to the design base shear, and the presently employed code design process cannot provide consistent protection for different structural system. In addition, the issue of damage control (serviceability) is not separated from the design against collapse.

2.3 Proposed Design Approach (Demand / Capacity)

This seismic design approach, which is summarized in Figs. 2.1 and 2.2 (Krawinkler, 1993), is based on the seismic demand and capacity concept and is the result of studies by Oстераas and Krawinkler (1990), Nassar and Krawinkler (1991), and the research summarized in this report. In the previous studies the effects of soft soils as well as strength deterioration of structures were not considered. The main objective of this research is to develop and calibrate simplified analytical models that permit the derivation of seismic demand spectra from a combination of rock motion and soil column information. In addition, the effects of strength deterioration and stiffness degradation of structures is investigated. The results of this study provide detailed data and input for the proposed seismic design methodology. In this section the proposed seismic design approach and its implementation are briefly reviewed.

The proposed approach is a dual level design approach in which serviceability and safety against collapse are treated as separate design levels associated with earthquakes of different probabilities of occurrence. Both limit states can be described by damage control, with the serviceability limit state defined by drift control and small (negligible) cumulative damage and the safety limit state defined by an adequate margin of safety against the cumulative damage approaching a limit value associated with collapse. This study is concerned only with the issue of design for safety against collapse during severe earthquakes.

Seismic design is an attempt to assure that strength and deformation *capacities* of structures exceed the *demands* imposed by severe earthquakes with an adequate margin of safety. The basic capacity parameters of structures are the strength and ductility (or deformation) of individual elements, which, when assembled into structural configurations, define the strength and ductility (or deformation) capacities of complete

structures. Ductility or deformation capacities of elements of structures can be estimated from experimental studies and empirical damage models.

The design process consists of estimating ductility capacities and deriving the strength required to "assure" that the ductility demands do not exceed the available ductility capacities. For design this implies that ductility capacity is a predetermined target and strength is a derived quantity that depends on the characteristics of the earthquake ground motions. Thus, the required strength (strength demand) for a specified target ductility becomes the primary seismic demand parameter, which needs to be evaluated with due regard to all pertinent structural and ground motion characteristics. Single degree of freedom (*SDOF*) systems are often utilized to evaluate this parameter.

Complications in this process arise from the fact that the ductility capacities may depend strongly on cumulative damage effects, i.e., the number and relative magnitudes of damaging cycles. One widely used measure of cumulative damage effects is the hysteretic energy that has to be dissipated during an earthquake. Detailed incorporation of cumulative damage aspects is a complex issue, but in a simplified approach the ductility capacities can be modified (weighted) to account for the anticipated number of inelastic cycles and hysteretic energy dissipation. Thus, for a specified target ductility, the number of inelastic cycles and the hysteretic energy dissipation demands, which again depend on structural and ground motion characteristics, become additional important demand parameters for design.

In summary, consistent seismic protection can be accomplished through a design process that is based on predefined target ductility capacities (which depend on the type of structural system and design detailing) and ground motion dependent strength demands. Thus, strength demands and energy demands (to account for cumulative damage effects) are the most important seismic demand parameters. Effects of soil amplification and deterioration of structure properties on these seismic demands are the focus of this study.

Figure 2.3 illustrates some of the important features of the proposed design approach in a simple flow chart. The demand vs. capacity approach is based on the estimation of structure ductility capacities which are then used to derive inelastic strength demands. Thus, the basic design information is the ductility or inelastic deformation capacity of structural elements. The ductility capacity is 1.0 or less for brittle elements

(e.g., many types of connections, columns subject to buckling, etc.), and a quantity to be obtained from experimental work and analytical studies for "ductile" elements. For any given element the ductility capacity is not a constant but is a function of the deformation history, which may be characterized by the number and magnitudes of inelastic excursions and the energy dissipated by the element. Every inelastic excursion causes damage, and cumulative damage models must be utilized to weight the ductility capacity with respect to anticipated demands.

The weighted ductility capacity of structural elements becomes the starting point for design. Through geometric transformations the element ductility capacities need to be converted into story ductility capacities, which are then used to derive "*inelastic strength demands*" for design.

By using the appropriate relationships presented in Section 2.5, these inelastic strength demands are derived first for *SDOF* systems with a bilinear hysteresis model for ground motion on rock or firm soil sites. Modifications need then be applied to account for the effects of the hysteresis model and soft soils on the *SDOF* inelastic strength demands, and further modifications are needed to account for response characteristics in real *MDOF* structures (Nassar and Krawinkler, 1991). The so derived strength demands identify requirements on the strength of the structure at the mechanism level.

Strength design can be performed directly using plastic design concepts. Since current design practice is more familiar with elastic design rather than plastic design, elastic design at the member strength level may be performed by converting the structure strength level to the member strength level. This transformation can be carried out by estimating the ratio of ultimate strength (E_g) of the structure to the strength level associated with the strength of the weakest element (E_l). These two levels of strength are shown in Fig. 2.4. Previous studies (Osteraas and Krawinkler, 1990) have shown that this transformation may involve an iteration process. Following preliminary strength and stiffness design, a necessary step is design verification and fine-tuning by using either a nonlinear static incremental load analysis (push-over) or a nonlinear time history analysis to verify that the ductility (deformation) demands in critical elements do not exceed the available capacities.

In order to implement the design approach (*demand vs capacity*) much research has to be carried out on the different aspects that are involved in this design process. On the

demand side, Nassar and Krawinkler (1991) provided statistical information on the elastic and inelastic strength, displacement, and cumulative damage demands, and on basic modifications for *MDOF* systems. In that study representative ground motions for rock and firm soil sites were used to derive statistical information on the seismic demands.

On the capacity side of the design approach much more work is required to identify the ductility capacities of individual elements of structures. The member ductility capacity depends on the material properties, detailing, function of the element as a part of the structure, and the effects of cumulative damage on the member ductility. More research is also needed to establish relationships between member ductilities and structure deformation parameters (e.g., interstory ductility).

In the context of the proposed design approach, the following questions concerning the effects of deterioration of structural properties and the effects of amplification of ground motions in soft soils on seismic demands are addressed in this study:

- How can important structural restoring force characteristics, including deterioration in strength and degradation in stiffness, be represented in *SDOF* hysteresis models?
- How sensitive are the seismic demand parameters to characteristics of the hysteresis models used to represent structures?
- How can one quantify site soil effects and incorporate them into ground motion analysis and seismic design?
- To what extent are the seismic demand parameters affected by site soil conditions?
- How can seismic demands derived for rock sites together with the characteristics of soil deposits be used to define seismic demands for soft soil sites?

2.3.1 Seismic Demand Parameters and Cumulative Damage Models

Seismic demands represent the requirements imposed by ground motions on relevant structural performance parameters. In a local domain this could be the demand on axial load of a column or the rotation of a plastic hinge in a beam, etc.. Thus, the localized demands depend on many local and global response characteristics of structures, which cannot be considered in a study that is concerned with a global evaluation of damage potential. In this study only *SDOF* systems are used as structural models. Assuming that these models have a reasonably well defined yield strength, the following basic seismic demand parameters play an important role in the proposed design approach. Some of the terms used in these definitions are illustrated in Fig. 2.5.

Elastic Strength Demand, $F_{y,e}$. This parameter defines the yield strength required of the structural system in order to respond elastically to a ground motion. For *SDOF* systems the elastic acceleration response spectra provide the needed information on this parameter.

Ductility Demand, μ . This parameter is defined as the ratio of maximum deformation over yield deformation for a system with a yield strength smaller than the elastic strength demand $F_{y,e}$.

Inelastic Strength Demand, $F_{y(\mu)}$. This parameter defines the yield strength required of an inelastic system in order to limit the ductility demand to a value of μ .

Strength Reduction Factor, $R_{y(\mu)}$. This parameter defines the reduction in elastic strength that will result in a ductility demand of μ . Thus, $R_{y(\mu)} = F_{y,e}/F_{y(\mu)}$. This parameter is often denoted as R .

Displacement Demand, δ . The elastic displacement demand (δ_e) defines the maximum displacement associated with elastic response to a ground motion. The inelastic displacement demand ($\delta_{in}(\mu)$) defines the maximum displacement of an inelastic system whose ductility demand is equal to μ . The displacement demand provides the information needed to control non-structural damage and to assess the importance of P-delta effects.

Energy and Cumulative Damage Demands. Repeated cyclic loading is known to have a detrimental effect on inelastic response characteristics. There are many attempts reported in the literature on assessment of cumulative damage effects through energy terms or specific cumulative damage models. The energy terms evaluated in this study are as follow.

- Input Energy, IE : The energy imparted to the structure by a ground motion
- Damping Energy, DE : The energy dissipated in the structure through viscous damping.
- Hysteretic Energy , HE : The energy dissipated in the structure through inelastic deformation.
- Total Dissipated Energy, TDE : $TDE = DE+HE$

Many cumulative damage models have been proposed in the literature, the simplest one being of the form

$$D = \sum_{i=1}^N \left(\frac{\Delta\delta_{pi}}{\delta_y} \right)^c \quad (2.3)$$

in which

- D = cumulative damage
- C, c = structural performance parameters
- N = number of inelastic excursions experienced in the earthquake
- $\Delta\delta_{pi}$ = the plastic deformation range of excursion i
- δ_y = yield displacement

For components of steel structures the exponent c was found to be in the range of 1.5 to 2.0 (Krawinkler, et. al., 1983). The coefficient C varies widely and depends strongly on the performance characteristics of the structures. The plastic deformation ranges $\Delta\delta_{pi}$ in this equation are not the ranges as they appear in the time history response. For the purpose of cumulative damage evaluation these ranges have to be reordered because small excursions have to be considered as interruptions of bigger ones. This can be accomplished with one

of several available cycle counting methods. For low-cycle fatigue damage the rain-flow cycle counting method was found to be the best suited one (Krawinkler, et. al., 1983). The plastic deformation ranges so identified, together with the number of inelastic excursions, N , provide basic information needed for cumulative damage modeling.

For bilinear systems, damage as expressed in Eq. (2.3) is identical (for elastic-plastic systems) or very close (for strain hardening systems) to the normalized cumulative hysteretic energy dissipation ($NHE = HE/F_y\delta_y$) if the structural performance parameters C and c are taken as 1.0; i.e.,

$$D = \sum_{i=1}^N \left(\frac{\Delta\delta_{pi}}{\delta_y} \right) \cong \frac{HE}{F_y\delta_y} = NHE \quad (2.4)$$

Thus, hysteretic energy dissipation is a subset of a more general damage model of the type given by Eq. (2.3). The advantage of using NHE as a damage parameter is that this quantity is always well defined whereas the plastic deformation ranges $\Delta\delta_{pi}$ are ill defined for stiffness degrading systems. The disadvantage of using NHE is that cycle counting methods no longer can be applied consistently and the use of an exponent c in a damage model based on NHE becomes ambiguous.

The list of seismic demand parameters enumerated here is by no means complete. But for conceptual studies much can be learned by using these parameters to assess the damage potential of ground motions. In the next three chapters, some of these seismic demand parameters are evaluated for rock and soft soil ground motions using different hysteresis models.

2.4 Hysteresis Model Issues

Using a realistic hysteresis model to represent the behavior of structural elements during cyclic loading is important for an accurate prediction of the damage that a structure sustains during severe earthquakes. These models should be capable of

representing all important structural characteristics that may significantly affect the response to ground motions.

Several types of hysteresis models are employed in research and engineering practice to predict the response of steel and reinforced concrete members subjected to cyclic loading. Clough and Takeda models are widely used to represent the cyclic behavior of reinforced concrete members. These models relate the degradation in stiffness to the maximum amplitude of deformation and assume that degradation is independent of the number of cycles. For steel structures simple bilinear models are used often to represent the load-deformation behavior of structural elements subjected to cyclic loading. The results of experimental studies (e.g., Krawinkler et. al. 1983) have shown that cumulative damage, which is a function of inelastic deformations and the number of excursions, may lead to a noticeable deterioration of initial strength after several load reversals. The effects of strength deterioration and stiffness degradation on the inelastic seismic demands has to be investigated and, if found to be important, incorporated in the seismic design of structures.

The sensitivity of inelastic demands to the type of hysteresis model used to represent the load-deformation characteristics of structures subjected to cyclic loading was studied already by Clough in 1966. In this study the response of *SDOF* systems with two different ranges of periods was investigated using elastoplastic and stiffness degrading models. For long period structures it was found that the response of both models are similar. However, short period structures ($T = 0.3$) with degrading stiffness properties were found to have significantly larger displacement ductility requirements compared to the elastoplastic system. The reason given in (Clough, 1966) is that the effective period of stiffness degrading models elongates more than that of the elastoplastic model. Since the quoted study as well as many others conducted since 1966 were of limited scope and led to somewhat different conclusions, the need persists to conduct a comprehensive study on the effects of hysteresis models on seismic demand parameters.

The seismic behavior of a structure subjected to a strong earthquake can be considered to be a process during which the mechanical properties of the structure (stiffness, strength) are modified during inelastic excursions. These modifications may significantly affect the response to ground motions. In order to evaluate these effects a general hysteresis model was developed in the research presented in this report. A

detailed discussion of this model and parametric studies of seismic demands using different model parameters will be presented in Chapter 3. Only *SDOF* systems are considered in this study.

2.5 SDOF Seismic Demands for Motions in Rock and Stiff Soils

A comprehensive study was performed by Nassar and Krawinkler (1991) to evaluate the seismic demand parameters for *SDOF* systems by using ground motions recorded on rock and stiff soil sites. In the following discussion the results of their study that are directly related to this research are briefly summarized.

The results summarized here are derived from a statistical study that used 15 Western US ground motion records from earthquakes ranging in magnitude from 5.7 to 7.7. The frequency characteristics of these records are similar in most cases and, in average, can be represented by a smoothed elastic response spectrum of the shape given in the *ATC-3* document for soil type *S₁*. Time history analysis for *SDOF* systems with bilinear and stiffness degrading hysteresis models was conducted for each record, using strain hardening ratios of $\alpha = 0, 2\%$, and 10% . In all analyses 5% damping was assumed. The yield levels of the *SDOF* systems were adjusted so that discrete predefined target ductility ratios of 2, 3, 4, 5, 6 and 8 were achieved. Statistical evaluation of elastic and inelastic strength demands, strength reduction factors *R*, and different types of energy demands was performed and the results were presented in terms of mean values and mean \pm standard deviation σ .

The strength reduction factors *R* were found to be dependent on the period of the *SDOF* system. To develop relationships between *R*, the period *T*, and the ductility ratio μ (*R- μ -T* relationships), Nassar and Krawinkler (1991) utilized a two-step nonlinear regression analysis on the *R*-factors obtained from the time history analysis of *SDOF* systems with a bilinear hysteresis model and strain hardening equal to 0, 2% and 10%. The regression analysis was performed in two stages, first regressing *R* versus μ for constant period *T*, and then evaluating the effect of period in a second step.

The following form of an *R- μ -T* relationship was employed:

$$R = \{c(\mu - 1) + 1\}^{1/c} \quad (2.5)$$

where

$$c(T, \alpha) = \frac{T^a}{1 + T^a} + \frac{b}{T} \quad (2.6)$$

The following values were obtained for the two regression parameters a and b for different α values:

for	$\alpha = 0\%$	$a = 1.00$	$b = 0.42$
for	$\alpha = 2\%$	$a = 1.00$	$b = 0.37$
for	$\alpha = 10\%$	$a = 0.80$	$b = 0.29$

A detailed discussion of the procedure used to develop these relationships is presented in the aforementioned reference.

These relationships together with mean or smoothed elastic response spectra can be used to develop inelastic strength demand spectra for rock and stiff soil sites. However, these R - μ - T relationships cannot be used directly for motions in soft soils, which exhibit strong amplification in their response spectra around the fundamental period of the soil deposit.

The mean R -factors for bilinear systems with 5% strain hardening (using 15- S_I records) are shown in Fig. 2.6(a) together with the regressed R -factors obtained from Eqs. (2.5) and (2.6). Fig. 2.6(b) shows the ATC S_I ground motion spectrum and inelastic strength demand spectra derived from this ground motion spectrum by utilizing these R - μ - T relationships. In the later chapters it is shown how to use spectra of this kind together with appropriate modification factors to derive strength demands for soft soil motions.

Using relationships discussed in Chapter 4, inelastic displacement spectra can be derived from the elastic spectrum and R - μ - T relationships. The displacement spectra corresponding to the strength demand spectra of Fig. 2.6(b) are presented in Fig. 2.7(a). Figure 2.7(b) shows normalized displacement demand spectra, defined as the ratios of inelastic over elastic displacement spectra for specified target ductilities. As indicated in this figure, these ratios are not much different from unity for periods larger than 0.5 sec., but increase rapidly and depend strongly on the target ductility for short period systems.

2.6 Soil Amplification Issues

A number of analytical studies have been carried out in the past to assess the effects of local subsurface condition on surface ground motions and resulting damage to structures caused by ground shaking. A review of some of these studies is presented in Chapter 4 to provide the background for the state-of-the knowledge on this subject.

Past studies have provided much information on specific aspects of soft soil amplification, such as methods of ground response analysis, dynamic properties of soil, and influence of different parameters on the modification of motions in soft soils. In regard to the response of structures to soft soil motions, past work has been limited almost exclusively to evaluations of elastic response spectra, and little attention has been paid to the effects of soft soils on inelastic seismic demands.

In order to investigate the effects of soft soil on surface motion characteristics many researchers have adopted one-dimensional vertical wave propagation models to compute the ground surface response. In most cases the spectral characteristics of the computed surface motions were in good agreement with those of recorded surface motions. The fundamental period of the soil deposit, T_s , which depends on the depth and the shear wave velocity of soil deposit layers, plays an important role in the frequency content of surface motions, the shape of response spectra, and the soil amplification.

Elastic response spectra of most soft soil motions show a clear hump in the vicinity of the fundamental period of the soil deposit. Structures with the natural period close to the fundamental period of the soil deposit will be subjected to a higher level of shaking compared to cases in which these periods are very different. This statement is correct if we assume the structures will respond elastically during a severe earthquake. But most structures will respond inelastically when subjected to strong ground motions and their effective period will lengthen. Therefore, using the elastic response spectrum together with the initial period of structures is inadequate for representing the effects of soft soil on the seismic demand parameters.

Fig. 2.8 illustrates the problem of using an elastic response spectrum to design structures on soft soils. Structure A has a natural period (T_a) smaller than the fundamental period of the soil column (T_s), whereas the period of structure B is approximately equal to T_s . During a strong earthquake these structures are expected to

respond inelastically and their effective period will increase to T'_a and T'_b for structures *A* and *B*, respectively. As indicated in the figure, the period of structure *A* moves into the hump of the elastic spectrum whereas the period of structure *B* moves away from the hump. As a consequence, the large hump of the elastic response spectrum, which is around the period of the soil column, diminishes in the inelastic strength demand spectra and even disappears at large ductility ratios.

This observation has significant implications for design. For structures with small ductility capacity the elastic strength demand spectrum will be an important design parameter and the required strength may be high and is very sensitive to the predominant soil period. For structures with large ductility capacity, which are expected to respond inelastically in severe earthquakes, the response will be less sensitive to the soil period and the amplification of response will be less significant. Thus, soil amplification will depend not only on the predominant soil period but also on the extent of nonlinearity expected in the response.

In this study much effort is devoted to the evaluation of soil amplification and its effect on elastic and inelastic strength demands. For this purpose the soil column is modeled as a multi-degree of freedom (*MDOF*) lumped mass system. The *MDOF* soil columns are subjected to recorded rock motions and the resulting response at the top (surface) is used as input for nonlinear time history analysis of *SDOF* systems. Elastic and inelastic spectra are computed for the soft soil motions and the rock motions from which the soil motions are derived, and the ratios of soft soil over rock spectra are used to evaluate the effects of soft soils on seismic demand parameters.

DESIGN OBJECTIVES AND PROCESSES

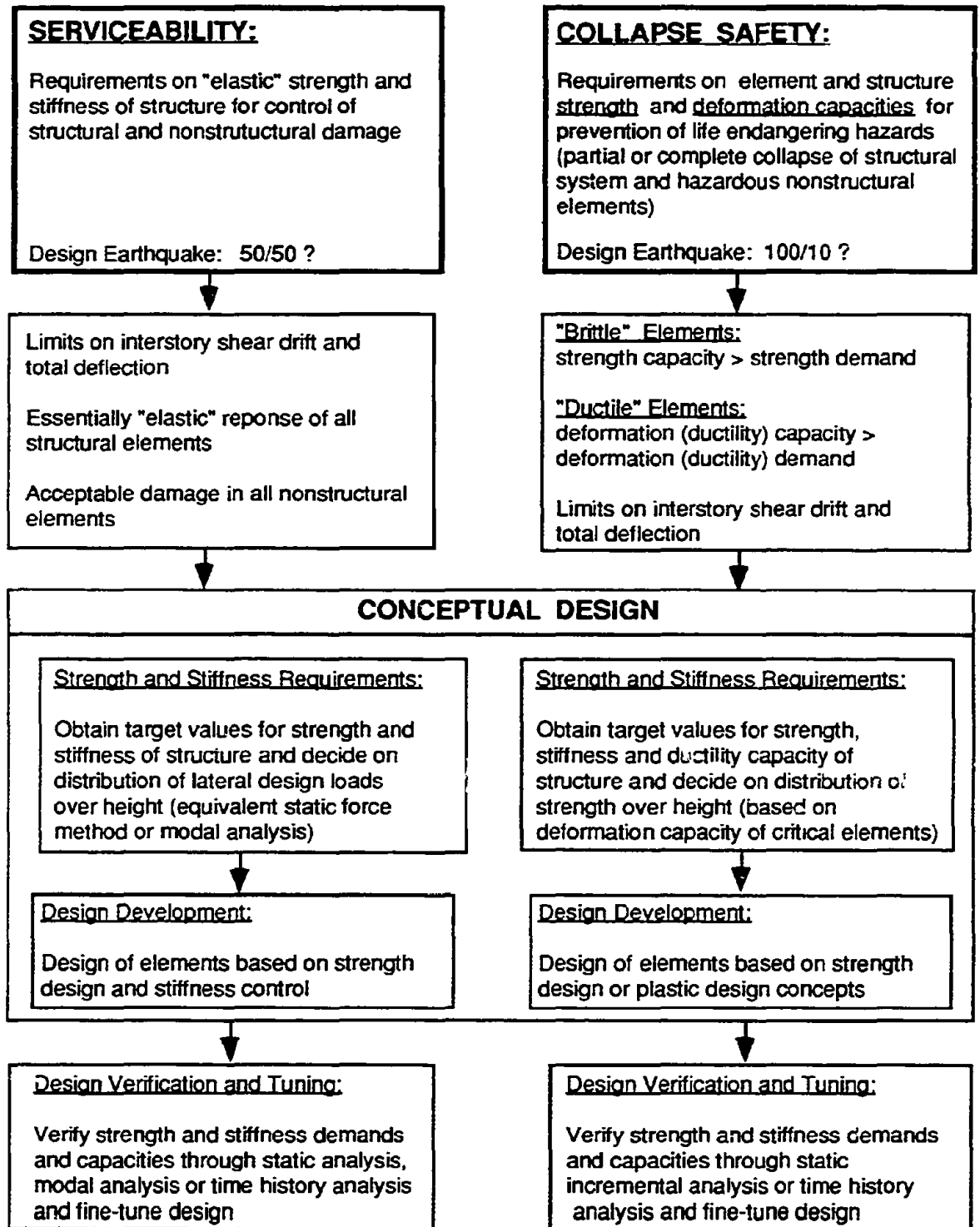


Fig. 2.1 Objectives and Processes for "Serviceability" and Collapse Safety" EQRD

DESIGN FOR COLLAPSE SAFETY: STRENGTH AND STIFFNESS REQUIREMENTS

Target Ductility Ratio for Structure:

"Known" Quantities:

Strength of elements

Cumulative damage models for deformation (ductility) capacity of critical elements

Examples:

$$D = C \sum \left(\frac{HE_i}{F_y \delta_y} \right)^c$$

$$D = \frac{\delta_m}{\delta_u} + \frac{\beta}{F_y \delta_u} \int dE$$

Determine available deformation (ductility) capacity of critical elements for structure to be designed:

- Dependence on period(s) of structure
- Dependence on strong motion duration and frequency content of ground motion

Convert element deformation (ductility) capacity into relevant structure deformation (ductility) capacity parameter:

- For frame structures:
Interstory drift (ductility) capacity
- For wall structures:
Interstory (ductility) capacity (if shear governs)
Global drift (ductility) or plastic hinge rotation capacity (if flexure governs)

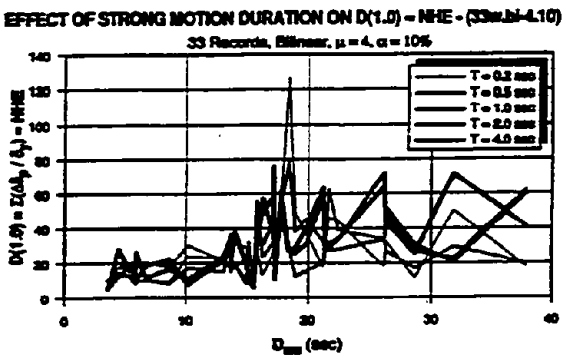
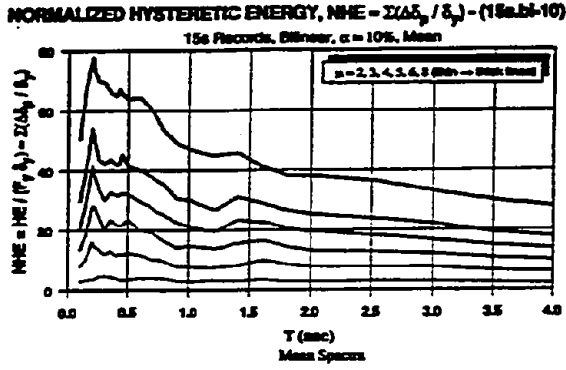
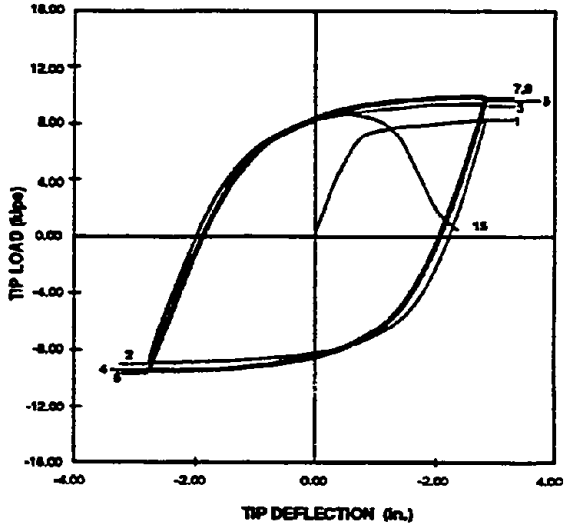


Fig. 2.2 Concepts and Steps Involved in EQRD for Collapse Safety

**DESIGN FOR COLLAPSE SAFETY:
STRENGTH AND STIFFNESS REQUIREMENTS, cont'd**

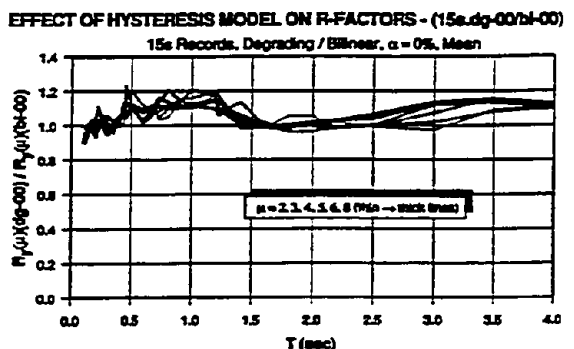
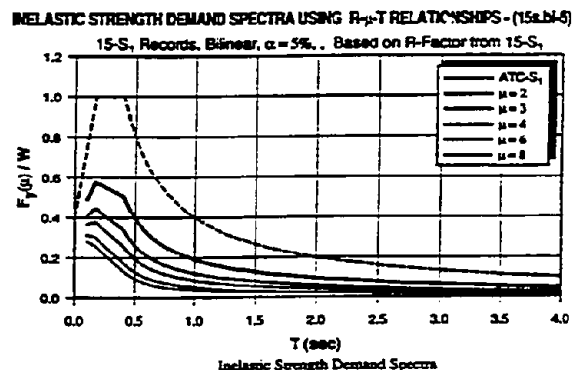
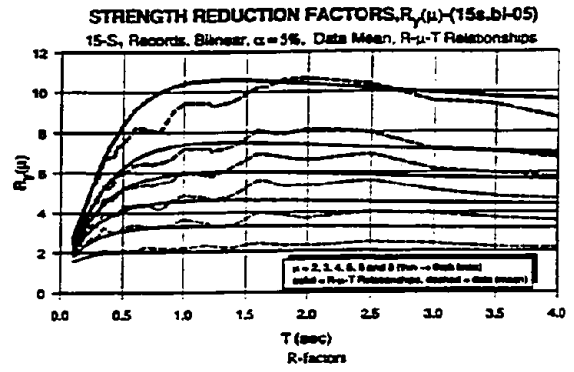
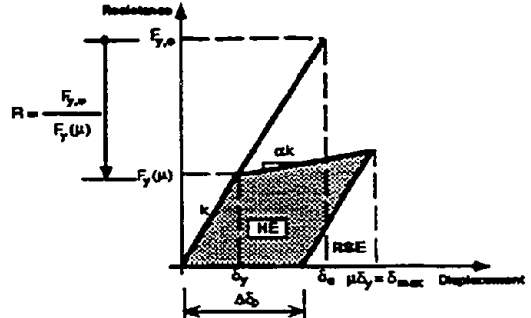
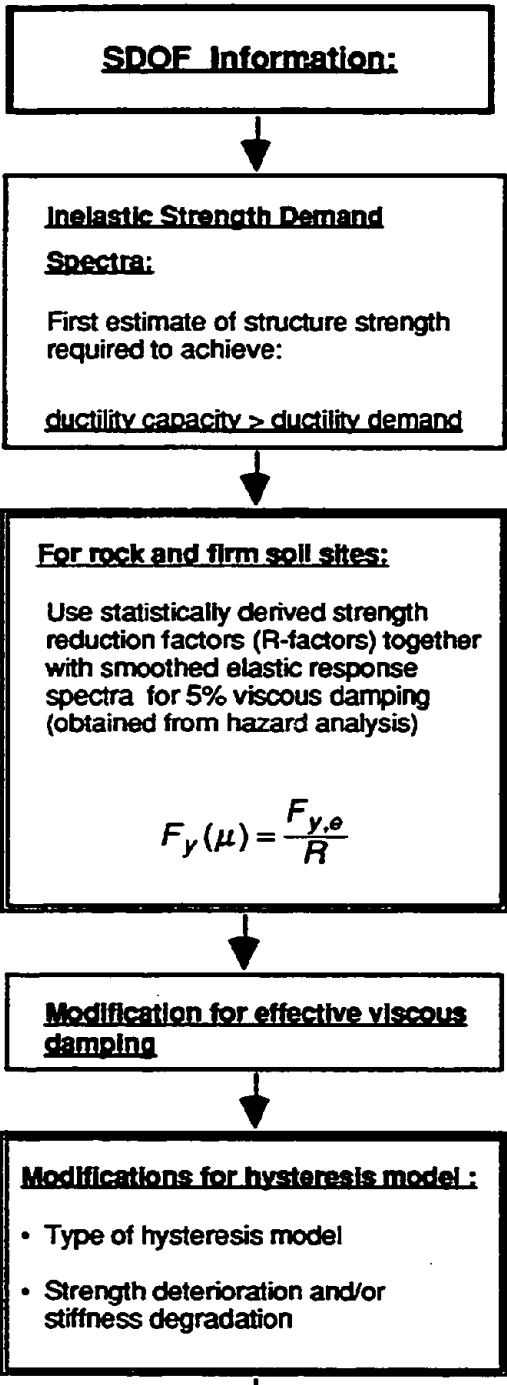


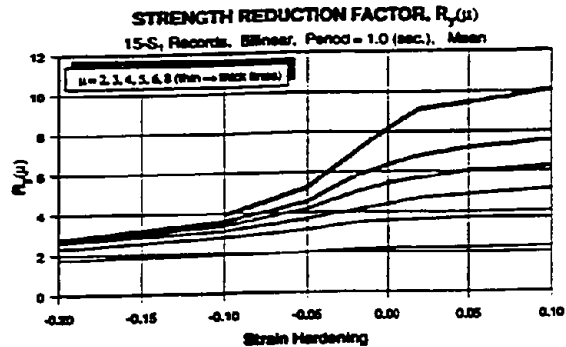
Fig. 2.2 (cont'd) Concepts and Steps Involved in EQRD for Collapse Safety

DESIGN FOR COLLAPSE SAFETY: STRENGTH AND STIFFNESS REQUIREMENTS, cont'd

Modification for P-delta effect:

Modification of R-factor
Effective hardening (softening)
stiffness:

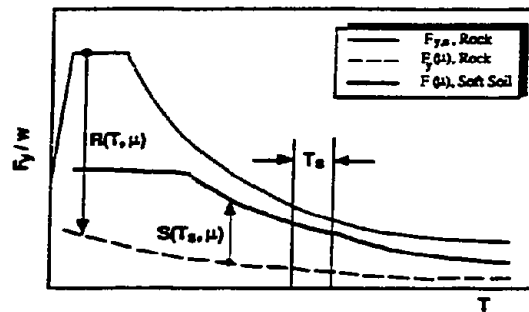
$$K_{in} = \alpha K_{el} \quad \alpha = \alpha_0 - \frac{P}{hK_{el}}$$



Modification for soft soil sites:

Soft soil modification function,
 $S(T_s, \mu)$

$$F_y^s(\mu) = \frac{F_{y,e}^r}{R} S(T_s, \mu)$$

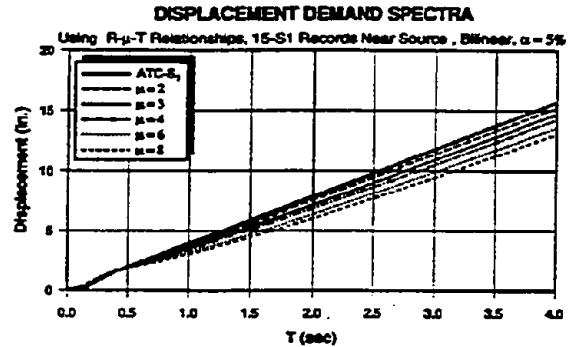


Inelastic Displacement

Demand Spectra:

For deformation control
For rock and firm soil sites:

$$\delta = \frac{\mu F_{y,e} g}{R W \omega^2}$$



For soft soil sites:

$$\delta_\theta^s = \frac{F_{y,e}^r}{W} \frac{g}{\omega^2} S(T_s, \mu = 1)$$

$$\frac{\delta_m^s}{\delta_\theta^s} = \frac{\mu S(T_s, \mu)}{R S(T_s, \mu = 1)}$$

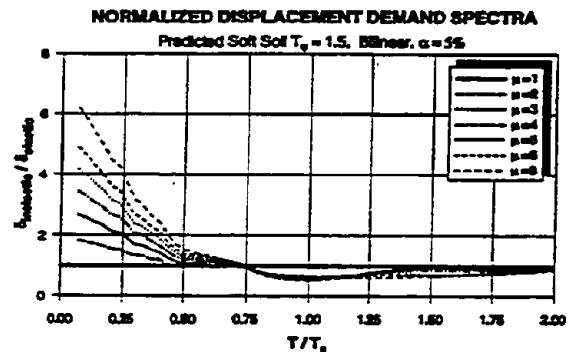


Fig. 2.2 (cont'd) Concepts and Steps Involved in EQRD for Collapse Safety

**DESIGN FOR COLLAPSE SAFETY:
STRENGTH AND STIFFNESS REQUIREMENTS, cont'd**

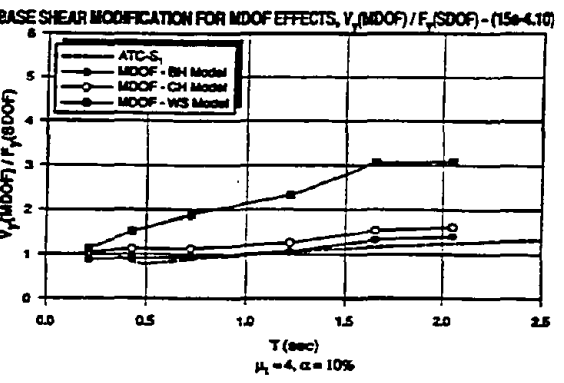
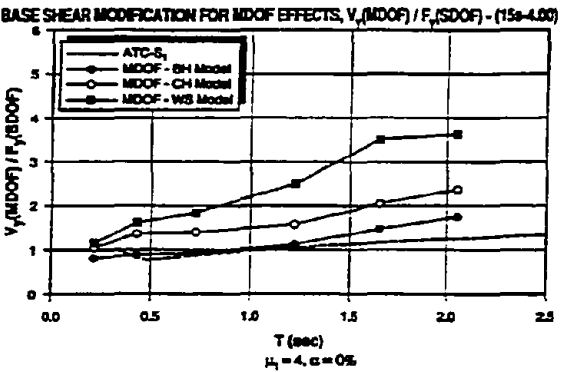
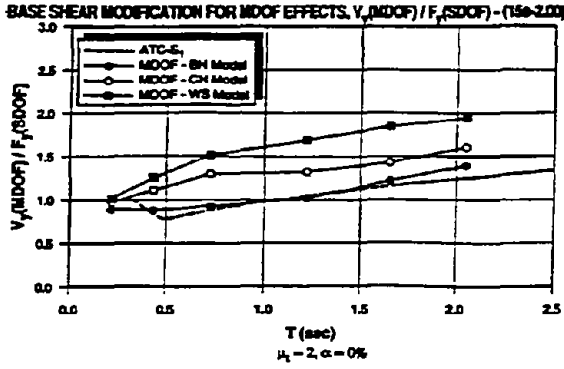
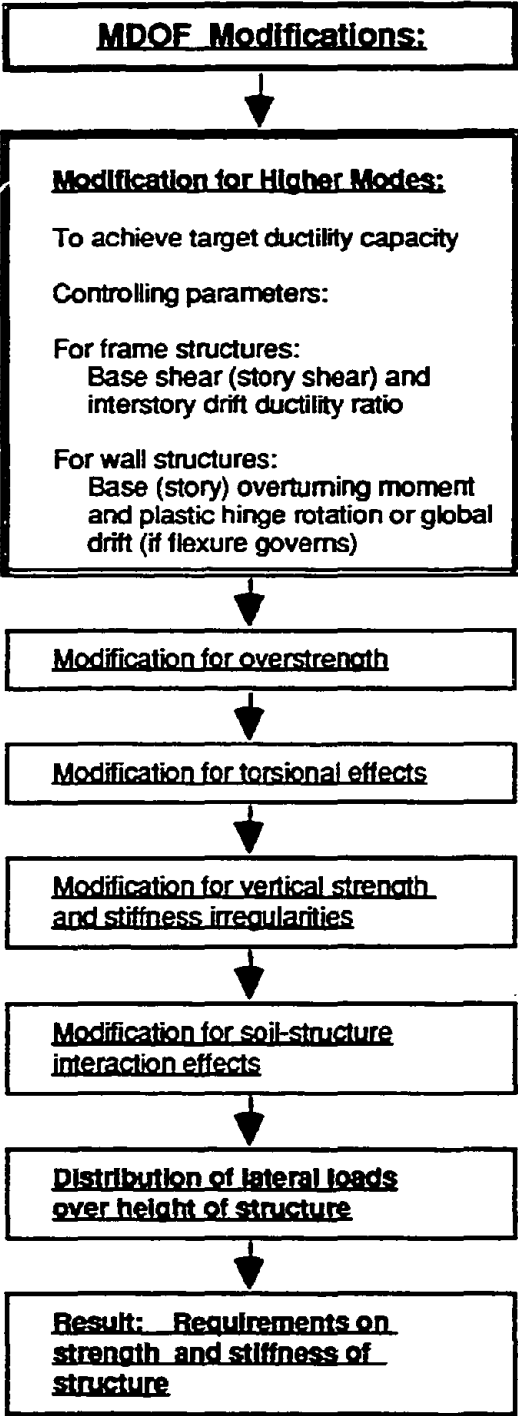


Fig. 2.2 (cont'd) Concepts and Steps Involved in EQRD for Collapse Safety

**DESIGN FOR COLLAPSE SAFETY:
DESIGN DEVELOPMENT**

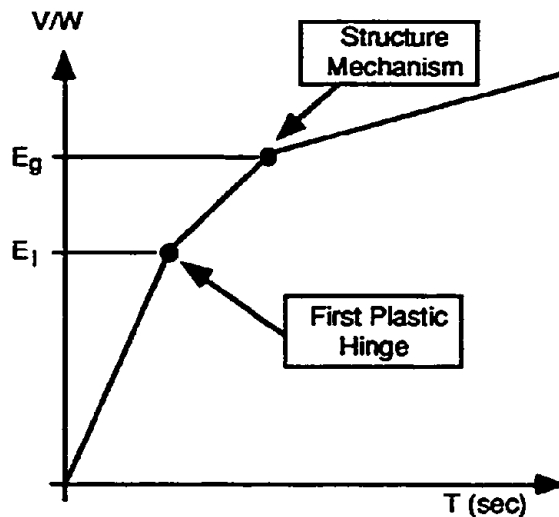
Member design for strength and deformation limits

Elastic design:

Based on strength of elements.
(Estimate difference between E_1 and E_g)

Plastic design

Design directly for required strength of structure (E_g)



**DESIGN FOR COLLAPSE SAFETY:
DESIGN VERIFICATION AND TUNING**

Verify strength and deformation (ductility) demands

- Static incremental analysis :
Push structure to estimated drift level, using one or more lateral load patterns
- Time history analysis:
Perform inelastic time history analysis of complete structure, using representative design ground motions

Identify strength demands (for brittle elements) and deformation (ductility) demands for critical elements and fine-tune the design

Fig. 2.2 (cont'd) Concepts and Steps Involved in EQRD for Collapse Safety

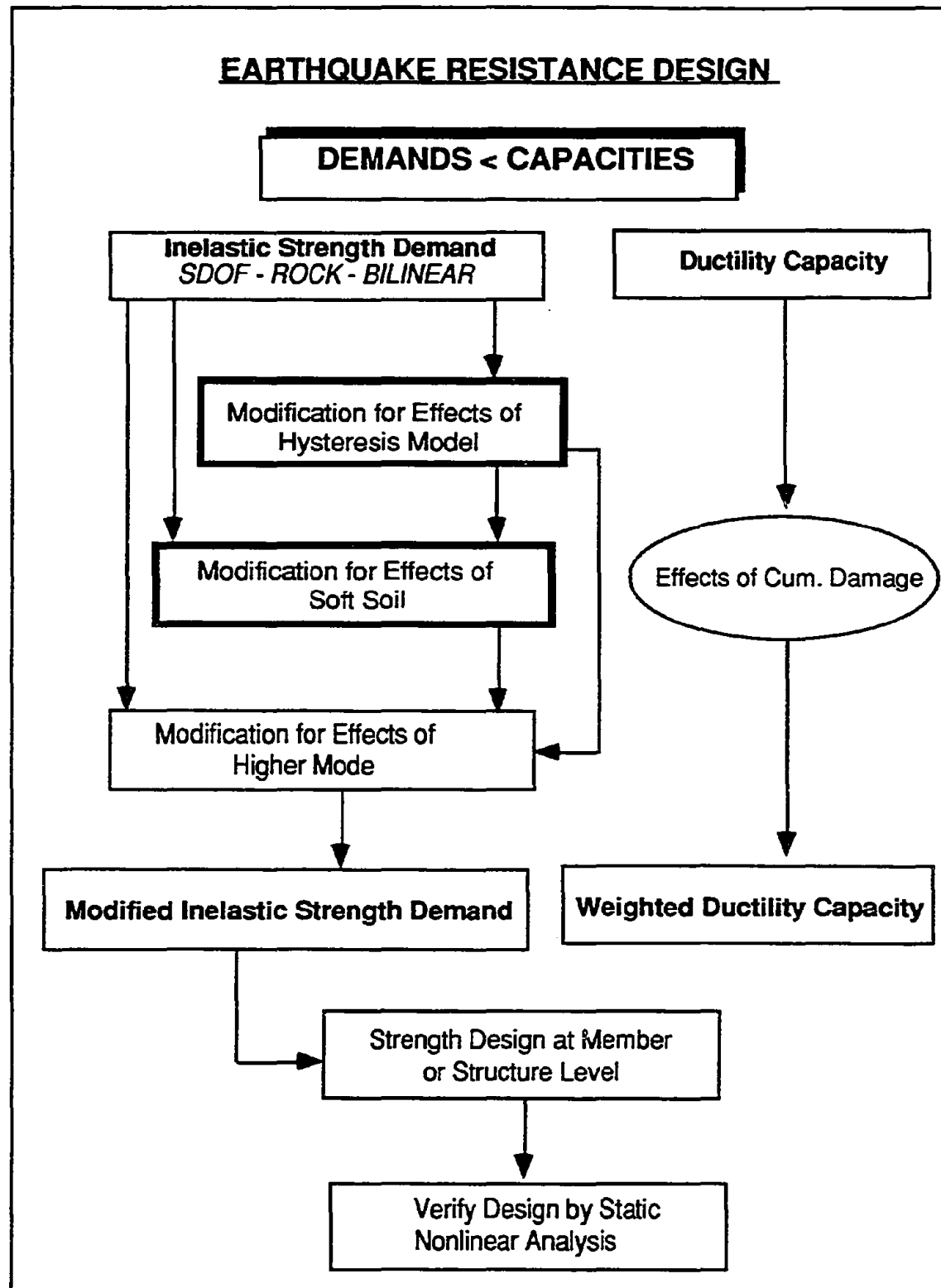


Fig. 2.3 Proposed Seismic Design Methodology

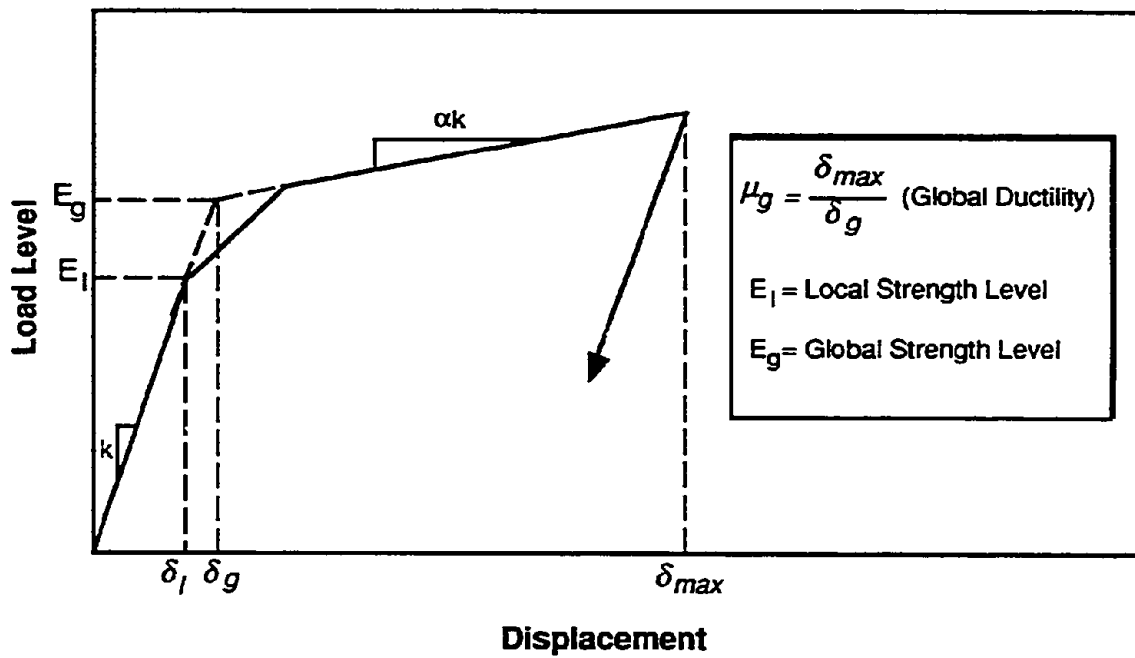


Fig. 2.4 Simplified Structure Model

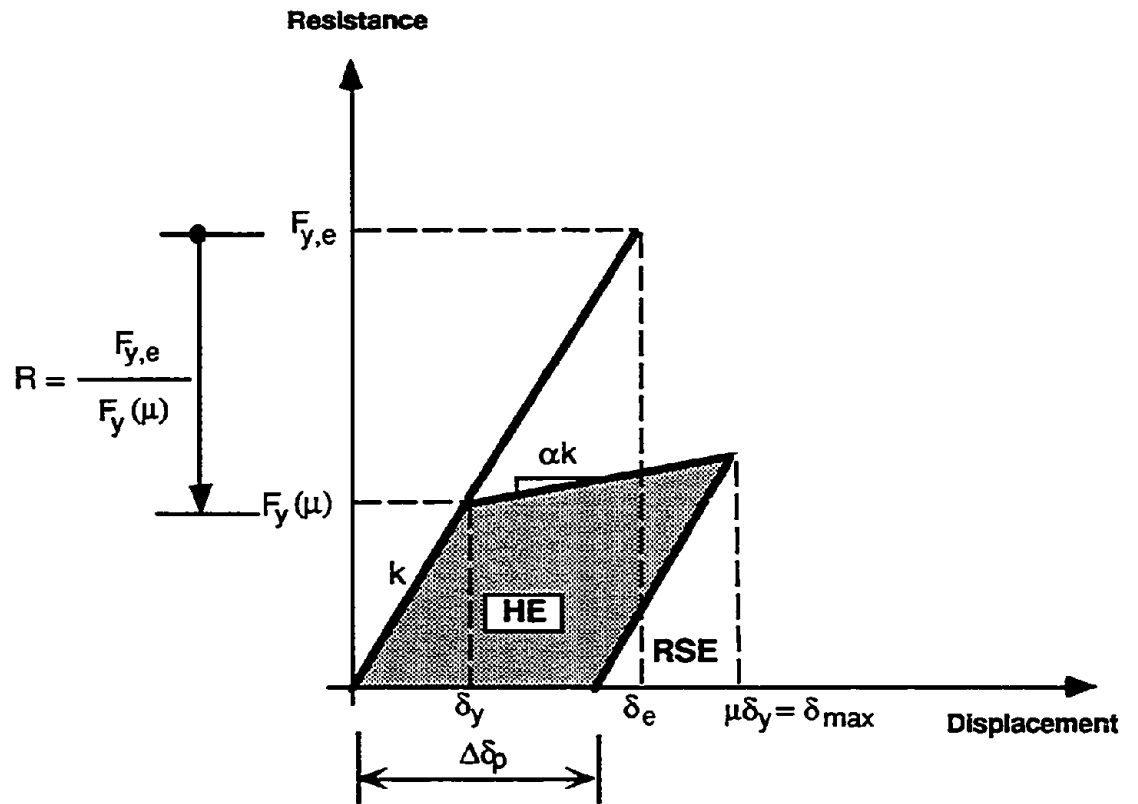
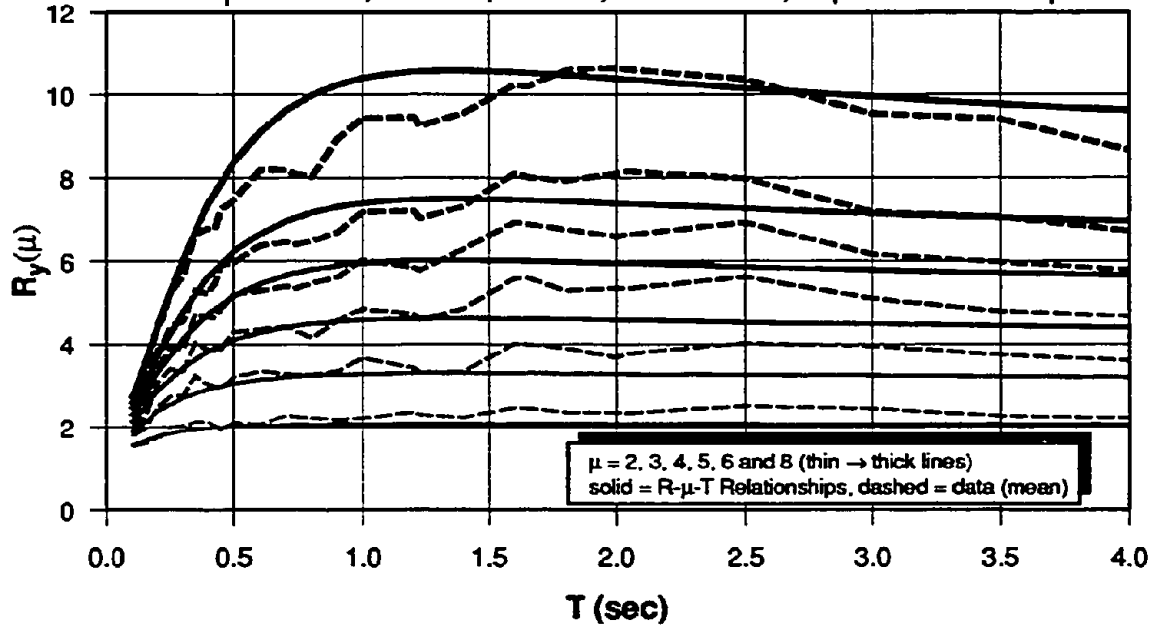


Fig. 2.5 Basic Seismic Demand Parameters

STRENGTH REDUCTION FACTORS, $R_y(\mu)$ -(15s.bi-05)

15-S₁ Records, Bilinear, $\alpha = 5\%$, Data Mean, R- μ -T Relationships



INELASTIC STRENGTH DEMAND SPECTRA USING R- μ -T RELATIONSHIPS - (15s.bi-5)

15-S₁ Records, Bilinear, $\alpha = 5\%$, , Based on R-Factor from 15-S₁

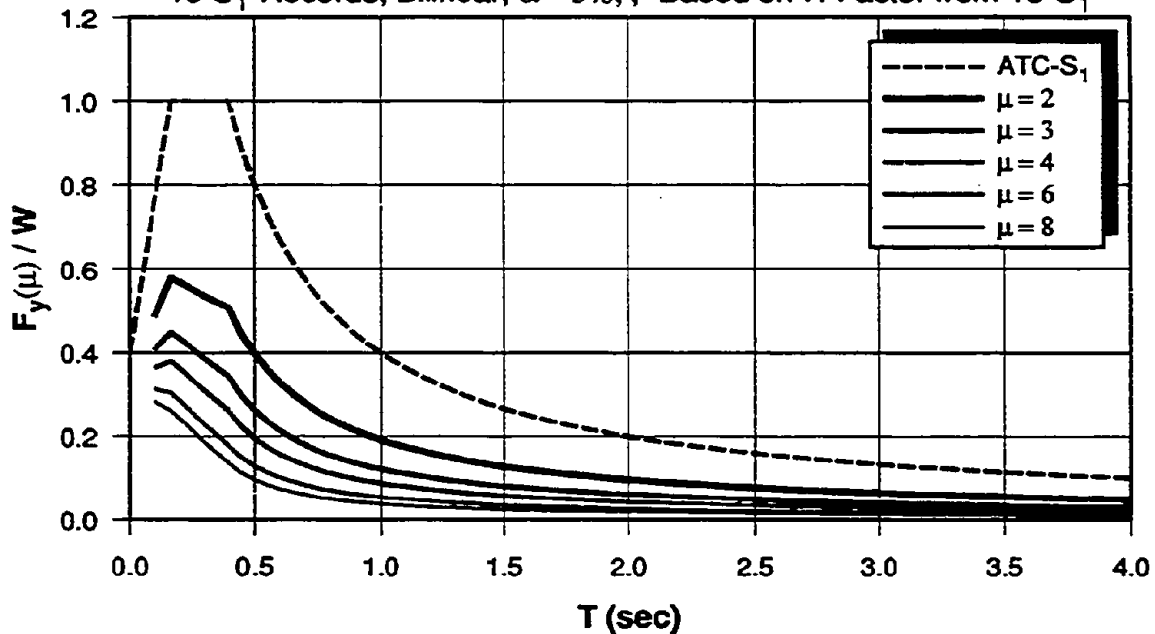
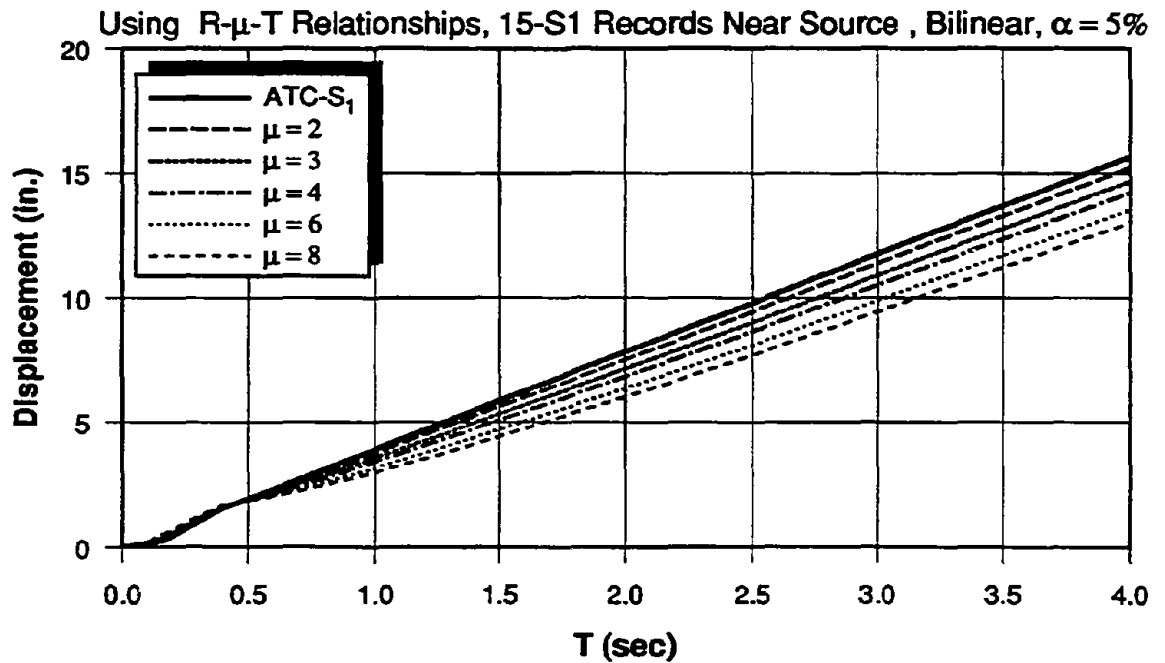


Fig. 2.6 R-factors and Inelastic Strength Demand Spectra for Soil Type S₁

DISPLACEMENT DEMAND SPECTRA



NORMALIZED DISPLACEMENT DEMAND SPECTRA

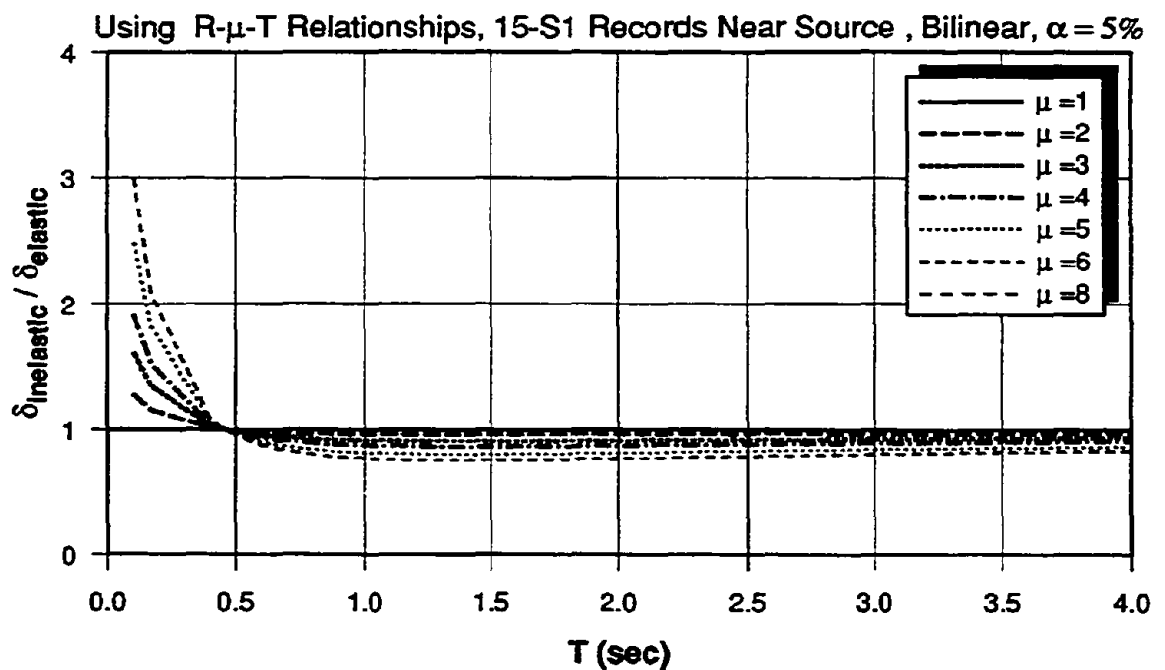


Fig. 2.7 Displacement Demands for Rock and Stiff Soil

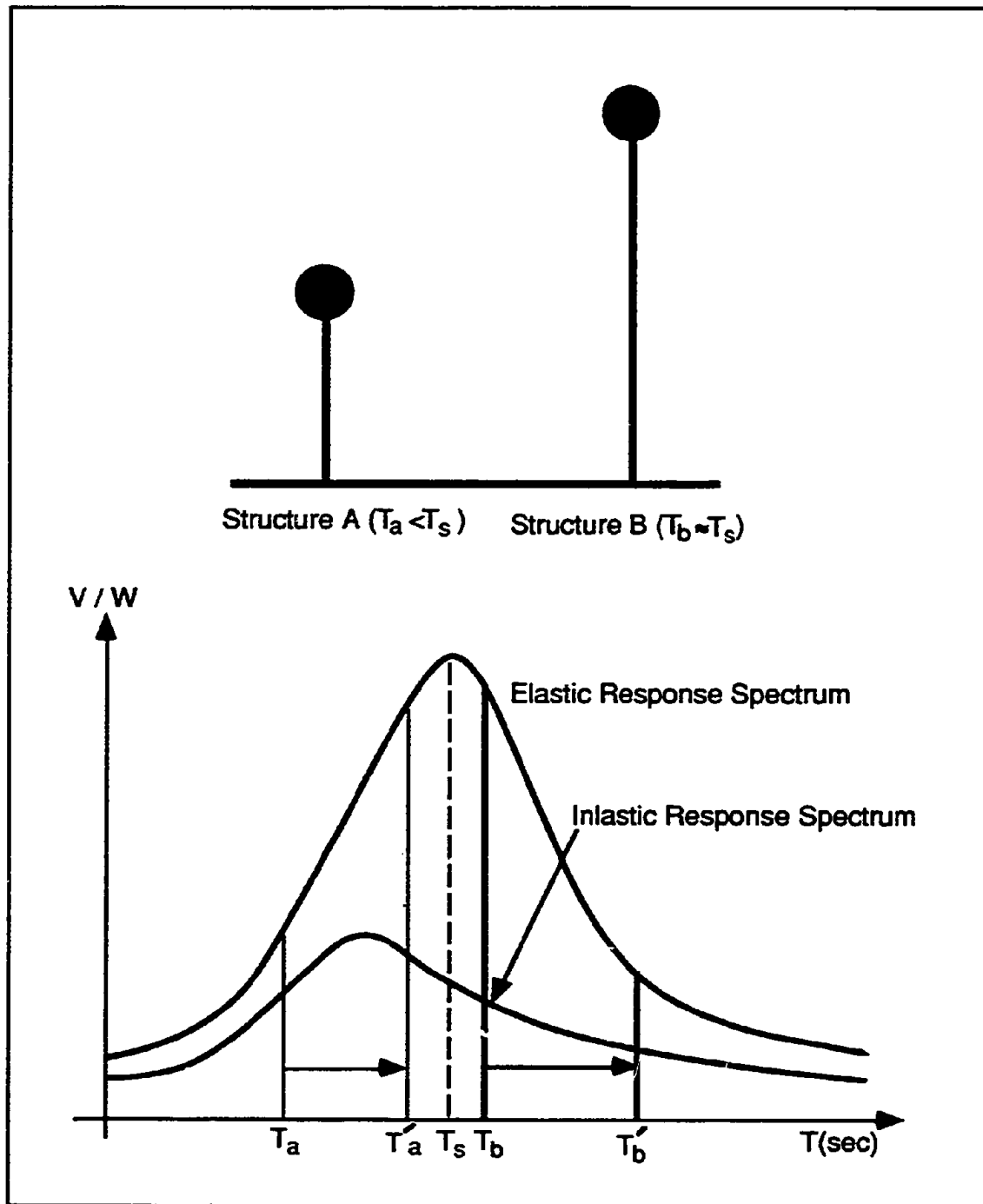


Fig. 2.8 Schematic Representation of the Variation of Strength Demand for Soft Soil Motions

CHAPTER 3

EFFECTS OF HYSTERESIS MODELS ON SDOF RESPONSE

3.1 Introduction

When structures are subjected to cyclic loading, the properties of structural elements, such as strength and stiffness, will deteriorate. Every excursion causes damage to the elements of structures, which brings them closer to a state of failure. The amount of damage sustained by structural elements depends upon the number of cycles, the amplitude of each cycle, and the material properties and detailing of elements. The rate of deterioration of the structural properties is related to the applied loading as well as the failure mode. For instance, for reinforced concrete elements the rate of deterioration of flexural strength is slower than that of shear strength.

Based on experimental results and analytical studies of different structural elements, many cumulative damage models have been developed. Response quantities such as maximum deformation, ductility ratio, cumulative inelastic deformation, number of excursions, and energy dissipation capacity are used to develop damage models. These models are used to identify the condition of the structure and the amount of damage sustained by elements of structures during cyclic loading. Most damage models, in one form or another, utilize the total hysteretic energy dissipation capacity as a damage indicator. This parameter is best suited to relate imposed seismic demands to available capacities. In this chapter we propose a model that accounts for the effects of deterioration of structural properties (strength, stiffness) on the seismic demands by using hysteretic energy to modify the structural properties after each excursion. In the following section, the classification of the hysteresis models is presented.

3.2 Classification of Hysteresis Models

The *SDOF* models used in this study are intended to represent global response characteristics of structures. As such, they should be capable of representing all important structural characteristics that may significantly affect the response to ground motions. In addition to basic elastic stiffness and yield strength, the following characteristics deserve consideration:

- Multilinear load-deformation response, representing either the propagation of cracking or the redistribution of internal forces after yielding of the weakest element. In the simplest case, such a model should be trilinear.
- Strain hardening or softening after formation of a mechanism.
- Degradation in stiffness.
- Deterioration in strength.
- Pinching of hysteresis loops caused by crack opening/closure in reinforced concrete structures and connection slip or post-buckling behavior in steel structures.

In order to incorporate these phenomena and study their effect on seismic demand parameters, a general hysteresis model was developed. The characteristics of this general model are shown in Fig. 3.1, and the types of specific hysteresis models that can be generated through rule modifications are summarized in Table 3.1. The specific hysteresis models that can be represented by the general model are of the following three types.

3.2.1 Nondeteriorating Models

These models are the basic bilinear and trilinear models, which have stable hysteresis loops with large energy dissipation capacity. One of the hysteresis models that has been used in this study to perform the parameter studies is the basic bilinear model.

This model, shown in Fig. 3.2 (a), is defined by the initial stiffness K_e , the hardening stiffness αK_e and the yield strength F_y .

3.2.2 Stiffness Degradation Models with Limited Memory

These models exhibit stiffness degradation which is based on memorizing only the largest positive and negative excursions of past loading cycles. The following two well known models are included in this category:

Peak Oriented Model or Modified Clough Model. In this well known model the reloading stiffness degrades to the extent that reloading is directed towards the previous maximum peak point in the direction of loading. This model was proposed by Clough and was an early attempt to account for pinching of hysteresis loops observed in experimental studies. From the many modification proposed for this model in the literature, the only one incorporated here is that proposed by Mahin and Bertero, 1975, since it improves the modeling of reloading following small excursions. This model has a bilinear skeleton curve which is defined by the yield strength F_y , the initial stiffness K_e and the hardening stiffness αK_e . The suggested modification for reloading is illustrated in Fig. 3.2 (b). After unloading, the reloading is directed toward either the previous unloading point (B) or the maximum displacement point (C), whichever provides a steeper slope.

Pinching Model. A more complex model for the representation of pinching is illustrated in Fig. 3.3. It is similar to the peak oriented model, with the major difference being that reloading consists of two steps. Initially, reloading is directed towards a point defined by the maximum displacement and a reduced target resistance F_p (points A, B, C, D in Fig. 3.3). This pinching stiffness defines the reloading path until the displacement attains a value equal to the permanent displacement of the largest previous excursion (points A', B', C', D'). Thereafter, the reloading path is directed towards the previous maximum peak point. Compared to the peak oriented model this model results in large pinching, with the amount of additional pinching determined by the difference between the pinching target resistance and the peak resistance of all previous excursions.

These two models have two important characteristics in common. First, the hysteresis loops are identical if several cycles of the same displacement amplitude are executed, therefore, no further stiffness degradation occurs in the additional cycles.

Secondly, if loading continues beyond the previous peak points, the loading path follows the originally defined skeleton curve and no strength deterioration occurs. Experimental evidence makes it necessary to refine these models further since history dependent stiffness degradation and deterioration may occur in elements and complete structures.

3.2.3 History Dependent Strength Deterioration and Stiffness Degradation Models

It is well established, from experimental work and analytical studies, that strength and stiffness properties of elements and structures deteriorate with time. Time implies here the complete load-displacement history experienced by the system. Materials, and therefore elements and structures, have a memory and the present state depends on the cumulative damage effect of all past states. In concept every excursion causes damage, and damage accumulates as the number of excursions increases. The damage caused by small (elastic) excursions is usually small and probably negligible in the context of seismic behavior. Thus, only inelastic excursions need to be considered, and from those the large ones cause significantly more damage than the smaller ones. Also, the cumulative damage may not lead to noticeable deterioration until several cycles have been executed. This is illustrated in Fig. 3.4(a), which shows the load-displacement response of a steel beam that failed by crack propagation at a weld. This failure mode exhibits a large deterioration threshold, but rapid deterioration is evident once unstable crack growth occurs, as is illustrated in Fig. 3.4(b). For other elements deterioration may be evident early in the loading history (small deterioration threshold) and may occur at a gradual rate. The response of such an element is shown in Fig. 3.5(a), and the mode of deterioration is illustrated in Fig. 3.5(b).

3.3 Hysteresis Rules for Strength Deterioration and Stiffness Degradation Models

The examples in the preceding paragraph show that it is necessary to model history dependent deterioration in a general hysteresis model that is supposed to capture all important phenomena that affect seismic response. Deterioration depends on a great many parameters, the simplest ones being the plastic deformation range $\Delta\delta_p$ (see Fig. 2.5) and the hysteretic energy dissipation in an excursion. The latter parameter is used here because hysteretic energy is a well defined quantity in all cases, whereas the plastic deformation range is an ambiguous quantity for stiffness degrading systems. It is assumed that the hysteretic energy dissipation capacity is a known quantity and that it is independent of the loading history. The latter assumption is hard to justify, but it has to

be made in order to make a parameter study manageable. The deterioration in excursion i is assumed to be defined by a deterioration parameter β_i , given by the following expression:

$$\beta_i = \left(\frac{E_i}{E_t - \sum_{j=1}^i E_j} \right)^c \quad (3.1)$$

where

- β_i = parameter defining the rate of deterioration in excursion i
- E_i = hysteretic energy dissipated in excursion i
- E_t = hysteretic energy dissipation capacity = $\gamma F_y \delta_y$
- $\sum E_j$ = hysteretic energy dissipated in all previous excursions
- c = exponent defining the rate of deterioration

This deterioration parameter is small at the beginning of loading, increases as more energy is dissipated through inelastic cycles, and approaches infinite as $\sum E_j$ approaches E_t . The latter state is associated with complete deterioration defined by zero strength or stiffness. The rate of deterioration can be controlled through the exponent c . A reasonable range for this exponent is between 1.0 and 2.0, as suggested for damage modeling of components of steel structures (Krawinkler et al., 1983). A value of 2.0 will slow down early deterioration and accelerate deterioration in later cycles, whereas a value of 1.0 implies an almost constant rate of deterioration. This is illustrated in the examples given in Figs. 3.9 and 3.10, which will be discussed later. The energy dissipation capacity E_t depends on the strength and ductility capacity of the system; we assume that it can be expressed as $\gamma F_y \delta_y$, where γ is a system dependent parameter and $F_y \delta_y$ is twice the elastic strain energy.

The parameter β can be utilized to incorporate various types of deterioration phenomena into the general hysteresis model. The following three phenomena are incorporated in this study.

3.3.1 Strength Deterioration

Deterioration in strength is modeled through a modification of the yield strength F_y and a corresponding translation of the strain hardening stiffness K_h . The modification of the yield strength is given by

$$F_i = (1 - \beta_i)F_{i-1} = \beta_s F_{i-1} \quad (3.2)$$

where

F_i = deteriorated yield strength after excursion i

F_{i-1} = deteriorated yield strength before excursion i

$\beta_s = (1 - \beta_i) > 0$, with the value of β_i given by Eq. 3.1, using the appropriate parameters to model strength deterioration.

The initial value for F_{i-1} is F_y , and the modification is applied after each inelastic excursion. The parameter β determined from Eq. (3.1) cannot exceed 1.0 in this case, or β_s would become negative. An inspection of Eq. (3.1) shows that a value of $\beta > 1.0$ will be obtained only when the system strength approaches zero.

Figure 3.6(a) shows the hysteresis rules for a bilinear model with strength deterioration. The parameter β which is updated after each unloading, is used to define the next target yield strength. Figure 3.7(a) illustrated the modified Clough model with strength deterioration. Specific rules for the modification of strength in Clough's model are presented in Fig. 3.8(a).

Two examples of the effect of applying this deterioration model to a bilinear hysteresis model are shown in Figs. 3.9 and 3.10. In both cases the displacement history is the same, consisting of constant amplitude cycles with an amplitude of $4\delta_y$. The value E_t is assumed to be $100F_y\delta_y$ (i.e., $\gamma = 100$), and the exponent c is taken as 1.0 in Fig. 3.9 and 2.0 in Fig. 3.10, respectively. As can be seen, the rate of deterioration is very different in the two cases because of this difference in c .

3.3.2 Degradation of Unloading Stiffness

Degradation in the unloading stiffness K_u is modeled in the same manner as strength deterioration. The modification of the unloading stiffness is given by

$$K_{u,i} = (1 - \beta_i)K_{u,i-1} = \beta_u K_{u,i-1} \quad (3.3)$$

where

$K_{u,i}$ = degraded unloading stiffness in excursion i

$K_{u,i-1}$ = degraded unloading stiffness before excursion i

β_u = $(1 - \beta_i) > 0$, with the value of β_i given by Eq. 3.1, using the appropriate parameters to model stiffness degradation.

The initial value for $K_{u,i-1}$ is the elastic stiffness, K_e , and the unloading stiffness is modified during each excursion. Fig. 3.6(b) shows the rules for bilinear systems with unloading stiffness degradation. All comments made for strength deterioration apply here as well. Two examples illustrating degradation of unloading stiffness are shown in Fig. 3.11.

3.3.3 Accelerated Degradation of Loading Stiffness

Basic degradation of the loading stiffness is modeled by the previously described peak oriented or Clough model. This model does not account for stiffness degradation caused by cumulative loading effects. This additional effect can be superimposed on the peak oriented model by modifying the target displacement, δ_i , to which the loading stiffness is directed. This target displacement, which in the basic model is the maximum displacement of past cycles, δ_{max} , (unless the modification discussed in Mahin and Bertero 1975, applies) can be modified in a manner very similar to that proposed for strength deterioration. The objective is to increase this target displacement in a manner so that the reloading stiffness degrades in a cumulative manner expressed by the deterioration parameter β . The following model is used to modify the target displacement:

$$\delta_{t,i} = (1 + \beta_i)\delta_{t,i-1} = \beta_k \delta_{t,i-1} \quad (3.4)$$

where

$\delta_{t,i}$ = target displacement in excursion i

$\delta_{t,i-1}$ = target displacement before excursion i

β_k = $(1 + \beta_i)$, with the value of β_i given by Eq. (3.1), using the appropriate parameters to model accelerated degradation of the loading stiffness.

The initial value for $\delta_{t,i-1}$ is δ_y , and the modification is applied after each inelastic excursion. When $\sum E_j$ approaches E_t , the target displacement approaches infinity which causes a complete loss of stiffness. Figures 3.7b and 3.8b illustrate the rules used in the modified Clough model for considering the cumulative effects of cyclic loading on the degradation of reloading stiffness. The reloading stiffness will decrease at an accelerated rate as the number of excursions increases.

The hysteresis response for constant amplitude cycling of a peak oriented model with accelerated stiffness degradation is shown in Fig. 3.12(a), using $E_t = 100F_y\delta_y$ (i.e., $\gamma = 100$) and $c = 1.0$. When this response is compared to that of the peak oriented model with strength deterioration (see Fig. 3.12(b)) the deterioration patterns appear to be similar. However, this comparison is misleading as no strength deterioration is associated with the model shown in Fig. 3.12(a). If for any of the repeated cycles the loading would be continued beyond the displacement of $4\delta_y$, the reloading stiffness would be maintained until the original skeleton curve is reached, whereas in the strength deterioration model, shown in Fig. 3.12(b), the stiffness would change to the strain hardening stiffness at a displacement of $4\delta_y$. The differences between the two models are evident in the two histories shown in Fig. 3.13, which consist of 4 cycles with amplitude $4\delta_y$, followed by 4 cycles with amplitude $8\delta_y$.

3.4 Nonlinear Dynamic Analysis of SDOF Systems

3.4.1 Method of Analysis

A computer program *NLDYNA* (Nonlinear Dynamic Analysis) has been developed to analyze the nonlinear response of single-degree-of-freedom (*SDOF*) systems subjected to ground motions. In order to investigate the effects of hysteresis models on the seismic demand parameters, several of the models discussed in the previous section are incorporated into the program. These models include the basic bilinear model, bilinear models with strength deterioration and unloading stiffness degradation, modified Clough model.

The equation of motion for an elastic *SDOF* system subjected to an acceleration time history may be written as:

$$m\ddot{v}(t) + c\dot{v}(t) + kv(t) = -m\ddot{v}_g(t) \quad (3.5)$$

where v and \dot{v} are the relative displacement and velocity of the mass with respect to the ground, k , m and c are the stiffness, mass, and damping coefficient of the system, and $\ddot{v}_g(t)$ is the ground acceleration. This equation may also be written as:

$$\ddot{v}(t) + 2\omega\xi\dot{v}(t) + \omega^2v(t) = -\ddot{v}_g(t) \quad (3.6)$$

where ξ is the damping ratio and ω is the natural frequency of the system. For inelastic analysis of *SDOF* systems it is convenient to rewrite equation 3-6 in the following dimensionless form (Mahin and Lin 1983):

$$\ddot{\mu}(t) + 2\omega\xi\dot{\mu}(t) + \omega^2\rho(t) = -\frac{\omega^2}{\eta} \frac{\ddot{v}_g(t)}{\ddot{v}_{g,\max}} \quad (3.7)$$

where

$$\rho(t) = \frac{F(t)}{F_y} \quad (3.8)$$

$$\eta = \frac{F_y}{m\ddot{v}_{g,\max}} = \frac{CW}{m\ddot{v}_{g,\max}} \quad (3.9)$$

In equation (3.7) $\mu(t)$ is the displacement ductility ratio, the quantity $\rho(t)$ is the normalized restoring force, and the nondimensional parameter η relates the system yield strength to the peak ground acceleration. The parameter η is used to vary the system yield strength in the analysis. The yield strength F_y can be expressed in terms of the seismic coefficient C and the weight of the system W . A more detailed discussion of the derivation of the above equations is presented in S. Mahin and J. Lin (1983).

NLDYNA uses the linear acceleration method to solve the equation of motion. A variable time step scheme is implemented in the program. The time step specified by the user is compared with the digitization interval of the record and the smaller value is taken as the initial time step. When the load path changes direction the time step is reduced to a smaller value in order to minimize the error caused by overshooting. Figure 3.14 illustrates the procedure that is adopted for loading and unloading cases. When a target value is overshoot by an amount greater than a specified tolerance, the time step is subdivided. The number of subdivisions is the integer closest to the ratio of the incremental displacement to the difference between the displacement at the previous step and the target displacement. Thus, the subdivision of the time step is related to the amount of overshooting, thereby increasing the efficiency of the solution scheme. The program will back up to the previous step, continue the analysis with the smaller time step, and repeat this procedure until the incremental displacement is in the range of specified tolerance. Once this is achieved the original time step will be used again for integration along the new load path.

NLDYNA performs iterations on the yield level in order to find the yield level corresponding to a specified target ductility ratio. There are two problems that may be encountered; both of them are illustrated in Fig. 3.18. First, the relationship between the yield level and ductility demand is not necessarily a monotonic function, and there are cases in which several yield levels correspond to a specific target ductility. In such a case the program will select the highest yield level for the target ductility μ . Secondly, the ductility demand may become very sensitive to small changes in the yield strength, particularly for systems with negative "strain hardening". This may require a great number of iterations or larger tolerances as is discussed further in Section 3.5.

3.4.2 Response Parameters

The program *NLDYNA* computes a comprehensive set of response parameters that can be used to evaluate the behavior of the *SDOF* system subjected to earthquake ground motion. These parameters include maximum displacement, velocity and acceleration response, displacement ductility, cyclic ductility, normalized hysteretic energy, number of excursions, number of zero crossings, and different kinds of energy. Some of these parameters are discussed in Section 2.3.1; the energy expressions that are incorporated into the program are summarized here.

During an earthquake part of the energy imparted to a structure is dissipated by viscous damping and inelastic deformations, and the rest is temporarily stored in the structure in the form of kinetic and elastic strain energy. As is pointed out by Uang and Bertero (1988), the input energy can be expressed in terms of absolute or relative energy depending upon the type of velocity (absolute or relative) that is used to define the kinetic energy. For a constant displacement ductility, Uang and Bertero have shown that the relative and absolute energies are very similar for systems with periods of practical interest (0.30 to 5.0 sec.). In this study the absolute input energy is used.

The integration of the equation of motion with respect to the displacement v leads to the following expression:

$$\int m\ddot{v}_t dv + \int c\dot{v}dv + \int f_s dv = 0 \quad (3.10)$$

where m is the mass of system, c is the viscous damping, v_t is total displacement, v and \dot{v} are the relative displacement and velocity, respectively, and f_s is the restoring force. The above equation can also be written in the following form:

$$m \int_0^t \ddot{v}_t dt + c \int_0^t \dot{v}^2 dt + \int_0^t f_s \dot{v} dt = m \int_0^t \ddot{v}_g \dot{v} dt \quad (3-11)$$

This equation represents an energy equilibrium equation. The first term on the left hand side represents the kinetic energy (*KE*), the second term represents the energy dissipated by viscous damping (*DE*), and the third term represent the sum of the

hysteretic energy and the strain energy ($HE+RSE$). Therefore, at any instance of time the total input energy can be written in the form of

$$IE = KE + DE + HE + RSE \quad (3.12)$$

At every time step the program *NLDYNA* computes all the energies term and checks energy balance. As was discussed previously, the computed hysteretic energy HE is used to modify the yield strength and/or stiffness whenever deteriorating hysteresis models are employed.

3.4.3 A Damage Indicator for Deteriorating Hysteresis Models

For deteriorating structures, maximum deformation or ductility alone does not satisfactorily define the state of damage and other parameters, such as cumulative inelastic deformations or cumulative energy dissipation, need to be considered to model damage. A review of widely used cumulative damage models is presented by Y.S. Chung et. al. (1987). For the deterioration models used in this study a simple damage indicator, which is based on the deterioration parameter β , can be derived.

This damage indicator is a measure of deterioration, which reaches a value of 1.0 when strength or stiffness has deteriorated to zero. For instance, the damage indicator for strength deterioration can be written as

$$D = \frac{F_y - F_i}{F_y} = 1 - \frac{F_i}{F_y} \quad (3.13)$$

where D is the damage indicator due to strength deterioration, F_y is the initial yield strength and F_i is the deteriorated yield strength after the i^{th} excursion. The deteriorated strength F_i can be evaluated by using the deterioration parameter β from equation (3.1) and substituting its value into equation (3.2), i.e.,

$$F_i = (1 - \beta_i)F_{i-1} \quad (3.14)$$

where

F_i = deteriorated strength after the i^{th} excursion

F_{i-1} = strength before the i^{th} excursion
 β_i = deterioration parameter for excursion i

By substituting for F_{i-1} , equation 3.14 becomes

$$F_i = (1 - \beta_i)(1 - \beta_{i-1})F_{i-2} \quad (3.15)$$

Repeated substitution for the deteriorated strength in all previous cycles will yield the following expression for the deteriorated strength after i excursions:

$$F_i = F_y \prod_{j=1}^i (1 - \beta_j) \quad (3.16)$$

Substituting the above equation into equation (3.13) provides the following expression for the damage indicator D :

$$D = 1 - \prod_{j=1}^i (1 - \beta_j) \quad (3.17)$$

The same expression can be employed for stiffness degradation if the damage indicator is defined as

$$D = \frac{K_e - K_i}{K_e} = 1 - \frac{K_i}{K_e} \quad (3.19)$$

where D is the damage indicator for stiffness degradation, K_e is the initial elastic stiffness, and K_i is the stiffness of the system after the i^{th} excursion.

The effect of cyclic loading on the strength deterioration is illustrated in the following example, using a *SDOF* system with the period of 0.5 second and the *EW* component of the El-Centro 1940 record as input ground motion. The basic bilinear and bilinear with strength deterioration hysteresis models with 5% strain hardening are used to represent the restoring force characteristics of the system. The yield strength for both cases is chosen such that the ductility demand for the basic bilinear system is limited to 4.0. In the bilinear model with strength deterioration, the hysteretic energy capacity (E_T) is assumed to be $40F_y\delta_y$ (i.e., $\gamma = 40$). This hysteretic energy capacity is very close to the total hysteretic energy dissipated by the system using the basic bilinear model. The

exponent c , which identifies the rate of deterioration, is assumed to be 1.0. The hysteresis response of this system, using both the basic bilinear and bilinear with strength deterioration models, is presented in Fig. 3.15. The ductility ratio of the system with strength deterioration is 6.02, compared to a ductility of 4.0 for the basic bilinear model. This indicates that the required strength of the deteriorating system would have to be significantly higher in order to limit the ductility ratio to 4.0. The displacement time histories for both models are presented in Fig. 3.16(a). The histories are similar only for the first 3 seconds, thereafter the displacement of the deterioration model increases significantly compared to the basic bilinear model.

For the system with strength deterioration, Fig. 3.16(b) shows the increase in the damage indicator D with the number of inelastic excursions. The rate of deterioration is controlled by the exponent c . A value of 1.0 causes early deterioration and slow-down of deterioration in later cycles as compared to c equal to 1.5.

3.4.4 Parametric Study of Seismic Demands for SDOF Systems

The objective of the study reported in this chapter is to provide basic information on seismic demand parameters, and to investigate the effects of hysteresis model, negative strain "hardening" (P-delta), and deterioration of structural properties on the seismic response of structures during an earthquake.

In order to perform a statistical evaluation of seismic demands for *SDOF* systems with different kinds of hysteresis models, the 15 rock and stiff soil records used by Nassar and Krawinkler (1991) are utilized for the nonlinear dynamic analysis. Pertinent information on the characteristics of these records are presented in Table 3.2. The frequency characteristics of these records are different but in average their response spectra reasonably match the shape given in the ATC-3 document for soil type S_1 . The records are from Western US earthquakes ranging in magnitude from 5.7 to 7.7. The strong motion durations D_{sm} listed in Table 3.2 are based on the definition given by McCann and Shah (1979). They define the end of strong motion as the point in time when the time derivative of the cumulative root mean square function is positive for the last time. The beginning of the strong motion is obtained similarly by applying the same procedure to the reversed time history of the record. The unscaled *PGA* and *PGV* values are listed in Table 3.2 together with the values obtained by scaling the *PGA* to 0.40 g.

From here on these records are referred to as the *15-S_j* record set. Further details about these records can be found in Nassar and Krawinkler (1991) and Hadidi-Tamjed (1988).

In this study the seismic demands are evaluated for systems whose yield levels are adjusted for each record to correspond to target ductility demands of $\mu = 1$ (elastic response), 2, 3, 4, 5, 6 and 8. The yield levels are, therefore, the strength demands $F_{y,e}$ and $F_y(\mu)$ for μ equal to 2, 3, 4, 5, 6 and 8. Thus, all information pertains to systems that may have different yield levels but equal ductility demands for the 15 ground motions. In the context of the proposed design approach this is the relevant information, as the available ductility capacity is the basis for design and the required strength is a quantity derived from the criterion that the ductility demand should not exceed the available ductility capacity.

Parametric studies for the basic bilinear model (Fig. 3.2(a)) and modified Clough model (Fig. 3.2(b)) were completed by Nassar and Krawinkler (1991). They assumed strain hardening ratios of 0, 2, and 10%. A conclusion of their study is that it makes little difference in strength demands whether the hysteretic behavior of a *SDOF* system resembles that of a bilinear system or that of a system with stiffness degradation of the type represented by a peak oriented model, provided that the systems have positive strain hardening. In the following two sections the effects of negative strain "hardening" (which may be caused by P-delta effects) and of strength deterioration on seismic demand parameters will be investigated. As will be shown, both negative "hardening" and strength deterioration may have a significant effect on seismic demands.

3.5 Effects of Negative Strain "Hardening" (P-Delta) on Seismic Demand Parameters

Lateral displacements lead to a decrease in stiffness and effective strength because of second order effects caused by gravity loads (P-delta effects). When a mechanism forms in a structure these second order effects may lead to a negative stiffness, which causes an increase in lateral displacement that ultimately may lead to incremental collapse. Thus, when a negative mechanism stiffness exists (negative strain "hardening"), the strength of the structure needs to be increased compared to a structure with positive hardening in order to limit lateral deflections to an acceptable level. This section summarizes a study on the effects of gravity loads on the dynamic response of *SDOF* systems and provides quantitative information on the increase in strength required to limit

the ductility ratio of *SDOF* systems to a prescribed value. This increase in strength demand is reflected in a decrease in the strength reduction factor R defined in Section 2.3.1.

For an *SDOF* system the effect of gravity loads can be incorporated into the equation of motion as follows:

$$m\ddot{v}(t) + c\dot{v}(t) + f(t) - \frac{mg}{h}v(t) = -m\ddot{v}_g(t) \quad (3.20)$$

where mg is the weight, h is the height of the structure and $f(t)$ is the lateral restoring force. This equation shows that the gravity load tends to reduce the lateral stiffness of the structure. Figure 3.17(a) illustrates how the dimensionless parameter $\theta = \frac{mg}{kh}$ can be used to represent this decrease in stiffness and strength. The elastic stiffness k is modified to $(1-\theta)k$, and the strain hardening stiffness $\alpha'k$ is modified to $(\alpha'-\theta)k$. In this formulation α' is the strain hardening ratio of the system without P-delta effect, and $\alpha'-\theta$ is the strain hardening ratio with P-delta effect. From here on the quantity $\alpha'-\theta$ will be denoted as α , the effective strain hardening ratio. If the effect of P-delta on the elastic stiffness is neglected, the *SDOF* system with P-delta effects takes on the form shown in Fig. 3.17(b).

This study focuses on the effect of the strain hardening ratio α on the seismic strength demand, with an emphasis on negative values of α (strain softening), which may be the consequence of P-delta effects. In the parameter study summarized here the objective is to evaluate the effect of α on the strength demand for prescribed target ductility ratios. As Fig. 3.17(b) shows, an increase in strength demand for a prescribed ductility ratio implies also a proportional increase in displacement demand. One needs to be aware of this observation when the results of this study are being interpreted.

Furthermore, it needs to be pointed out that most of the results presented here are mean values obtained from records with different strong motion durations. Interpretation of results must be done with caution since it is clear that strong motion duration affects the strength demands for systems with negative stiffness. This issue is addressed in Section 3.5.3.

For the purpose of assessing the effects of strain hardening/softening on seismic demand parameters, time history analyses are performed on the following 71,820 permutations:

- For 38 discrete periods ranging from $T = 0.10$ to 4.0 seconds
- For nine strain hardening ratios $\alpha = +10, +5, +2, 0, -2, -5, -10, -15,$ and -20%
- For target ductility ratios $\mu = 1$ (elastic), 2, 3, 4, 5, 6, and 8
- For two hysteresis models (basic bilinear and modified Clough models)
- For the 15- S_I ground motions (Table 3.2).

In all analyses 5% viscous damping is assumed. Statistical averaging is performed on the results to evaluate patterns and variations of the aforementioned seismic demand parameters. Only mean values are reported in this section.

3.5.1 Observations from Time History Analyses

For *SDOF* systems with negative strain hardening the determination of the required strength for a specified target ductility ratio involves more iterations compared to a system with zero or positive strain hardening. At lower strength levels the ductility demands are very sensitive to small changes in the strength of the system, which requires the use of a larger tolerance to converge to solutions. In this study the tolerance is assumed to be 1% of the target ductility ratio. Figure 3.18 shows typical relationships between strength capacities assumed in the analysis and computed ductility demands, using a basic bilinear system with a period of 0.5 seconds and -5% strain hardening. Both Figs. 3.18(a) and (b) show that around a strength of 0.1W the ductility demand increases rapidly, which indicates that the system is close to incremental collapse. Figure 3.18(a) shows a monotonic relationship between $F_y(\mu)$ and μ , whereas Fig. 3.18(b) shows a special case in which the ductility ratio does not increase monotonically as the yield level decreases. As can be seen, for a ductility of 4.0 there are three distinct yield levels. The largest of these three levels is the strength demand corresponding to a target ductility ratio of 4.0.

In order to illustrate the effects of different hysteresis models on the response of a system with negative "hardening" stiffness (*P-delta*), results obtained with the bilinear and modified Clough models for *SDOF* systems with 5% negative strain hardening and periods of 0.20 and 1.0 seconds are shown in Figs. 3.19 and 3.20. These systems are

subjected to the 1952 Taft earthquake (*N21E*). The yield level of the system with a period of 0.2 sec. is defined by $\eta = 1.0$, and the yield level of the system with a period of 1.0 sec. is adjusted to a value that gives a ductility ratio of 3 for this ground motion.

Figure 3.19 shows the load-displacement diagrams for the bilinear and degrading models with a period of 0.2 seconds. The bilinear model reaches incremental collapse at a displacement that is about four times as large as the maximum displacement of the stiffness degrading model. However, the amount of hysteretic energy dissipated by the bilinear model is much smaller than that dissipated by the stiffness degrading model. The displacement time histories of both models are presented in Fig. 3.21(a). As can be seen, the displacement time history of the bilinear model drifts strongly to one direction whereas the response history of the stiffness degrading model is almost symmetric. Thus, for this case the behavior of the stiffness degrading model is far superior to that of the bilinear model.

Figure 3.20 shows the load-displacement diagrams for the bilinear and degrading models with a period of 1.0 second. In this case the bilinear model has a stable hysteresis response and the number of inelastic excursions is small compared to the system with a period of 0.2 seconds. The displacement time histories for both models, which are presented in Fig. 3.21(b), are similar and the maximum displacement of the bilinear model is only slightly larger than that of the degrading model.

These examples were presented to illustrate that the response of systems with negative strain "hardening" is very sensitive to the type of hysteresis model, the period of the structural system, and the frequency content of the ground motion. In general, however, the response of stiffness degrading models is far superior to that of bilinear models if P-delta effects lead to a negative "hardening" stiffness. This conclusion is supported in the next section, which presents mean value data on strength demands represented by strength reduction factors.

3.5.2 Effects of Strain Hardening/Softening on the Strength Reduction Factor R

The strength reduction factor R , or more specifically $R_y(\mu)$, defines the reduction in the elastic strength demand that will result in a ductility demand of μ . This factor can be thought of as an effectiveness factor; the larger the R-factor, the smaller the inelastic strength demand. The following discussion is based on the statistical evaluation of data

obtained from time history analyses with bilinear and degrading models, using strain hardening ratios that vary from +10% to -20%. The dependence of the results on the earthquake severity is eliminated by using R -factors, which represent the ratios of elastic to inelastic strength demands.

Figures 3.22 and 3.23 illustrate the large effects of strain hardening on the strength reduction factor for specific cases, i.e., bilinear and stiffness degrading (Clough model) $SDOF$ systems with periods of 0.5 and 1.0 seconds. The graphs shown here are obtained from mean values for the $15-S_1$ record set. The presented results lead to the following conclusions, which hold true also for systems of different periods.

- The R -factor decreases consistently with a decrease in strain hardening (or increase in strain softening). For positive strain hardening the bilinear and stiffness degrading models give similar results, but the results differ greatly for negative strain hardening.
- For bilinear models the R -factor decreases rapidly for small negative hardening ratios and levels off to a small - almost ductility independent - value for larger negative hardening ratios. Thus, for larger negative hardening ratios the relationship between strength and ductility becomes unstable, which indicates that the system is close to incremental collapse. As was shown in Fig. 3.19(a), the displacement response of bilinear systems drifts to one side and in many cases stability cannot be maintained. The conclusion is that large negative strain hardening ratios (e.g., $\alpha = -0.15$ for $T = 0.5$ sec.) must be avoided unless a structure is designed with sufficient strength to respond almost elastically to the design ground motion.
- For stiffness degrading models negative hardening is much less critical than for bilinear models. The R -factors do decrease, but at a much smaller rate than for bilinear systems. As Fig. 3.19(b) shows, the drifting of stiffness degrading models is much smaller, if at all present. The conclusion is that stiffness degrading systems of the type represented by the modified Clough model behave better than bilinear systems if large P-delta effects are present.

- The sensitivity of the R -factor to strain hardening increases with the ductility ratio. For a ductility ratio of 2 the dependence of R on α is small, whereas it becomes predominant for large ductility ratios.

Comprehensive data on the effects of strain hardening on the strength reduction factors for bilinear systems are presented in Figs. 3.24 to 3.29. Figures 3.24 and 3.25 show mean values of ductility dependent strength reduction factors for systems with strain hardening $\alpha = +10, 0, -10, \text{ and } -20\%$, respectively. Figures 3.26 and 3.27 present the variation of strength reduction factors with strain hardening for systems with a ductility of 2, 4, 6, and 8, respectively. Figures 3.28 and 3.29 show the same results, but normalized with respect to the R -factor of systems with zero strain hardening (elastic-plastic).

These figures confirm the conclusions drawn from Figs. 3.22 and 3.23, and provide data that can be used to assess the importance of P-delta effects and to account for P-delta effects in design. As can be seen from Figs. 3.28 and 3.29, a relatively small negative stiffness may necessitate a very large increase in strength in order to limit the ductility ratio to a prescribed target value. Let us assume that a structural system with a fundamental period between 0.2 and 1.5 seconds develops a mechanism that causes fully plastic behavior (no strain hardening, $\alpha' = 0.0$) without considering P-delta effects. If the P-delta effect causes a 10% reduction in elastic stiffness, which is not unusual for many structures, then $\alpha = \alpha' - \theta$ becomes -0.1 and the strength of the structure would have to be increased by a factor of approximately $1/0.7 = 1.4$ if the ductility ratio is to be limited to a value of 4 (see Fig. 3.28(b)). For larger target ductilities or negative strain hardening ratios the required strength may be easily twice the strength of an elastic-plastic system. These quantitative conclusions are based on the data presented in Figs. 3.28 and 3.29, and using the relationship

$$F_y^\alpha(\mu) = F_y^0(\mu) \frac{R_y^0(\mu)}{R_y^\alpha(\mu)} \quad (3.21)$$

It should be noted that some of the data shown here are outside the practical range of interest. For instance, for a system with $\mu = 6$ and $\alpha = -0.2$ the strength at maximum displacement is zero, an undesirable condition, indeed, since it is associated with dynamic P-delta instability.

Results similar to those shown in Figs. 3.24 to 3.27 are presented for stiffness degrading systems (modified Clough model) in Figs. 3.30 to 3.33. The behavior patterns are similar for both types of models, but the effect of negative hardening on R -factors is much smaller for stiffness degrading systems than for bilinear systems. The quantitative differences in the behavior of the two types of models are best represented by the ratios of reduction factors for degrading and bilinear systems, which are shown in Figs. 3.34 and 3.35 for strain hardening of 0, -5, -10, -20 percent and different ductility ratios. For systems with zero (or positive) strain hardening these ratios are close to 1.0 for all ductilities and periods, as is shown in Fig. 3.34(a) and was reported already by Nassar and Krawinker (1991). However, these ratios may become significantly larger than 1.0 when negative hardening is present, particularly if the periods are short and the ductility demands are high. The better performance of the stiffness degrading model can be explained by the fact that this model spends most of its time in "inner" loops in which the loading stiffness is always positive, rather than on the skeleton curve where the negative stiffness leads to drifting of the displacement response (see Fig. 3.19).

The results of this study have shown that for systems with negative strain hardening the R -factor, and therefore the inelastic strength demand, is strongly dependent on the strain hardening ratio, ductility ratio, and the period of the system. So called "secondary" effects due to P -delta may become primary effects and may lead to large increases in displacements and possibly to incremental collapse unless this problem is addressed explicitly in design. Most codes take into account the P -delta effect by using the results from a static elastic analysis. The P -delta effect is often evaluated by comparing the P -delta shear ($P\delta/h$) with the primary story shear. If the ratio of $(P\delta/h)/V$ is less than 0.1, P -delta effects are usually ignored, otherwise they are included through a simple elastic force and displacement magnification factor. This procedure ignores the effects of ductility and structure period in the assessment of P -delta effects, which in this study were found to be critical.

3.5.3 Effects of Strong Motion Duration on Seismic Demands for Systems with Negative Strain Hardening

In $SDOF$ systems that can be represented by a bilinear model, negative hardening will lead to drifting of the displacement response. Depending on the frequency content of the ground motion, the duration of motion may have great or negligible effect on this drifting and, therefore, on the inelastic strength demand. Attempts were made in this

study to correlate strong motion duration (using various definitions) with seismic demand parameters, but little success was achieved. The general conclusion is that there is no clear pattern between strong motion duration - as it is presently defined - and inelastic seismic demand parameters. In future research on the effect of duration on demand parameters explicit consideration will have to be given to the frequency content of the ground motion and the period and extent of nonlinearity (ductility) of the structural system.

For bilinear systems with negative hardening the dependence of demand parameters on strong motion duration, D_{sm} , can be judged from Figs. 3.36 to 3.40. The 15-S₇ record set is used to assess strong motion duration effects. Figure 3.36 illustrates the effect of strong motion duration on the strength demands for *SDOF* systems with periods of 0.50 and 1.0 second and a ductility ratio of 4, using bilinear models with 5, 10, and 20% negative strain hardening. The strength demands are normalized to the strength demand of the same system with zero strain hardening. The increase in strength demand with an increase in negative hardening is very consistent, but the increase with duration is not. There is a discernible pattern of increase in strength demand with duration, but the exceptions are too large to draw any general conclusions.

Figure 3.37 shows the effect of strong motion duration on the normalized hysteretic energy (*NHE*) for the same *SDOF* systems. The figure shows that *NHE* increases, in general, with D_{sm} provided the system has little or no negative strain hardening. For larger negative hardening the dependence decreases or disappears. There is, however, a clear pattern of decrease in *NHE* with an increase in negative hardening. Both observations can be explained with the same argument, which is illustrated in Figs. 3.38 and 3.39. With increasing negative hardening the response of a bilinear system is driven more and more by non-reversing excursions that lead to cumulative drifting of the displacement response. Consequently, the total hysteretic energy dissipation will not be much larger than the area under the monotonic force-displacement curve. This can be observed in the force-displacement response shown in Fig. 3.38(b), which is obtained from a bilinear system with a period of 0.5 sec. and $\alpha = -5\%$ subjected to the Castaic record ($D_{sm} = 15.1$ sec. in Fig. 3.37(a)). On the other hand, systems with positive or zero strain hardening will respond more in a symmetric displacement mode and hysteretic energy will be dissipated in many excursions, leading to large cumulative energy dissipation (see Fig. 3.38(a)). In the illustrated case the *NHE* for the system with zero strain hardening is approximately 6 times as large as that for the system with -5%

hardening. The differences in the response are evident also in the displacement time histories presented in Fig. 3.39.

For the case illustrated even the non-normalized hysteretic energy dissipation of the system with zero strain hardening is approximately 1.4 times as large as that for the system with $\alpha = -5\%$ in spite of the much larger strength demand (by a factor of 2.1) for the latter system. The general observation was made that the great differences in the normalized hysteretic energy ($NHE = HE/F_y\delta_y$) between elastic-plastic systems and systems with negative hardening (see Fig. 3.37) diminish and in many cases disappear when the non-normalized hysteretic energies are compared.

Results on the hysteretic energy dissipation (per unit mass) are shown in Fig. 3.40. In order to compare the HE dissipated by $SDOF$ systems, the $15-S_1$ records, which have different severity, are scaled to a common PGA of $0.4g$. As Fig. 3.40 shows, the dependence of HE on the strain hardening ratio is not very pronounced even though the strength demands may differ greatly as seen from Fig. 3.36. The duration dependence of HE is similar to that of strength demand and NHE , and in all three cases is not very pronounced.

3.6 Effects of Strength Deterioration and Stiffness Degradation on Seismic Demand Parameters

A pilot study was performed to investigate the effects of strength deterioration and unloading stiffness degradation on seismic demand parameters. In this pilot study only bilinear systems with periods of 0.5 and 1.0 sec. and 5% strain hardening are considered. The $15-S_1$ record set is used as input ground motions.

The models discussed in Section 3.3 are utilized to describe strength deterioration and unloading stiffness degradation. In these models deterioration is based on the total energy capacity of the system and the amount of energy dissipated during each excursion. The energy capacity is expressed as $\gamma F_y\delta_y$. In this study the value of γ is assumed to be equal to 100, 75, 50 and 25. Figure 3.41 illustrates the meaning of this range of γ values in the context of the mean hysteretic energy demands for nondeteriorating bilinear systems. The values of F_y and δ_y of these nondeteriorating systems are used to define the energy capacity. The exponent c in equation (3.1), which defines the rate of deterioration, is assumed to be equal to 1.0.

In Section 3.4.3 the El-Centro record (1940), which has a relatively long duration, was used to illustrate the effect of strength deterioration on the response of a system with the period of 0.50 second. The same system is used here to illustrate the effect of unloading stiffness degradation as well as combined strength deterioration and unloading stiffness degradation on the seismic response. The undeteriorated yield level is taken as the value that gives a ductility demand of 4.0 for this ground motion using the basic bilinear model with 5% strain hardening.

Figure 3.42(a) shows the force-displacement response of the bilinear system with unloading stiffness degradation. The ductility demand for this system is 4.63, compared to 4.0 for the basic bilinear model. Fig. 3.42(b) presents the force-displacement response of the bilinear system with strength deterioration and unloading stiffness degradation. For this model the ductility demand is 6.40, compared to 6.02 for the same model without unloading stiffness degradation. This example shows that unloading stiffness degradation has some effect on the seismic response, but that this effect is small compared to strength deterioration effects. Thus, the following discussion focuses on strength deterioration only.

Figure 3.44(a) shows the effect of strength deterioration on ductility demands, using mean values for *SDOF* systems with a period of 0.5 sec. subjected to the 15- S_1 records. The results are presented in terms of the ratio of ductility demands of deteriorated to undeteriorated systems for different γ values. As shown in the figure, the effect of strength deterioration is very much dependent on the γ value, which reflects the energy capacity of system, as well as the ductility of the system. The curve for $\gamma = 25$ terminates at a ductility of 6, since for a ductility of 8 the system strength in the response to three of the 15 S_1 records deteriorated to the extent that failure (zero residual strength) occurred.

Figure 3.44(b) presents mean values of the ratio of hysteretic energy of deteriorated to undeteriorated systems. This ratio decreases as the ductility increases and γ decreases. The conclusion to be drawn is that systems with strength deterioration need to dissipate less energy than undeteriorated systems. Similar results for *SDOF* systems with a period of 1.0 second are presented in Fig. 3.45.

The results presented in Figs. 3.44 and 3.45 show that strength deterioration leads to an increase in displacement (ductility), but they also show that this increase is not very

large unless the strength deteriorates to a very small value. Strength deterioration, which is assumed to be controlled by dissipated energy, is slowed down by the decreased energy demand imposed on deteriorating systems.

The effect of strength deterioration on seismic response is more pronounced for ground motions having longer strong motion duration and several large peak values. The responses to two different motions, the Taft N21E (1952) and San Fernando N69W (1971) records, are used to illustrate this point.

Figure 3.46 shows the force-displacement responses of basic bilinear and strength degrading *SDOF* systems with a period of 0.5 seconds and equal yield strength, subjected to the Taft (1952) record. The Taft record, which is shown in Fig. 3.47(a), has several strong pulses and, as a consequence, the hysteresis response of the *SDOF* system exhibits several large inelastic excursions that contribute to further deterioration of strength and to a significant increase in the displacement. On the other hand, the maximum displacements of the basic bilinear and strength degrading systems are equal if the San Fernando (1971) record, which has only one strong pulse early in the time history (see Fig. 3.49(a)), is used as input. In this case the maximum displacement is governed by the early pulse during which no deterioration has yet occurred (see Fig. 3.48(b)). Later cycles exhibit significant deterioration but no increase in displacement because of the low intensity of the pulses occurring later in the time history.

The results of this pilot study have given a preliminary indication of the importance of strength degradation in seismic response. Significant degradation will occur when the hysteretic energy demand approaches the energy dissipation capacity of the structural system. This does not necessarily imply a large increase in displacement (ductility). A significant increase in displacement will occur only if the ground motion has several large pulses, such that the later large pulses will act on an already deteriorated system. Thus, again, the frequency content of the ground motion, the time history envelope, and the strong motion duration will play an important role. Further research in this area is needed before quantitative conclusions can be drawn.

Table 3.1 Specific Hysteresis Models Generated from the General Model Shown in Fig. 3.1

MODEL	SKELETON PARAMETERS					HYSTERESIS PARAMETERS					
	K_e	K_t	K_h	F_y	F_s	K_u	K_r	K_p	F_t	F_p	δ_t
Basic Trilinear	K_e	K_t	K_h	F_y	F_s	K_e	K_e	—	—	—	—
Basic Bilinear	K_e	—	K_h	F_y	—	K_e	K_e	—	—	—	—
Bilinear with Strength	K_e	—	K_h	F_y	—	K_e	K_e	—	$\beta_s F_{i-1}$	—	—
Bilinear with Unloading Stiffness Degradation	K_e	—	K_h	F_y	—	$\beta_u K_{u,i-1}$	$\beta_u K_{u,i-1}$	—	—	—	—
Clough Model with Basic Stiffness Degradation	K_e	—	K_h	F_y	—	K_e	Rule	—	—	—	δ_{max}
Clough Model with Acc. Stiffness Degradation	K_e	—	K_h	F_y	—	K_e	Rule	—	—	—	$\beta_k \delta_{t,i-1}$
Clough Model with Strength Deterioration	K_e	—	K_h	F_y	—	K_e	Rule	—	$\beta_s F_{i-1}$	—	δ_{max}
Clough Model with Unloading Stiff. Degradation	K_e	—	K_h	F_y	—		Rule	—	—	—	δ_{max}
Basic Pinching Model	K_e	—	K_h	F_y	—	K_e	Rule	Rule	—	Rule	δ_{max}
Pinching and Accelerated Stiffness Degradation	K_e	—	K_h	F_y	—	K_e	Rule	Rule	—	Rule	$\beta_k \delta_{t,i-1}$
Pinching and Strength Deterioration	K_e	—	K_h	F_y	—	K_e	Rule	Rule	$\beta_s F_{i-1}$	Rule	δ_{max}

Table 3.2 Typical Western U.S. Ground Motion Records Used in this Study
(15-S₁ Record Set)

Earthquake	Name (Station)	Mag.	e (km)	Dsm (sec)	PGA (cm/sec ²)	PGV (cm/sec.)
Kern County CA 1952	Taft Lincoln School Tunnel 1952, N21E	7.7	43.0	11.2	152.7	15.7
Kern County CA 1952	Taft Lincoln School Tunnel 1952, S69E	7.7	43.0	12.6	175.9	17.7
Lower California CA 1934	El Centro Imperial Valley 1934, N00E	6.5	64.0	13.0	156.8	20.5
Lower California CA 1934	El Centro Imperial Valley 1934, N90E	6.5	64.0	15.6	179.1	11.5
Western Washington WA 1949	Olympia Washington HWY Test Lab 1949, S04E	7.0	16.0	19.8	161.6	21.4
Western Washington WA 1949	Olympia Washington HWY Test Lab 1949, S86W	7.0	16.0	19.2	274.6	17.0
Puget Sound WA 1965	Olympia Washington HWY Test Lab 1965, S86W	6.5	61.0	11.2	194.3	12.7
San Fernando CA 1971	Castaic Old Ridge Route 1971, N69W	6.6	29.0	15.1	265.4	27.2
Long Beach CA 1933	Public Utilities Bluding 1933, South	6.3	27.0	5.6	192.7	29.3
Long Beach CA 1933	Public Utilities Bluding 1933, West	6.3	27.0	6.4	156.0	15.8
Imperial Valley CA 1979	Holtville P.O. 1979, 225	6.6	19.0	6.7	246.2	44.0
Imperial Valley CA 1979	Calexico Fire Station 1979, 225	6.6	15.0	10.9	269.6	18.2
Coyote Lake CA 1979	San Yasidro School 1979, 360	5.7	12.0	7.9	246.2	32.9
Coyote Lake CA 1979	San Yasidro School 1979, 270	5.7	12.0	6.4	228.1	24.9
Coalinga CA 1983	Parkfield Zone 16 1983, 0	6.5	39.10	8.2	178.7	14.7

GENERAL HYSTERETIC MODEL

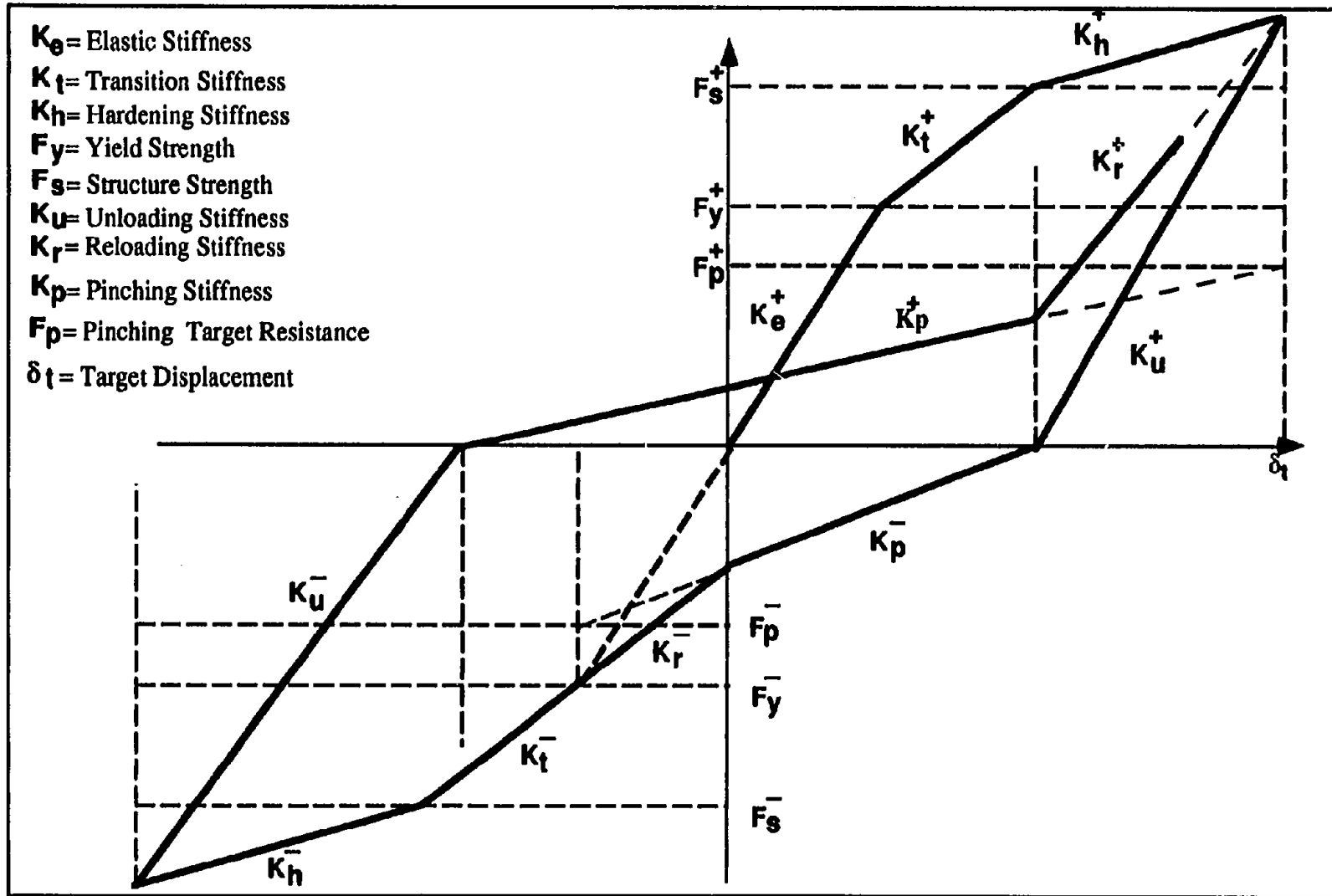


Fig. 3.1 Parameters of General Hysteresis Model

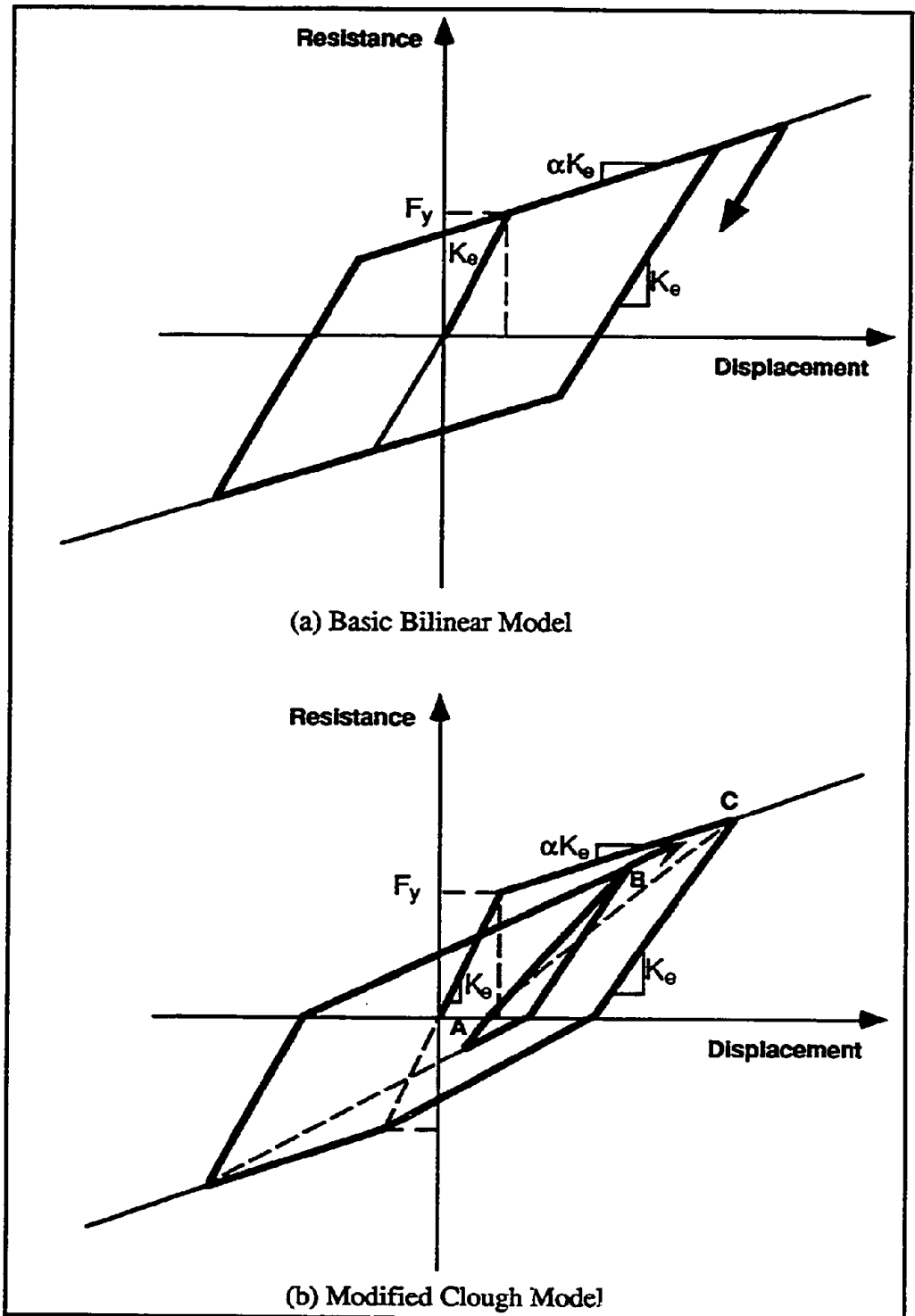


Fig. 3.2 Basic Hysteresis Models

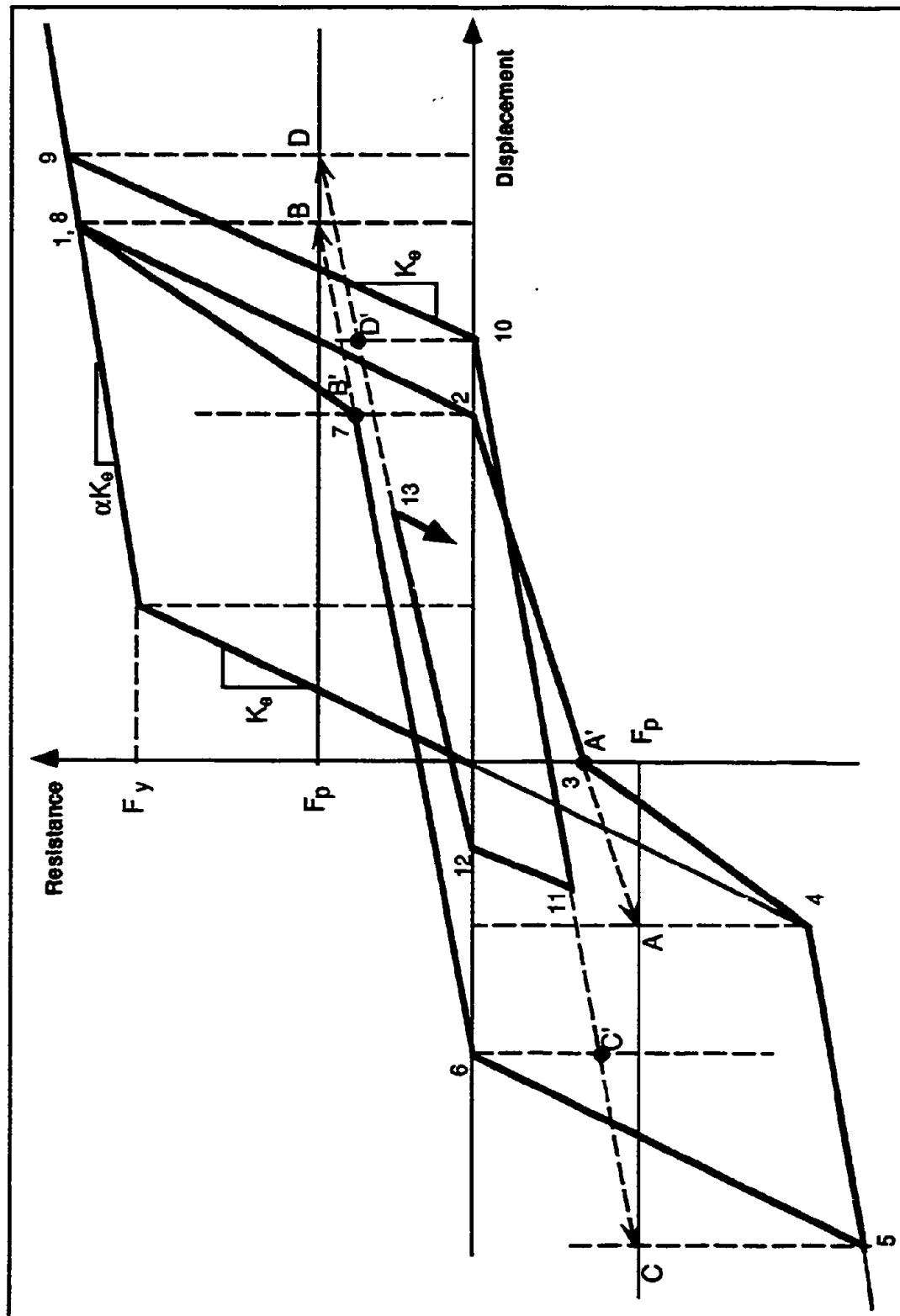


Fig. 3.3 Pinching Hysteresis Model

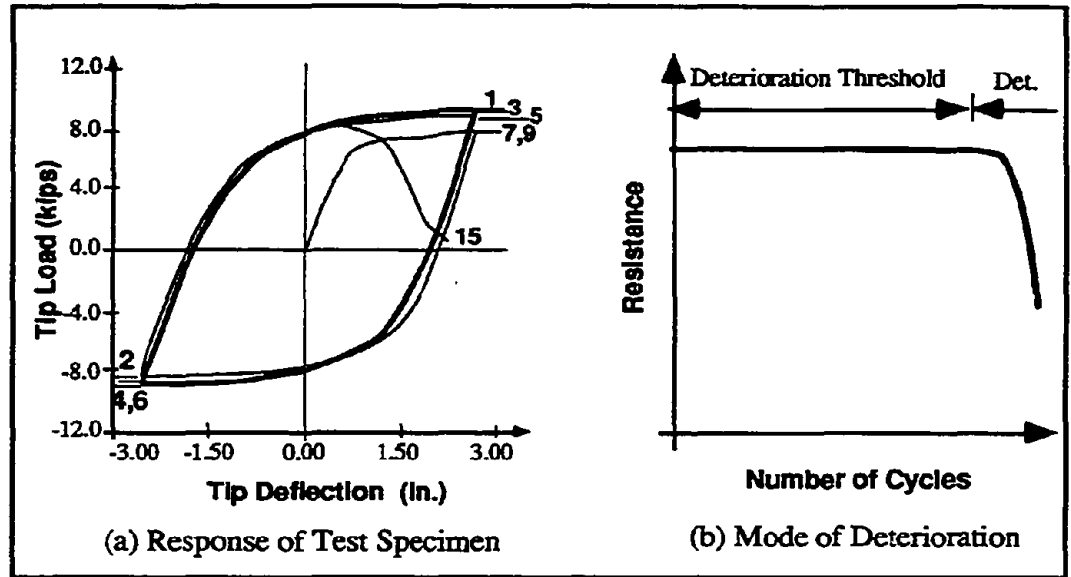


Fig. 3.4 Test Specimen with Large Deterioration Threshold (Krawinkler et. al. 1983)

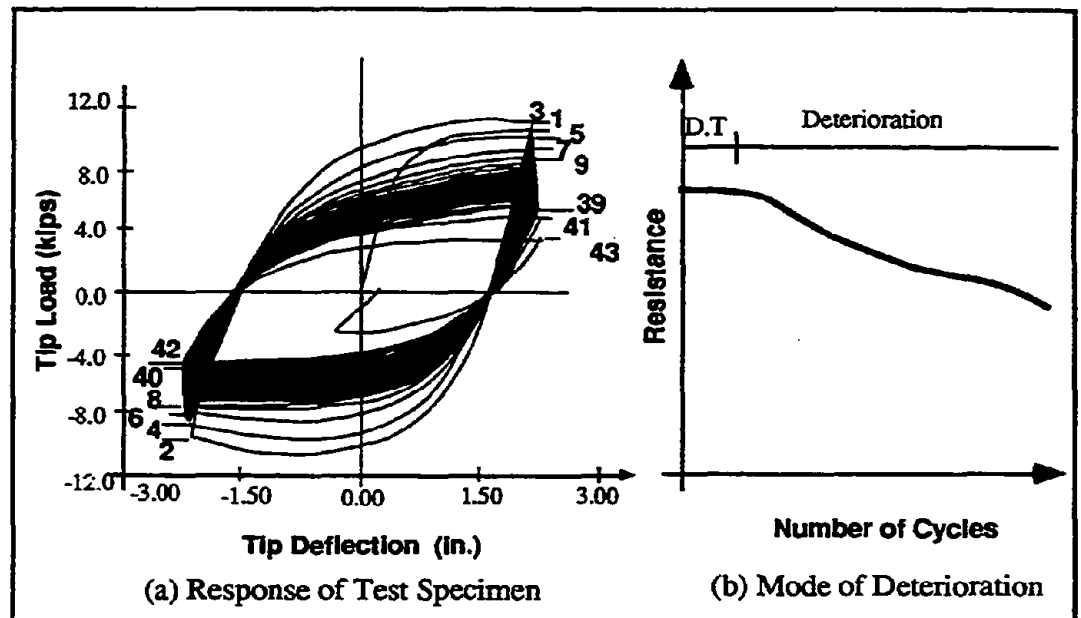


Fig. 3.5 Test Specimen with Small Deterioration Threshold (Krawinkler et. al. 1983)

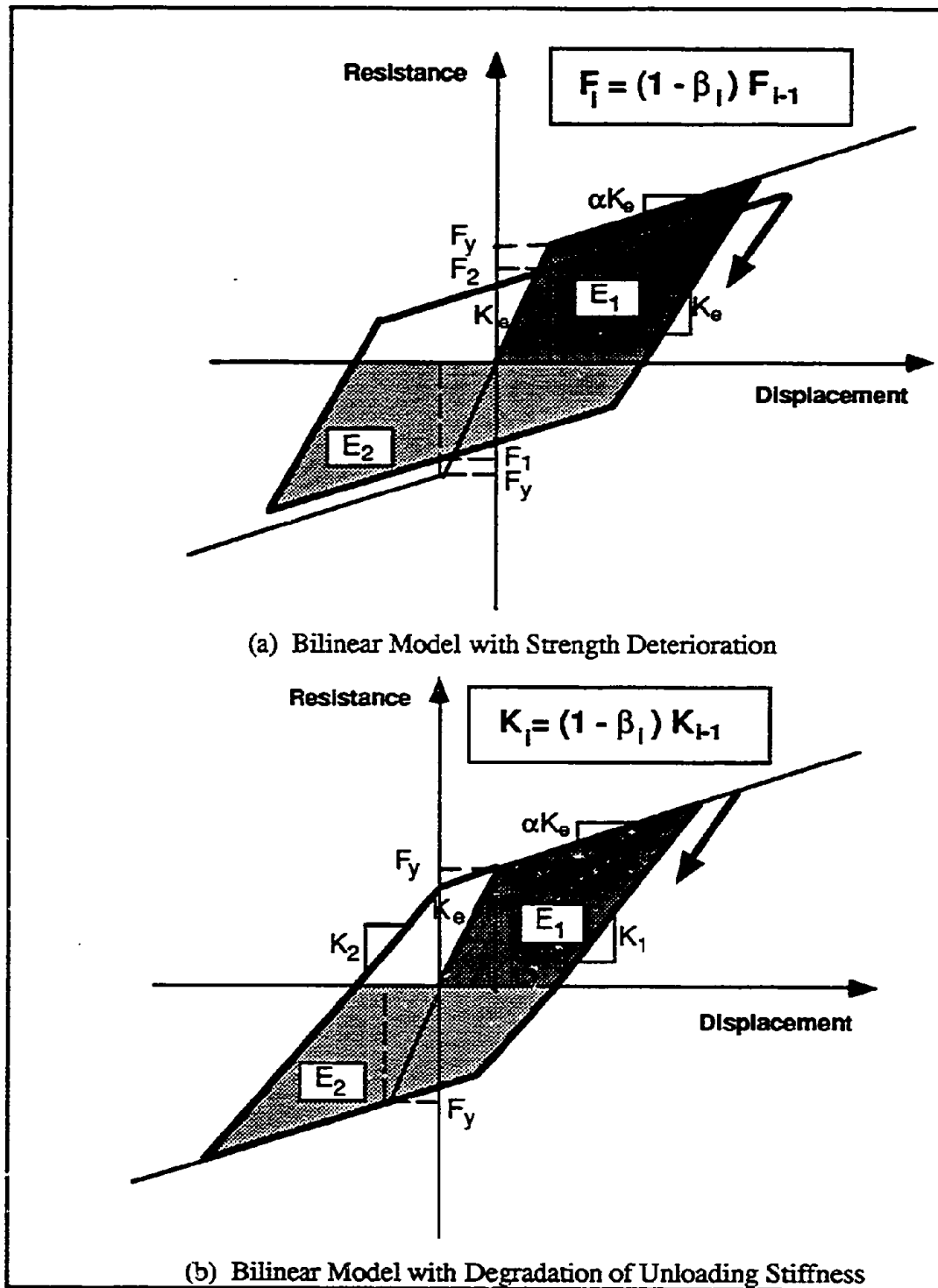


Fig. 3.6 Effects of Deterioration of Structural Properties in Bilinear Model

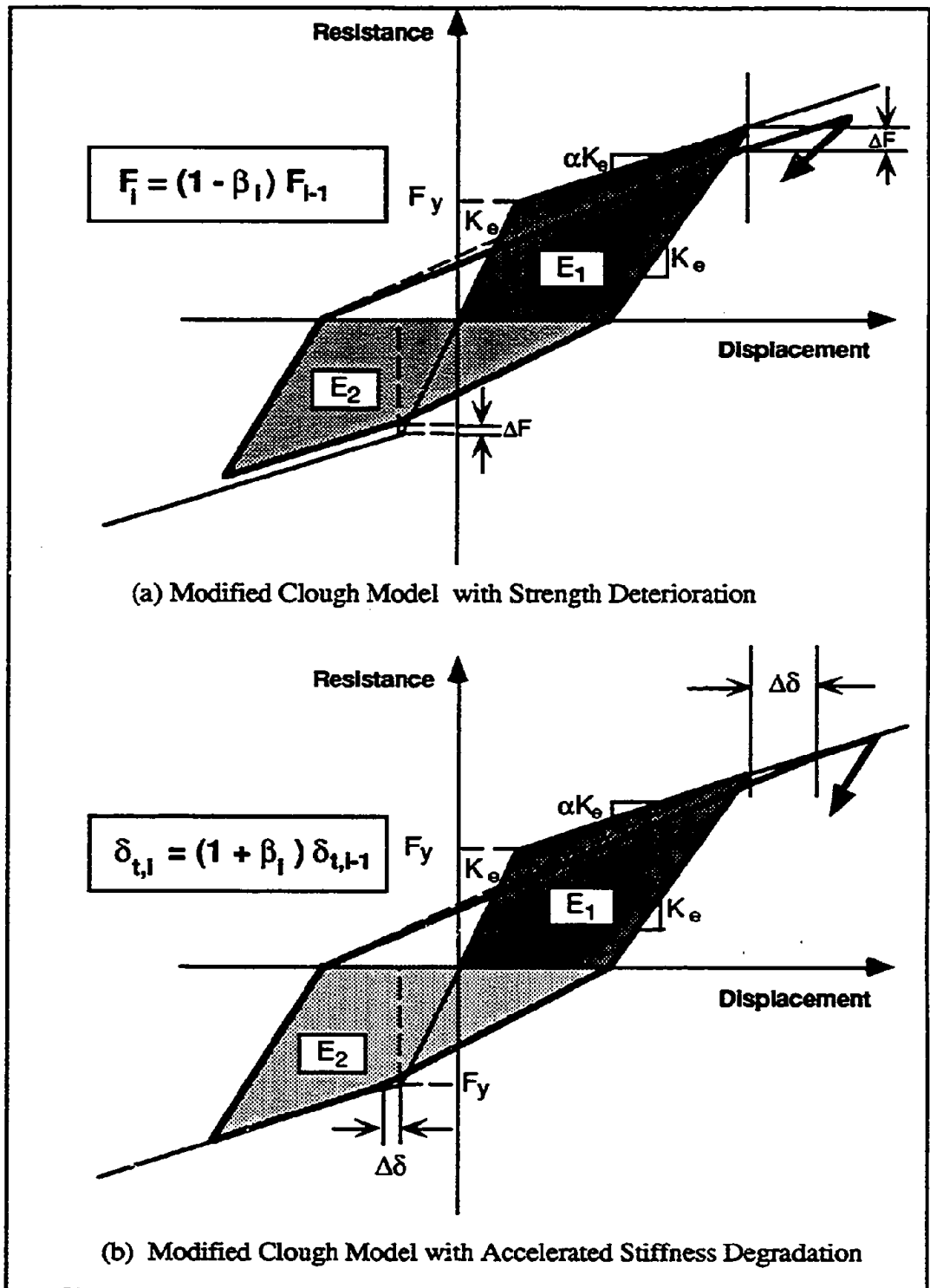


Fig. 3.7 Effects of Deterioration of Structural Properties in Modified Clough Model

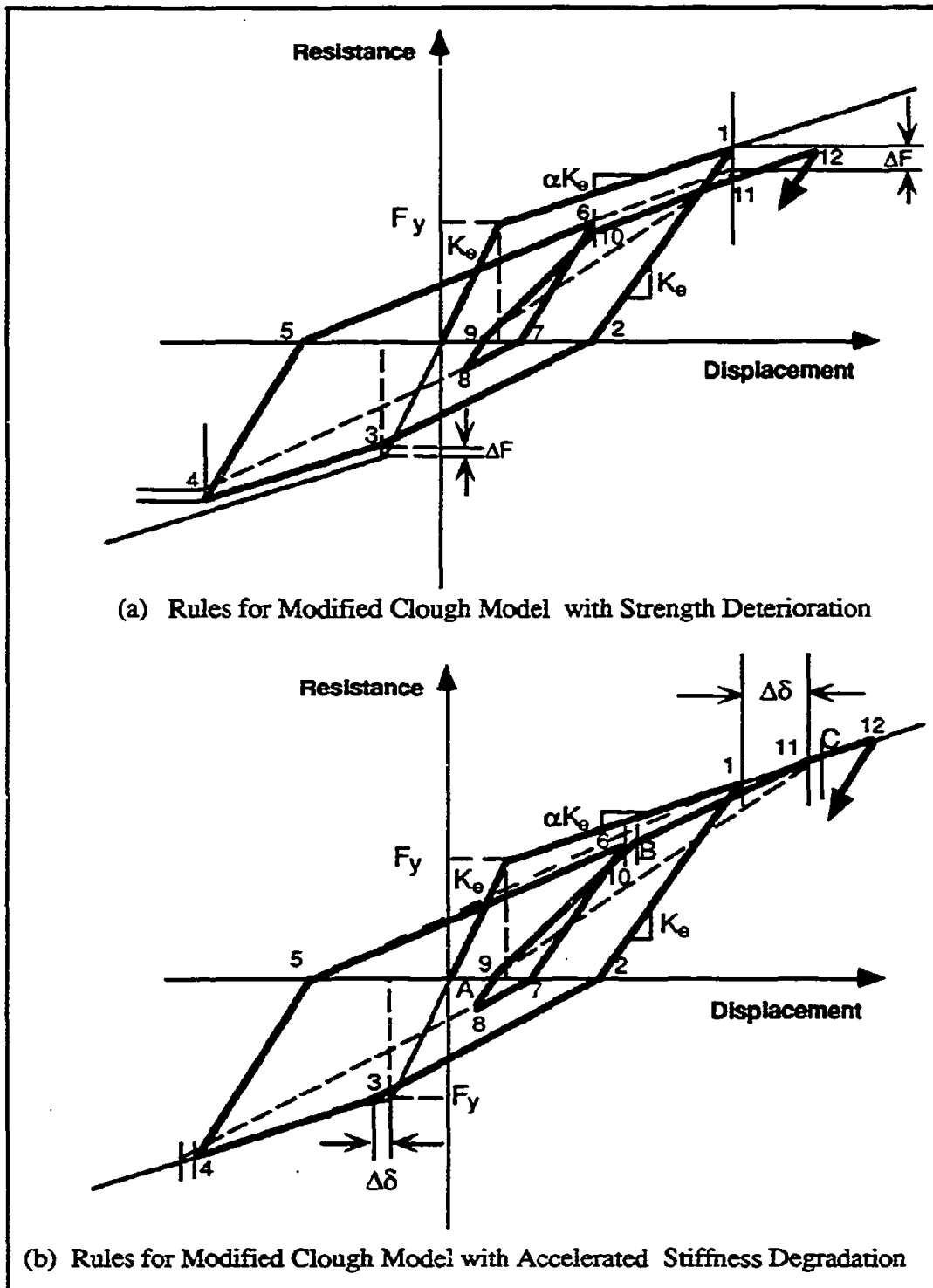
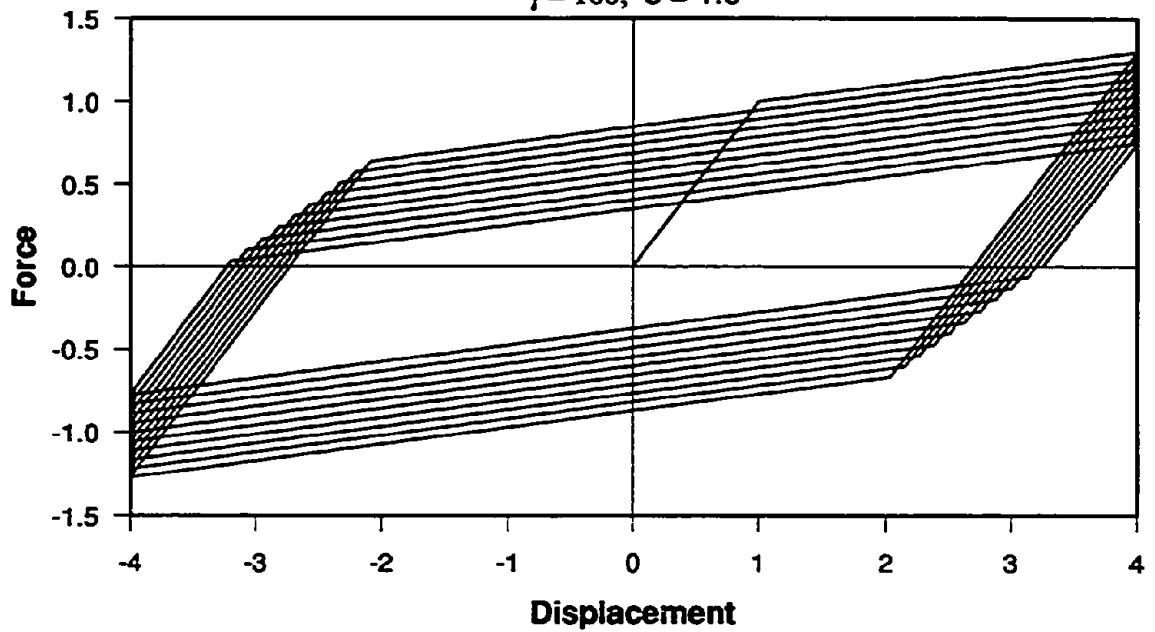


Fig. 3.8 Rules for Modified Clough Model with Deterioration of Structural Properties

BILINEAR MODEL WITH STRENGTH DETERIORATION

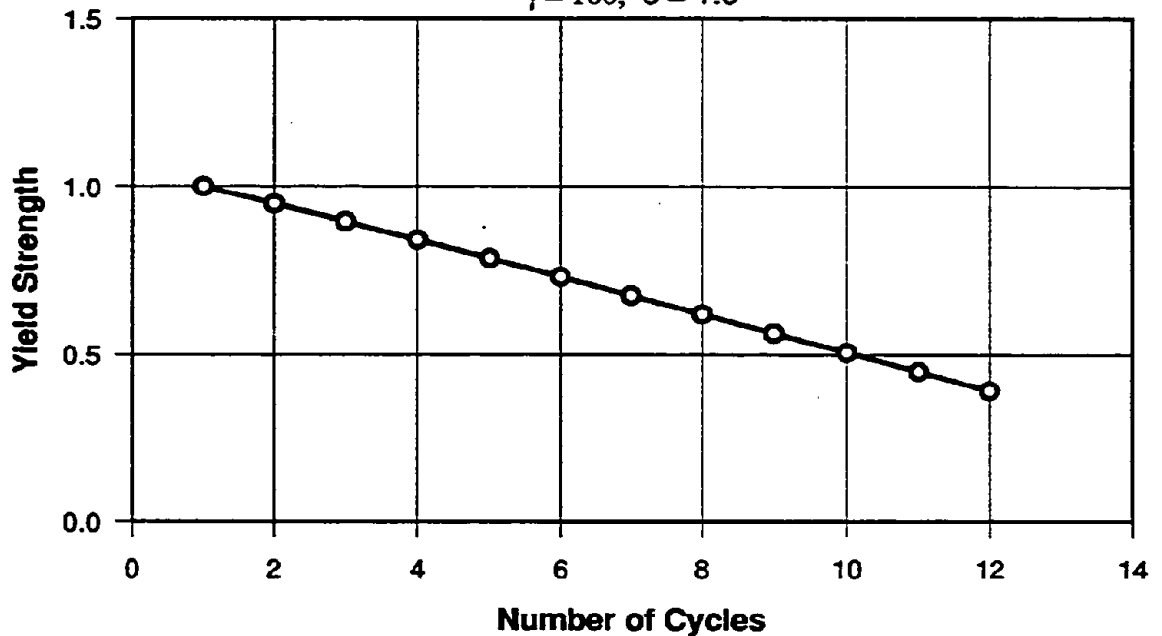
$\gamma = 100, c = 1.0$



(a) Hysteresis Model

RATE OF DETERIORATION OF YIELD STRENGTH

$\gamma = 100, c = 1.0$

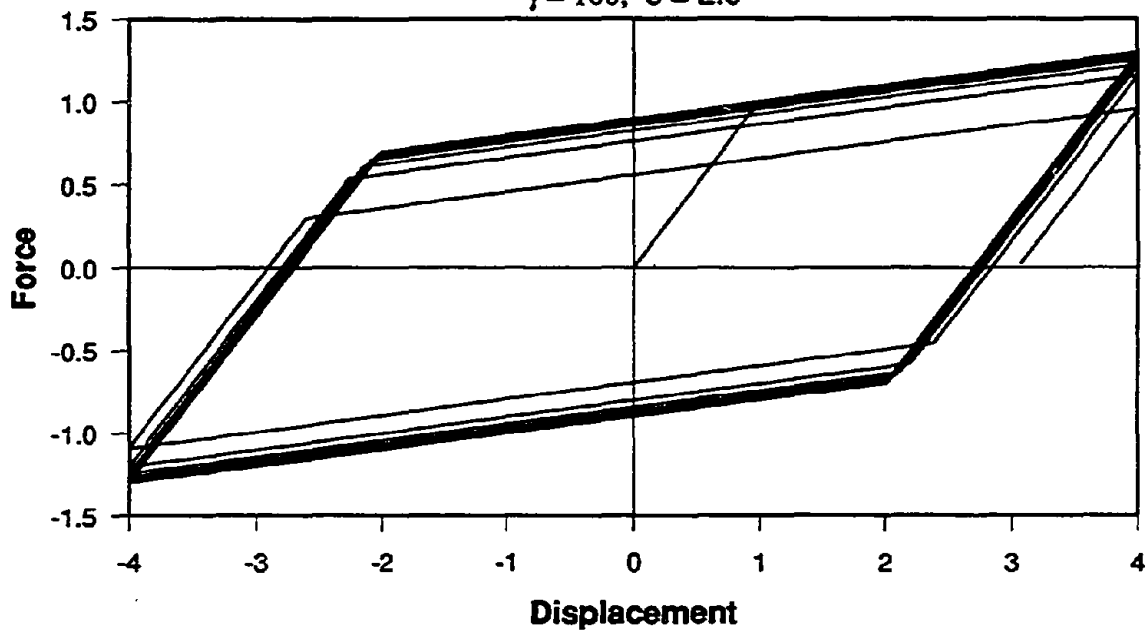


(b) Deterioration in Yield Strength with Number of Cycles

Fig. 3.9 Strength Deterioration in Bilinear Hysteresis Model - $c = 1.0$

BILINEAR MODEL WITH STRENGTH DETERIORATION

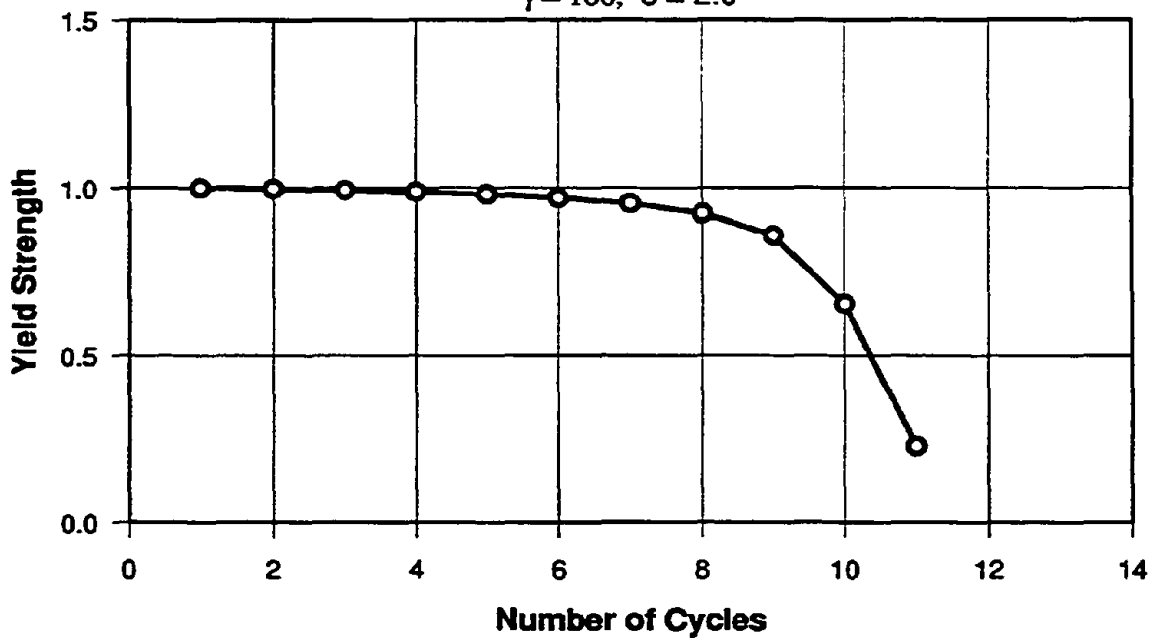
$$\gamma = 100, c = 2.0$$



(a) Hysteresis Model

RATE OF DETERIORATION OF YIELD STRENGTH

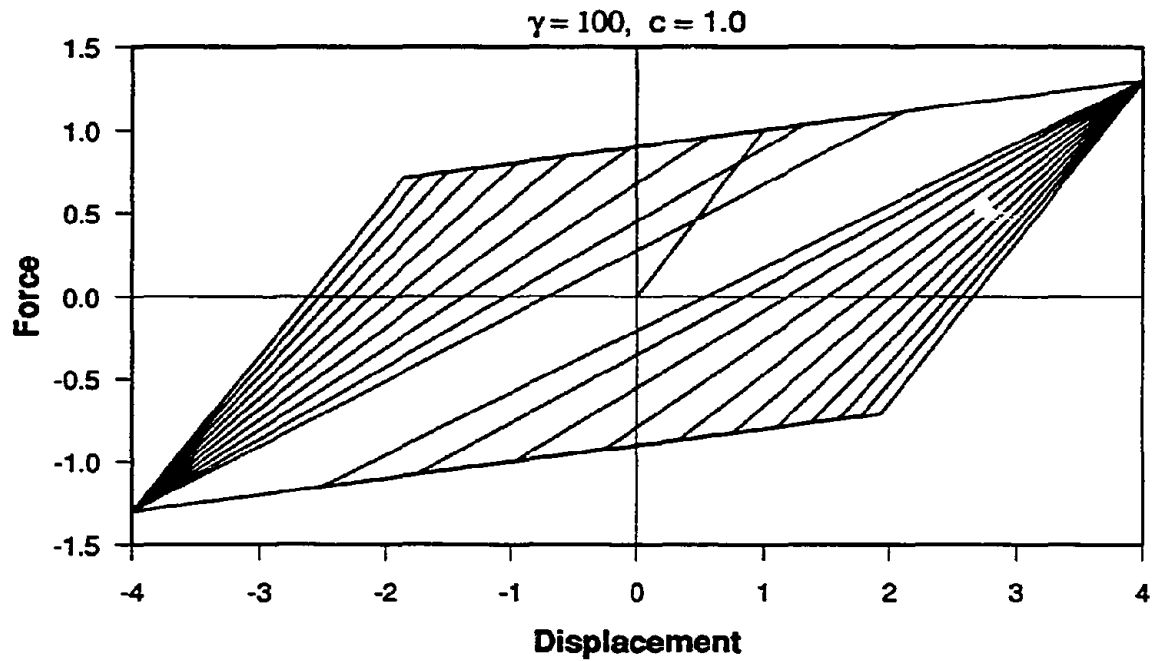
$$\gamma = 100, c = 2.0$$



(b) Deterioration in Yield Strength with Number of Cycles

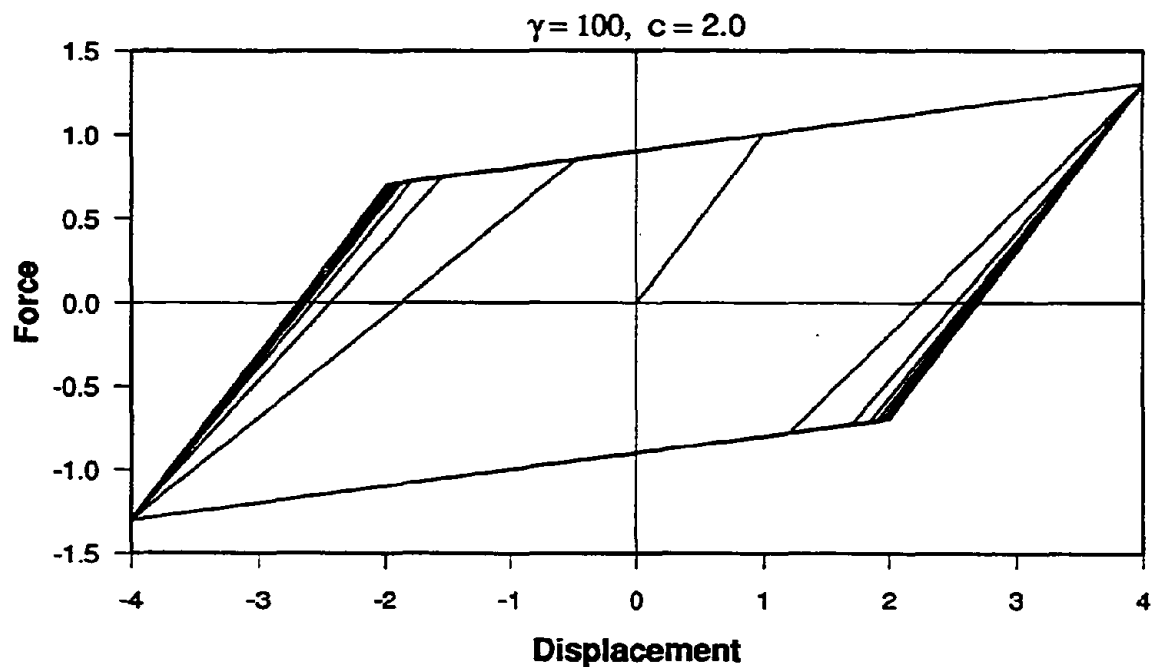
Fig. 3.10 Strength Deterioration in Bilinear Hysteresis Model - $c = 2.0$

BILINEAR MODEL WITH DEGRADATION OF UNLOADING STIFFNESS



(a) Hysteresis Model for $\gamma = 100$, and $c = 1.0$

BILINEAR MODEL WITH DEGRADATION OF UNLOADING STIFFNESS

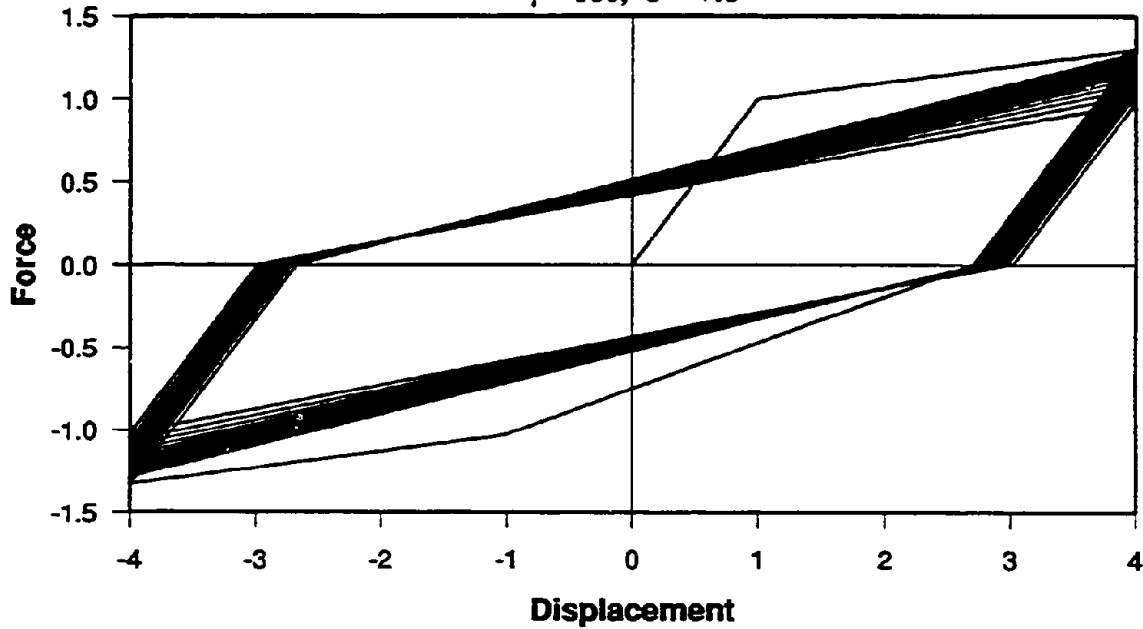


(a) Hysteresis Model for $\gamma = 100$, and $c = 2.0$

Fig. 3.11 Degradation of Unloading Stiffness in Bilinear Hysteresis Model

Clough Model with Accelerated Stiffness Degradation

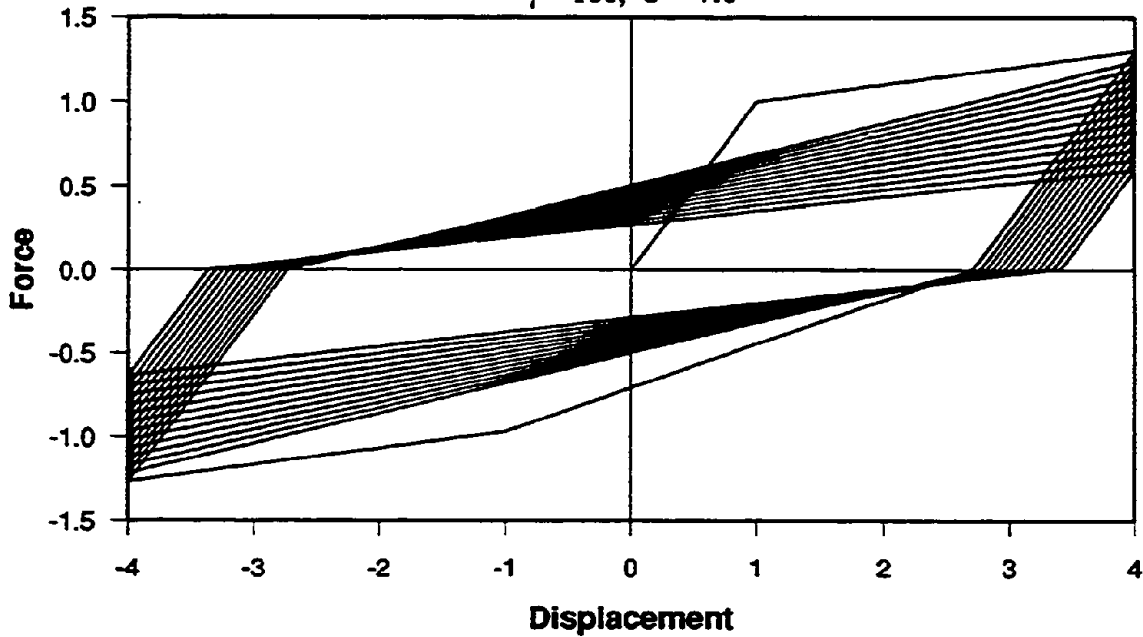
$$\gamma = 100, c = 1.0$$



(a) With Accelerated Stiffness Degradation

Clough Model with Strength Deterioration

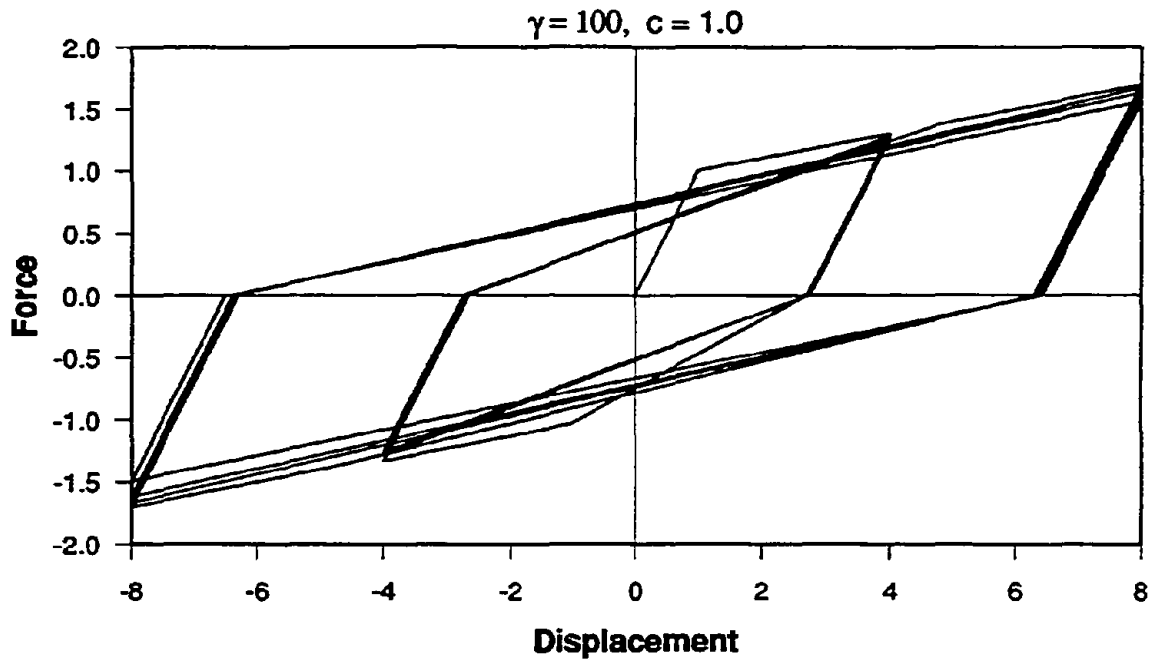
$$\gamma = 100, c = 1.0$$



(a) With Strength Deterioration

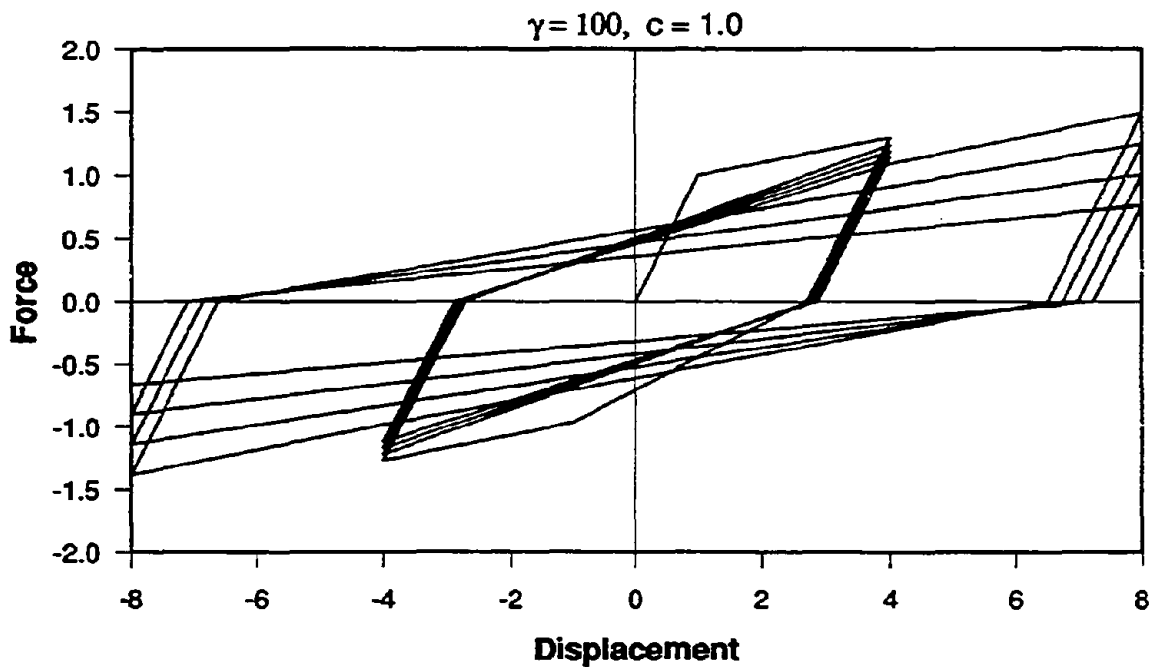
Fig. 3.12 Deterioration in Peak Oriented Models Subjected to Constant Amplitude Cycling

COUGH MODEL WITH ACCELERATED STIFFNESS DEGRADATION



(a) With Accelerated Stiffness Degradation

COUGH MODEL WITH STRENGTH DETERIORATION



(a) With Strength Deterioration

Fig. 3.13 Deterioration in Peak Oriented Models Subjected to Cycling with Different Amplitudes

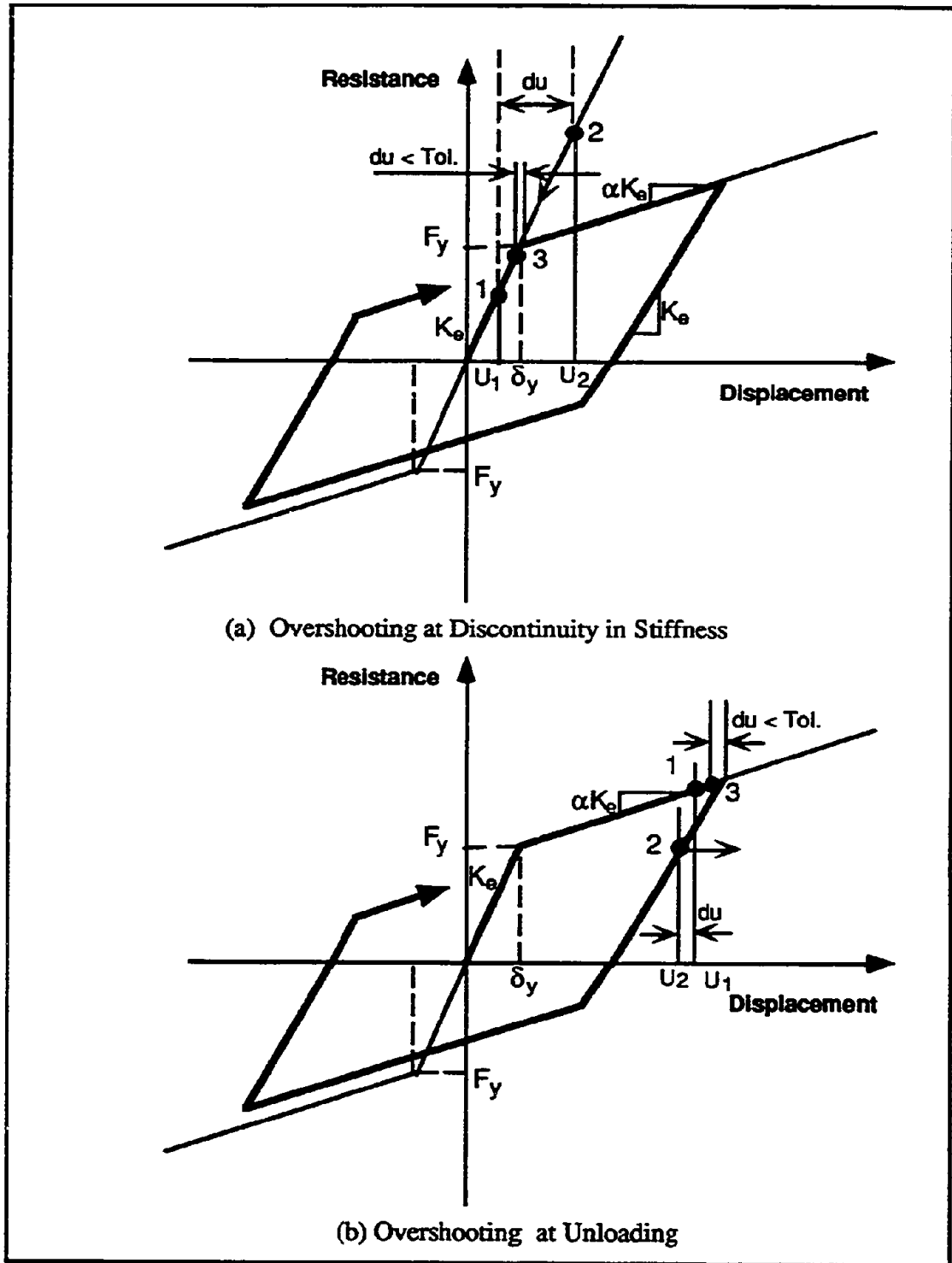
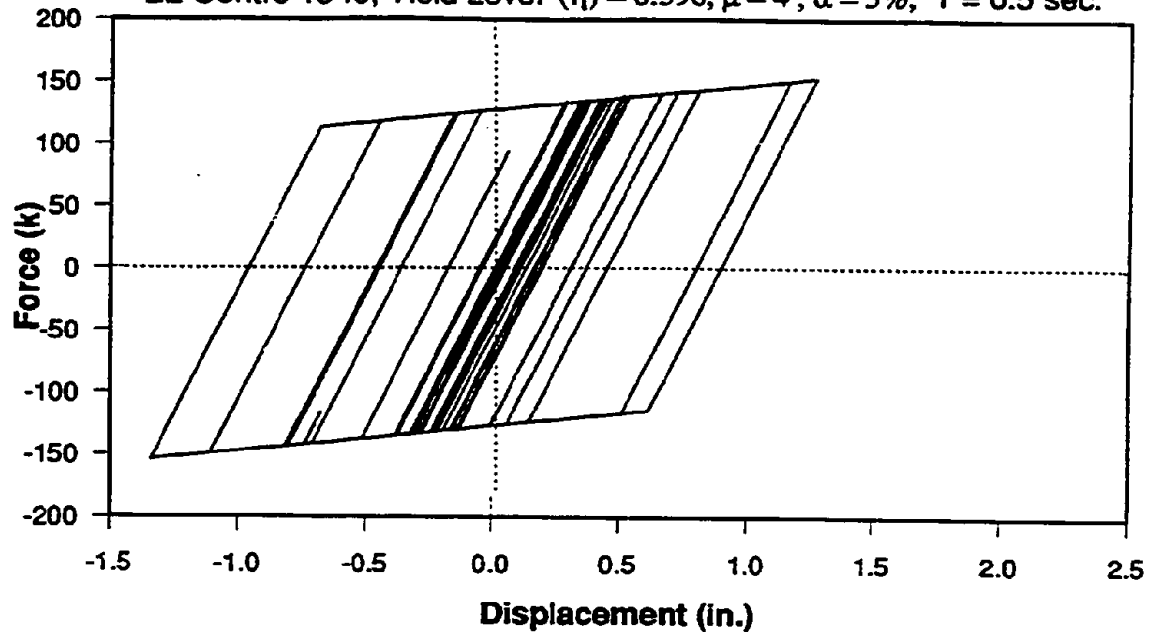


Fig. 3.14 Procedure to Correct Overshooting

BILINEAR HYSTERESIS MODEL

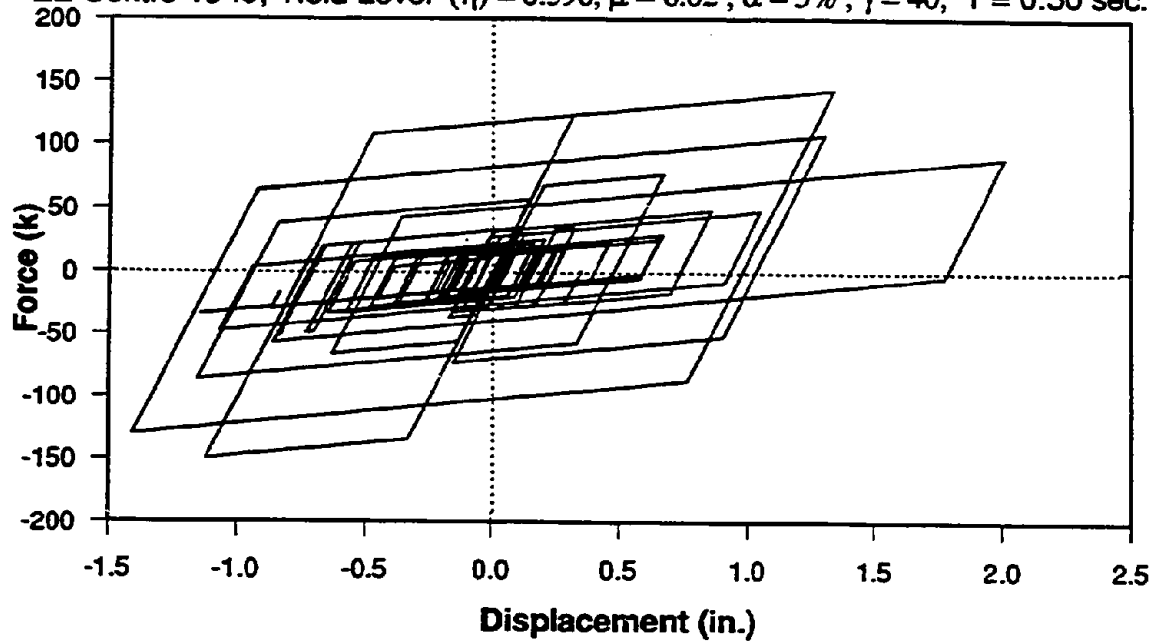
EL-Centro 1940, Yield Level (η) = 0.396, $\mu = 4$, $\alpha = 5\%$, $T = 0.5$ sec.



(a) Basic Bilinear Model

BILINEAR STRENGTH DETERIORATION MODEL

EL-Centro 1940, Yield Level (η) = 0.396, $\mu = 6.02$, $\alpha = 5\%$, $\gamma = 40$, $T = 0.50$ sec.

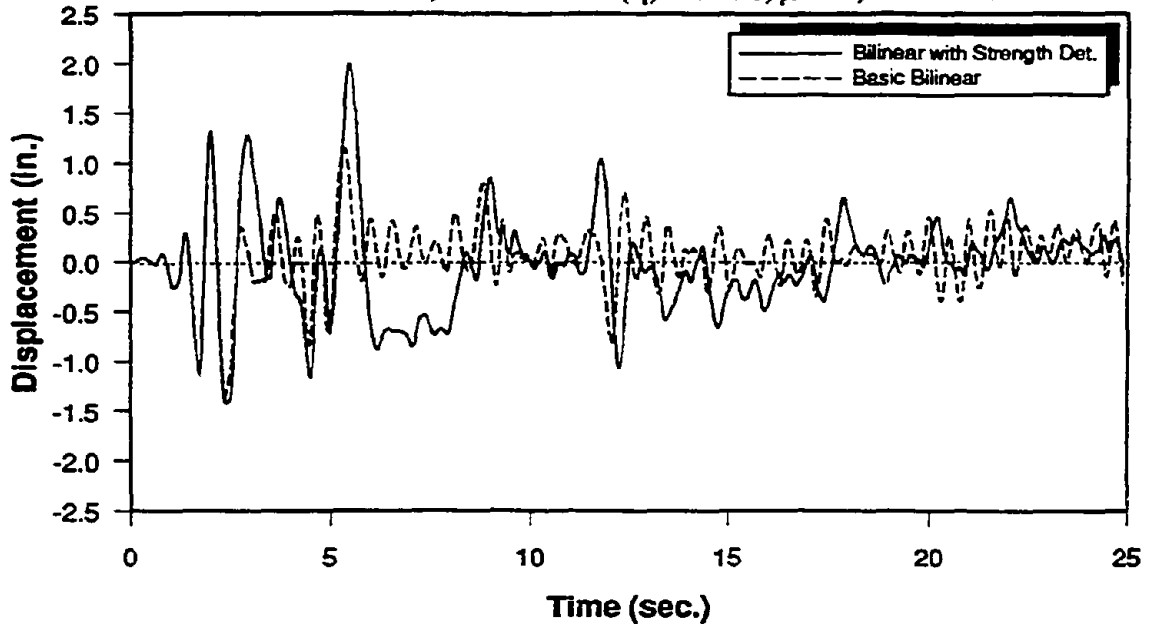


(b) Bilinear Model with Strength Deterioration

Fig. 3.15 Force-Displacement Response without and with Strength Deterioration

DISPLACEMENT TIME HISTORIES FOR DIFFERENT HYSTERESIS MODELS

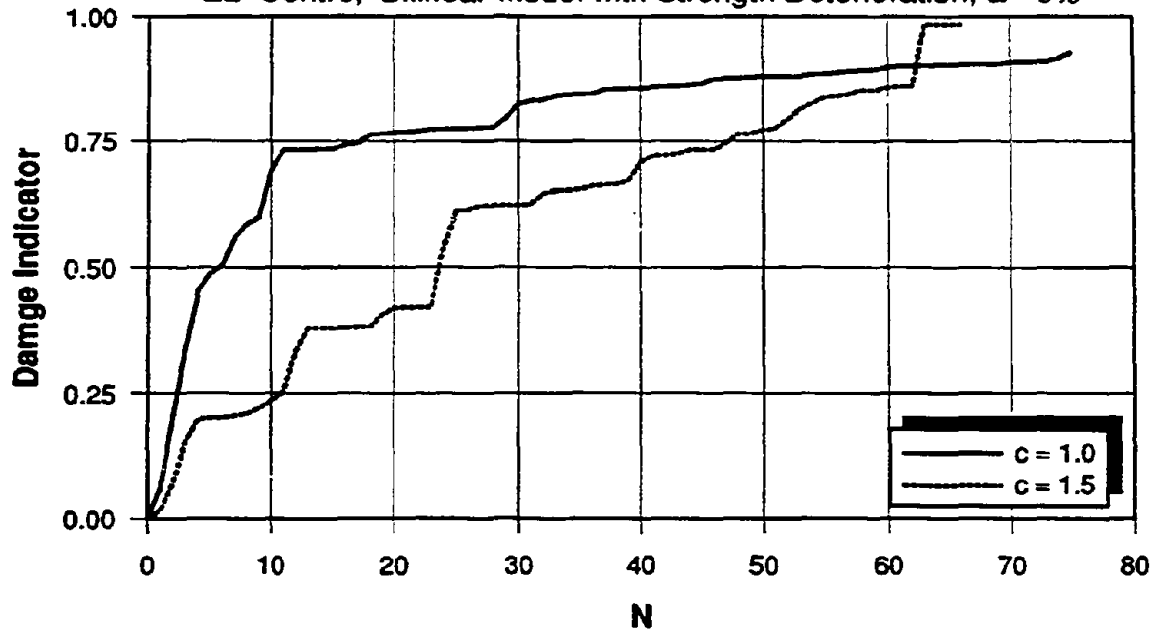
EL-Centro 1940, Yield Level (η) = 0.396, $\mu = 4$, $\alpha = 5\%$ $c = 1$



(a) Displacement Time History

VARIATION OF DAMAGE INDICATOR WITH NO. OF INELASTIC EXCURSIONS

EL- Centro, Bilinear Model with Strength Deterioration, $\alpha = 5\%$



(b) Variation of Damage Indicator

Fig. 3.16 Displacement Time History and Variation of Damage Index for a System with Period 0.50 sec.

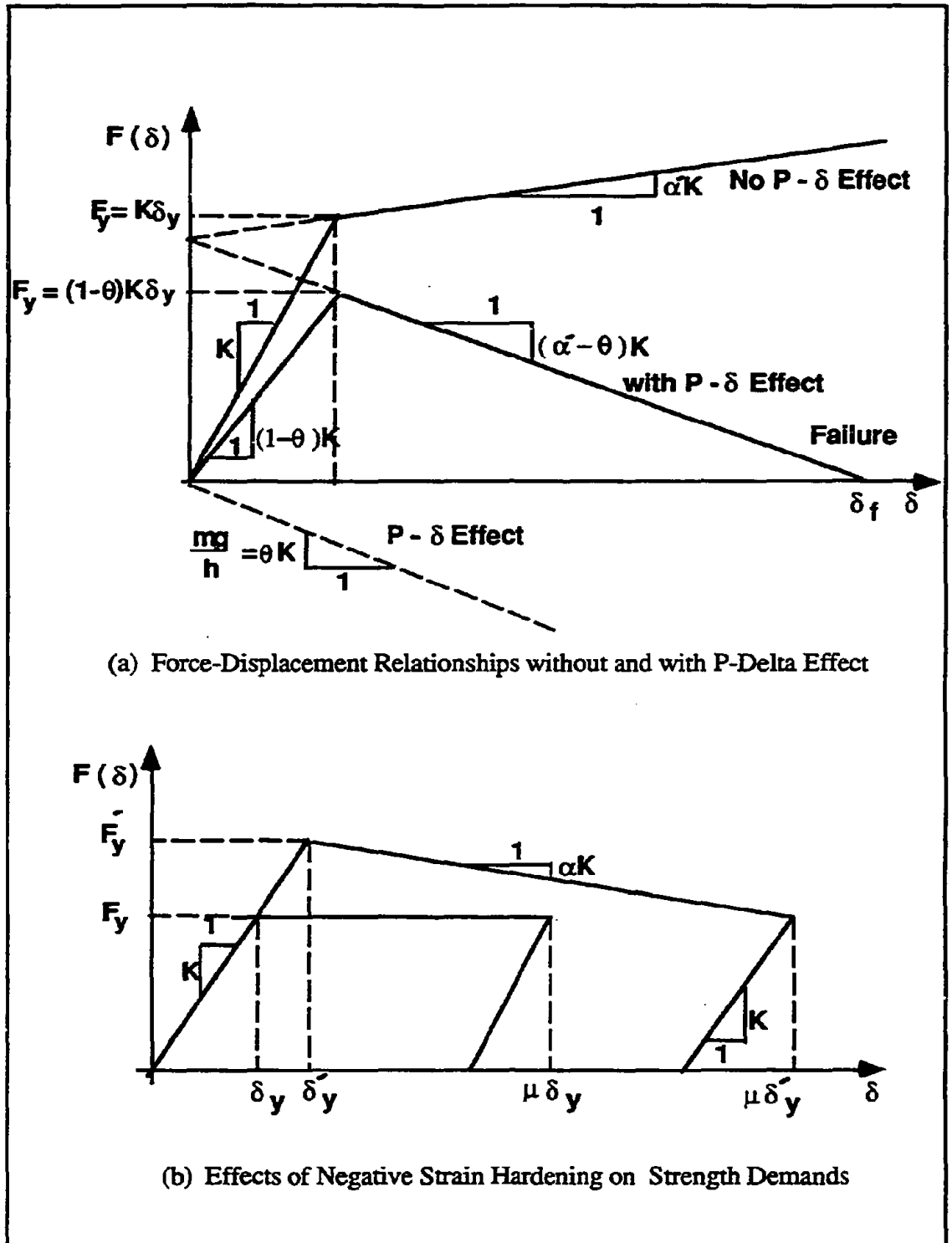
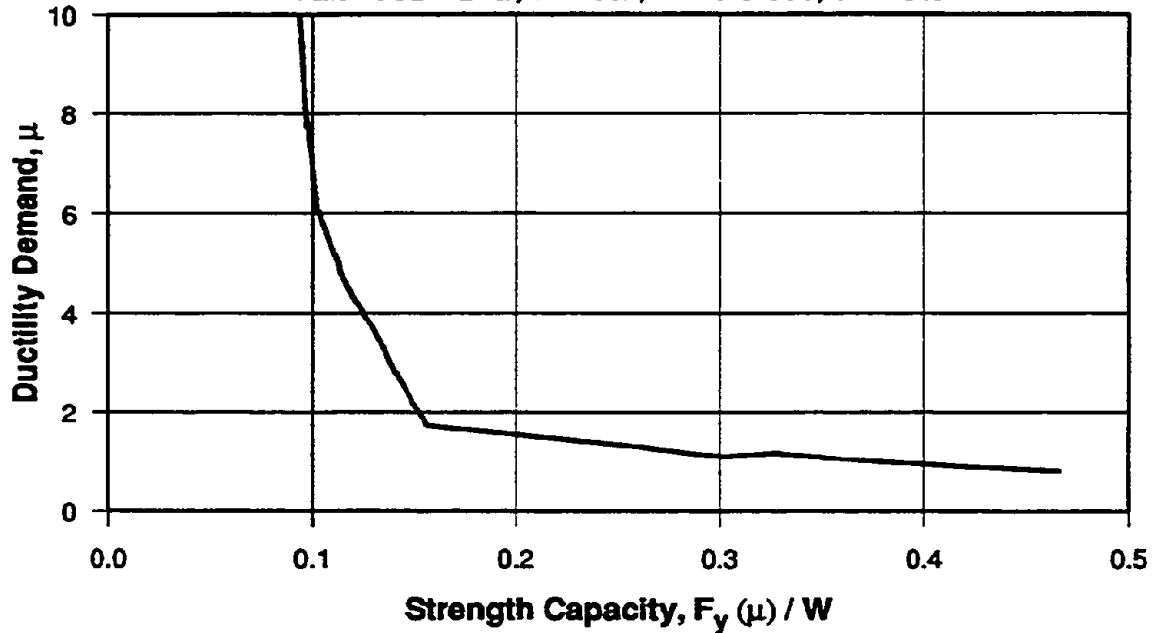


Fig. 3.17 Effect of P-Delta and Negative Strain Hardening on Seismic Demands

STRENGTH CAPACITY vs. DUCTILITY DEMAND

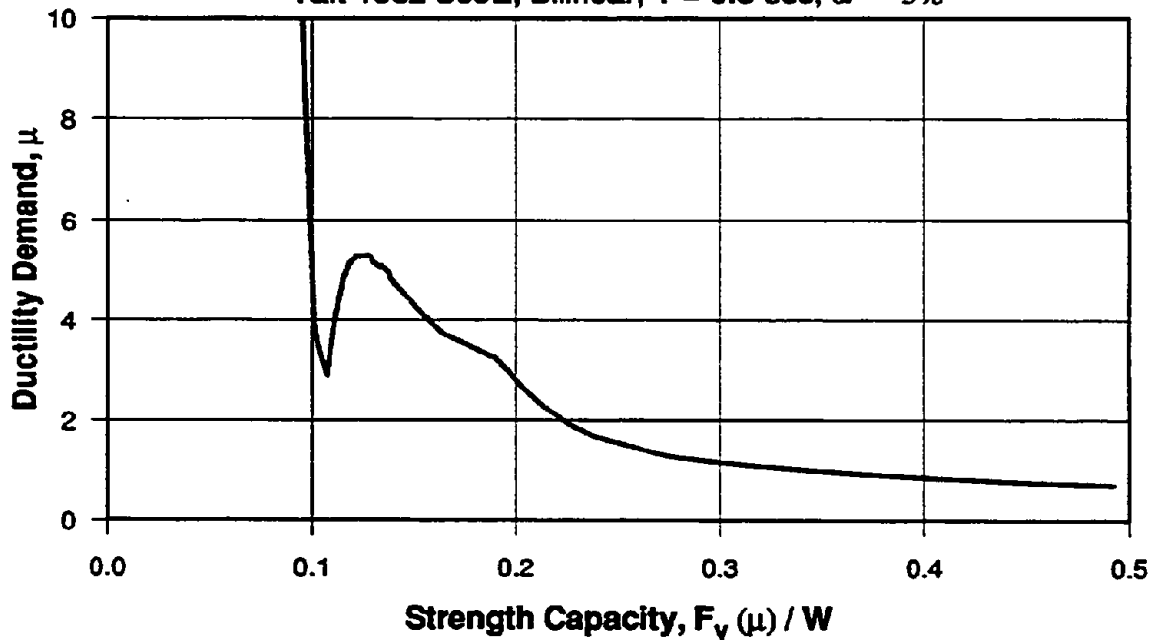
Taft 1952 N21E, Bilinear, $T = 0.5$ sec, $\alpha = -5\%$



(a) Monotonic Relationship Between $F_y(\mu)$ and μ

STRENGTH CAPACITY vs. DUCTILITY DEMAND

Taft 1952 S69E, Bilinear, $T = 0.5$ sec, $\alpha = -5\%$

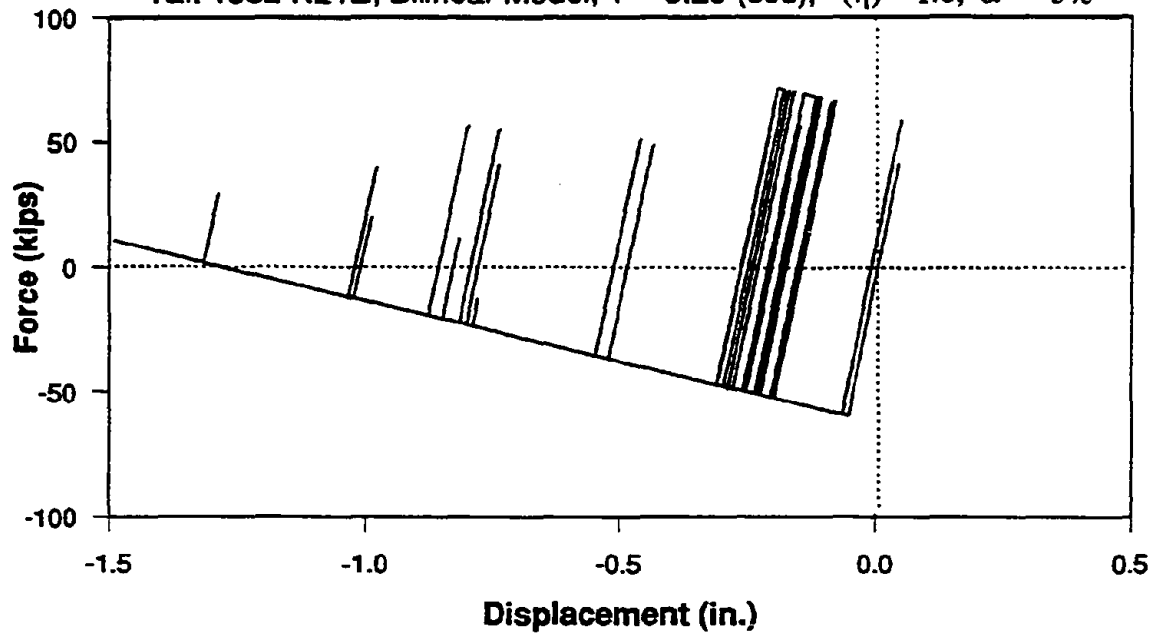


(b) Nonmonotonic Relationship Between $F_y(\mu)$ and μ

Fig. 3.18 Relationships Between Inelastic Strength Capacity $F_y(\mu)$ and Ductility Demand μ

FORCE-DISPLACEMENT DIAGRAM

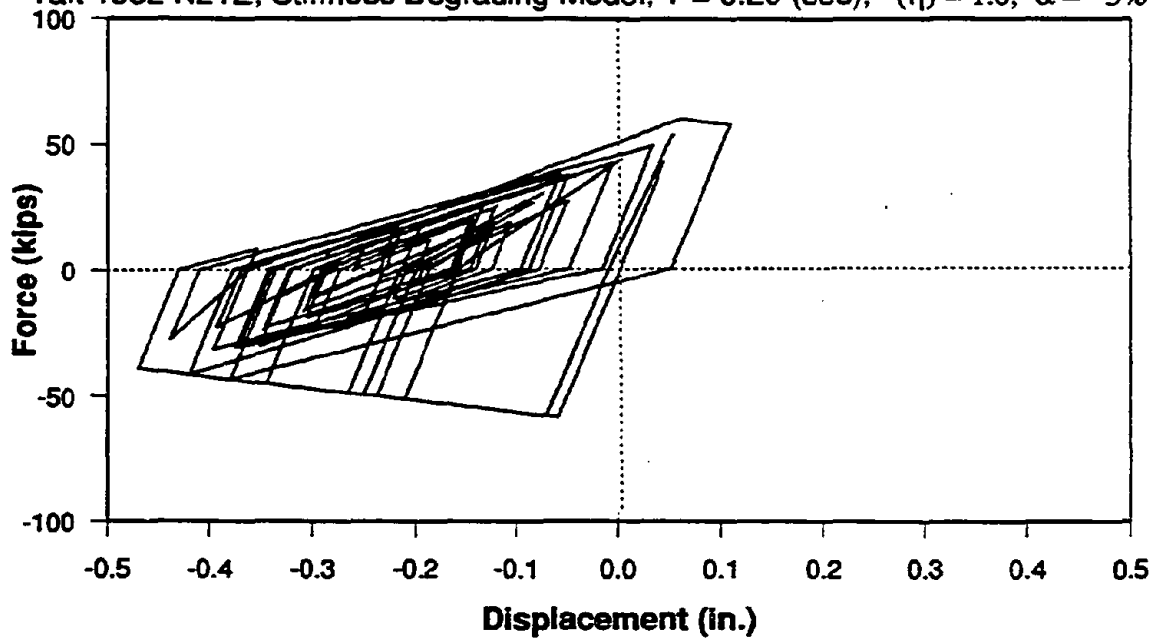
Taft 1952 N21E, Bilinear Model, $T = 0.20$ (sec), $(\eta) = 1.0$, $\alpha = -5\%$



(a) Bilinear Model

FORCE-DISPLACEMENT DIAGRAM

Taft 1952 N21E, Stiffness Degrading Model, $T = 0.20$ (sec), $(\eta) = 1.0$, $\alpha = -5\%$

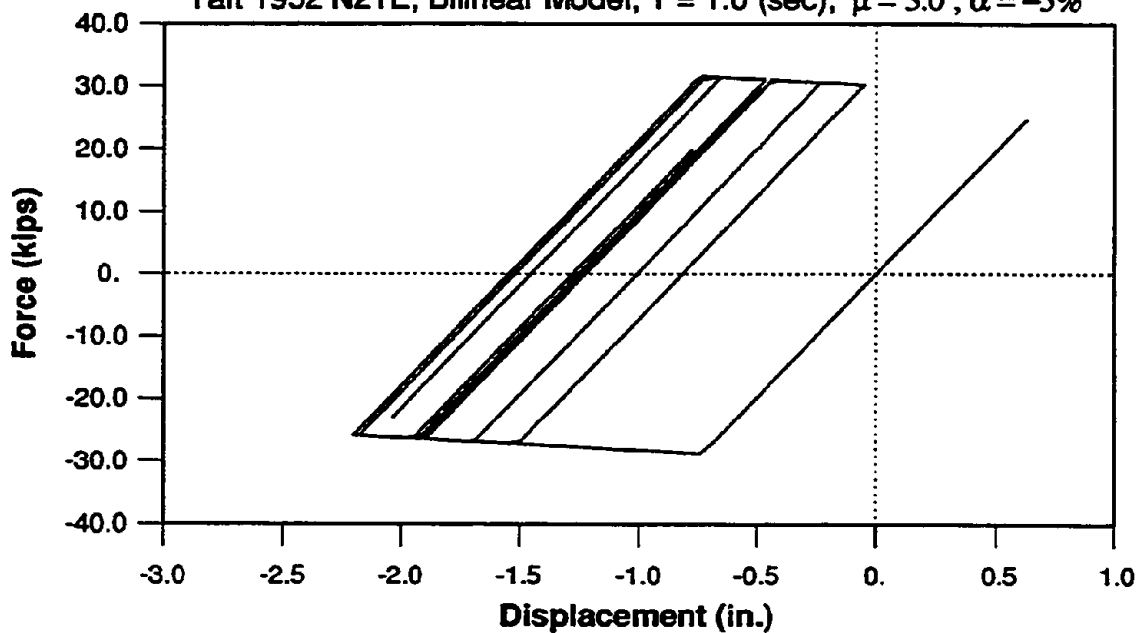


(b) Modified Clough Model

Fig. 3.19 Effect of Negative Strain Hardening on SDOF System with $T = 0.2$ sec.

FORCE-DISPLACEMENT DIAGRAM

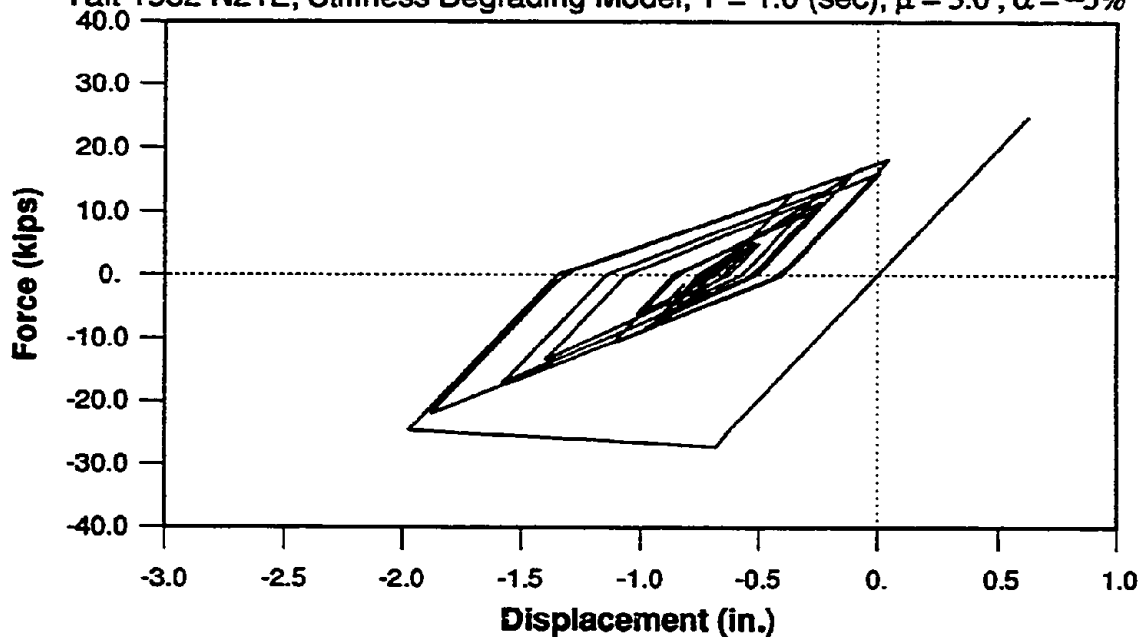
Taft 1952 N21E, Bilinear Model, $T = 1.0$ (sec), $\mu = 3.0$, $\alpha = -5\%$



(a) Bilinear Model

FORCE-DISPLACEMENT DIAGRAM

Taft 1952 N21E, Stiffness Degrading Model, $T = 1.0$ (sec), $\mu = 3.0$, $\alpha = -5\%$

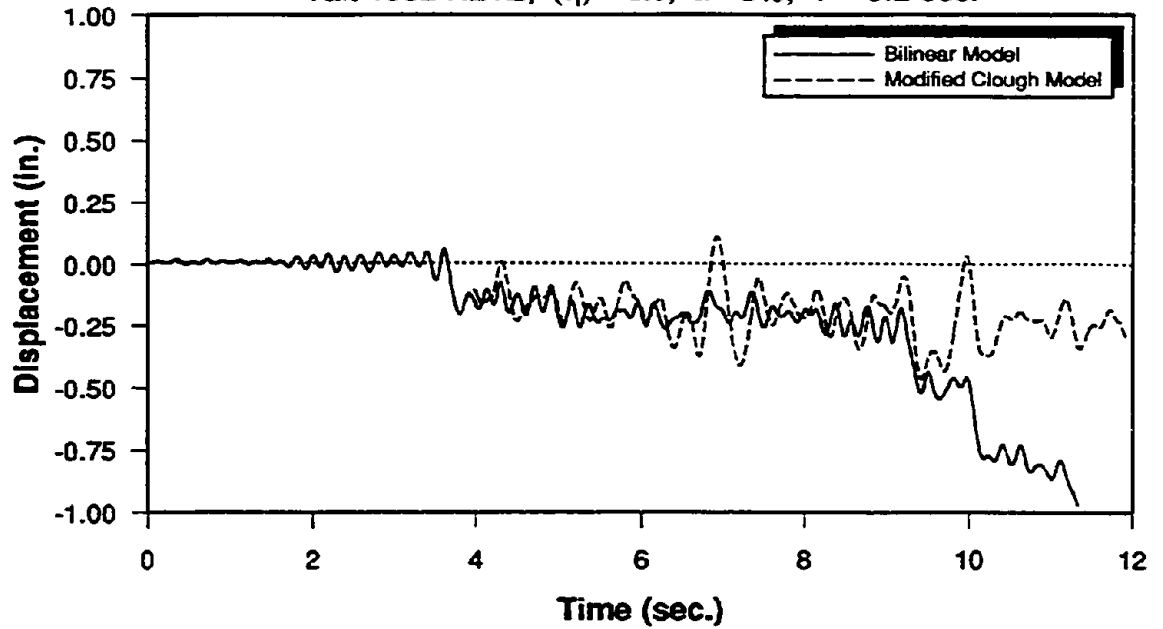


(b) Modified Clough Model

Fig. 3.20 Effect of Negative Strain Hardening on SDOF System with $T = 1.0$ sec.

DISPLACEMENT TIME HISTORY

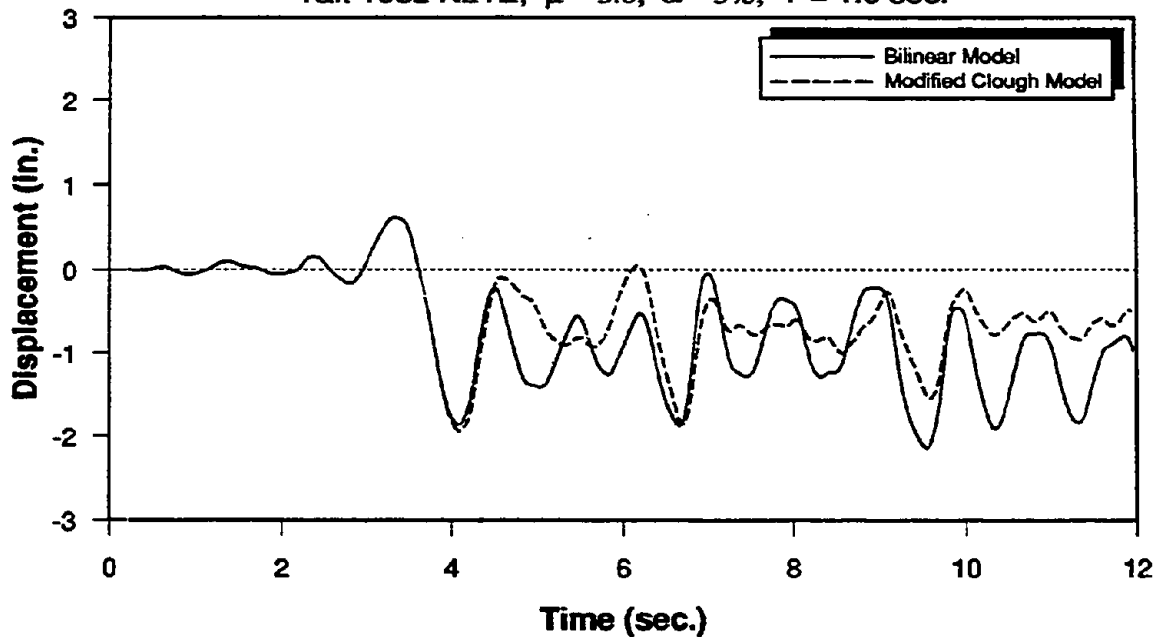
Taft 1952 N21E, (η) = 1.0, α = 5%, T = 0.2 sec.



(a) System with T = 0.2 sec.

DISPLACEMENT TIME HISTORY

Taft 1952 N21E, μ = 3.0, α = 5%, T = 1.0 sec.

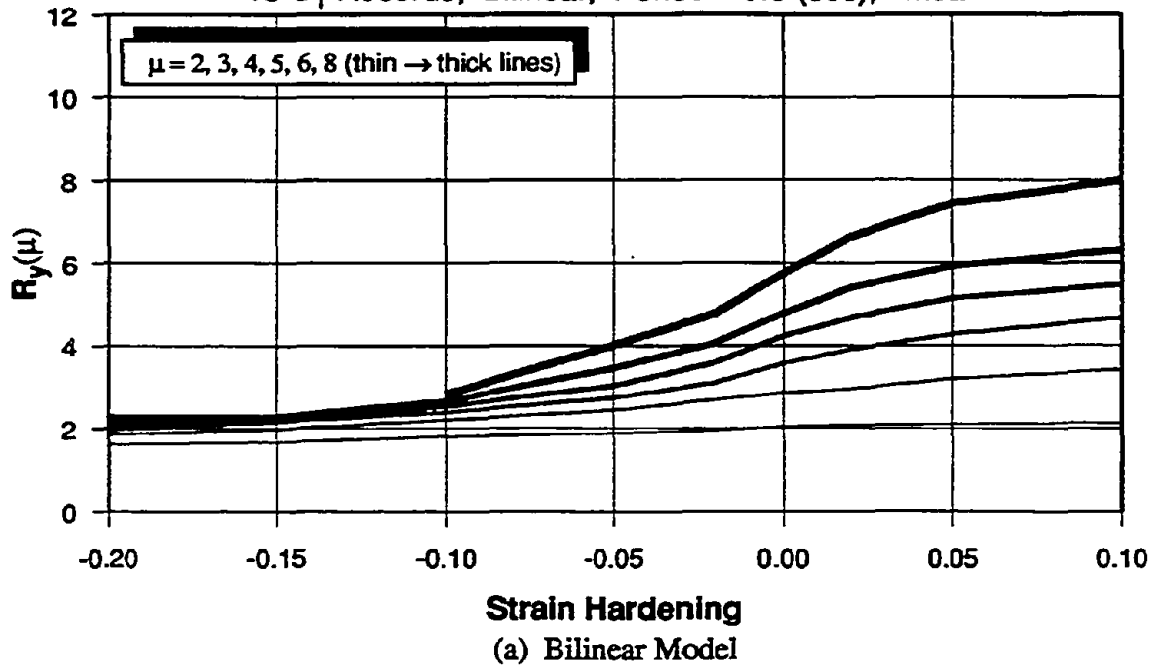


(b) System with T = 1.0 sec.

Fig. 3.21 Displacement Time Histories for Systems with -5% Strain Hardening

EFFECT OF STRAIN HARDENING/SOFTENING ON $R_y(\mu)$

15-S₁ Records, Bilinear, Period = 0.5 (sec), Mean



EFFECT OF STRAIN HARDENING/SOFTENING ON $R_y(\mu)$

15-S₁ Records, Stiffness Degradation, Period = 0.5 (sec), Mean

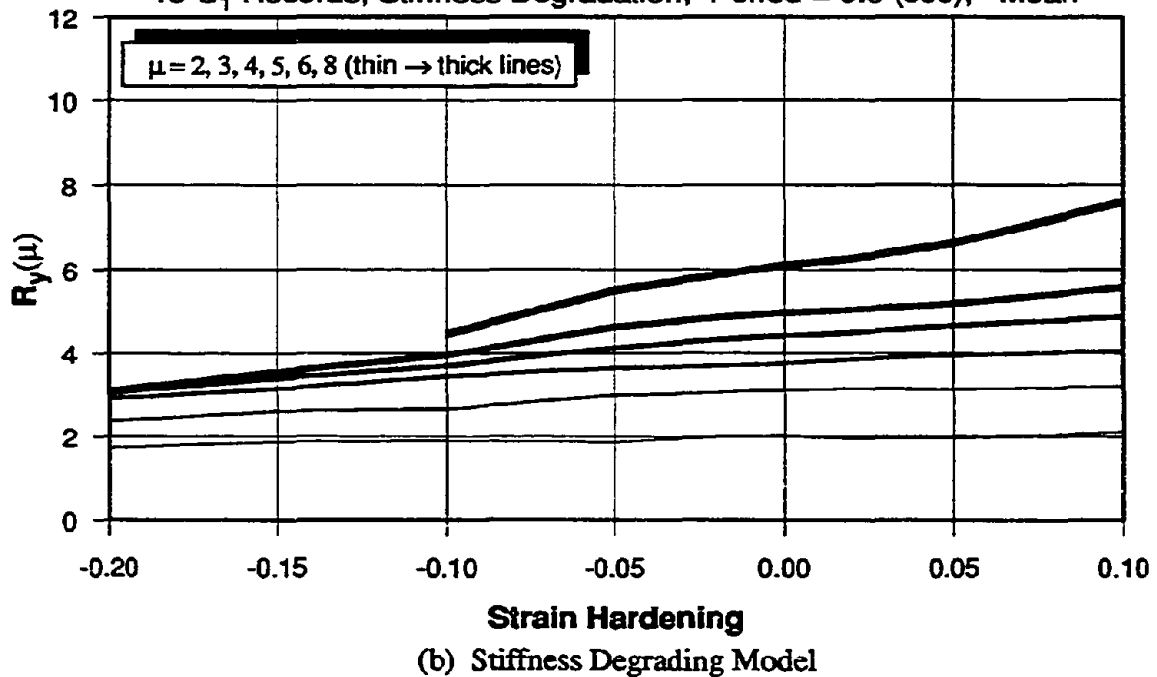
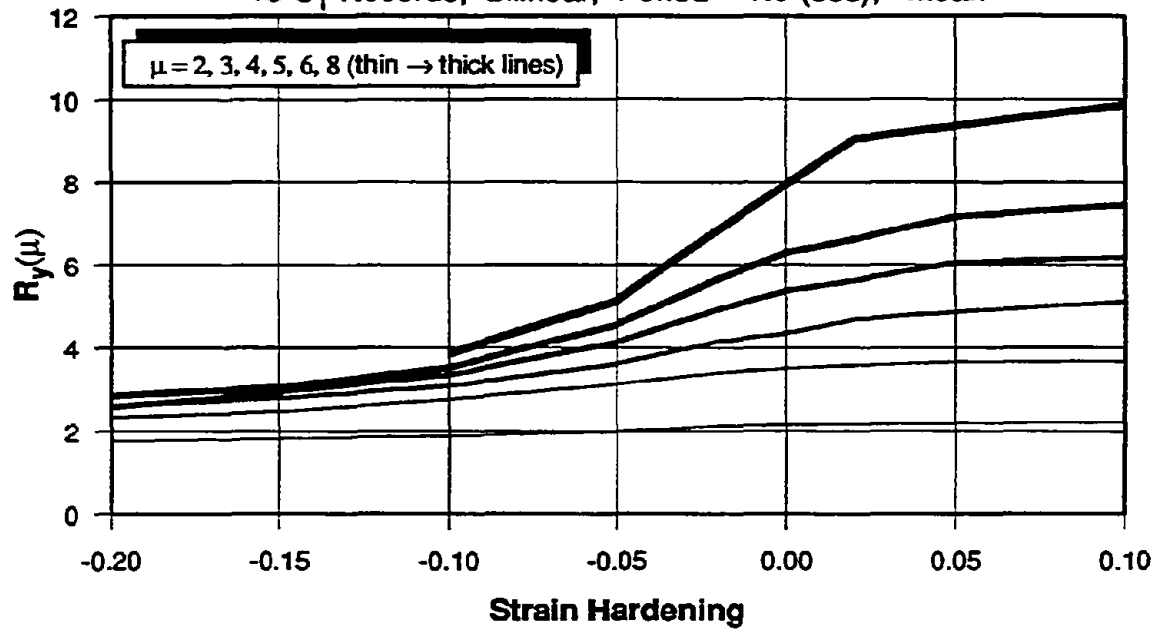


Fig. 3.22 Effect of Strain Hardening/Softening on R-factor for System with $T = 0.50$ sec.

EFFECT OF STRAIN HARDENING/SOFTENING ON $R_y(\mu)$

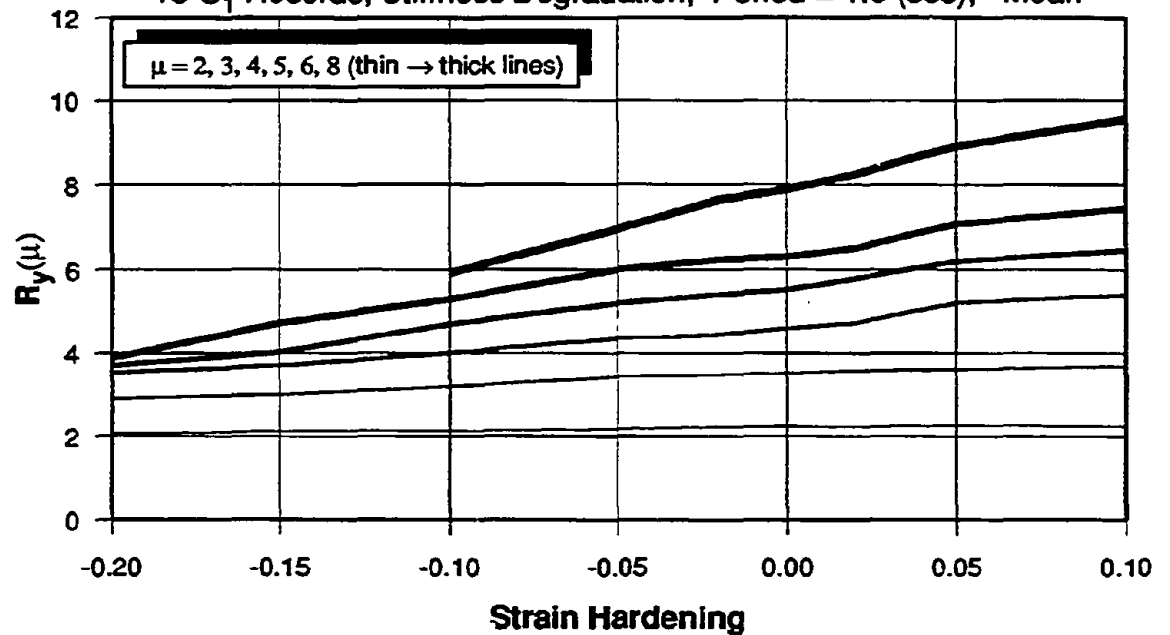
15- S_1 Records, Bilinear, Period = 1.0 (sec), Mean



(a) Bilinear Model

EFFECT OF STRAIN HARDENING/SOFTENING ON $R_y(\mu)$

15- S_1 Records, Stiffness Degradation, Period = 1.0 (sec), Mean

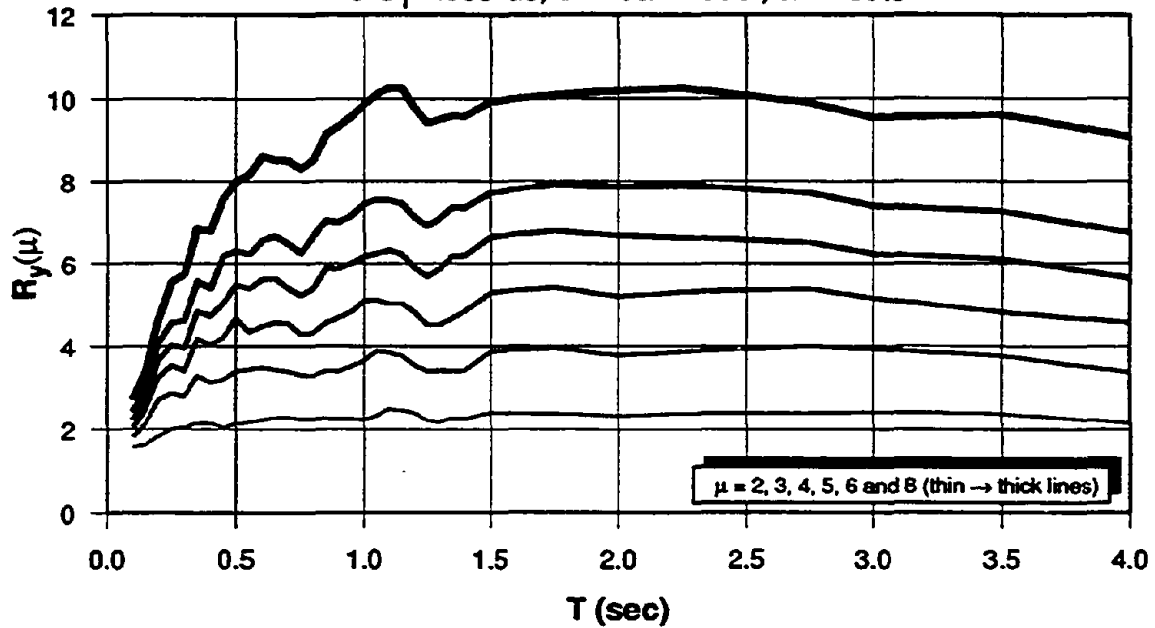


(b) Stiffness Degrading Model

Fig. 3.23 Effect of Strain Hardening/Softening on R-factor for System with $T = 1.0$ sec.

MEAN OF STRENGTH REDUCTION FACTORS, $R_y(\mu)$

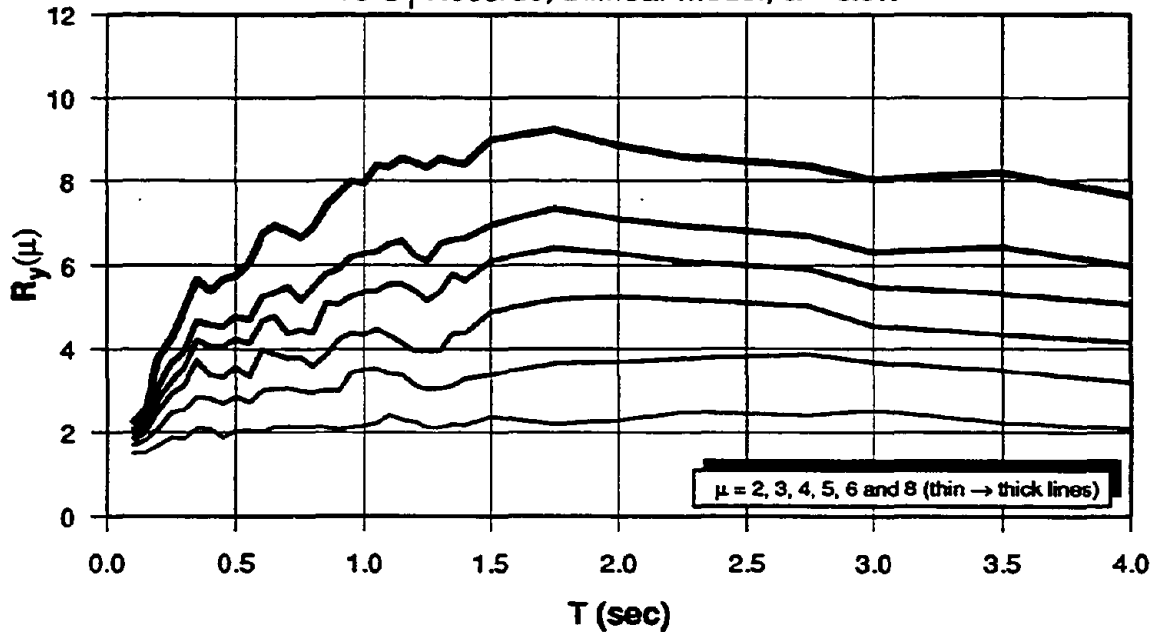
15-S₁ Records, Bilinear Model, $\alpha = +10\%$



(a) Bilinear Model with +10% Strain Hardening

MEAN OF STRENGTH REDUCTION FACTORS, $R_y(\mu)$

15-S₁ Records, Bilinear Model, $\alpha = 0.0\%$

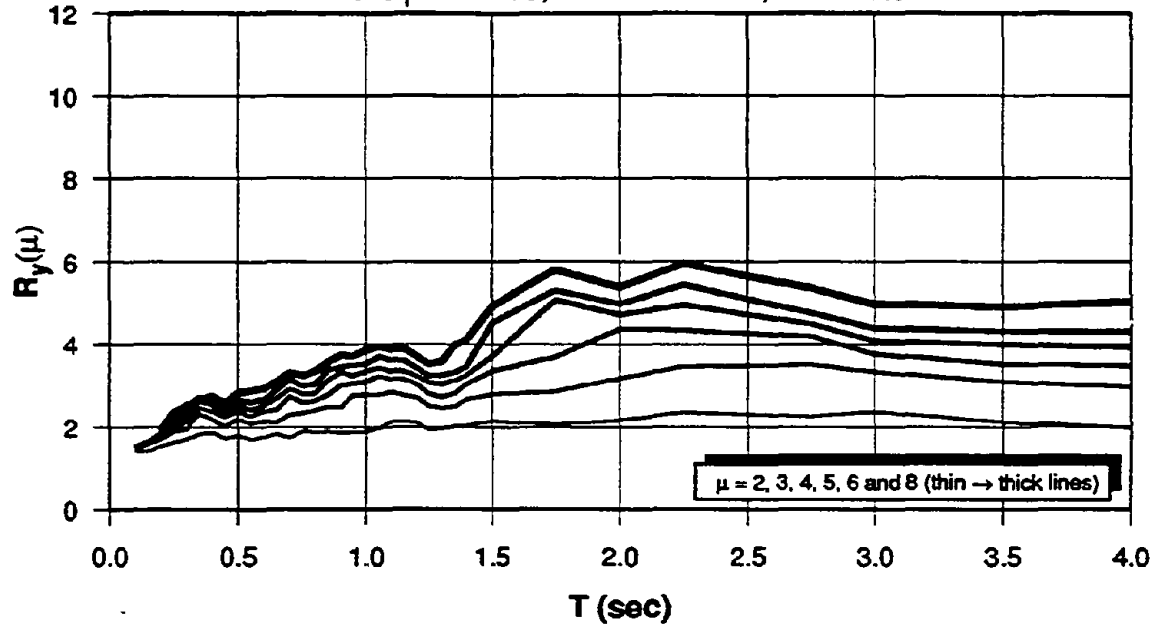


(b) Bilinear Model with Zero Strain Hardening

Fig. 3.24 Strength Reduction Factors for Bilinear Systems with $\alpha = 0.0$ and +10%

MEAN OF STRENGTH REDUCTION FACTORS, $R_y(\mu)$

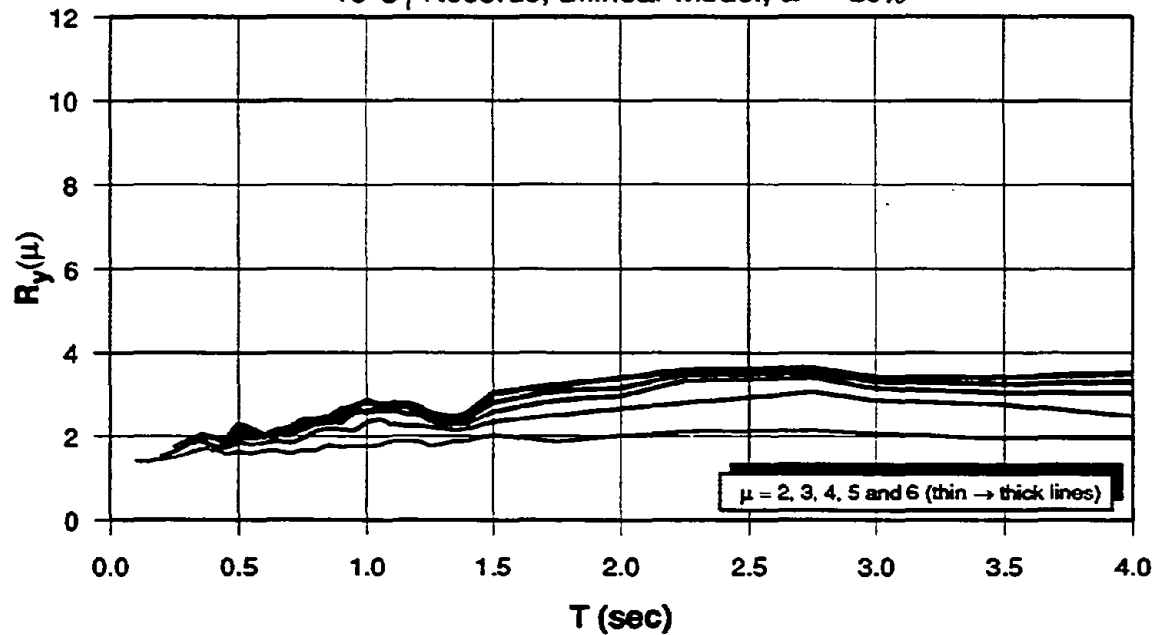
15- S_1 Records, Bilinear Model, $\alpha = -10\%$



(a) Bilinear Model with -10% Strain Hardening

MEAN OF STRENGTH REDUCTION FACTORS, $R_y(\mu)$

15- S_1 Records, Bilinear Model, $\alpha = -20\%$

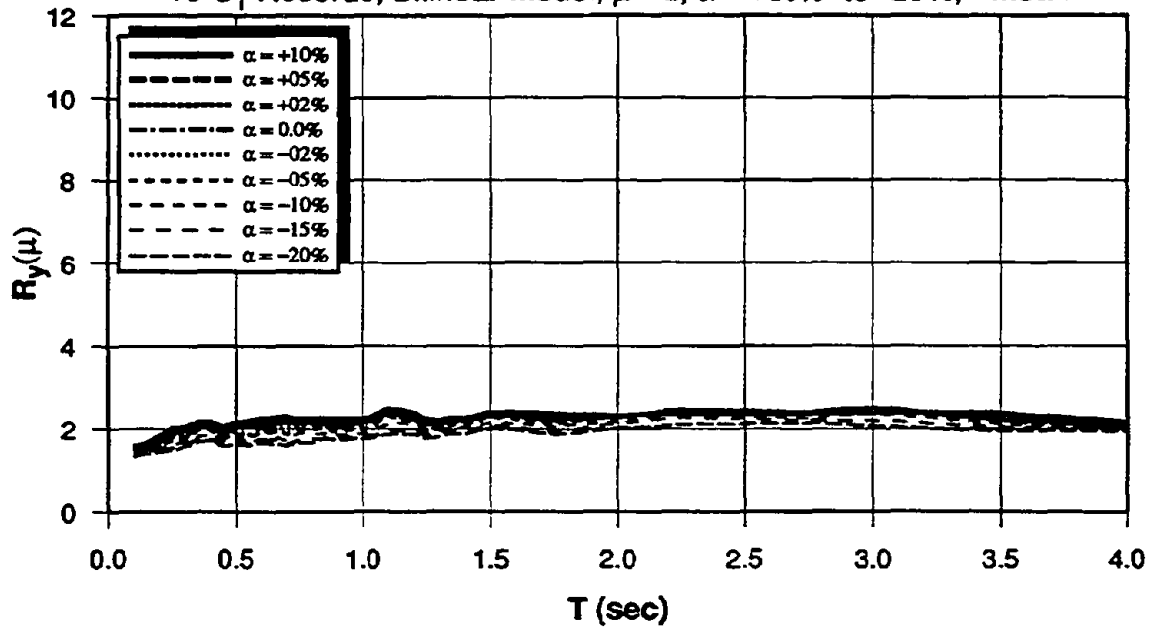


(b) Bilinear Model with -20% Strain Hardening

Fig. 3.25 Strength Reduction Factors for Bilinear Systems with $\alpha = -10$ and -20%

EFFECT OF STRAIN HARDENING/SOFTENING ON $R_y(\mu)$

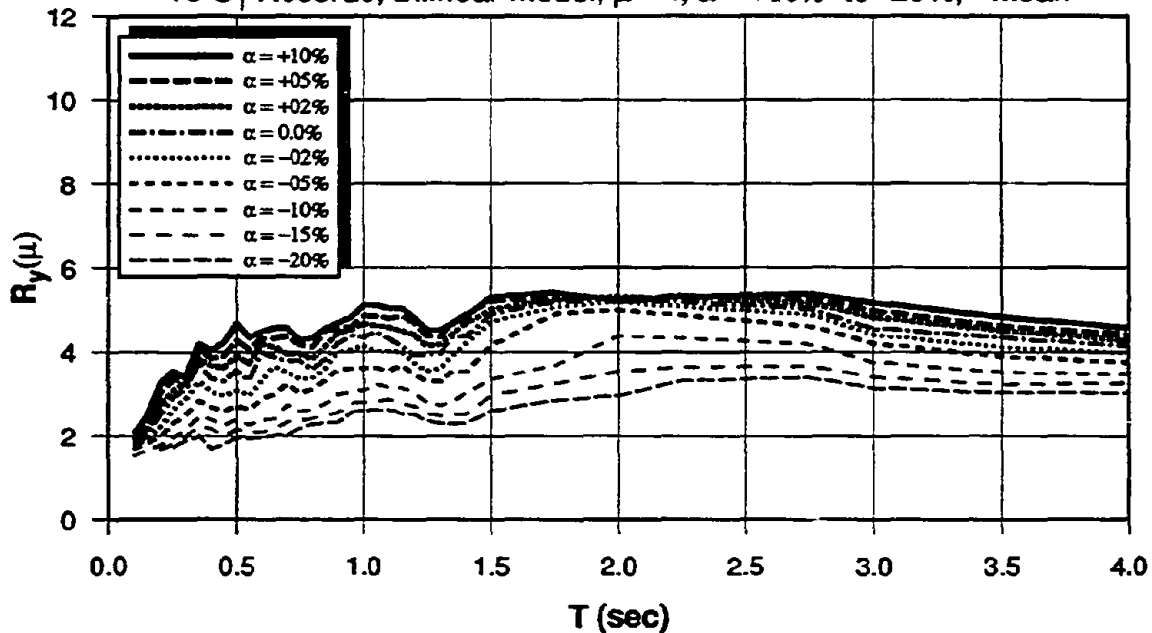
15- S_1 Records, Bilinear Model, $\mu = 2$, $\alpha = +10\%$ to -20% , - Mean



(a) Bilinear Model with Ductility $\mu = 2$

EFFECT OF STRAIN HARDENING/SOFTENING ON $R_y(\mu)$

15- S_1 Records, Bilinear Model, $\mu = 4$, $\alpha = +10\%$ to -20% , - Mean

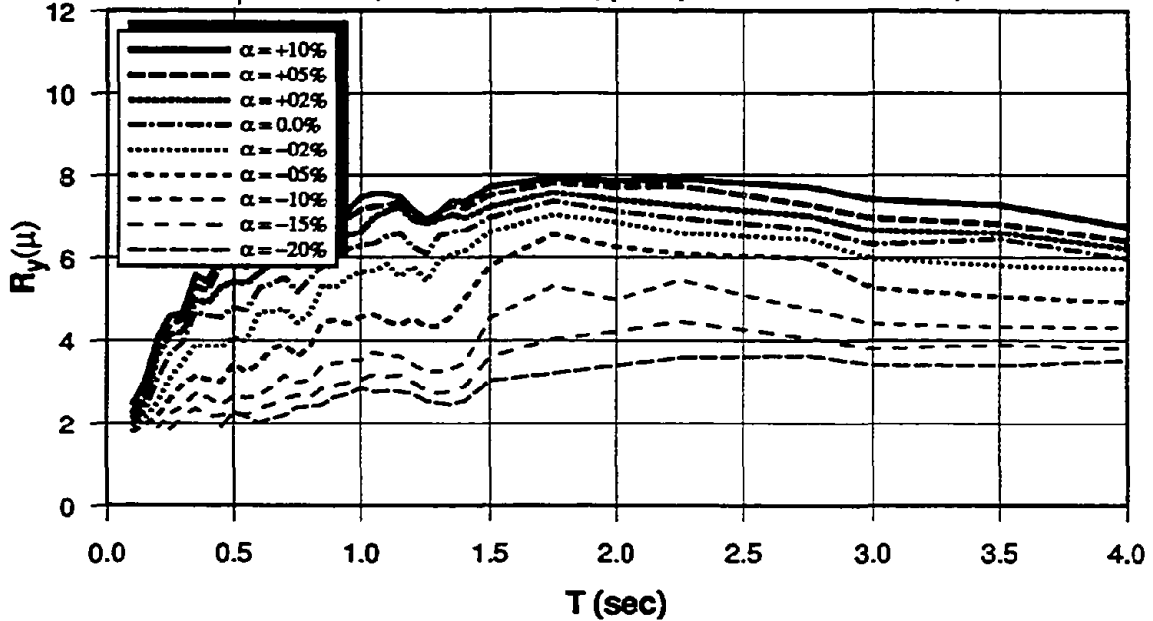


(b) Bilinear Model with Ductility $\mu = 4$

Fig. 3.26 Variation of R-factor with Strain Hardening Using Bilinear Model

EFFECT OF STRAIN HARDENING/SOFTENING ON $R_y(\mu)$

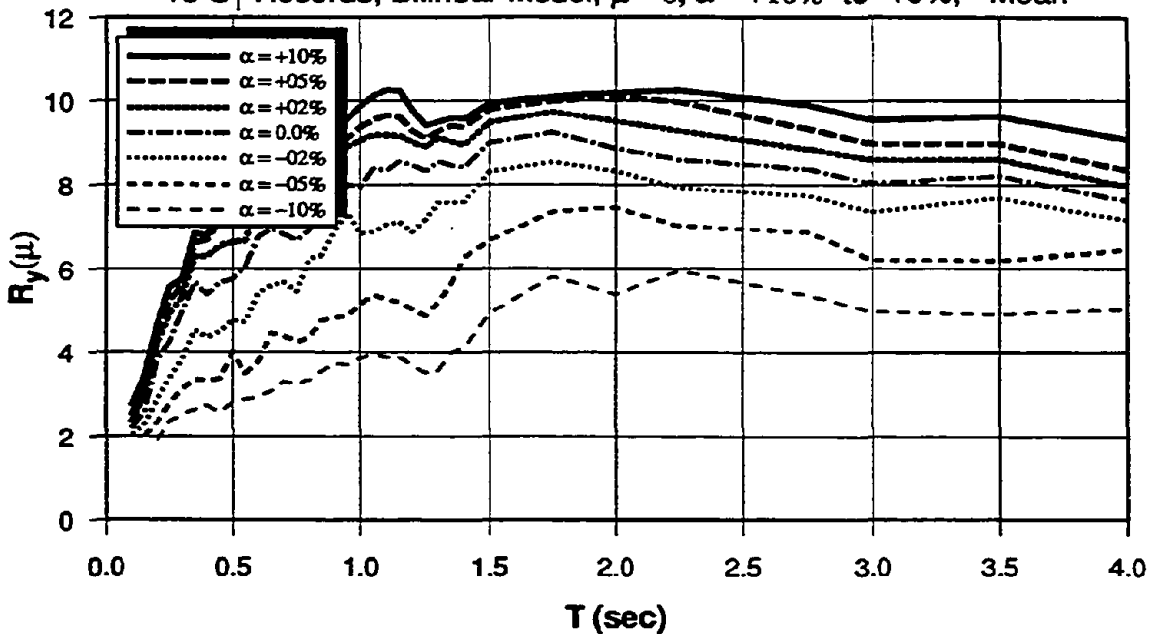
15-S₁ Records, Bilinear Model, $\mu = 6$, $\alpha = +10\%$ to -20% , - Mean



(a) Bilinear Model with Ductility $\mu = 6$

EFFECT OF STRAIN HARDENING/SOFTENING ON $R_y(\mu)$

15-S₁ Records, Bilinear Model, $\mu = 8$, $\alpha = +10\%$ to -10% , - Mean

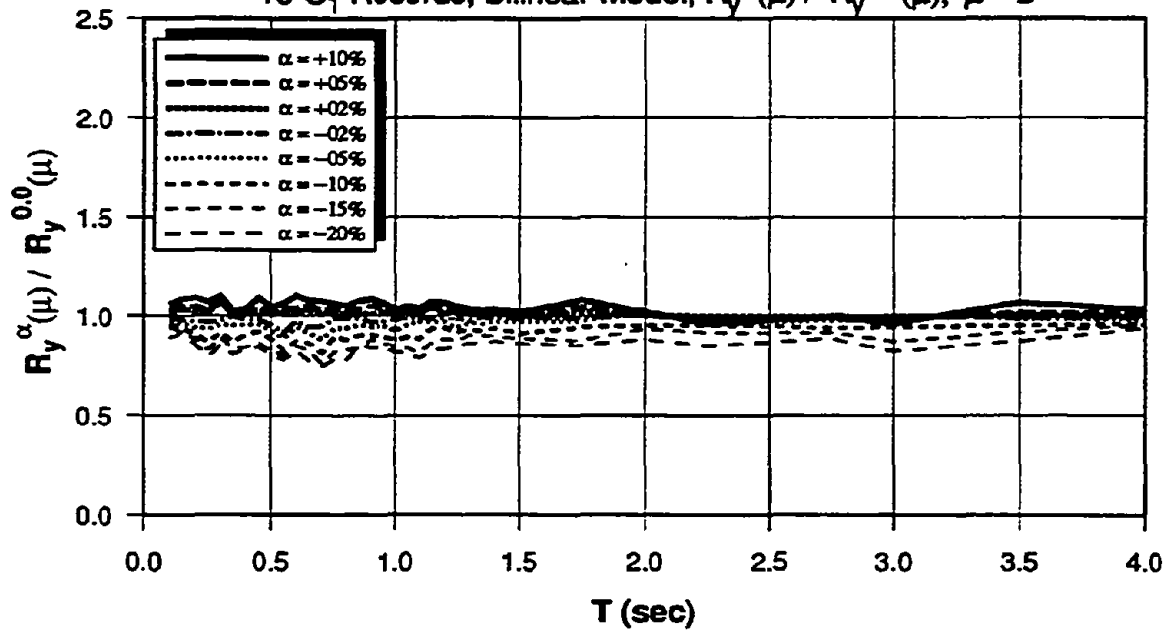


(b) Bilinear Model with Ductility $\mu = 8$

Fig. 3.27 Variation of R-factor with Strain Hardening Using Bilinear Model

EFFECT OF STRAIN HARDENING/SOFTENING ON $R_y(\mu)$

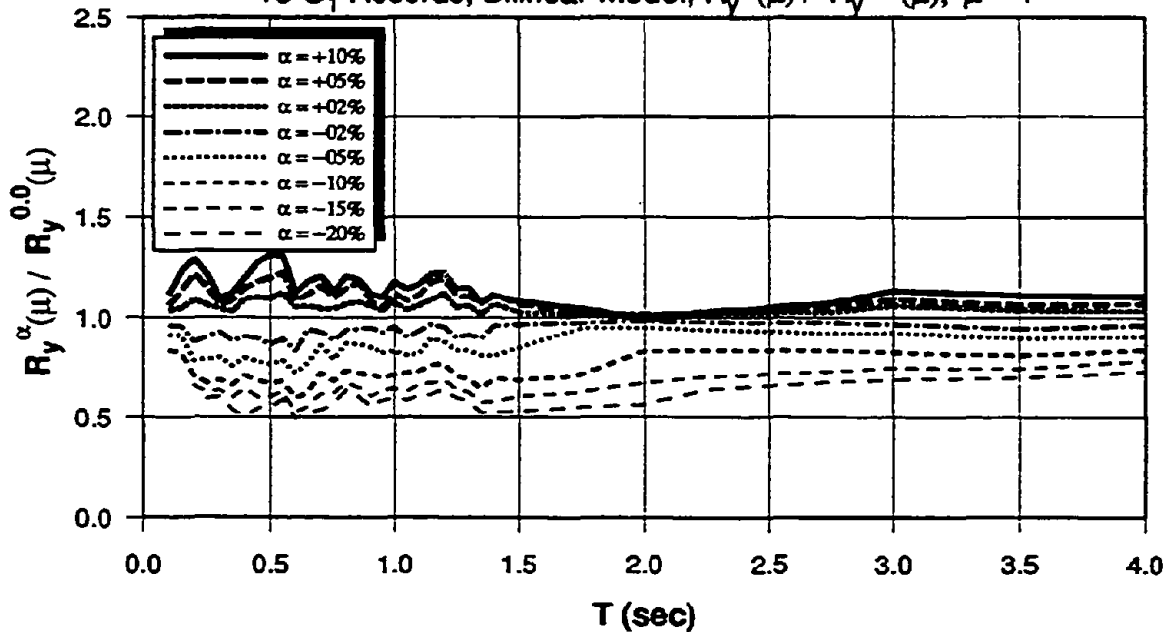
15-S₁ Records, Bilinear Model, $R_y^\alpha(\mu) / R_y^{0.0}(\mu)$, $\mu = 2$



(a) Bilinear Systems with Ductility $\mu = 2$

EFFECT OF STRAIN HARDENING/SOFTENING ON $R_y(\mu)$

15-S₁ Records, Bilinear Model, $R_y^\alpha(\mu) / R_y^{0.0}(\mu)$, $\mu = 4$

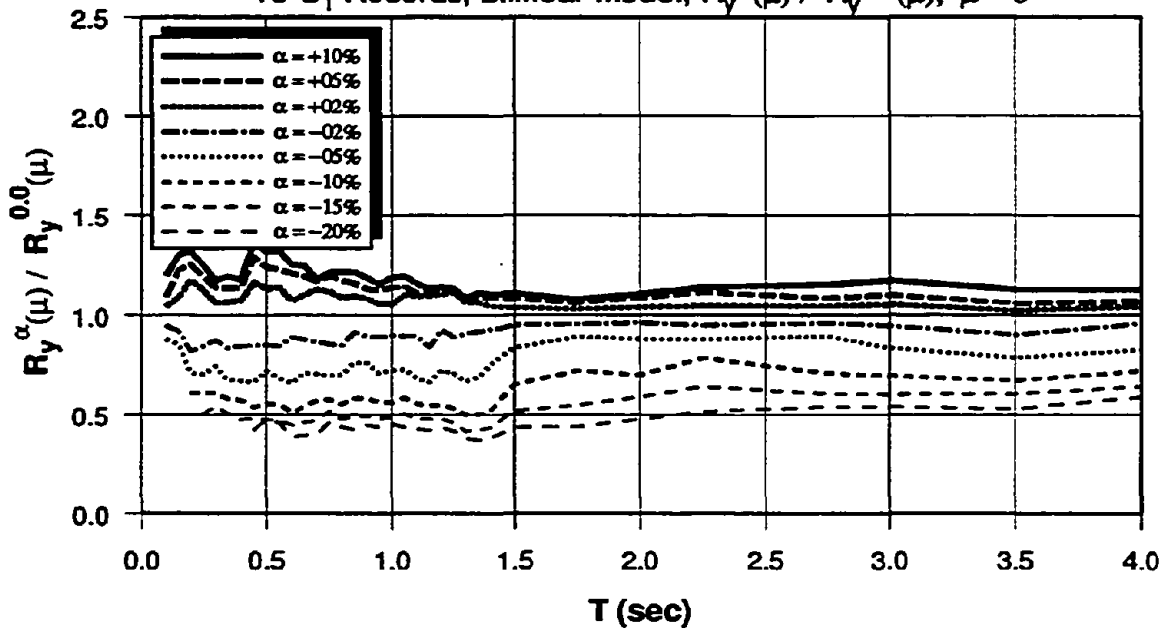


(b) Bilinear Systems with Ductility $\mu = 4$

Fig. 3.28 Effects of Strain Hardening/Softening on R-factors for Bilinear Systems with $\mu = 2, 4$

EFFECT OF STRAIN HARDENING/SOFTENING ON $R_y(\mu)$

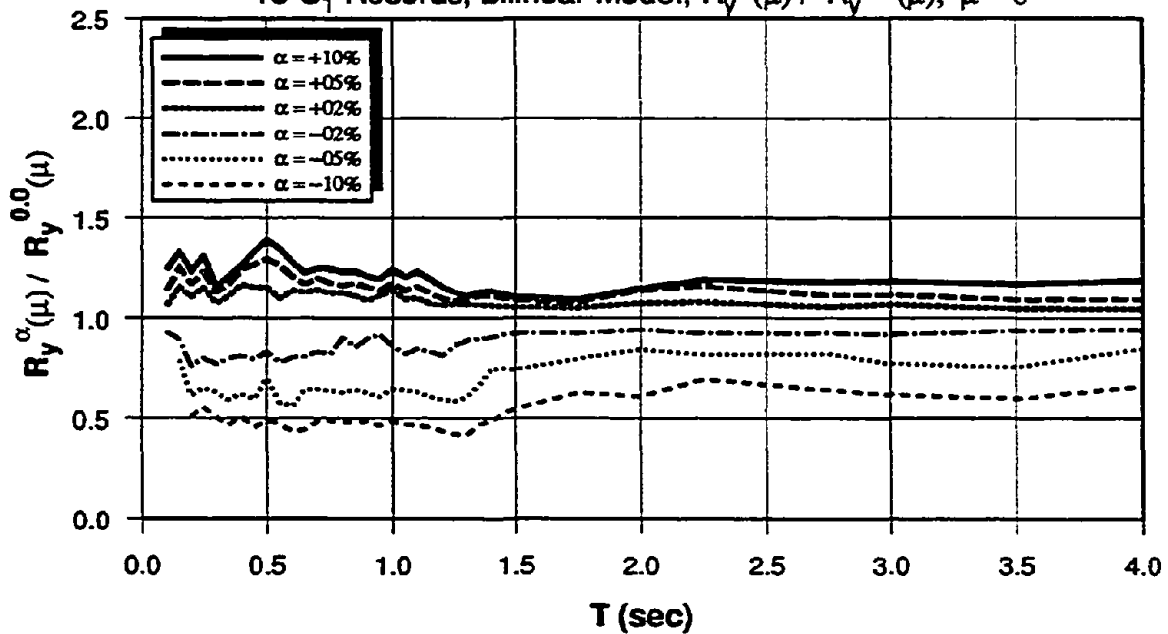
15-S₁ Records, Bilinear Model, $R_y^\alpha(\mu) / R_y^{0.0}(\mu)$, $\mu = 6$



(a) Bilinear Systems with Ductility $\mu = 6$

EFFECT OF STRAIN HARDENING/SOFTENING ON $R_y(\mu)$

15-S₁ Records, Bilinear Model, $R_y^\alpha(\mu) / R_y^{0.0}(\mu)$, $\mu = 8$

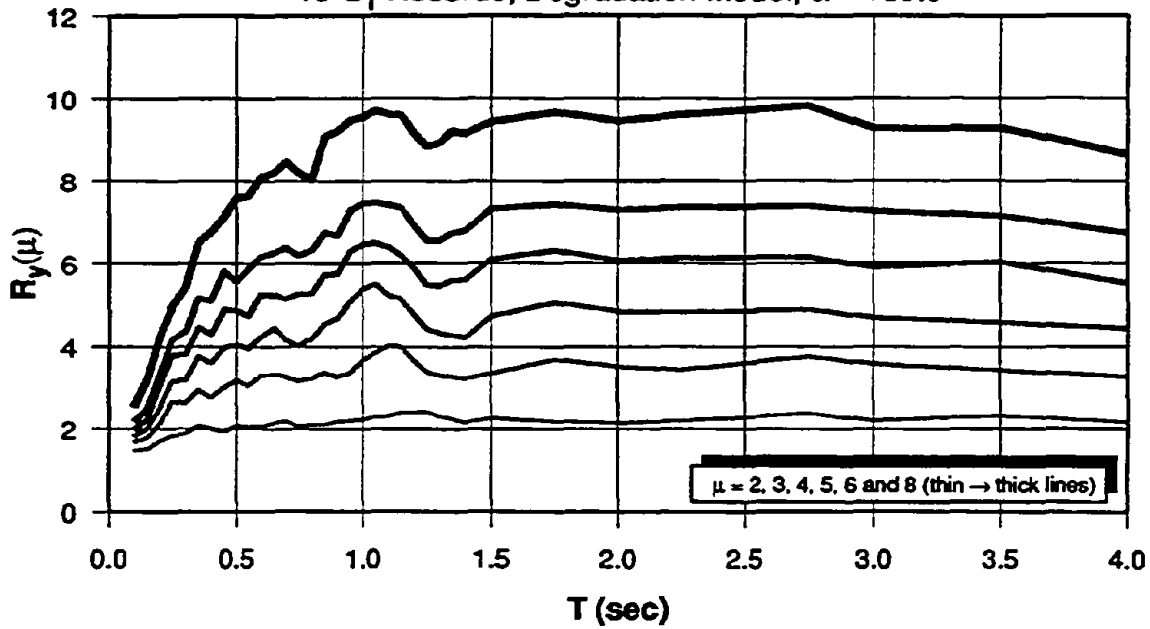


(b) Bilinear Systems with Ductility $\mu = 8$

Fig. 3.29 Effects of Strain Hardening/Softening on R-factors for Bilinear Systems with $\mu = 6, 8$

MEAN OF STRENGTH REDUCTION FACTORS, $R_y(\mu)$

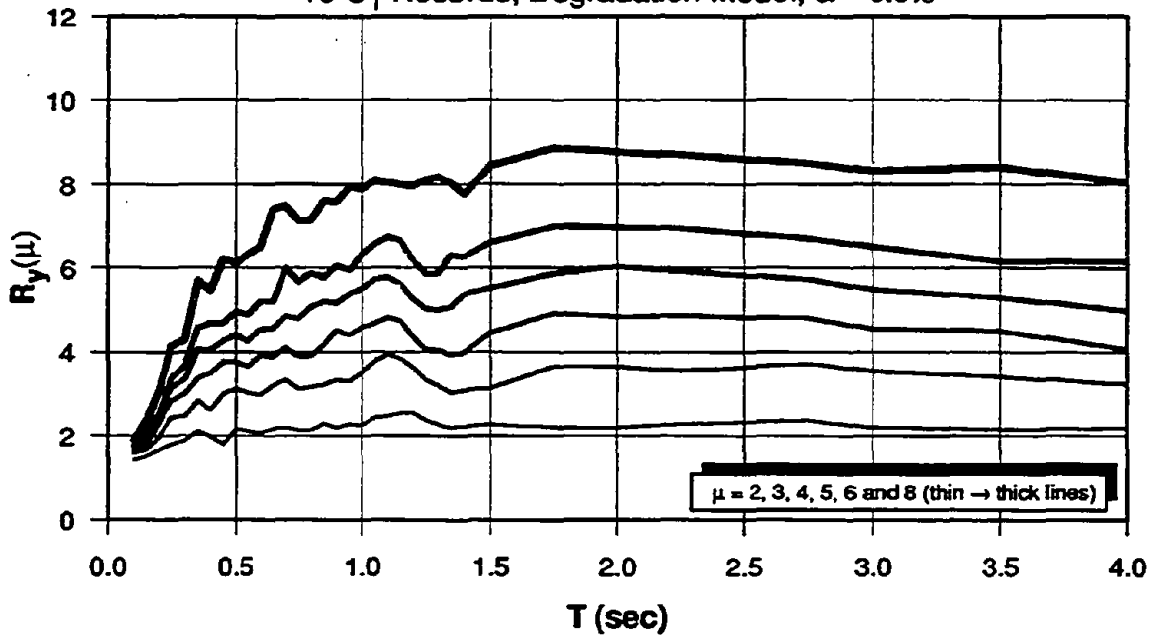
15-S₁ Records, Degradation Model, $\alpha = +10\%$



(a) Degradation Model with +10% Strain Hardening

MEAN OF STRENGTH REDUCTION FACTORS, $R_y(\mu)$

15-S₁ Records, Degradation Model, $\alpha = 0.0\%$

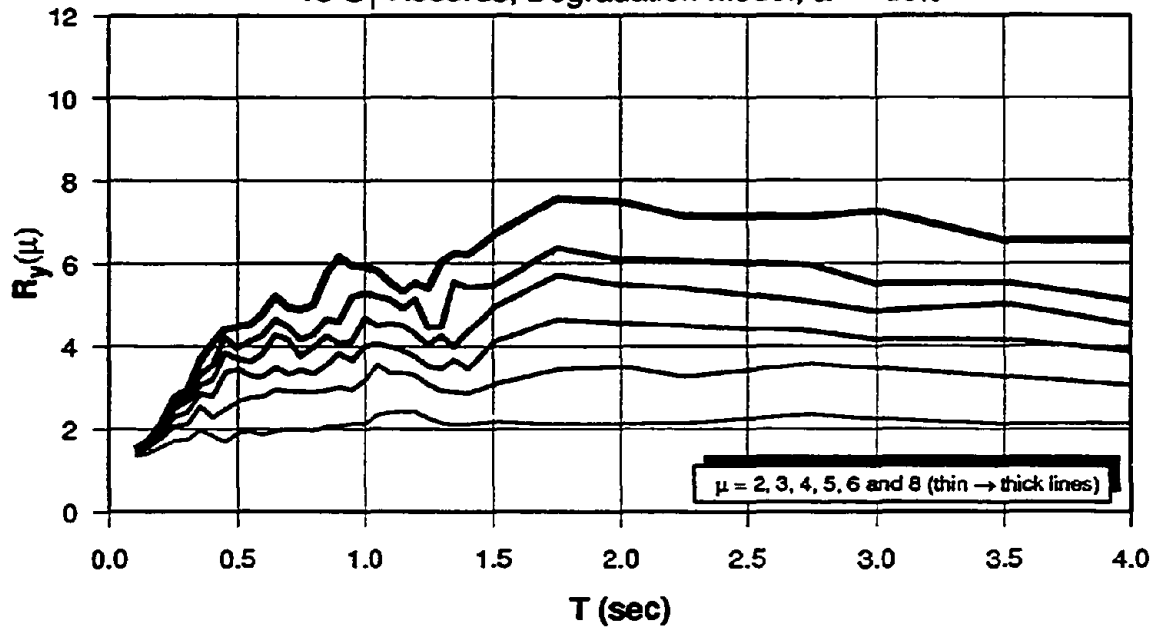


(b) Degradation Model with Zero Strain Hardening

Fig. 3.30 Strength Reduction Factors for Degrading Systems with $\alpha = 0.0$ and +10%

MEAN OF STRENGTH REDUCTION FACTORS, $R_y(\mu)$

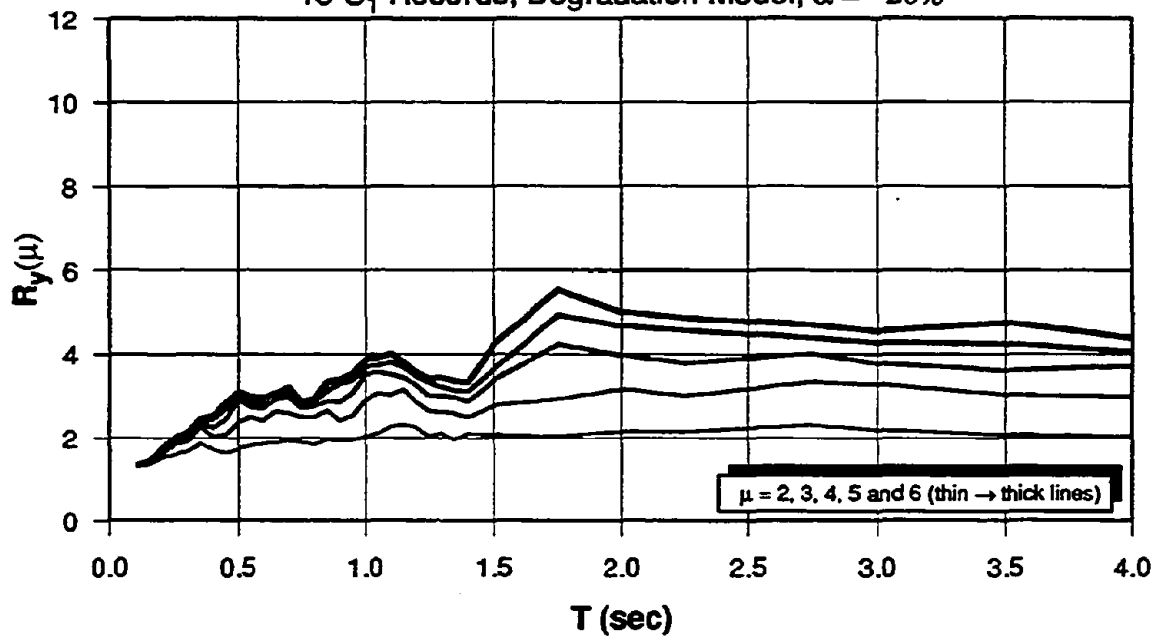
15- S_1 Records, Degradation Model, $\alpha = -10\%$



(a) Degradation Model with -10% Strain Hardening

MEAN OF STRENGTH REDUCTION FACTORS, $R_y(\mu)$

15- S_1 Records, Degradation Model, $\alpha = -20\%$

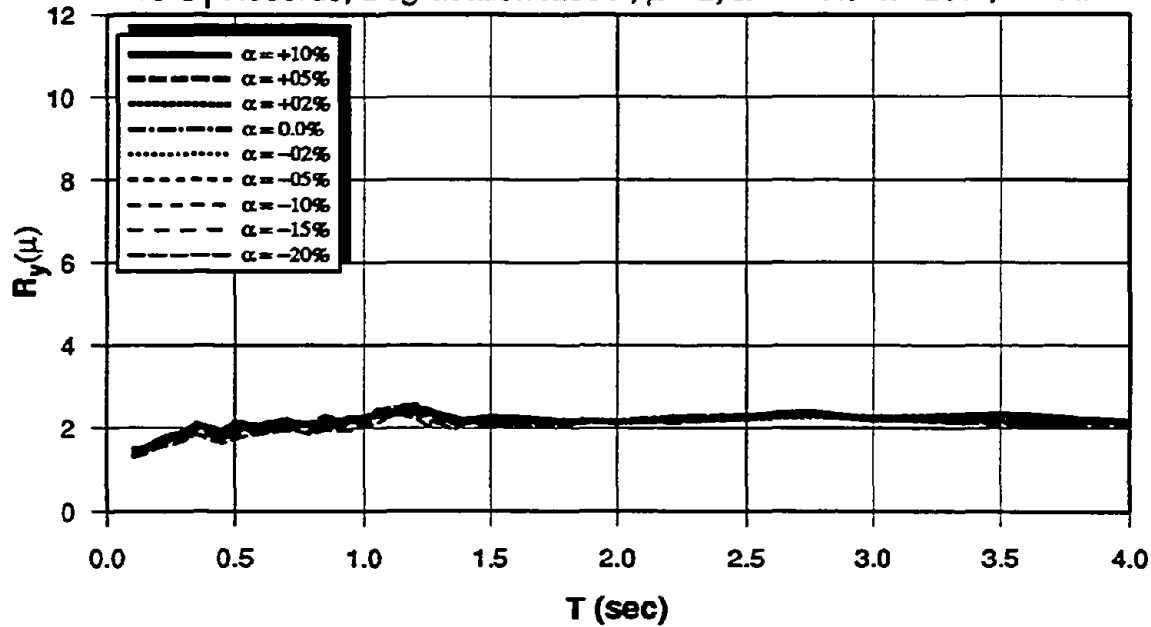


(b) Degradation Model with -20% Strain Hardening

Fig. 3.31 Strength Reduction Factors for Degrading Systems with $\alpha = -10$ and -20%

EFFECT OF STRAIN HARDENING/SOFTENING ON $R_y(\mu)$

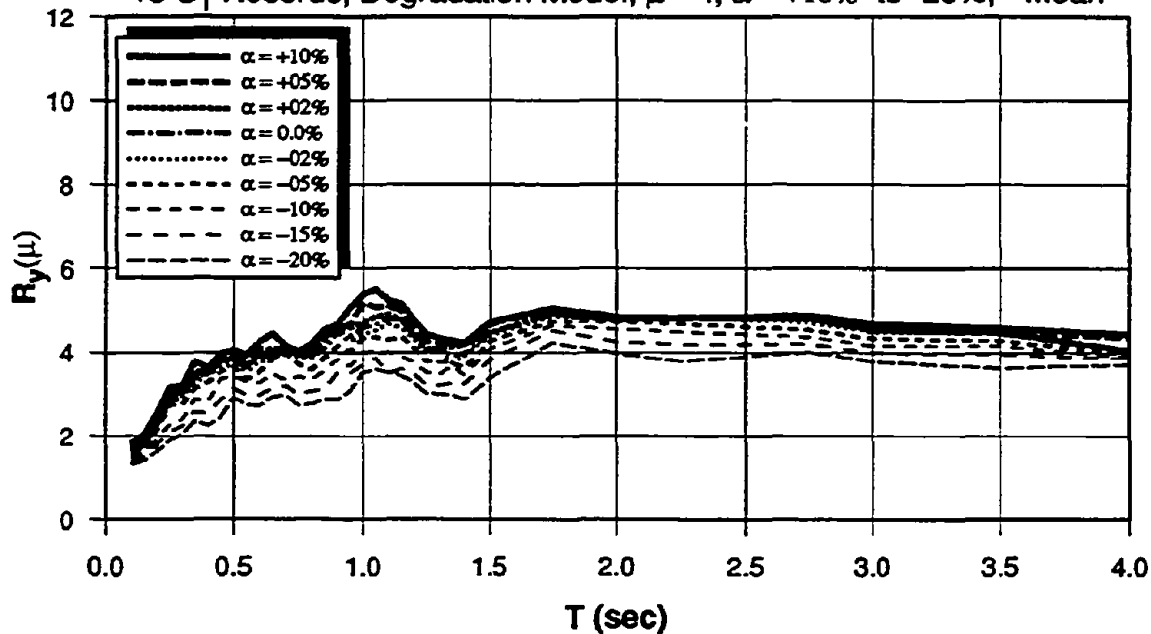
15-S₁ Records, Degradation Model, $\mu = 2$, $\alpha = +10\%$ to -20% , - Mean



(a) Degradation Model with Ductility $\mu = 2$

EFFECT OF STRAIN HARDENING/SOFTENING ON $R_y(\mu)$

15-S₁ Records, Degradation Model, $\mu = 4$, $\alpha = +10\%$ to -20% , - Mean

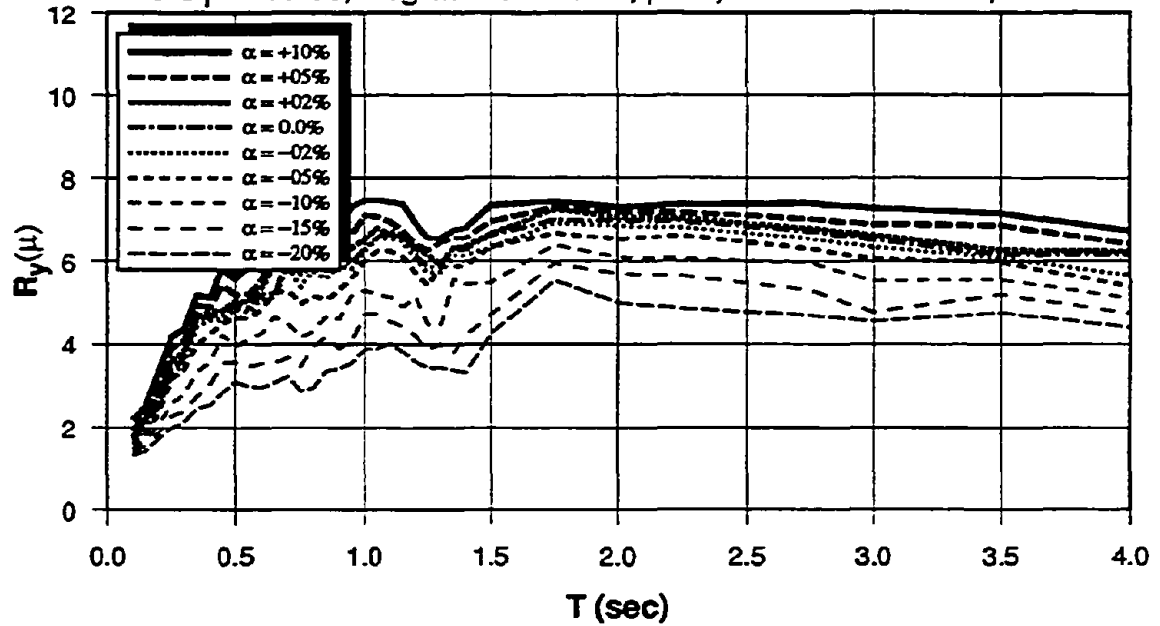


(b) Degradation Model with Ductility $\mu = 4$

Fig. 3.32 Variation of R-factor with Strain Hardening Using Stiffness Degradation Model

EFFECT OF STRAIN HARDENING/SOFTENING ON $R_y(\mu)$

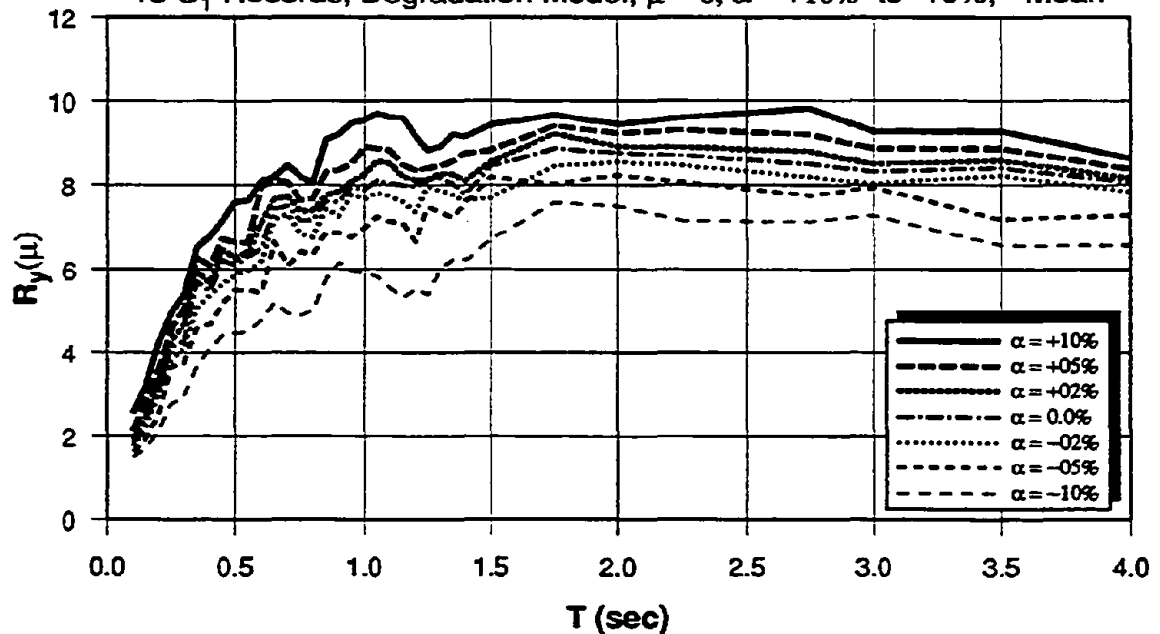
15-S₁ Records, Degradation Model, $\mu = 6$, $\alpha = +10\%$ to -20% , - Mean



(a) Degradation Model with Ductility $\mu = 6$

EFFECT OF STRAIN HARDENING/SOFTENING ON $R_y(\mu)$

15-S₁ Records, Degradation Model, $\mu = 8$, $\alpha = +10\%$ to -10% , - Mean

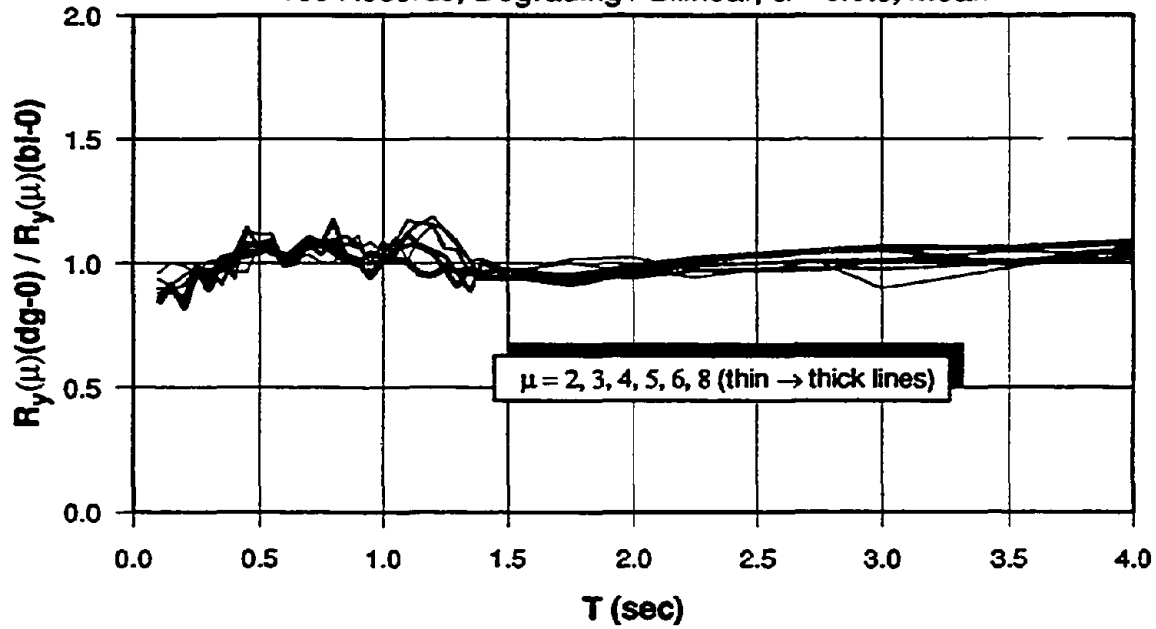


(b) Degradation Model with Ductility $\mu = 8$

Fig. 3.33 Variation of R-factor with Strain Hardening Using Stiffness Degradation Model

EFFECT OF HYSTERESIS MODEL ON R-FACTORS

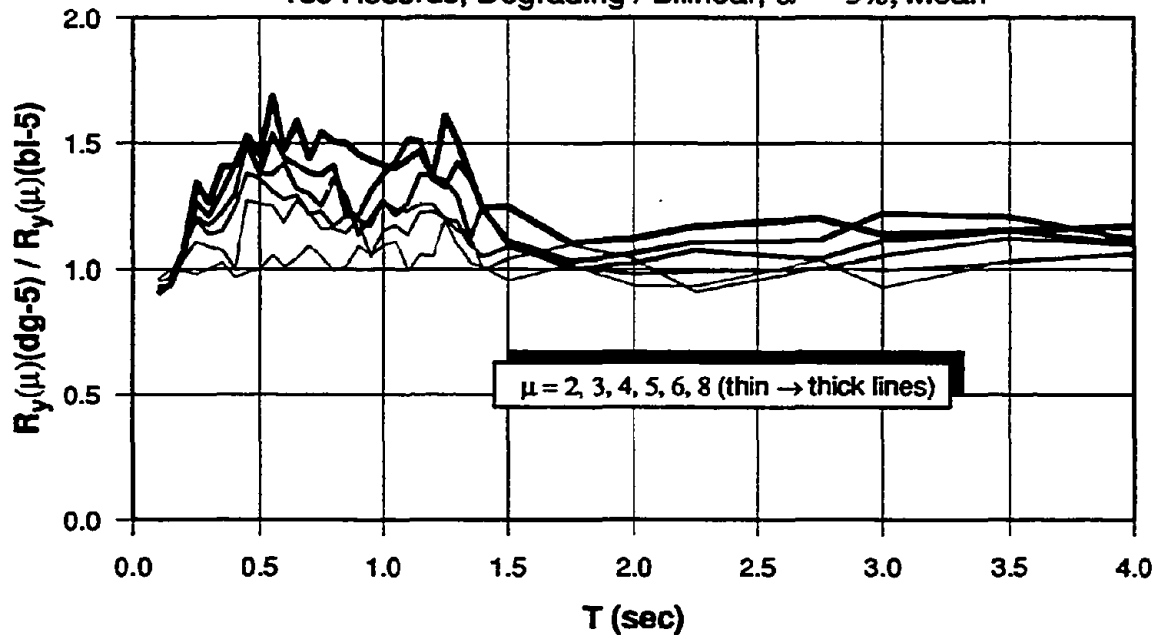
15s Records, Degrading / Bilinear, $\alpha = 0.0\%$, Mean



(a) Ratio of R-factors for Systems with Zero Strain Hardening

EFFECT OF HYSTERESIS MODEL ON R-FACTORS

15s Records, Degrading / Bilinear, $\alpha = -5\%$, Mean

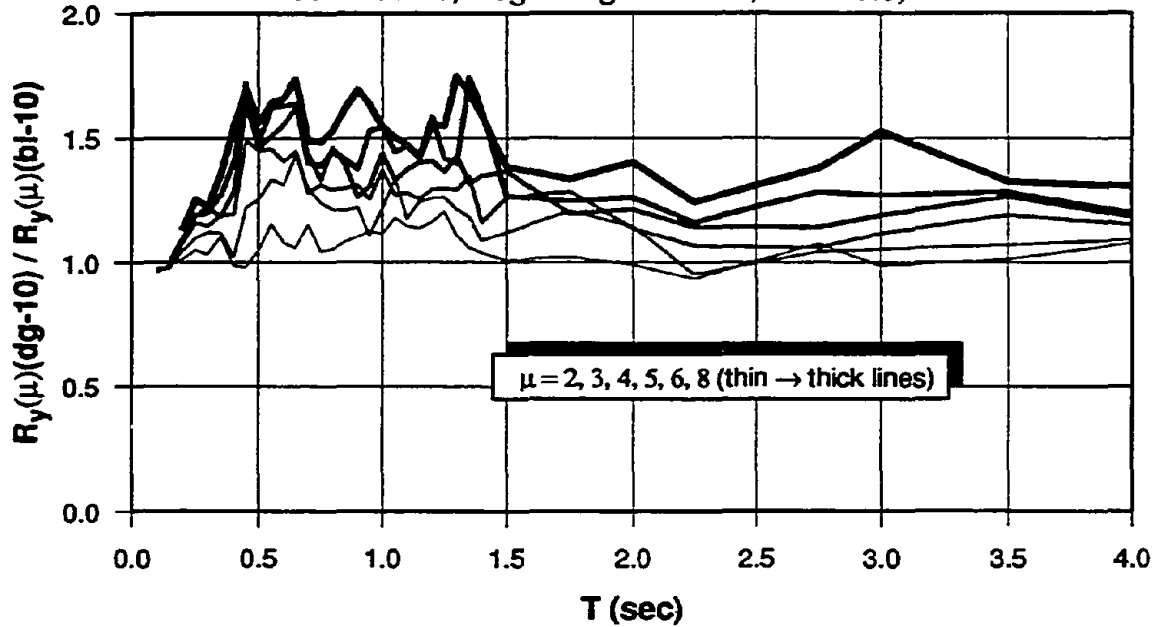


(b) Ratio of R-factors for Systems with -5% Strain Hardening

Fig. 3.34 Effect of Hysteresis Model on the Strength Reduction Factors

EFFECT OF HYSTERESIS MODEL ON R-FACTORS

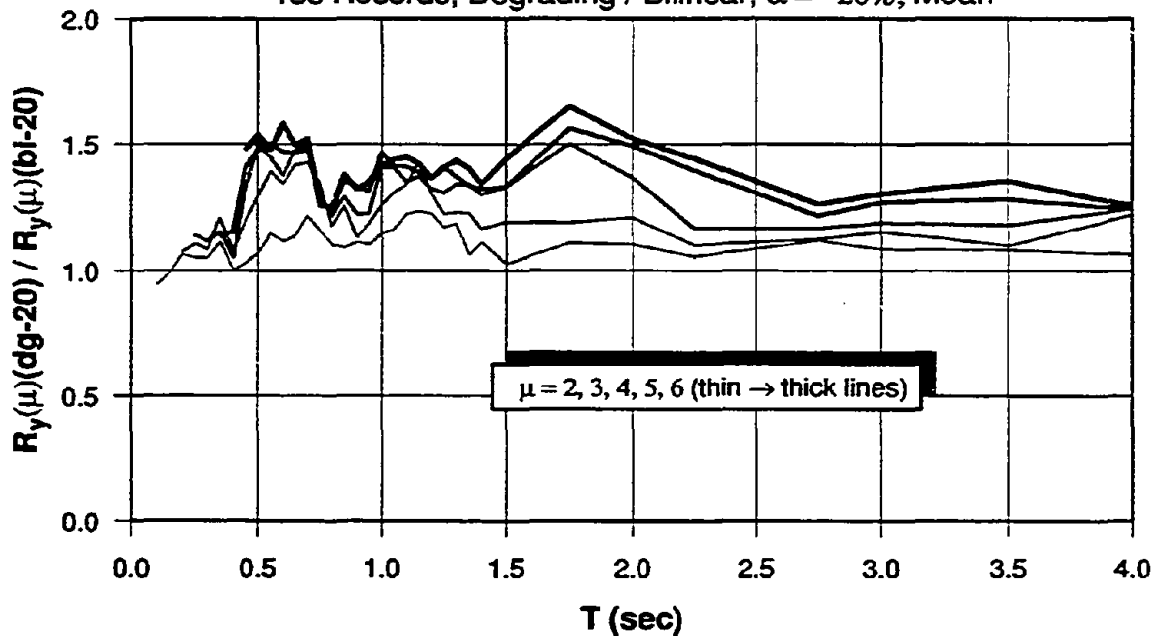
15s Records, Degrading / Bilinear, $\alpha = -10\%$, Mean



(a) Ratio of R-factors for Systems with -10% Strain Hardening

EFFECT OF HYSTERESIS MODEL ON R-FACTORS

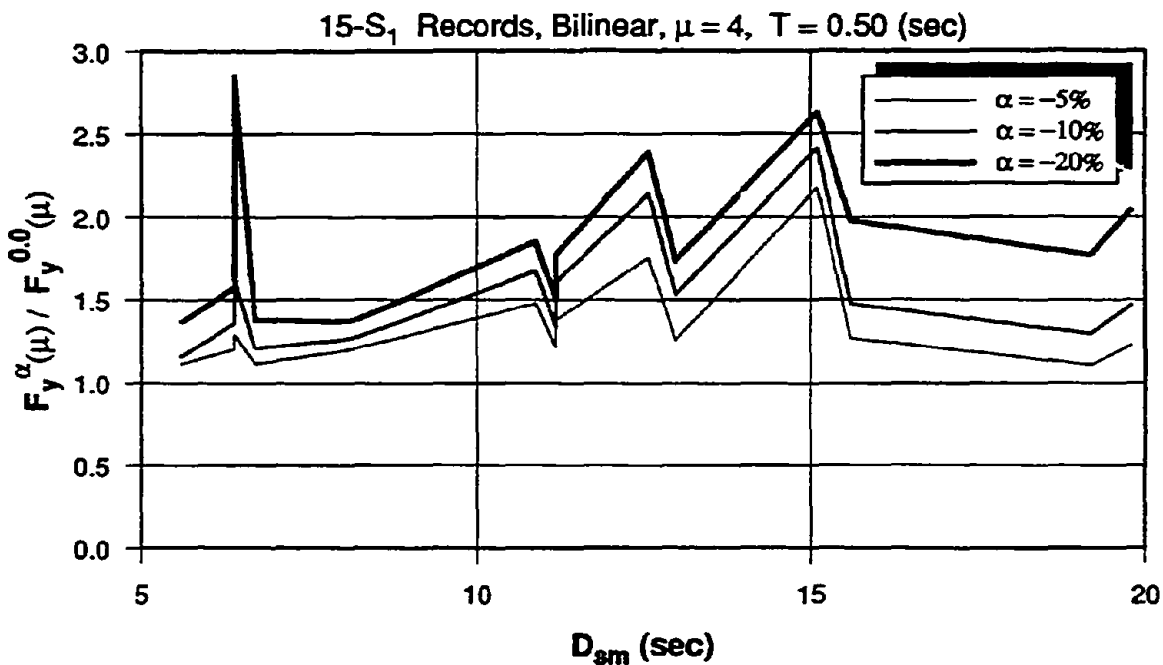
15s Records, Degrading / Bilinear, $\alpha = -20\%$, Mean



(b) Ratio of R-factors for Systems with -20% Strain Hardening

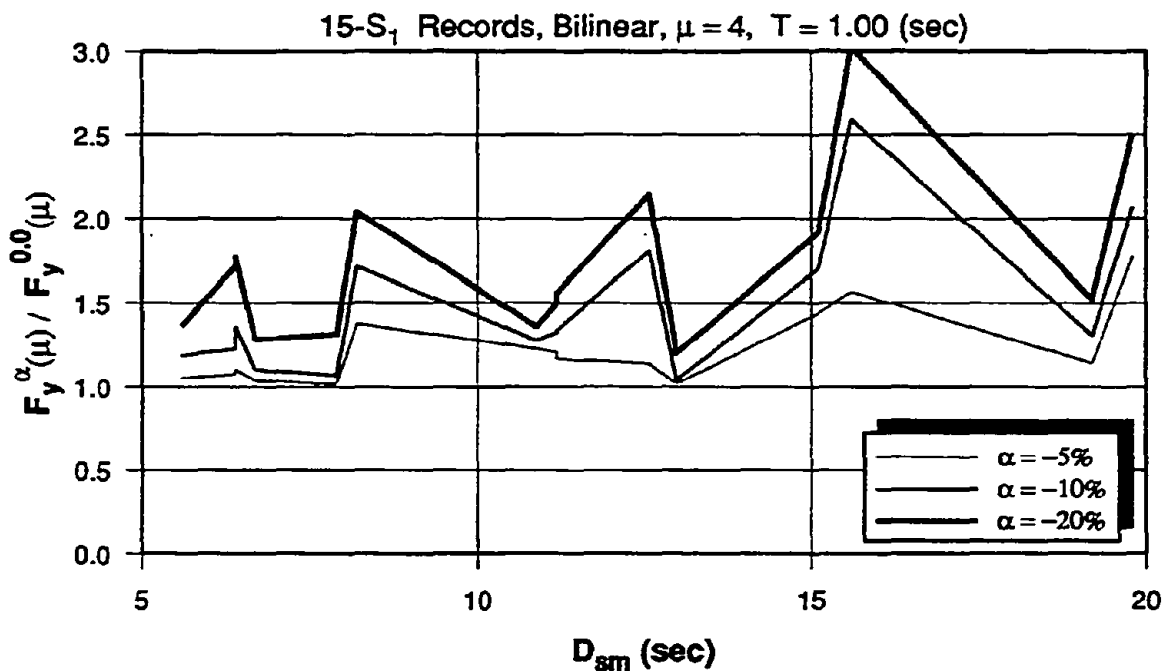
Fig. 3.35 Effect of Hysteresis Model on the Strength Reduction Factors

EFFECT OF STRONG MOTION DURATION ON STRENGTH DEMAND



(a) SDOF System with $T = 0.50$ sec.

EFFECT OF STRONG MOTION DURATION ON STRENGTH DEMAND

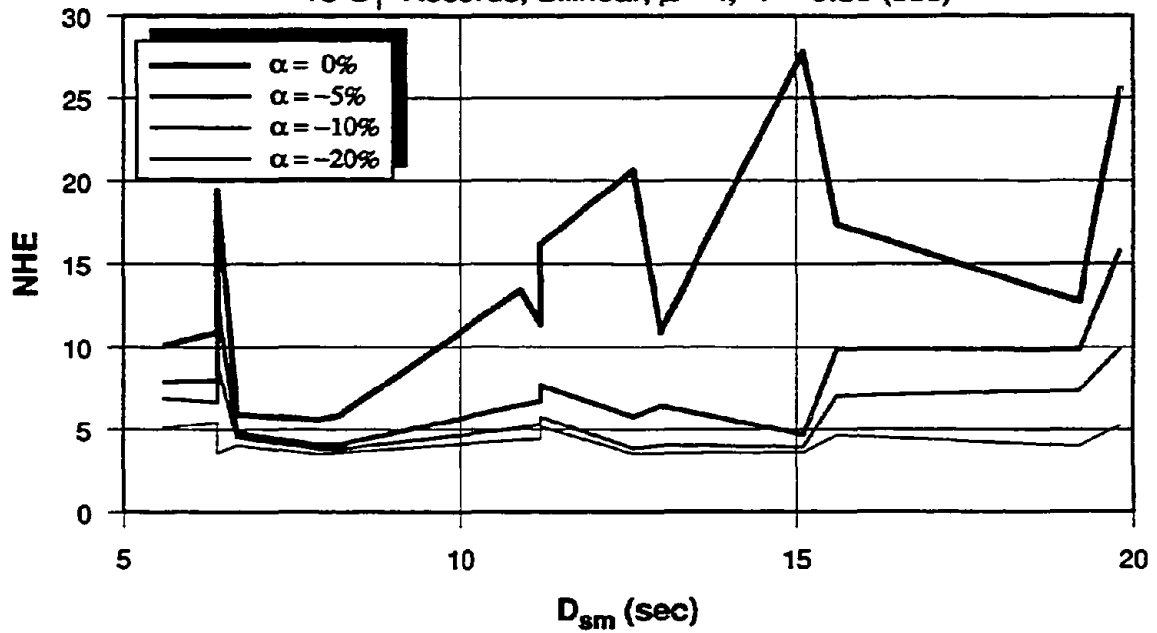


(b) SDOF System with $T = 1.0$ sec.

Fig. 3.36 Effect of Strong Motion Duration on Strength Demand Using Bilinear Models with $\mu = 4$

EFFECT OF STRONG MOTION DURATION ON NHE

15-S₁ Records, Bilinear, $\mu = 4$, $T = 0.50$ (sec)



EFFECT OF STRONG MOTION DURATION ON NHE

15-S₁ Records, Bilinear, $\mu = 4$, $T = 1.0$ (sec)

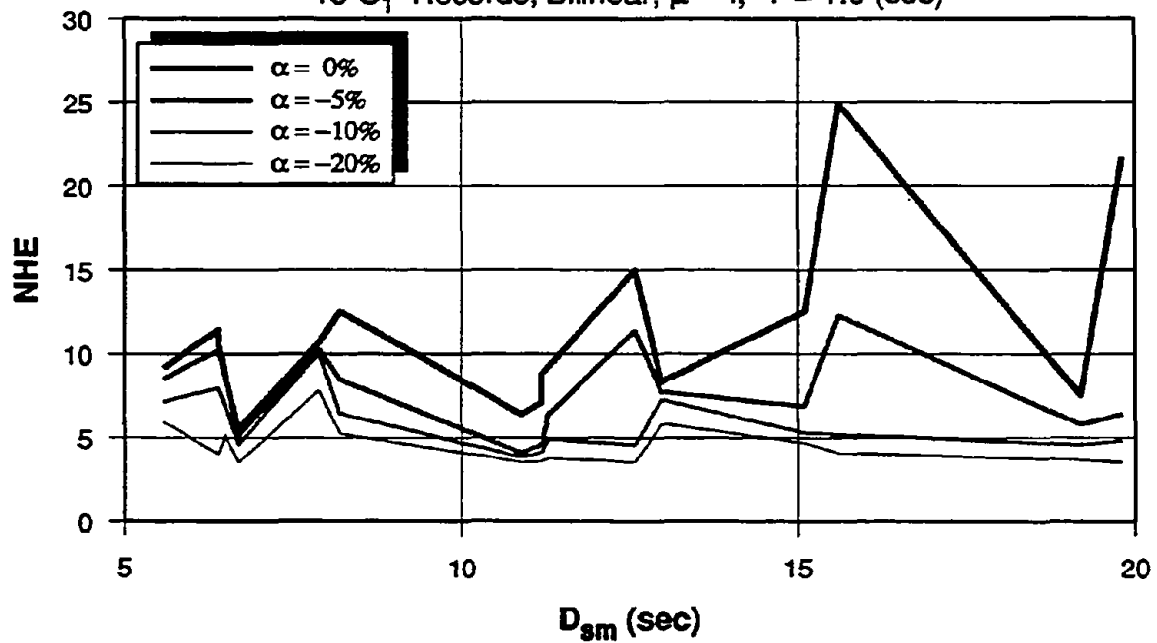
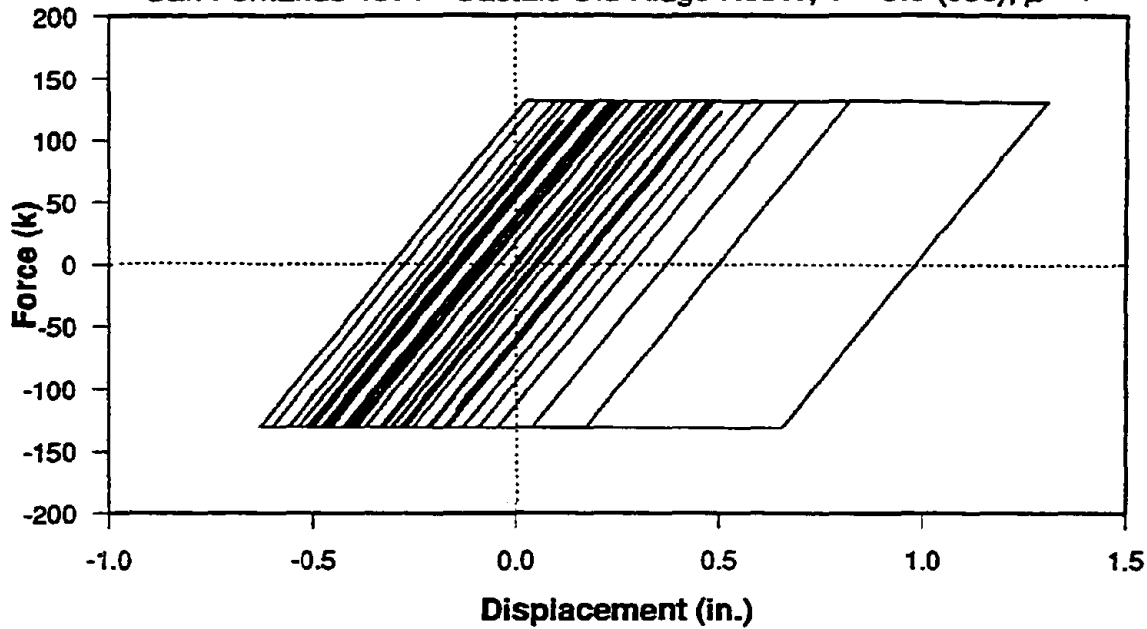


Fig. 3.37 Effect of Strong Motion Duration on NHE Using Bilinear Models with $\mu = 4$

FORCE-DISPLACEMENT RESPONSE - $\alpha = 0.0$

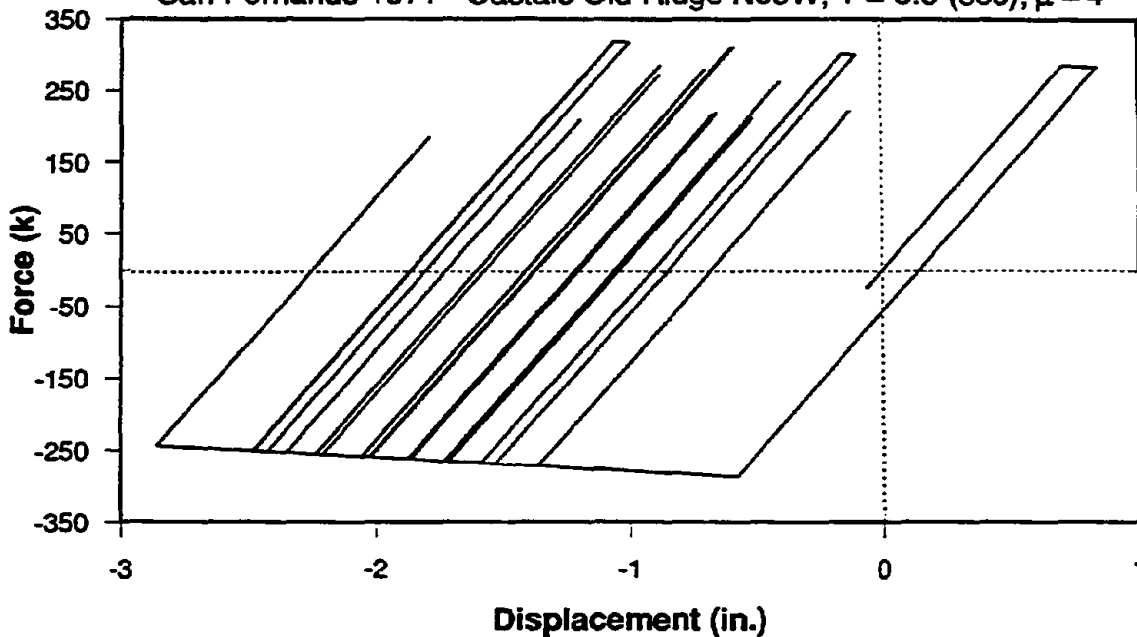
San Fernando 1971 - Castaic Old Ridge N69W, $T = 0.5$ (sec), $\mu = 4$



(a) Bilinear Model - $\alpha = 0$

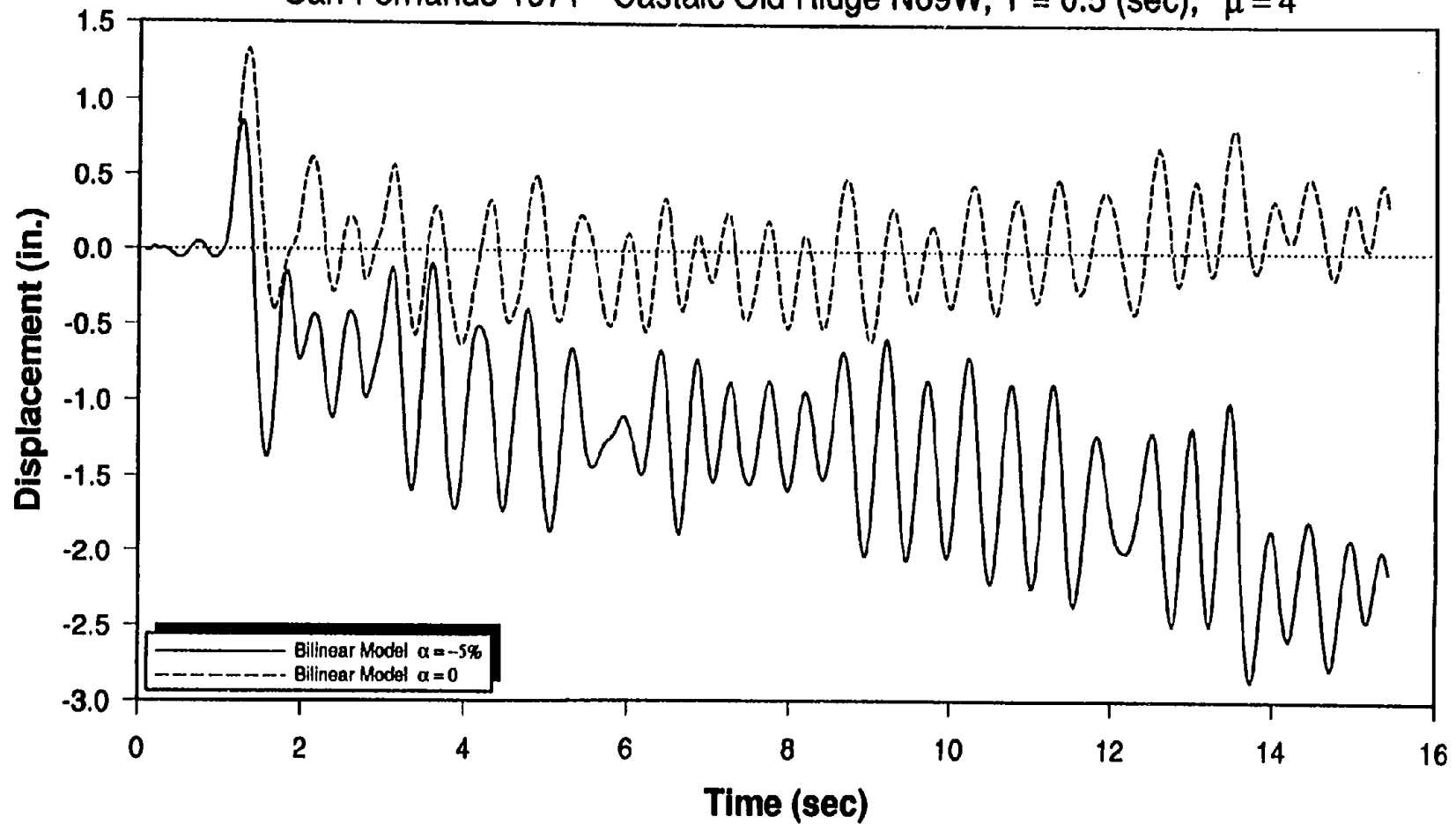
FORCE-DISPLACEMENT RESPONSE - $\alpha = -5\%$

San Fernando 1971 - Castaic Old Ridge N69W, $T = 0.5$ (sec), $\mu = 4$

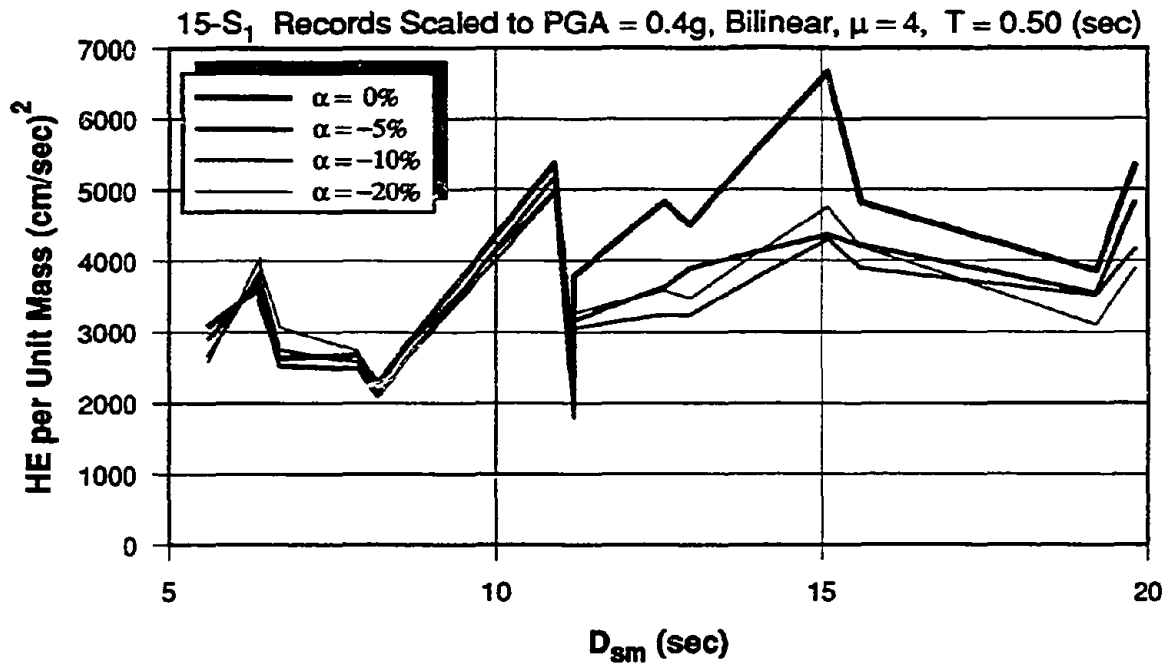


(b) Bilinear Model - $\alpha = -5\%$

Fig. 3.38 Force-Displacement Responses of SDOF System Using Bilinear Model with $\alpha = 0$ and $\alpha = -5\%$

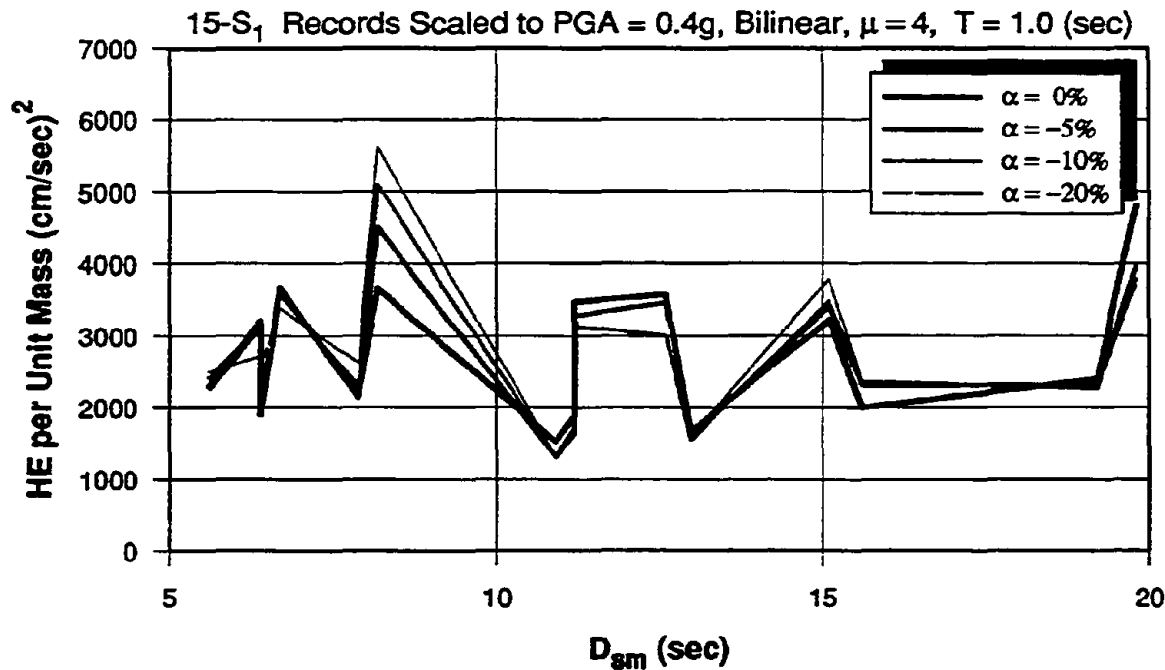
DISPLACEMENT TIME HISTORIES FOR BILINEAR MODELSan Fernando 1971 - Castaic Old Ridge N69W, $T = 0.5$ (sec), $\mu = 4$ Fig. 3.39 Displacement Time Histories of SDOF System Using Bilinear Model with $\alpha = 0$ and $\alpha = -5\%$

EFFECT OF STRONG MOTION DURATION ON HYSTERETIC ENERGY



(a) SDOF System with $T = 0.50$ sec.

EFFECT OF STRONG MOTION DURATION ON HYSTERETIC ENERGY



(b) SDOF System with $T = 1.0$ sec.

Fig. 3.40 Effect of Strong Motion Duration on Hysteretic Energy Using Bilinear Models with $\mu = 4$

NORMALIZED HYSTERETIC ENERGY, NHE (15s.bi-05)

15-S₁ Records, Bilinear, $\alpha = +5\%$, Mean

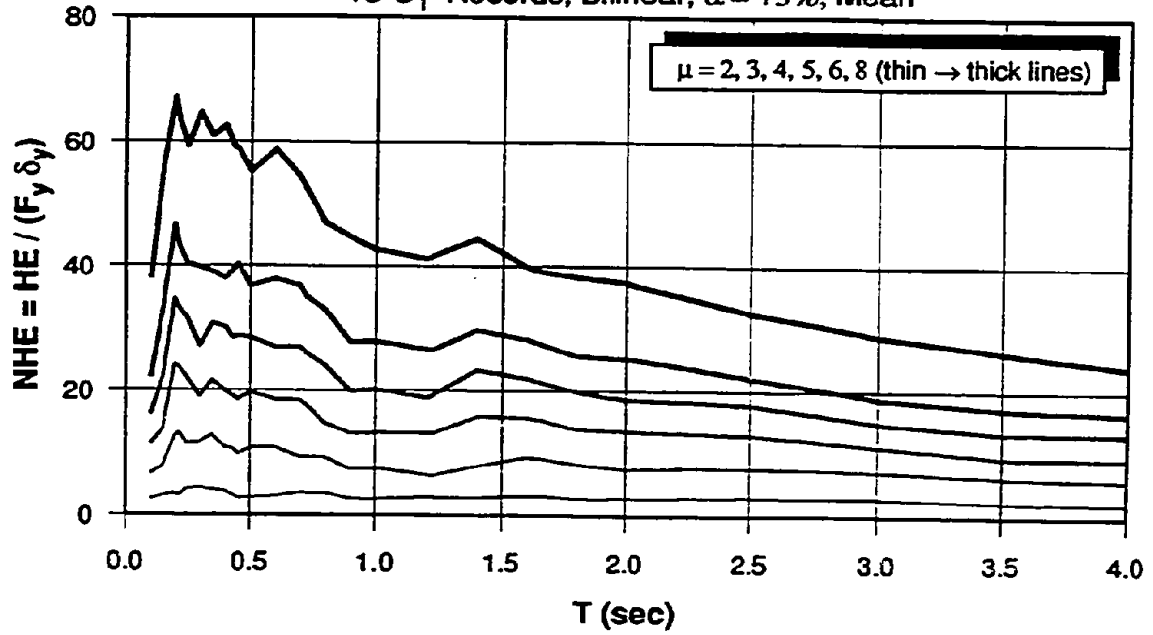
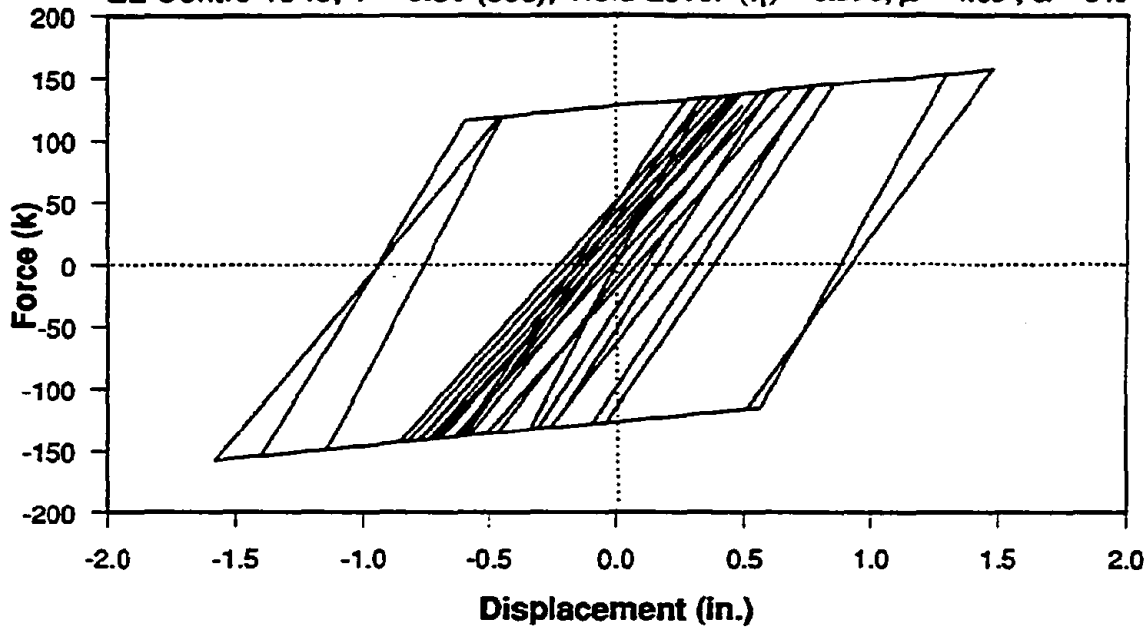


Fig. 3.41 Normalized Hysteretic Energy for Bilinear Systems with 5% Strain Hardening - Mean

BILINEAR STIFFNESS DEGRADATION HYSTERESIS MODEL

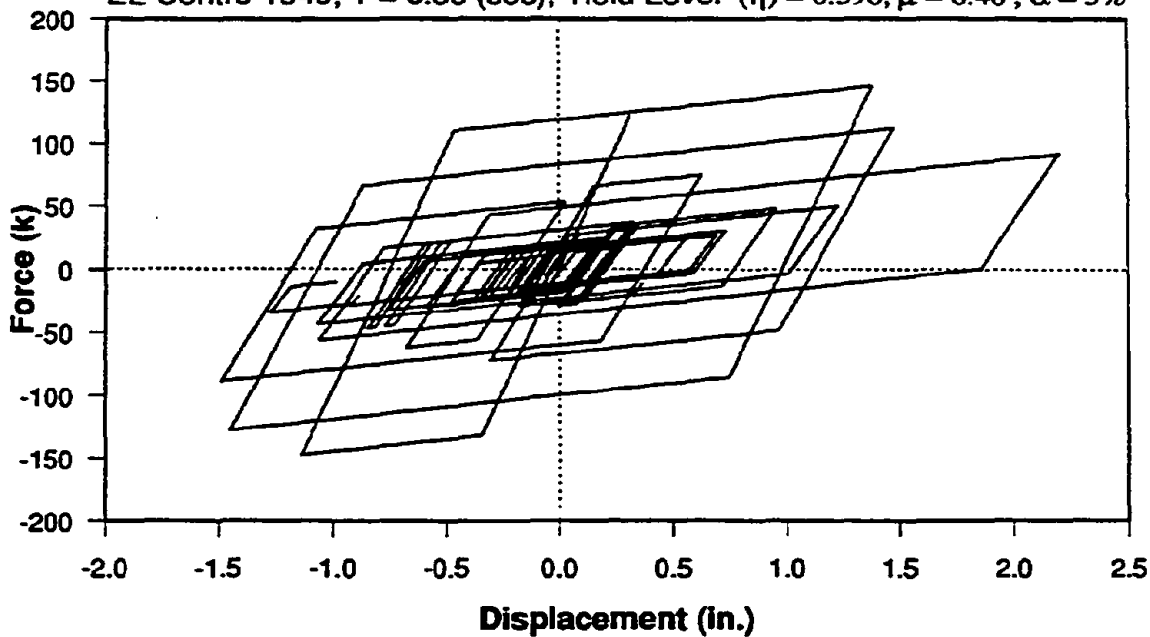
EL-Centro 1940, $T = 0.50$ (sec), Yield Level (η) = 0.396, $\mu = 4.63$, $\alpha = 5\%$



(a) Bilinear Unloading Stiffness Degradation Model, $T = 0.50$ sec.

BILINEAR STRENGTH DETERIORATION MODEL

EL-Centro 1940, $T = 0.50$ (sec), Yield Level (η) = 0.396, $\mu = 6.40$, $\alpha = 5\%$



(b) Bilinear Strength and Stiffness Deterioration Model, $T = 0.5$ sec.

Fig. 3.42 Force-Displacement Responses with Stiffness Degradation and Strength Deterioration

DISPLACEMENT TIME HISTORIES FOR DIFFERENT HYSTERESIS MODELS

EL-Centro 1940, $T = 0.5$ (sec), Yield Level $(\eta) = 0.396$, $\mu = 4$, $\alpha = 5\%$, $c = 1$

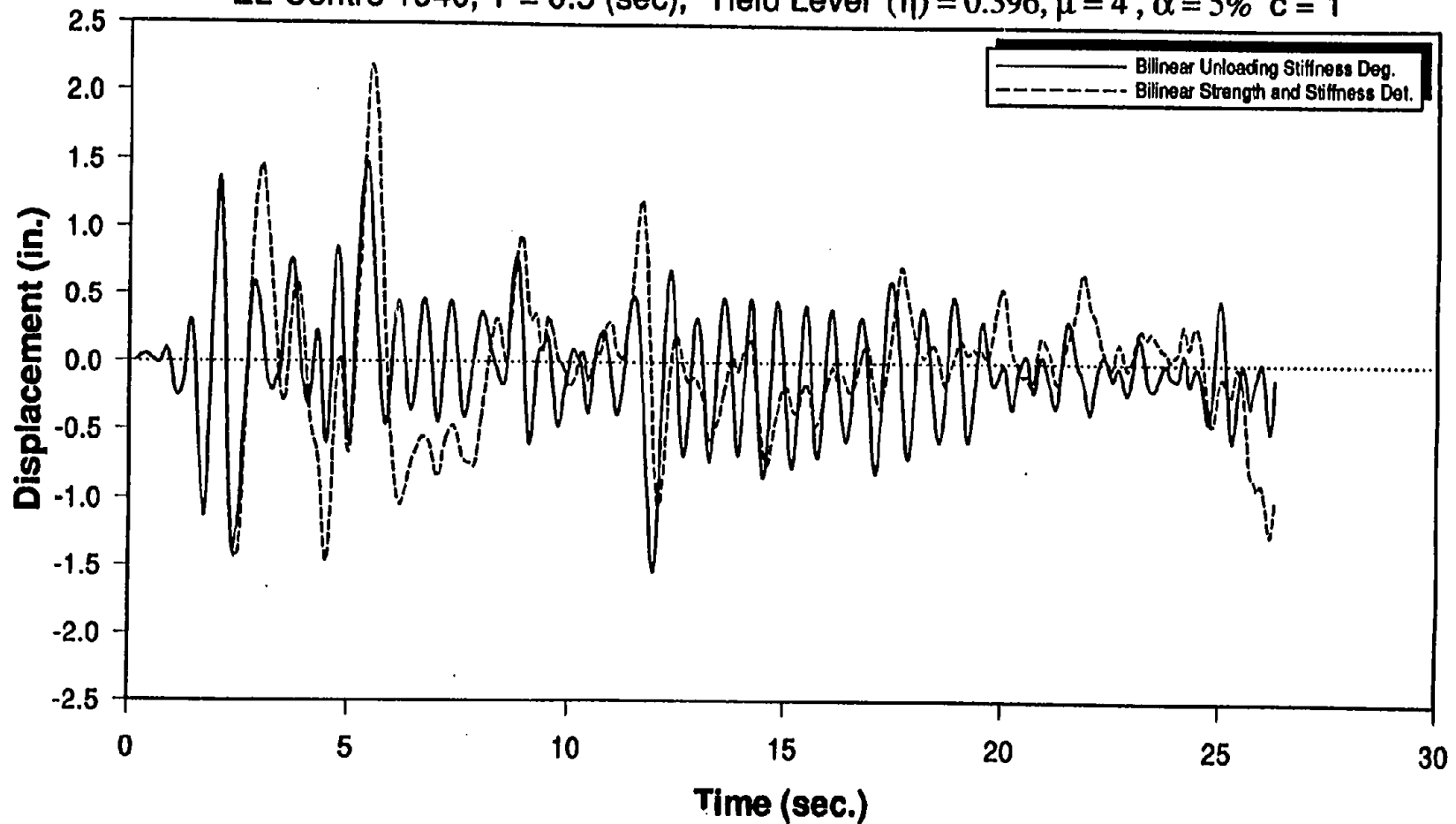
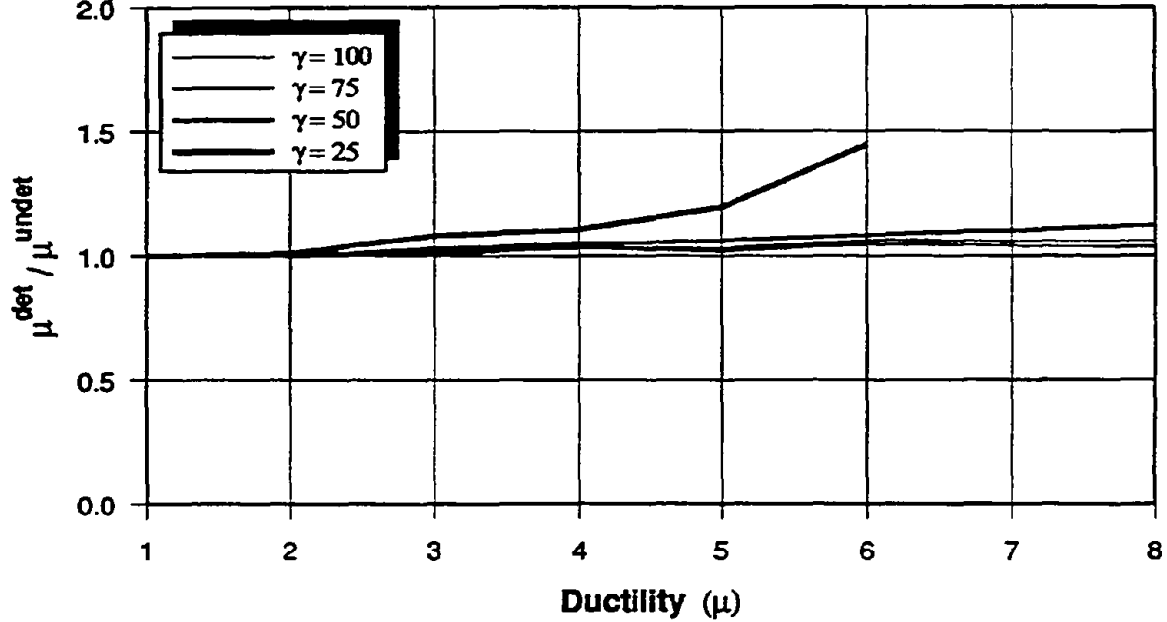


Fig. 3.43 Displacement Time Histories of System with Period of 0.50 Seconds Using Different Hysteresis Model

EFFECT OF STRENGTH DETERIORATION ON DUCTILITY

15-S₁ records, Bilinear Model with Strength Deterioration, T = 0.50 (sec) - Mean



(a) Ratio of Ductilities

EFFECT OF STRENGTH DETERIORATION ON HYSTERETIC ENERGY

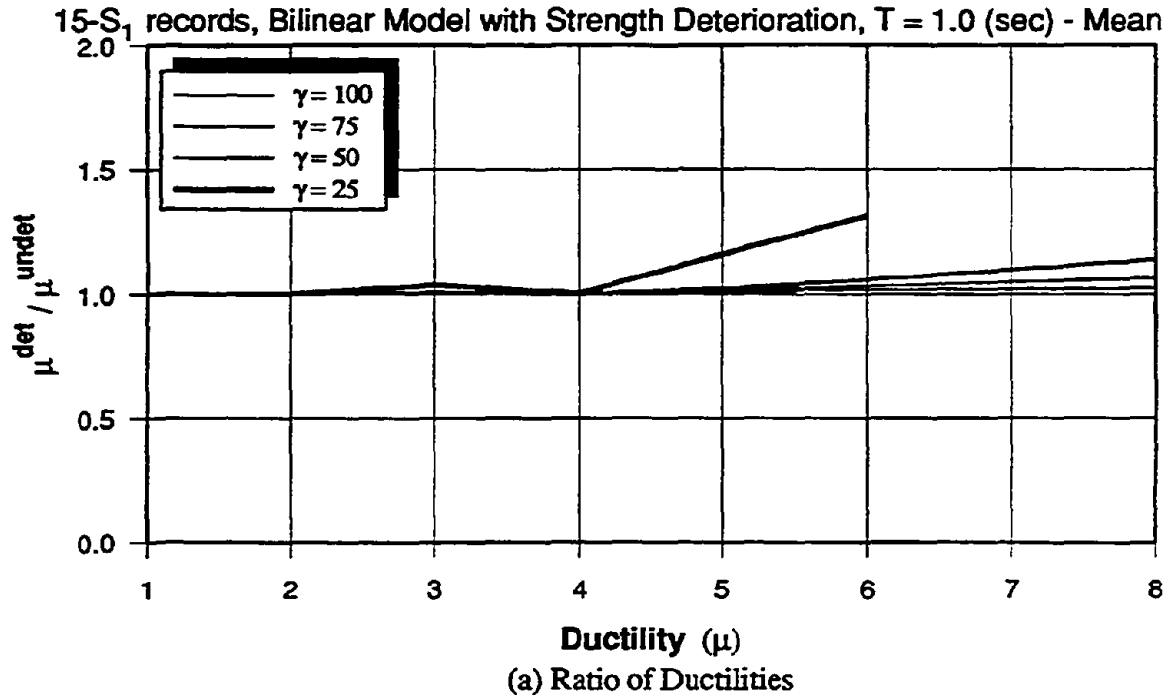
15-S₁ records, Bilinear Model with Strength Deterioration, T = 0.50 (sec) - Mean



(b) Ratio of Energies

Fig. 3.44 Effect of Strength Deterioration on Ductility and Hysteretic Energy of Systems with T = 0.50 sec.

EFFECT OF STRENGTH DETERIORATION ON DUCTILITY



EFFECT OF STRENGTH DETERIORATION ON HYSTERETIC ENERGY

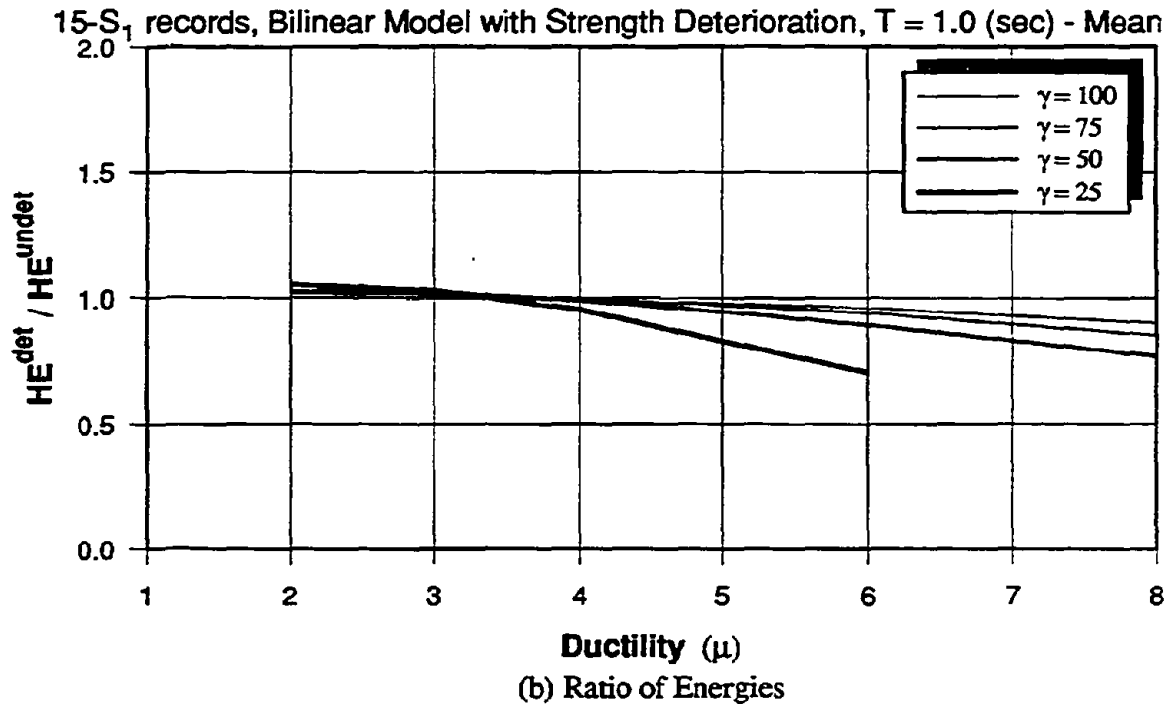
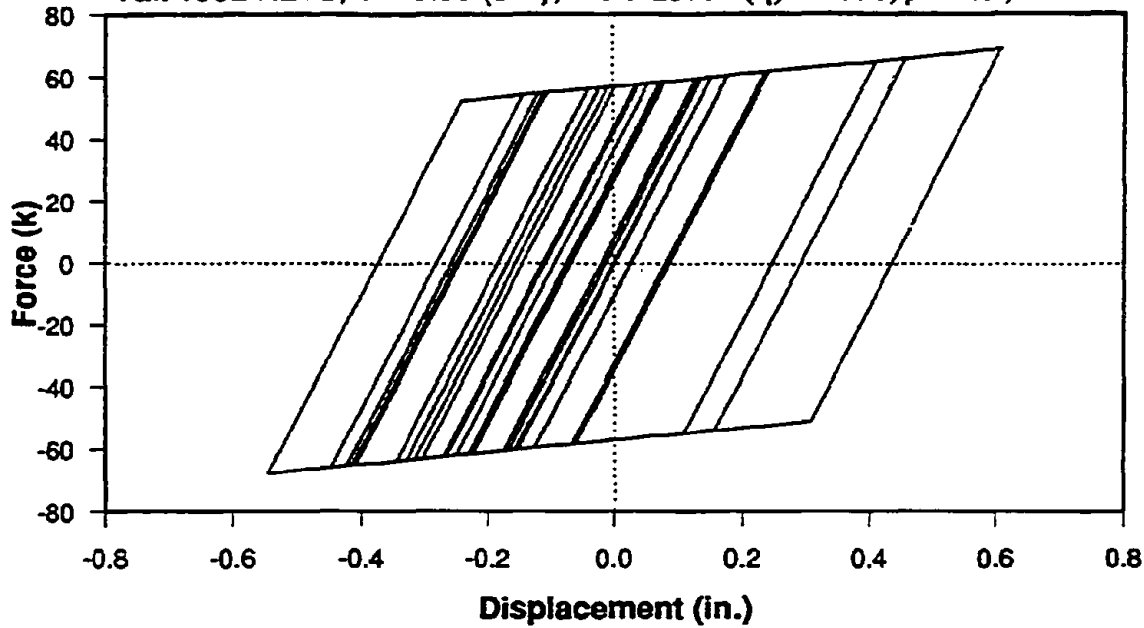


Fig. 3.45 Effect of Strength Deterioration on Ductility and Hysteretic Energy of Systems with T = 1.0 sec.

BILINEAR HYSTERESIS MODEL

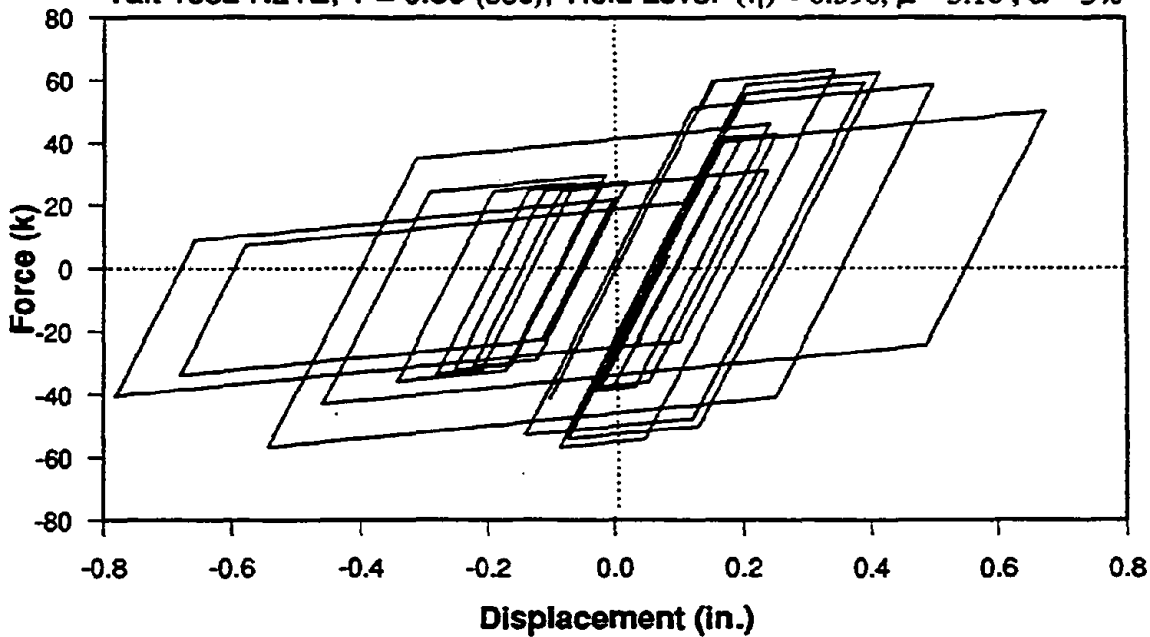
Taft 1952 N21E, $T = 0.50$ (sec), Yield Level (η) = 0.398, $\mu = 4.0$, $\alpha = 5\%$



(a) Bilinear Model, $T = 0.50$ sec.

BILINEAR STRENGTH DETERIORATION MODEL

Taft 1952 N21E, $T = 0.50$ (sec), Yield Level (η) = 0.398, $\mu = 5.16$, $\alpha = 5\%$

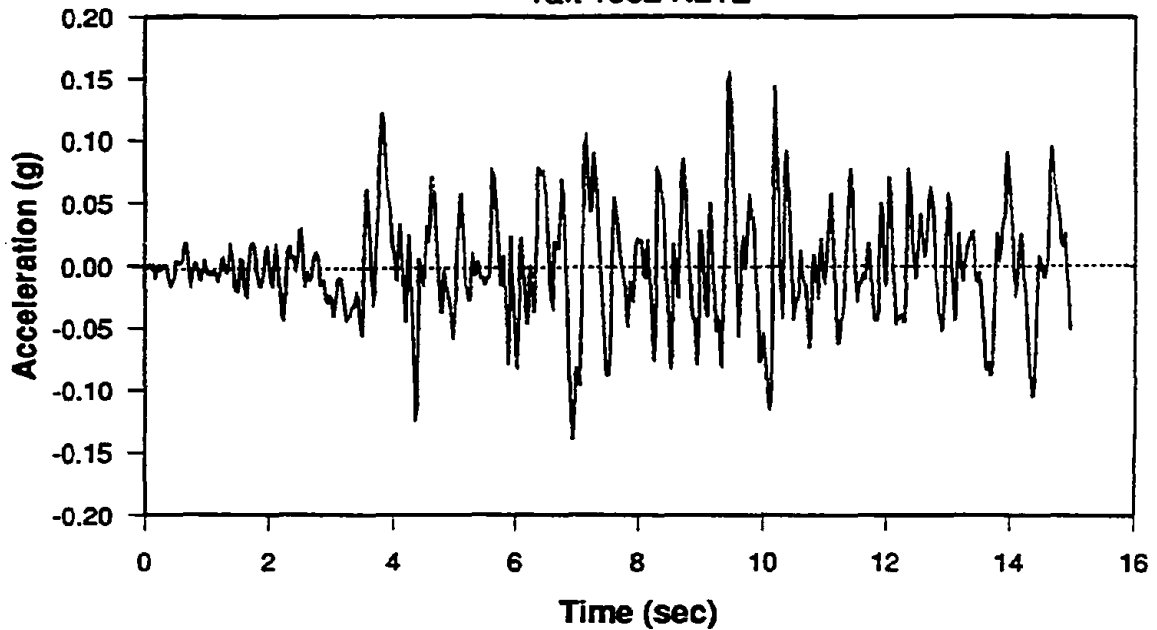


(b) Bilinear Strength Deterioration Model, $T = 0.50$ sec.

Fig. 3.46 Force-Displacement Response without and with Strength Deterioration

ACCELERATION TIME HISTORY

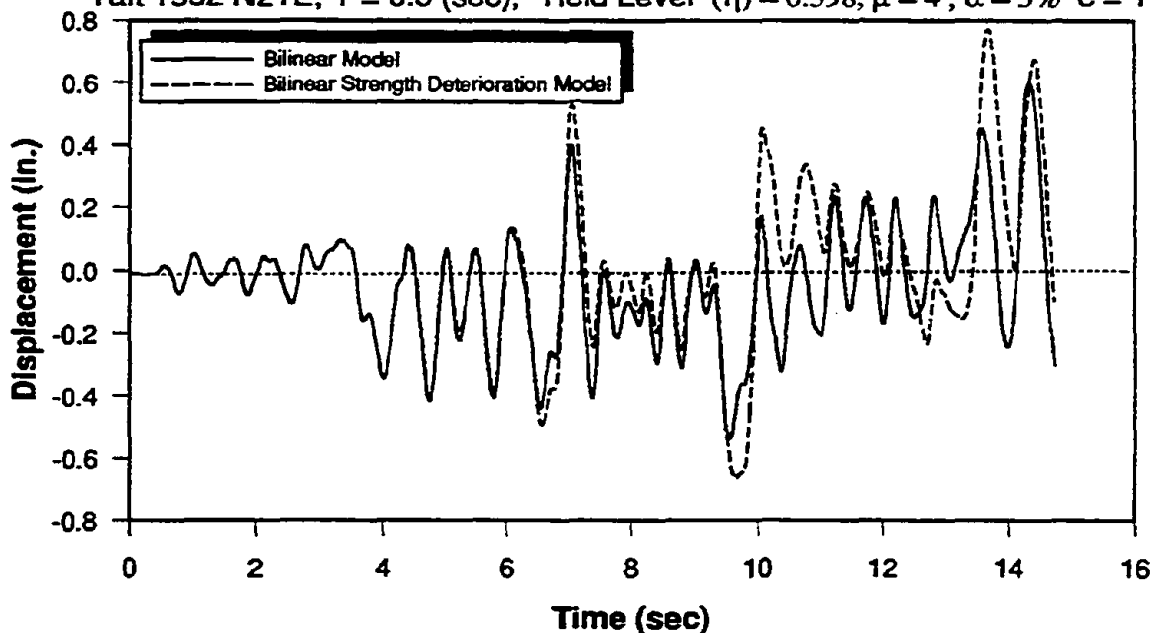
Taft 1952 N21E



(a) Acceleration Time History of Ground Motion

DISPLACEMENT TIME HISTORIES FOR DIFFERENT HYSTERESIS MODELS

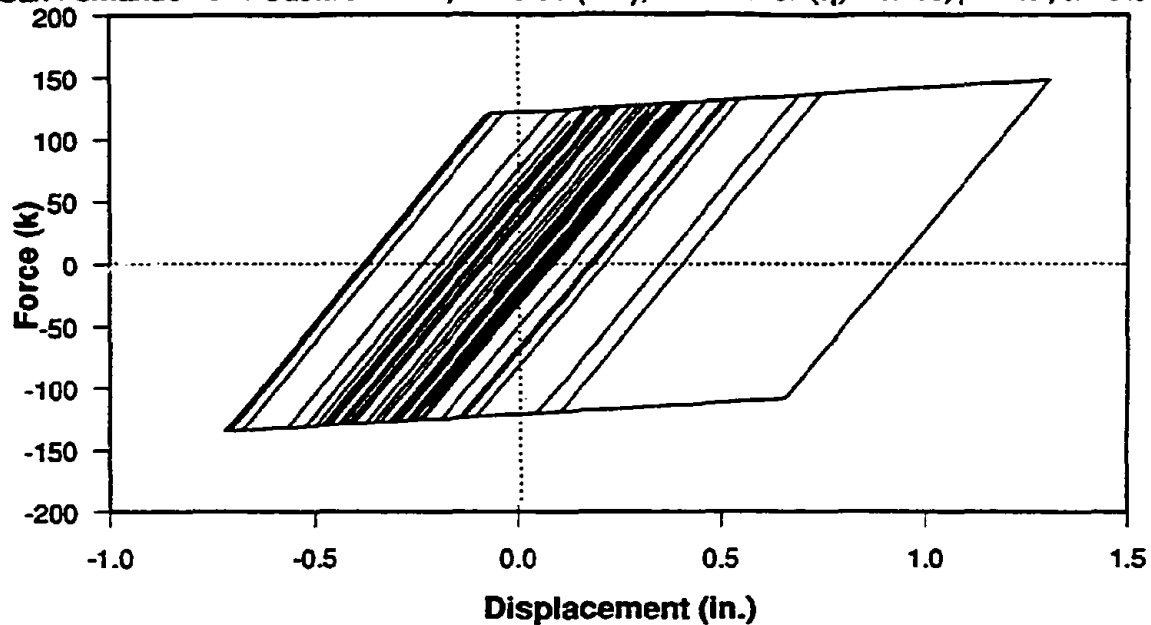
Taft 1952 N21E, $T = 0.5$ (sec), Yield Level (η) = 0.398, $\mu = 4$, $\alpha = 5\%$, $c = 1$



(b) Displacement Time Histories of Bilinear Model without and with Strength Deterioration
Fig. 3.47 Taft Acceleration Record and Displacement Time Histories of System with $T = 0.50$ sec.

BILINEAR HYSTERESIS MODEL

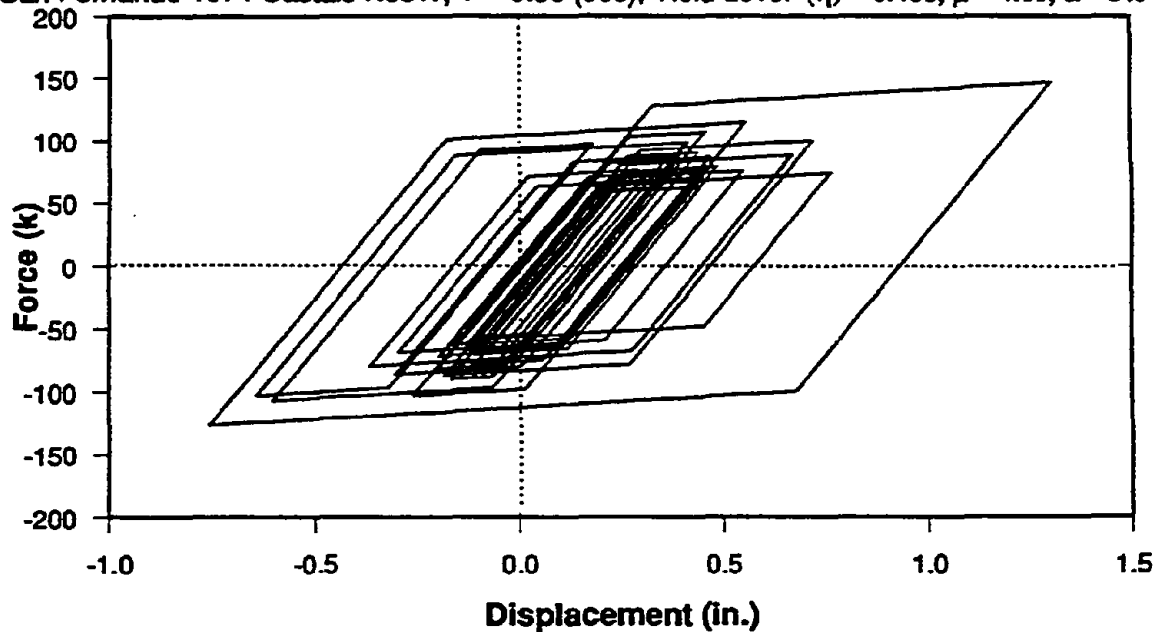
San Fernando 1971 Castaic N69W, $T = 0.50$ (sec), Yield Level $(\eta) = 0.488$, $\mu = 4.0$, $\alpha = 5\%$



(a) Bilinear Model, $T = 0.50$ sec.

BILINEAR STRENGTH DETERIORATION MODEL

San Fernando 1971 Castaic N69W, $T = 0.50$ (sec), Yield Level $(\eta) = 0.488$, $\mu = 4.01$, $\alpha = 5\%$

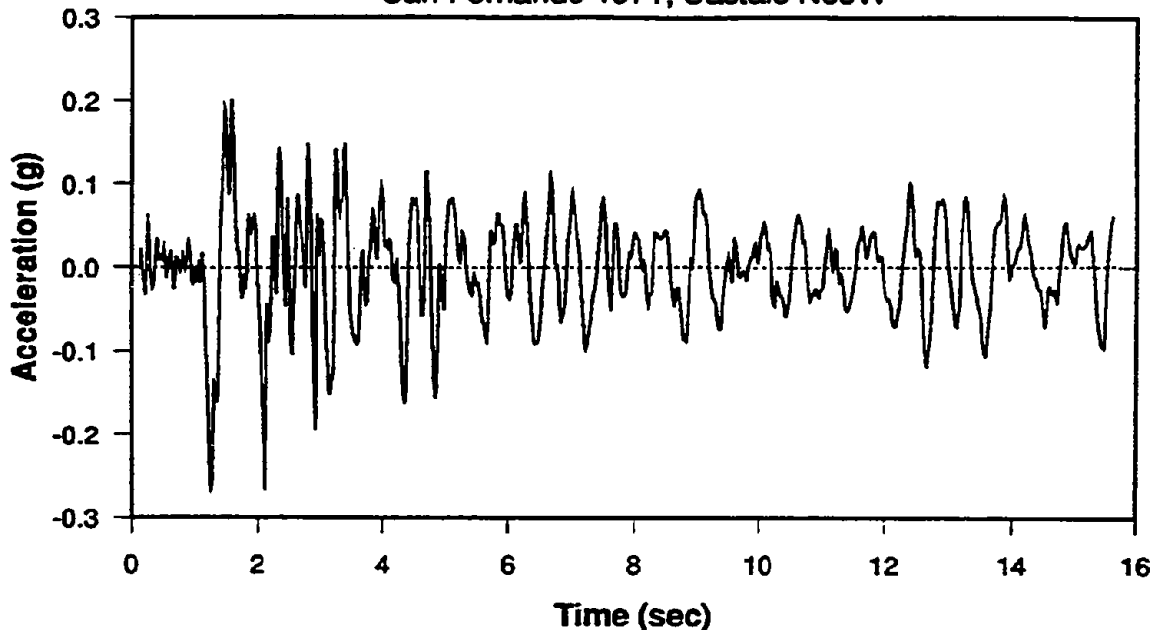


(b) Bilinear Strength Deterioration Model, $T = 0.50$ sec.

Fig. 3.48 Force-Displacement Response without and with Strength Deterioration

ACCELERATION TIME HISTORY

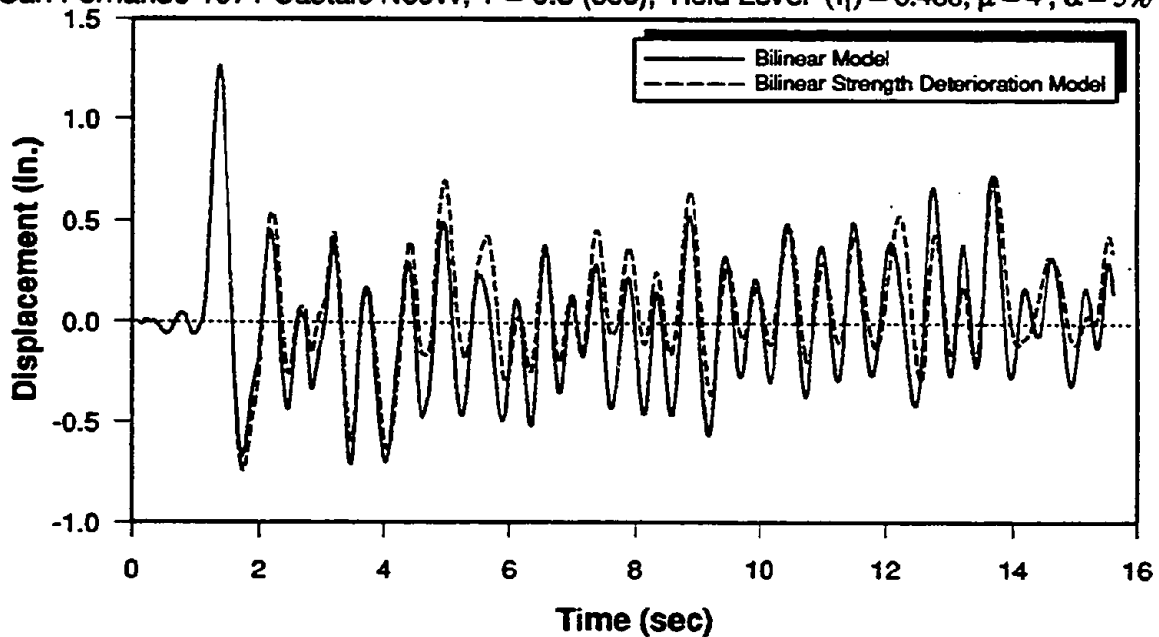
San Fernando 1971, Castaic N69W



(a) Acceleration Time History of Ground Motion

DISPLACEMENT TIME HISTORIES FOR DIFFERENT HYSTERESIS MODELS

San Fernando 1971 Castaic N69W, $T = 0.5$ (sec), Yield Level (η) = 0.488, $\mu = 4$, $\alpha = 5\%$



(b) Displacement Time Histories of Bilinear Model without and with Strength Deterioration
Fig. 3.49 San Fernando Acceleration Record and Displacement Time Histories of System with $T = 0.50$ sec.

CHAPTER 4

EFFECTS OF SOIL CONDITIONS ON SEISMIC DEMANDS OF LOMA PRIETA GROUND MOTIONS

4.1 Introduction

It is well recognized that the intensity of ground motion during earthquakes and the resulting damage to structures are influenced by local soil conditions. The characteristics of strong ground motions are affected not only by the magnitude of earthquake and the distance from the fault rupture but also by the source mechanism, the geological characteristics of the transmission path, and the local soil conditions.

Subsoil characteristics have an influence on the amplitude, the frequency content and the duration of shaking. Seismic waves will be modified as they pass from the underlying rock formations through the soil medium. This modification of ground motions depends on the depth and shear wave velocity of soil layers. Usually the effects of soil modification can be seen in various characteristics of earthquake ground motion such as peak ground acceleration, peak ground velocity and the shape of the response spectrum in most cases, the elastic response spectra of surface motion show usually a clear sign of amplification and concentration of energy around the fundamental period of the soil.

As mentioned in Chapter two, current seismic codes are using a soil factor S to account for soil site effects, but in an empirical manner that does not reflect the inelastic behavior of structures during severe earthquakes. The procedure of modifying the base shear by constant S factors cannot provide a consistent level of protection and may penalize structures whose natural periods are not in the range of periods affected by soil

amplification. Thus, a consistent approach, that accounts for the effects of soft soil on elastic and inelastic strength demands in a rational and transparent manner, is needed.

The Loma Prieta earthquake and most other recent earthquakes have shown the sensitivity of the observed damage of structures to the soil and local geological conditions. In recent years extensive research has been conducted regarding the characteristics of earthquake motions, the effect of local soil conditions on the ground surface motions, and on the extent of structural damage. In the following paragraphs a few of these studies that are related to the soft soil issues are briefly discuss.

Seed H.B. et al. (1976-1) discussed the frequency dependent effects of local site amplification. They analyzed the shapes of the average response spectra of 104 ground motion records obtained from 23 earthquakes in the western part of the United States. These records are representative of four different site conditions. These sites were classified as rock, stiff soil, deep cohesionless soil and soft to medium clay and sand. The results of this study show wide differences in spectral shapes depending on the soil conditions especially at periods greater than 0.50 seconds.

Seed H.B. et. al. (1976-2) studied the influence of local soil conditions on the attenuation of peak ground acceleration and peak ground velocity. Attenuation studies of ground motion parameters (*PGA and PGV*) were conducted using eight Western United States earthquakes with magnitude of about six. The results of this study show that there is little difference between the mean values of *PGA* obtained on rock and stiff soil sites. But there are large differences between *PGAs* in rock and those developed in deep cohesionless soil deposits. In this study the relationships between mean peak acceleration values in rock and those developed at different soil sites at equal distance were presented by curves that are shown in Fig. 4.1(a). The branch of the proposed curve for *PGA* of soft soil greater than 0.30g was based on the authors' experience. This curve has been modified by Idriss (1990) based on the new sets of ground motion records obtained from the 1989 Loma Prieta and 1985 Mexico City earthquakes and it is presented in Fig. 4.1(b). The results of Idriss' study show that for soft soil sites the horizontal accelerations are amplified at sites with peak accelerations in the underlying rock less than about 0.4g. For higher levels of rock accelerations the *PGA* of surface motions will be deamplified due to the soil nonlinearity. His results indicate that at very low levels of rock accelerations the amplification of *PGA* on soft soil sites could be in the range of 6 to 10. In this study the effect of fundamental period that reflects the site properties (depth and

shear wave velocity) is not considered. The 1989 Loma Prieta earthquake clearly shows the dependency of the amplification of *PGA* for soft soil sites in the San Francisco / Oakland area on the characteristics and frequency content of rock motions as well as the fundamental period of the soil deposit.

Singh R.D. et. al. (1981) investigated the nonlinear seismic response of soft clay sites during earthquakes. The ground response analysis was conducted using one-dimensional shear wave propagation. The Ramberg - Osgood formulation was adopted in order to represent the soil nonlinearity. The *R-O* parameters were defined based on cyclic loading tests reported by Idriss (1978). The results of nonlinear ground response analysis were compared with those obtained by the equivalent linear method using the *SHAKE* program. The comparison of spectral values of generated surface motion using these two methods of ground response analysis indicated that in the short period range the acceleration spectral values of surface motions for the equivalent linear method are higher than those obtained using nonlinear analysis. The spectral values in the long period range for computed surface motions using nonlinear method are higher or about equal to those obtained by using the *SHAKE* program. The results of both methods of analysis were in good agreement with the spectra of recorded motions at the low level of rock input motions.

Martin P.P. and Seed H.B. (1982) conducted one-dimensional response analysis of six soft soil sites. The analyses were performed using both the equivalent linear method (*SHAKE* program) and the nonlinear finite element approach. The Davidenkov model was used to represent soil nonlinearity. The results of this investigation show that the response spectra of computed surface motions obtained with both methods are very similar for all six sites. The acceleration spectra of motions computed by both methods were in good agreement with spectral values of recorded motions.

Seed H.B. et al. (1988) used one-dimensional vertical wave propagation to analyze the ground response for five soft soil sites in Mexico City. The response spectra of computed motions were similar to the response spectra of recorded motions.

Seed H.B. and Sun I.J. (1989) used the 1985 Mexico City earthquake to examine the factors that are likely to have influence on the response and extent of damage to structures. The results of a part of this study were used to investigate the extent of damage to structures on sites underlain by clay in the San Francisco area.

In most of the studies mentioned above available data from major earthquakes were used to study the soft soil effects. In these investigations emphasis was placed on the amplification of *PGA* and *PGV* or the amplification and shape of the elastic response spectra.

Under severe earthquake ground motions most buildings and other structures behave inelastically and dissipate energy through inelastic deformations. Therefore, it is equally relevant for seismic design of structures to investigate the effects of soft soil on the amplification of inelastic strength demands and find out to what extent the seismic demand parameters are affected by site soil conditions. The objectives of the study presented in this and the next chapter is to develop procedures and information that permit an explicit incorporation of the effects of site surface geology on the seismic demands imposed on structures by strong ground motions. The study of soft soil effects consists of two parts. In the first part, which is presented in this chapter, advantage is taken of the extensive set of ground motions recorded during the Loma Prieta earthquake and available data on local soil conditions at recording stations. These data sets are utilized to improve the basic understanding of the phenomena involved and to identify the most relevant parameters. In the second part of the study, which will be presented in Chapter 5, a simplified soil column model is employed for an extensive parameter study of the effects of soft soil conditions on seismic demands.

In the following sections a detailed study on attenuation characteristics of motions recorded during the Loma Prieta earthquake will be presented. This includes the attenuation of elastic and inelastic strength demands of rock motions and its importance for site amplification of ground motions. Seismic demands for six recorded soft soil ground motions are discussed. The effects of different parameters, such as soil period and directivity, on the amplification of seismic demands are investigated.

4.2 Loma Prieta Ground Motion Records Used in This Study

Ground motions in the October 17, 1989 Loma Prieta earthquake have been recorded by several agencies and private organizations, the primary sources being the *CDMG* and *USGS*. The motions recorded by the latter two agencies are well documented (e.g., *CDMG*, 1989, and *USGS*, 1989), many of the records have been digitized and corrected in final format (e.g., *CDMG*, 1990, and *USGS*, 1990), and many discussions on

ground motion issues have been published already (e.g., Boore et al., 1989, and *Competing Against Time*, 1990, Campbell, 1991).

In the study summarized here, the digitized records made available by *CDMG* and *USGS* were utilized for a global evaluation of strength and ductility demands for bilinear single degree of freedom (*SDOF*) systems, with due consideration given to attenuation characteristics and local site conditions. Records from 51 stations were used for this purpose. The overriding consideration in the selection of records was that each record could be viewed as a "free-field" record. Thus, only records from instrument shelters or one to two story buildings were considered in order to avoid records that could be considerably contaminated by structural feedback.

The records were classified as either rock, alluvium, or soft site records. This classification was based in most cases on the information provided in *CDMG* (1989) and *USGS* (1990). However, because of the ambiguity of some of the information given in these references, and in view of the objectives of this study, several judgmental decisions had to be made in this soil classification. Rock and alluvium site records were used primarily to study attenuation patterns, and therefore, records which are known to be uncharacteristic for these two categories were eliminated. This applied to four records that were classified in *CDMG* (1989) as "alluvium" records, but which likely are soft soil records (see section on Strength Demands for Ground Motions in Soft Soils), and to the "rock" motion recorded at the San Francisco Presidio.

Properties of the records classified as rock, alluvium, and soft soil site records are summarized in Tables 4.1 to 4.3. For each station only the horizontal component with the larger *PGA* value is tabulated. With very few exceptions this component was also the record with the larger *PGV* and Arias intensity. The tabulated sets of motions for rock and alluvium sites are used in order to perform an attenuation study of *PGA*, *PGV*, and strength demands.

The next two sections focus on demand information obtained from time history response analyses, using these records as input to bilinear *SDOF* systems with 5% damping and 10% strain hardening for periods ranging from 0.10 to 4.0 second. The emphasis is on strength demand spectra.

4.3 Attenuation Characteristics for Motions in Rock and Alluvium

Attenuation characteristics are known to follow well established patterns for ground motions in rock and firm soil (Joyner and Boore, 1988). Thus, the two sets of records classified as rock and alluvium records were used to evaluate attenuation characteristics of *PGA* and *PGV* as well as of elastic and inelastic strength demands. For each parameter a regression analysis was performed, using the following relationship between the attenuating parameter y and the distance r :

$$\log y = a + d \log r + kr \quad (4.1)$$

where

$$r = (r_o^2 + h^2)^{0.5}$$

r_o = shortest horizontal distance from station to surface projection of the rupture surface (km), see Tables 4.1 and 4.2

h = a depth parameter

a, d, k = regression parameters.

This equation is of the form proposed by Joyner and Boore, 1988, without consideration of a site soil correction factor. Joyner and Boore set the value of d to -1.0, whereas in this study d was used as a free regression parameter. The only constraint on the regression parameters was that k had to be negative and was taken as zero if it turned out to be positive in an unconstrained regression analysis. In Joyner and Boore, 1988, the depth parameter h is obtained from a search procedure that minimizes the sum of the squares of the residuals, and is taken as 8.0 km for attenuation of *PGA* and 4.0 km for attenuation of *PGV*.

4.3.1 Attenuation of *PGA* and *PGV*

Both horizontal (*NS* and *EW*) components of the two record sets listed in Tables 4.1 and 4.2 for rock and alluvium ground motions were used in separate least square regression analyses to evaluate the attenuation of *PGA* and *PGV*. The sensitivity of the regression lines to the depth parameter h was investigated by using $h = 8$ and 15 km for *PGA* and $h = 4, 8,$ and 15 km for *PGV*. The first values are the values used by Joyner and Boor, and the 15 km value was used because the hypocenter of the Loma Prieta

earthquake is rather deep (approx. 18 km). As Figs. 4.2 and 4.3 show, the regressed near-source attenuation relationships are very sensitive to the choice of h , whereas for horizontal distances to the fault rupture exceeding 10 km the effect of different h values disappears. Thus, no confidence can be placed in the regression lines for distances of less than 10 km, and for all later discussed seismic demand parameters h was chosen as 8 km.

From Figs 4.2 to 4.5 the following observations can be made on the attenuation of PGA and PGV for different site condition (rock vs. alluvium) and different orientations (NS vs. EW component):

- As was pointed out already by Boore D.M. et al. (1989), Competing Against Time (1990), and is confirmed in Fig. 4.2 and 4.3, both the PGA and PGV attenuate much slower than predicted by Joyner and Boore (1988). The solid lines in these two figures show the Joyner and Boore predictions based on a moment magnitude 6.9 earthquake.
- Figs. 4.4(a) and 4.4(b) show the relative attenuation of PGA and PGV for the two horizontal components of the alluvium site and rock site records, respectively. All curves are normalized with respect to the regressed values at 10 km from the rupture. Except for the PGV of alluvium sites, the PGA and PGV of the EW component attenuate much slower than those of the NS component. The larger the distance from the fault rupture, the more predominant the EW component becomes. Thus, the motions show a definite directivity, with the predominant direction for far-source motions oriented orthogonal to the fault. Also, for rock sites (Fig. 4.4(a)) the PGV attenuates much slower than the PGA , an important characteristic since it is responsible for the considerable distance dependence of the strength demand spectra discussed later.
- Figs. 4.5(a) and 4.5(b) show the attenuation of PGA and PGV of the component with the large PGA . This component was used for the later discussed evaluation of seismic strength demands. As Fig. 4.5(a) shows, the PGA for alluvium sites is larger at all distances, and attenuates slower than the PGA for rock sites. However, the PGV for alluvium sites attenuates faster than that for rock sites and, as a consequence, the $PGVs$ for rock and alluvium sites are about equal at distances of 80 to 100 km, which are the distances for San Francisco and Oakland.

4.3.2 Attenuation of Strength Demand Spectra

Least square regression analysis was performed on period dependent ordinates of the strength demand spectra, using Equation (4.1) and the responses computed from the two record sets given in Tables 4.1 and 4.2. Performing the least square fit is expected to diminish the effects of local site irregularities and amplify behavioral patterns in demand parameters and in the relationships amongst response and ground motion parameters. The process employed in the regression analysis is simple but very computation intensive. For each spectral ordinate and for all the variables employed in the study (e.g., different ductility ratios and periods), the results obtained from the two sets of records were used for an independent regression analysis. The regression curves for the spectral ordinates were then used to derive distance dependent spectral information. Figs. 4.6 to 4.12 illustrate representative results obtained from the regression analysis.

Figure 4.6 shows, in solid lines, the attenuation of the elastic strength demand (acceleration response) spectra for rock and alluvium sites, using distances to the fault rupture, r_o , of 10, 20, 40, and 80 km. Also shown, in dashed lines, are the 1988 *UBC* code design values *ZC* for soil type S_1 in Fig. 4.6(a) (rock) and S_2 in Fig. 4.6(b) (alluvium). Comparing the *ZC* curves with the regressed elastic spectra gives an indication how close the elastic strength demand imposed by the Loma Prieta ground motions is to the code "design value." The two curves marked as *SMF88* and *CMF68* in Fig. 4.6 will be discussed later on.

There are clear differences in the shapes and attenuation characteristics of the elastic spectra for rock and alluvium sites. The near-source (10 km) rock spectrum exhibits one large peak at 0.3 sec. and rapid decay at longer periods, whereas the corresponding alluvium spectrum exhibits a short period plateau and slower decay at longer periods. For both the rock and alluvium spectra the attenuation with distance is rapid in the short period range whereas it is very slow for specific longer periods. This phenomenon results in a significant change in spectral shapes as a function of distance, as is illustrated in Fig. 4.7, which shows the same spectra but normalized with respect to the regressed *PGA* at the specified distances. Peaks in the spectra diminish with distance and are replaced by wider plateaus, resulting in almost constant spectral values from 0.2 to 1.0 second periods at a distance of 80 km (San Francisco). These phenomena are more pronounced for rock sites than alluvium sites.

The significant changes in shapes of the rock spectra with distance from the fault rupture may not be critical for the design of structures located on rock sites, since the design likely will be governed by spectra derived from near-site earthquakes. However, there is an important consequence to be considered. The elastic spectra shown in Figs. 4.6 and 4.7 represent frequency characteristics of the ground motions, and a broad plateau with relatively high spectral values at longer periods clearly indicates that soft soils over rock will be much more excited than anticipated from a typical near-source rock spectrum with peaks at short periods. There is no doubt that the slow attenuation of long period components of the ground motion, reflected in the wide plateaus of the far-source rock spectra (80 km), has contributed significantly to the amplification of motion in soft soils in and around San Francisco and Oakland. This conclusion is not new, but little documentation existed so far on the importance of this effect.

Figure 4.8(a) shows the regressed elastic strength demand spectra at 80 km as well as the mean strength demand spectra of ten rock motions recorded in the San Francisco / Oakland area. As shown in the figure, the strength demand spectra obtained by these two methods are in good agreement. The mean of normalized (w.r.t. *PGA*) elastic strength demand spectra of the ten far-source rock records is shown in Fig. 4.8(b). In this figure the dashed curve represents the normalized *ATC* ground motion spectrum for soil type *S₁*. The long "plateau" of the mean spectrum, reflects the characteristics of far-source motions. These far source rock motions are used in Chapter 5 as input motions to perform ground response analyses of soft soil sites.

Figures 4.9 and 4.10 show results similar to those of Figs. 4.6 and 4.7, but for inelastic strength demand spectra for $\mu = 4$. As was stated previously, these spectra identify the required strength of *SDOF* systems whose ductility is limited to a value of 4.0. The shapes of these spectra are relatively smooth and are very different from the elastic ones, indicating that the inelastic strength demands are not related to the elastic ones by a period independent reduction factor (*R-factor*) as is assumed in present design codes. The variation in spectra shapes with distance is illustrated in Fig. 4.9 and shows only minor variations for alluvium spectra, but great variations for rock spectra based on the much slower attenuation of strength demands for longer periods.

Figure 4.11 shows regressed strength demand spectra for $\mu = 1$ (elastic), 2, 3, and 4 at a distance to the fault rupture of 10 km. Again, the nonlinear relationship between elastic and inelastic spectra is evident, particularly in the rock spectrum where the peak in the elastic spectrum disappears already in the $\mu = 2$ spectrum.

Figure 4.12 shows the regressed strength reduction factors $R_y(\mu)$ at a distance of 10 km for $\mu=2, 3$ and 4. It can be seen from the figure, that the ratio of elastic to inelastic strength demand is by no means constant; it is smaller than μ for short periods and for periods with low elastic strength demands followed by period ranges of high elastic strength demands (hump in the elastic spectra). The reason for the latter is that the effective period of the inelastic system lengthens and shifts into the period range of high elastic strength demands. As a consequence, the strength demands for inelastic system becomes relatively large and the corresponding strength reduction factors are small. For the rock site motions the *R-factors* for periods exceeding one second are significantly larger than μ , indicating low long period energy content for rock motions near the fault rupture. This observation is confirmed also from the descending branch of the elastic strength demand spectrum (curve for $\mu=1$ in Fig. 4.11(a)), which is significantly below the curve displaying the product ZC for S_1 soil conditions.

4.4 Seismic Demands for Ground Motions on Soft Soils

It is well established by now that records at soft soil sites (particularly fill on bay mud) show great amplifications of *PGA* values compared to nearby firm soil records. However, it would be misleading to proportion seismic demands imposed on structures according to *PGA* alone, without regard to frequency characteristics of the ground motions. The following discussion focuses on an evaluation of the damage potential of Loma Prieta ground motions that were recorded on soft soil, utilizing the aforementioned elastic and inelastic strength demand spectra. Results from six individual ground motions are discussed and illustrated, since the records are site specific and no statistical evaluation is possible. These six ground motions, which are included in Table 4.3 were recorded on soft soils. *CDMG* (1989) classifies four of the six soft soil records under "alluvium," but all these stations are on soft soils and, in addition, at one site (Oakland Harbor) several feet of fill material were placed on top of fine-grained sand. Seismic demands of these soft soil records (strength and displacement) are presented in the following sections. The effects of different parameters on soft soil amplification are discussed.

4.4.1 Strength Demands and R-factor

Elastic as well as inelastic strength demand spectra and strength reduction factors for each of the records are shown in Fig. 4.13. Superimposed on the spectra are two sets

of curves that relate the spectra to code design considerations. The dashed curves ($S_2 - S_4$) represent the 1988 *UBC* code design coefficients ZC for soil types S_2 , S_3 , and S_4 , and are a measure of the elastic strength demand envisioned by the code. The dashed-dotted curves (*SMF88* and *CMF68*) will be discussed in Section 4.6. An inspection of this figure as well as of Fig. 4.14, which shows the variation of elastic and inelastic strength demands (for $\mu = 4$) of all six records, leads to the following observations on the seismic demands imposed by ground motions on soft soil.

- The shapes of the elastic strength demand (acceleration) spectra, which are shown in Fig. 4.14(a) (spectra normalized with respect to *PGA*, or dynamic amplification factors *DAF*) are very different for all six records. The elastic spectra show a clear signature of the soft and deep soil on which the motions were recorded. This signature is most evident in the large *DAF* of the Foster City / Redwood Shores record at a period of 0.7 seconds and at period of 1.0 second for the Redwood City Apeel Array 2 record and the wide humps of several of the other spectra, extending to and beyond a period of 1.5 seconds in the Emeryville spectrum.
- All six records exhibit a low high-frequency content, represented by the small *DAFs* at periods shorter than 0.25 seconds. This may help to explain the relatively "good" performance of most short-period structures, such as low-rise unreinforced masonry and tilt-up structures, in the vicinity of the record locations.
- As Fig. 4.13 shows, with few exceptions the elastic strength demand imposed by the Loma Prieta earthquake was smaller, and in many cases much smaller, than the strength demand implied by the 1988 *UBC* for a design earthquake (probably soil type S_4 should be used for all records). It must be concluded that in this earthquake most structures did not experience the severity of motion for which modern codes intend to provide protection against collapse, and we should derive no comfort from the observation that modern structures survived this earthquake without collapse.
- For many soft soil sites it must be concluded that the code prescribed S_4 elastic force demand is too low in the period ranges in which soil response magnifies the *DAF*. For instance, if the elastic Emeryville spectrum is

scaled up to a *PGA* of $0.4g$, the spectrum will exceed the S_4 curve considerably in the period range of 1.0 to 1.5 seconds. Site specific design spectra need to be utilized for such soil sites.

- The shapes of the inelastic strength demand spectra are quite different from those of the elastic strength demand spectra. This is evident from Fig. 4.13, which shows plots of the strength reduction factor for the six soft soil ground motions for $\mu = 2, 3, 4, 5, 6$ and 8 . The peaks and valleys of these plots coincide with those of the corresponding elastic strength demand spectrum. The consequence of this phenomenon is that the peaks evident in the elastic spectra diminish and ultimately disappear in inelastic strength demand spectra for increasing μ values.
- The observation made in the previous paragraph has significant implications for design. For structures with small ductility capacity the required strength will be high and the elastic strength demand spectrum will be an important design parameter. For structures with large ductility capacity the inelastic strength demand spectra, which are very different from the elastic spectra, should control the design. This implies that more knowledge needs to be acquired on the magnitude and shape of inelastic strength demand spectra. The data discussed here show that the shape is site dependent, but in a different manner than the elastic spectra. This can be seen by comparing the normalized elastic strength demand spectra of Fig. 4.14(a) with the normalized inelastic strength demand spectra for $\mu = 4$ shown in Fig. 4.14(b).
- The elastic strength demand imposed on structures on soft soil may be easily 6 times as high as that imposed on nearby structures built on rock. This factor is obtained as the product of *PGA* ratios and *DAF* ratios of soft-site to rock-site records.

4.4.2 Elastic and Inelastic Displacement Demands

As mentioned in Chapter 2 the proposed design approach (demand vs. capacity) is based on the estimation of structure ductility capacity, which is used to define inelastic strength demands. Thus, the basic design parameter is ductility or normalized inelastic deformation of structural elements. This design methodology provides a consistent level of seismic protection for structures during severe earthquakes. However, additional criteria need to be considered in order to limit non-structural damage and provide protection against excessive deflections. The 1989 Loma Prieta earthquake has highlighted the need to do so. In order to control the amount of damage to nonstructural elements during severe earthquakes it is necessary to limit the maximum displacement (drift) of structures. Therefore, to design structures for safety against collapse, and at the same time control the amount of nonstructural damage, another design criterion needs to be considered. The elastic and inelastic displacement spectra provide additional information that can be used together with the strength demands for this purpose.

Because of the relationship that exists between displacement ductility, displacement and strength demand, the displacement spectra can be derived directly from the strength demand spectra for a target ductility μ . In the following paragraphs the method of computing displacement demand spectra and observations on the displacement demands of six soft soil records are discussed.

In Fig. 2.5 δ_e is the maximum displacement of a system that respond elastically to a ground motion and δ_{max} is the maximum displacement of an inelastic system with a ductility of μ . The maximum inelastic displacement demand can be expressed in terms of the *R-factor* (reduction factor), elastic displacement and μ as follow:

$$\delta_{max} = \frac{\mu}{R} \delta_e \quad (4.2)$$

Thus, the ratio of inelastic to elastic displacement is given by

$$\frac{\delta_{max}}{\delta_e} = \frac{\mu}{R} \quad (4.3)$$

The maximum inelastic displacement can be written also in terms of yield strength for a system with initial period T and target ductility μ as follows

$$\delta_{\max} = \frac{T^2}{4\pi^2} \mu F_y(\mu) \quad (4.4)$$

The above expressions were used to calculate the elastic and inelastic displacement demands of six soft soil records from the 1989 Loma Prieta earthquake. Figs. 4.15 and 4.16 show the *SDOF* displacement demands and normalized displacement spectra of these records. From these plots the following observations on the displacement demands imposed by ground motions on soft soils can be made.

- The shapes of the elastic displacement demands spectra are very different for all six records (see Fig. 4.16). For some of the records, similar to the elastic strength demands, a clear peak exists in the elastic displacement demand spectra around the fundamental period of the site. This effect is most evident in the displacement spectra computed from the ground motion recorded at Apeel Array 2 (around a period of 1.10 second) and for the Emeryville record (around a period of 1.5 second).
- The inelastic displacement demands at periods shorter than the fundamental site period are quite different from the elastic displacement demands. The normalized displacement spectra show that at short periods the ratio of inelastic to elastic displacement demand is strongly dependent on the ductility ratio and period. For a period range greater than the predominant period of the site, the inelastic displacements are usually smaller and not much different from the elastic displacement demands.
- The observations from these figures indicate that a methodology for the derivation of inelastic displacement demands from elastic displacement demands independent of ductility may lead to significant errors in the short period range, specially for soft soil sites.
- The displacement spectra presented here show that the shapes are site dependent, and they are different from the displacement spectra obtained on rock sites such as those shown in Fig. 2.7. These site specific displacement

spectra are similar to the mean displacement spectra reported by Bertero V.V. and Miranda E. (1991) based on a statistical study of displacement demands from twelve soft soil records.

- The reduction of inelastic displacement and strength demands in the vicinity of the site period has significant implications for design of structures located at soft soil sites.

4.5 Factors Effecting Soil Amplification

As the seismic waves propagate from the underlying rock to the soil surface they will be modified. Some of the main parameters that affect the amplification of surface motion are the dynamic properties of the soil deposit (shear modulus, damping, degree of nonlinearity), the characteristics of the rock motions such as frequency content and magnitude of earthquake, source mechanism, source-site distance, directivity and topography of bedrock and site. A few specific items are discussed in this section.

The observations made in this section are based on an evaluation of rock and soft soil motions recorded in the San Francisco / Oakland area and the Mid-Peninsula. The locations of the recording stations are shown in Fig. 4.17 and relevant information on the stations and records is presented in Tables 4.4 and 4.5.

4.5.1 Predominant Soil Period

The predominant period of the soil deposit, which is a function of the depth and the stiffness of the soil layers, plays an important role in the characteristics of surface motions. Fig. 4.13 illustrates the strength demands at specific soft soil sites. As can be seen from the presented spectra, around the period of the site there is a concentration of energy in the elastic response spectra. It is a matter of much debate in the profession whether it is necessary to identify predominant soil periods in order to assess soil amplifications, or whether it is adequate to use average shear wave velocities (for the top 100 feet, or less if the soil layer is shallow) for this purpose. In this work the period of the soil deposit is used as a basic parameter.

Dobry R. et al. (1976) have presented a comprehensive review of different methods available to estimate the predominant period of a soil deposit. In our study

several approximate methods were examined. For a single layer of uniform properties, the modal periods of the site can be computed by the following formula:

$$T_n = \frac{1}{2n-1} \frac{4H}{V_s} \quad (4.5)$$

In this equation T_n is the modal period of the deposit, n is an integer corresponding to each mode of vibration, V_s is the shear wave velocity of the layer, and H is the depth of the layer.

This equation can be used to compute an approximate value of the period of a soil deposit with different layers by using an average value for the shear wave velocity. This average shear wave velocity is evaluated using the thickness and the shear wave velocity of each layer of the soil profile. This approach was employed to estimate the period of the soil deposits for the Loma Prieta soft soil sites used in this study, utilizing soil profile information obtained from different sources.

Another way of estimating the period of soil deposits is to represent the soil deposit by a *MDOF* lumped mass model, as will be discussed in Chapter 5. In this method the soil properties of the site are used to define the stiffness and mass matrix of a lumped mass structural model in order to compute the period of the soil. For the Loma Prieta soft soil sites the periods calculated by this method are very close to those computed using equation 4.5.

Velocity, Fourier amplitude, or power spectra of soft soil records may be used to estimate the period of sites. Figure 4.18 shows these spectra for the Emeryville component 260. The predominant period here is defined as the period corresponding to the maximum spectral values of these three spectra (i.e., $T_s = 1.5$ seconds). Because of the relationships that exist among the velocity, Fourier amplitude and power spectra, the periods computed from these spectra are almost identical.

In the process of estimating the period of soil deposits from velocity spectra it became evident that the so estimated period may vary significantly depending on which component of the record is used. This can be seen in Figure 4.19, which shows the velocity spectra of two horizontal components of ground motions recorded in Foster City and Oakland Harbor Wharf. In many cases it was observed that at periods corresponding

to the peaks in the velocity spectrum of one component there are valleys in the spectrum of the other component. This points out the danger of estimating soil periods from these spectra.

Figure 4.20 shows the velocity spectra of the same motions after transforming the records into the radial and tangential directions with respect to the epicenter. As indicated in the figure, a much better match of peaks and valleys of the velocity spectra is obtained. Similar observations are made for the other five soft soil motions used in this study. In most cases the periods estimated from velocity spectra of radial and tangential components are nearly equal and the patterns of velocity spectra in both directions are consistent. The predominate period obtained from the velocity spectra of records in the tangential direction is very close to that computed by equation 4.5 and to the one evaluated by the *MDOF* lumped mass model. For example, the velocity spectra of the E-W component of the record at Treasure Island site indicates a value of 0.65 seconds for the predominate period as compared to 1.30 seconds computed by the *MDOF* lumped mass system. However, predominant period of this site obtained from the velocity spectrum of the record in the tangential direction is similar to that obtained from the *MDOF* lumped mass system. Thus, the radial and tangential directions of ground motions appear to provide more consistent information and, therefore, in most of the analyses discussed in Chapter 5 these directions of motions were utilized for both rock and soft soil motions. The peak values of *PGA* and *PGV* in these directions are shown in Tables 4.4 and 4.5.

4.5.2 Directivity Effects

The topography and geological characteristics of rock formations and the local site conditions have various effects on the travel path of seismic waves. The direction of the incident seismic waves, the reflection and refraction of waves at the boundaries of different layers of the soil deposit, together with focusing of seismic waves pose a very complex 3-D problem that has a major effect on the characteristics of surface motions.

The rock and soft soil motions recorded in the Loma Prieta earthquake show clear but different directivity characteristics. On the average, the rock motions in the radial direction (w.r.t the epicenter) exhibit significantly smaller strength demands than the motions in the tangential direction. This is evident from Fig. 4.21 (a), which shows the mean elastic strength demand spectra obtained from the tangential and radial components

as well as from the larger of the two recorded components of ten Loma Prieta rock motions recorded in the San Francisco / Oakland area (see Fig. 4.17). Fig. 4.21(b) shows the mean of the normalized elastic strength demand spectra for those records in the tangential and radial directions, superimposed on the *ATC-3-06* normalized ground motion spectra for soil type *S₁*. Even in the normalized domain the spectrum in the tangential direction significantly exceed, that in the radial direction for periods greater than 1.0 second.

For the soft soil records, however, the elastic spectra for the radial and tangential components differ usually by a much smaller amount, which leads to the conclusion that soil amplification in the radial direction is significantly larger than in the tangential direction. This is illustrated in Fig. 4.22(b) with the amplification factors for elastic spectra obtained from radial and tangential components of nearby soft soil and rock records. The higher amplification of the weak direction of motion (radial direction) in the Loma Prieta earthquake was pointed out also by Borchardt (1990).

4.5.3 Attenuation Characteristics of Rock Motions

In Section 4.3.2 the attenuation of inelastic strength demands (acceleration spectra) for ground motions recorded on rock sites was discussed in detail. The regressed spectra at different distances from the fault rupture indicate a consistent attenuation pattern with a rapid decrease in short period spectral values. Peaks in the spectra diminish with distance and are replaced by wider plateaus. The wide plateau with relatively high spectral values at longer periods for the far-source spectra demonstrates that soft soils over rock will be much more excited than anticipated from a typical near-source rock spectrum with peaks at short periods. The data from the Loma Prieta earthquake show that the average dynamic amplification factors at long periods in far-source rock spectra are almost three times as large as those in near-source rock spectra. Thus, good reasons exist to consider near- as well as far-source rock motions in the evaluations of soil site effects, as will be done in the next Chapter.

4.6 Damage Potential of Soft Soil Ground Motions

In order to assess the damage potential of the Loma Prieta ground motions, the strength capacities of structures must be compared to the strength demands imposed by the ground motions. These capacities must be estimated with due consideration given to

the real strength of structures. For many reasons structures are stronger, and sometimes much stronger, than is implied by the seismic base shear coefficients used in code design. The strength of five types of code designed buildings, considering most but not all sources of overstrength, was estimated by Oстераas and Krawinkler (1990) and Nassar and Krawinkler (1991) and is illustrated in Fig. 4.23. Four of these five types of structures were designed in conformance with the 1988 *SEAOC* Blue book (*SBF88* = steel braced frames, *SMF88* = steel moment frames, *SPF88* = steel perimeter frames, and *CMF88* = concrete moment frames), and one type was designed in conformance with the 1968 *SEAOC* Bluebook (*CMF68* = concrete moment frames).

The strength capacity curves of the strongest and weakest structure types (*SMF88* and *CMF68*, respectively) provide a range of the expected strength of modern code designed structures and are used here to assess the damage potential of the Loma Prieta ground motions. These two capacity curves are superimposed on the strength demand spectra illustrated in Figs. 4.6, 4.9, 4.11, and 4.13 and are left to the reader for interpretation, with only a few observations summarized here.

Figure 4.6 indicates that even for code designed structures located on rock, small inelastic deformation demands have to be expected in some cases as far away as 80 km from the fault rupture, considering that the *CMF68* curve falls partly below the elastic strength demand spectra for this distance. Fig. 4.9 indicates that global ductility demands of 4 are anticipated as far away as 20 km from the fault rupture. Fig. 4.11 indicates that at a distance from the fault rupture of 10 km the ductility demands could have exceeded the value of 4 considerably for *CMF68* structures with period between 0.2 and 1.0 seconds and located on alluvial soils. Clearly, these observations are more qualitative than quantitative, since the spectra are obtained from a regression analysis and represent average rather than site specific conditions, and since significant deviations from the estimated values of structure strength have to be anticipated.

Figure 4.13 shows clearly that in soft soils, where the shaking was severe even at large distances, the ductility demands for modern structures could have been substantial. This holds true particularly for early-70 vintage low- and mid-rise reinforced concrete frame buildings (*CMF68*), except for 2-story buildings. The global ductility demand for modern steel moment frames (*SMF88*) was small for low-rise and high-rise construction and moderate for mid-rise buildings.

The demand and capacity curves shown in Figs. 4.6, 4.9, and 4.13 illustrate the variation of expected damage (assuming that ductility is an acceptable measure of damage) with source-site distance and site soil conditions, from the viewpoint of demands, and types of structural system and number of stories (period), from the viewpoint of capacities. In none of the cases illustrated, the ductility demand is severe enough to justify collapse of a modern structure. But relatively high ductility demands are evident in some cases even though the ground motions were significantly smaller (except close to the source) than anticipated by present code philosophy. This indicates that excessive ductility demands may have to be anticipated in some code designed structures if the ground motions approach the level envisioned in design codes. This holds true particularly for structures located on soft soils. It is understood that soft soil *PGA* amplification decreases as the rock *PGA* increases (Idriss, 1990, estimates that at rock *PGAs* exceeding 0.4g no soft soil *PGA* amplification occurs), but there is good reason to believe that significantly larger soft soil strength demands can be generated in a severe earthquake than those shown in Fig. 4.13 therefore, the ductility demands for modern structures may be much higher than those shown in this figure.

4.7 Summary

The Loma Prieta earthquake has again demonstrated the sensitivity of ground motions to source-site distance and directivity, travel path through geologic media, and local site conditions. Moreover, the earthquake has also demonstrated the great dependence of the elastic as well as inelastic structural response on the frequency characteristics of the ground motion. The simple conclusion is that the demands imposed by an earthquake on a structure, which should be the basis for protective design, must be evaluated with due consideration given to all the aforementioned factors. This conclusion points towards the need for detailed microzoning and raises questions on the appropriateness of presently employed global seismic zoning. It is recognized that detailed microzoning is a long way from reality because much of the needed information is not yet available. However, the Loma Prieta earthquake provided an excellent opportunity to assess seismic demands based on recorded ground motions, as a first step in identifying the sensitivity of the demands to known site conditions and structural response characteristics.

In this chapter the characteristics of ground motions, attenuation of strength demands for rock and alluvium motion, and displacement and strength demands for selected soft soil sites were examined. Since the number of available ground motions recorded on soft soil sites are limited, it is difficult to draw general conclusion based on the limited site specific study. Therefore, it is necessary to use the available soil column information together with nearby rock motions in order to generate soft soil surface motions. The comparison of the strength demands of recorded and computed surface motions will provide guidelines to develop a procedure for generating surface motions for ranges of soil column period. This information will be used in Chapter 5 to generate soft soil motions and investigate the effects of soft soil on the seismic demand parameters.

Table 4.1 Loma Prieta Rock Site Records Used in this Study

GROUND MOTIONS ON ROCK SITES						
Record No.	Name	Comp.	Distance (km)		PGA (cm/sec. ²)	PGV (cm/sec.)
			Epicenter	Rupture		
57007	Corralitos (Canyon Road)	0	7	1	618	55.2
47379	Gilroy #1 (Gavilan Coll.)	90	29	15	434	33.8
58065	Santa Cruz (UCSC/ Elec. Lab.)	0	16	16	433	21.2
1601	Stanford Univ. (Slac Test Lab.)	360	51	33	282	28.4
58127	Woodside (Fire Station)	90	55	36	80	14.7
47189	Sago South (Hol. Cienegaa Rd.)	261	54	39	71	10.3
47377	Monterey (City Hall)	0	49	44	69	3.3
58219	Hayward (CSUH Stadium)	90	71	53	83	7.4
58130	SF. (Dimond Heights)	90	92	73	111	14.3
58338	Piedmont (Jr. High Grounds)	45	93	74	81	9.2
58151	SF. (Rincon Hill)	90	95	76	89	11.6
58163	Yerba Island (Yerba Buena)	90	95	77	89	11.6
58133	SF. (Telegraph Hill)	90	97	78	91	9.6
58131	SF. (Pacific Heights)	270	97	78	60	14.3
58132	SF. (Cliff House)	90	99	80	106	21.0
58043	Ptbonita (Point Bonita)	297	104	85	71	13.6

Table 4.2 Loma Prieta Alluvium Site Records Used in this Study

GROUND MOTIONS ON ALLUVIUM SITES						
Record No.	Name	Comp.	Distance (km)		PGA cm/sec. ²	PGV cm/sec.
			Epicenter	Rupture		
58065	Saratoga (Aloha Ave.)	0	27	9	494	41.3
47125	Capitola (Fire Station)	0	9	14	463	36.1
47380	Gilroy #2 (Hwy 101/Bolsa Rd.)	0	30	16	344	33.3
47381	Gilroy #3 (Sewage Plant)	0	31	18	532	34.5
57066	Agnew (State Hospital)	0	40	25	163	30.9
57425	Gilroy #7 (Mantelli Ranch)	90	40	28	314	16.3
1656	Hollister (Differential Array)	255	45	30	281	36.6
57191	Halls Valley (Grant Park)	0	37	31	128	12.5
57382	Gilroy #4 (San Ysidro School)	0	32	32	408	39.1
47179	Salinas (John and Work St.)	250	46	34	110	15.8
57064	Fremont (Fire Station)	0	55	39	118	10.2
1686	Fremont (Emerson Court)	90	56	40	191	10.8
58393	Hayward (Muir School)	0	71	53	166	13.6
58498	Hayward (Bart Station)	310	73	55	155	11.8
58505	Richmond (City Hall Pkg. Lot)	280	108	89	123	17.1

Table 4.3 Loma Prieta Soft Soil Records Used in this Study

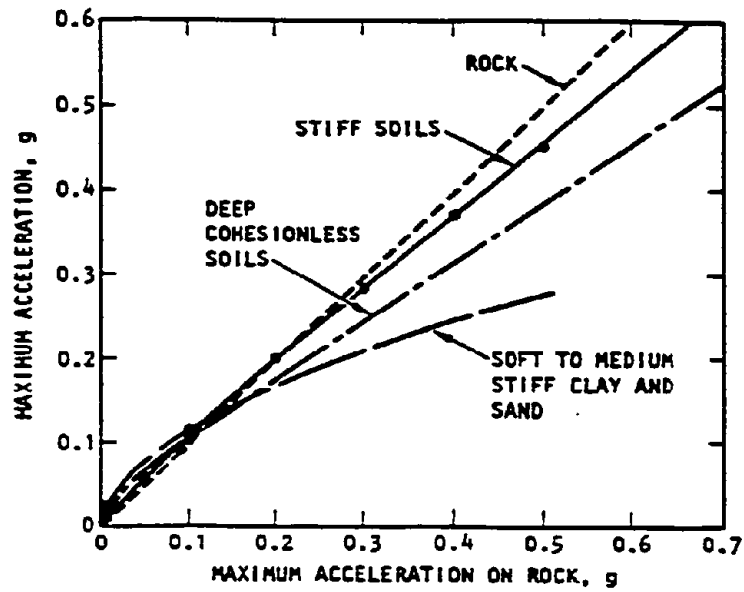
GROUND MOTIONS ON SOFT SOIL SITES						
Record No.	Name	Comp.	Distance (km)		PGA (cm/sec. ²)	PGV (cm/sec.)
			Epicenter	Rupture		
58117	Treasure Island (Fire Station)	90	98	79	156	33.4
1662	Emeryville (Christie Ave.)	260	97	79	255	41.1
1002	Redwood City (Apeel Array 2)	43	63	45	272	53.1
58375	Foster City (Redwood Shores)	90	63	44	278	45.4
58223	SF. (International Airport)	90	79	60	326	29.3
58472	Oakland (Outer Harbor Wharf)	35	95	76	281	40.8
58224	Oakland (2-Story Office Bldg.)	290	92	73	238	37.9

Table 4.4 Rock Motions Recorded in San Francisco / Oakland Area
(PGA and PGV in Tangential and Radial Directions)

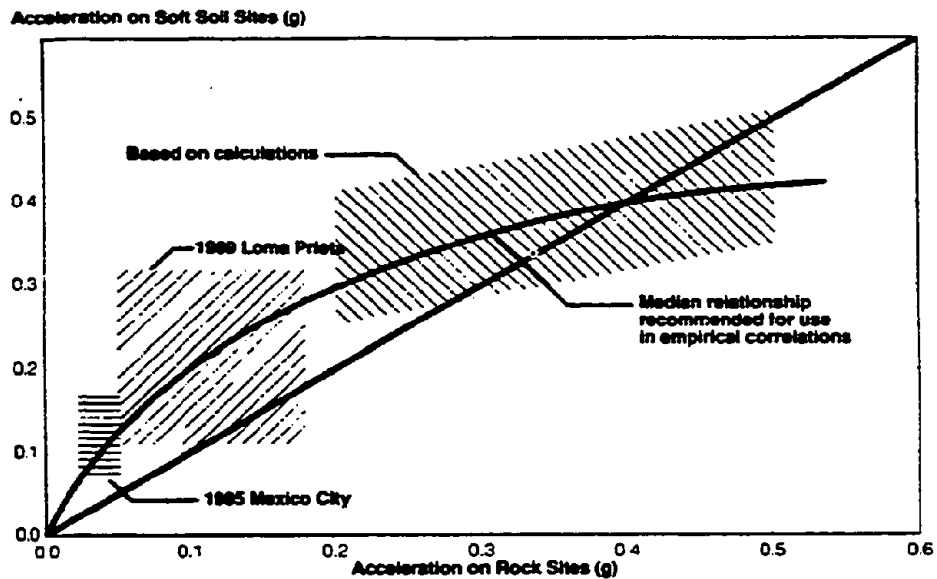
Record No.	Name	Distance (km)		Azimuth	PGA (Tan.) cm/sec. ²	PGA (Rad.) cm/sec. ²	PGV(Tan.) cm/sec	PGV (Rad.) cm/sec
		Ep	Rup.					
58163	Yerba Buena Island (YBI)	95	77	328	66.44	43.11	13.85	5.81
58338	Piedmont Jr. High G. (PJRH)	93	74	336	96.09	51.20	11.96	5.78
58151	SF. Rincon Hill (SFR)	97	76	326	96.67	64.76	13.15	4.22
58133	SF. Telegraph Hill (SFT)	97	78	325	86.30	86.77	8.73	5.54
58131	SF. Pacific Heights (SFP)	97	78	324	60.25	39.09	17.21	4.64
58132	SF. Cliff House (SFC)	99	80	320	89.30	87.13	21.44	11.57
58130	SF. Diamond Heights (SFD)	92	73	322	99.39	95.69	14.85	8.14
58043	Point Bonita (PTB)	104	85	321	60.25	73.17	12.30	10.39
1675	SF. Shfter Ave. (SFSH)	89	70	324	86.30	86.77	12.93	7.36
58539	SSF. Sierra Point (SSFS)	84	65	322	107.01	60.19	8.92	6.35

Table 4.5 Soft Soil Records Used in this Study
(PGA and PGV in Tangential and Radial Directions)

Record No.	Name	Distance (km)		Azimuth	PGA (Tan.) cm/sec. ²	PGA (Rad.) cm/sec. ²	PGV(Tan.) cm/sec	PGV (Rad.) cm/sec
		Ep	Rup.					
58117	Treasue Island (TRI)	98	76	328	135.68	128.49	32.42	14.68
1662	Emeryvill Christie Ave. (EMV)	97	78	333	245.92	239.90	34.86	31.76
1002	Redwood City Apeel2 (APL2)	63	44	323	267.74	197.72	54.46	32.79
58375	FC. - Redwood Shore (RSH)	63	44	326	293.60	275.48	41.67	34.79
58223	SF. Int. Airport (SFA)	79	60	318	376.00	217.12	34.06	19.40
58472	Oakland Harbor (OAKW)	95	76	331	314.82	256.75	46.61	29.04
58224	Oakland 2 Story Office (OAK2)	92	73	333	234.82	172.02	32.63	24.13



(a) Relationships Between PGA of Rock and PGA of Soil Sites (Seed et. al. 1976-2)



(b) Variation of PGA of Rock and Soil Sites (Idriss, 1990)

Fig. 4.1 Variation of Peak Ground Acceleration on Rock and Soil Sites

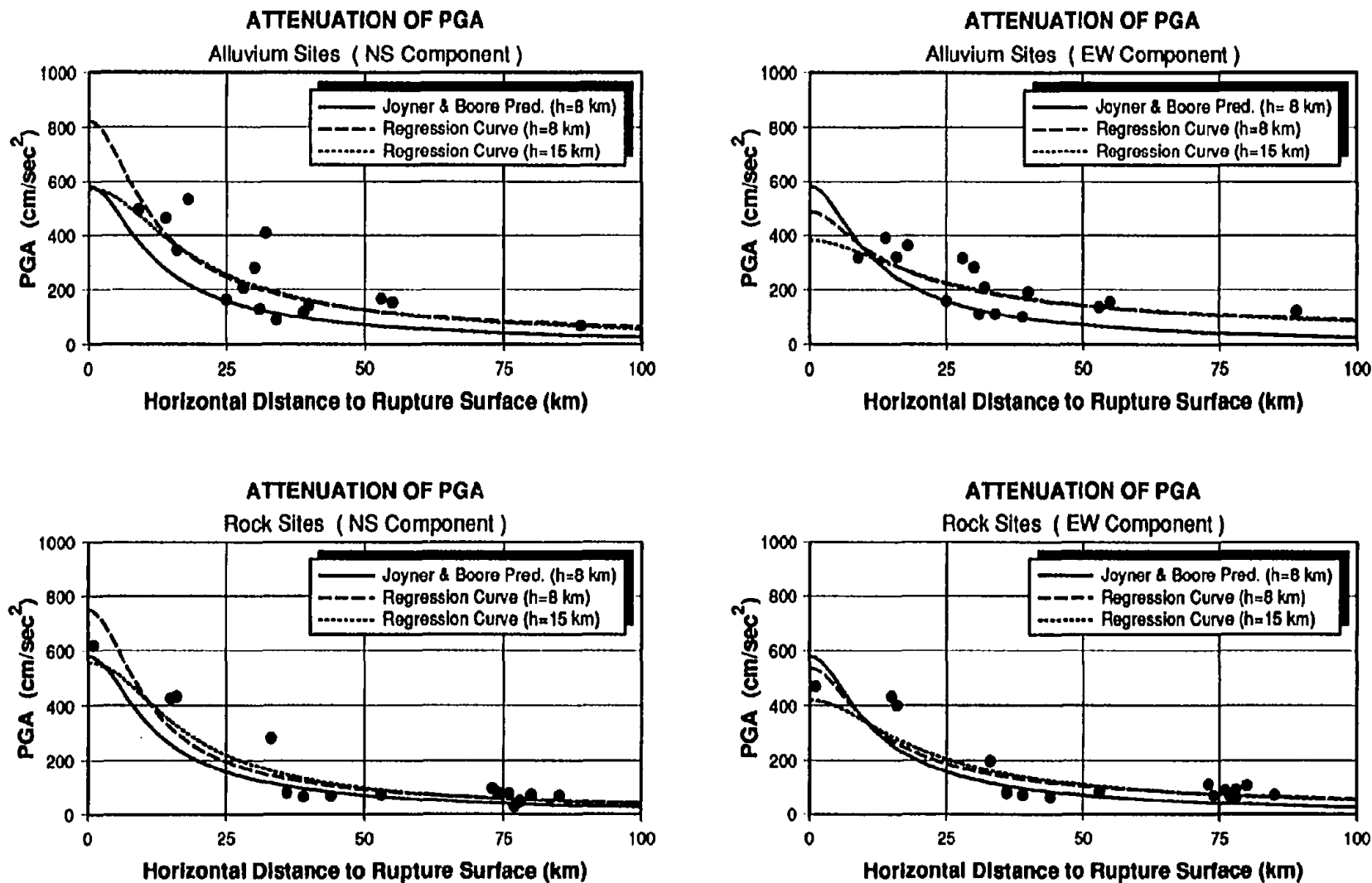


Fig. 4.2 Attenuation of PGA for Alluvium and Rock Sites (NS & EW Components)

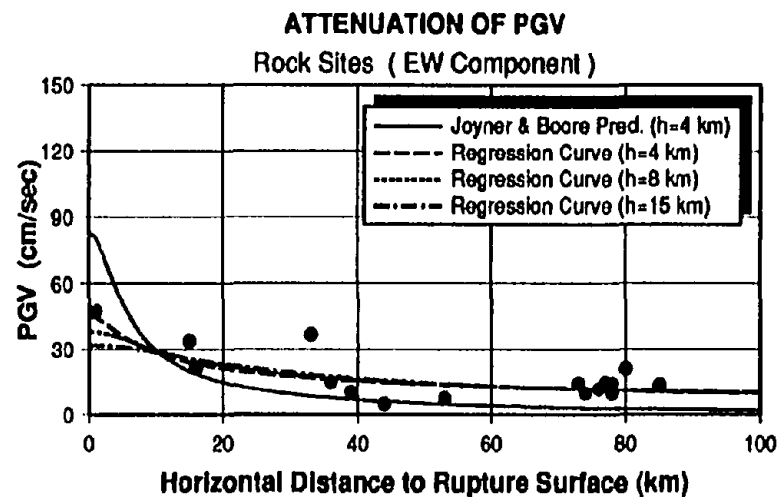
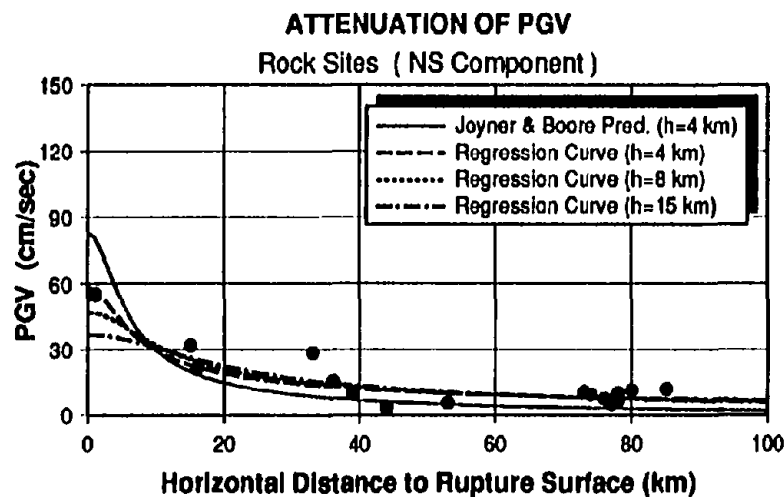
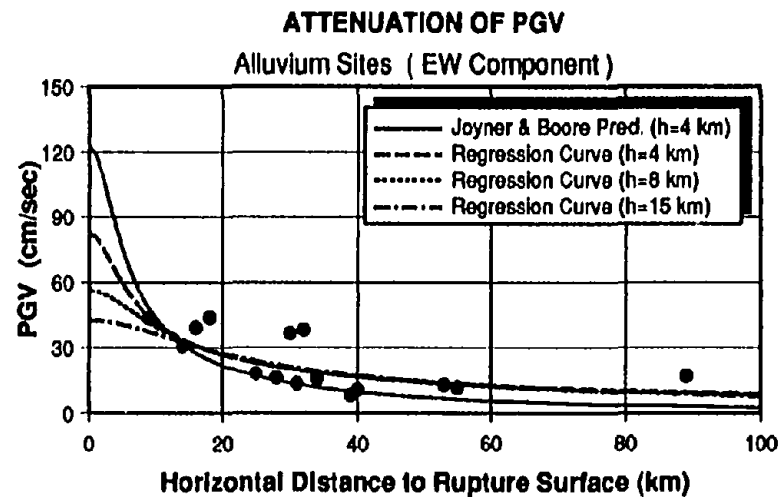
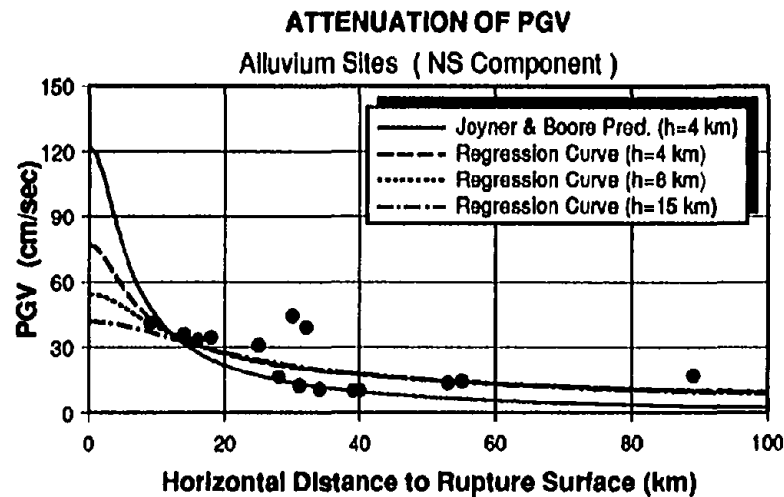
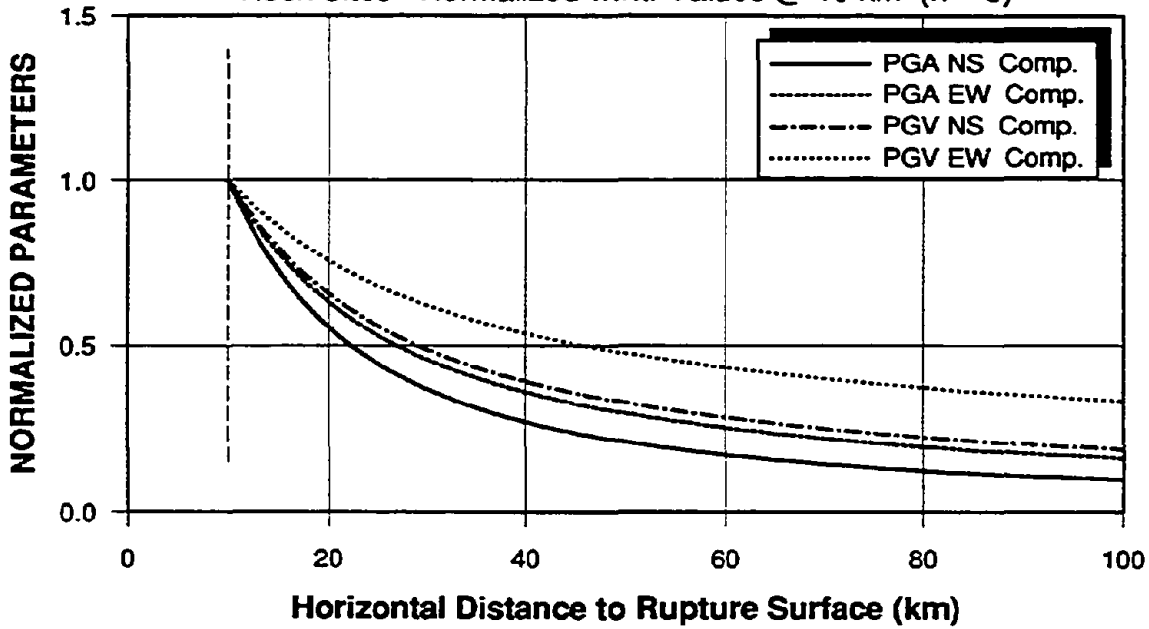


Fig. 4.3 Attenuation of PGV for Alluvium and Rock Sites (NS & EW Components)

NORMALIZED REGRESSION CURVES

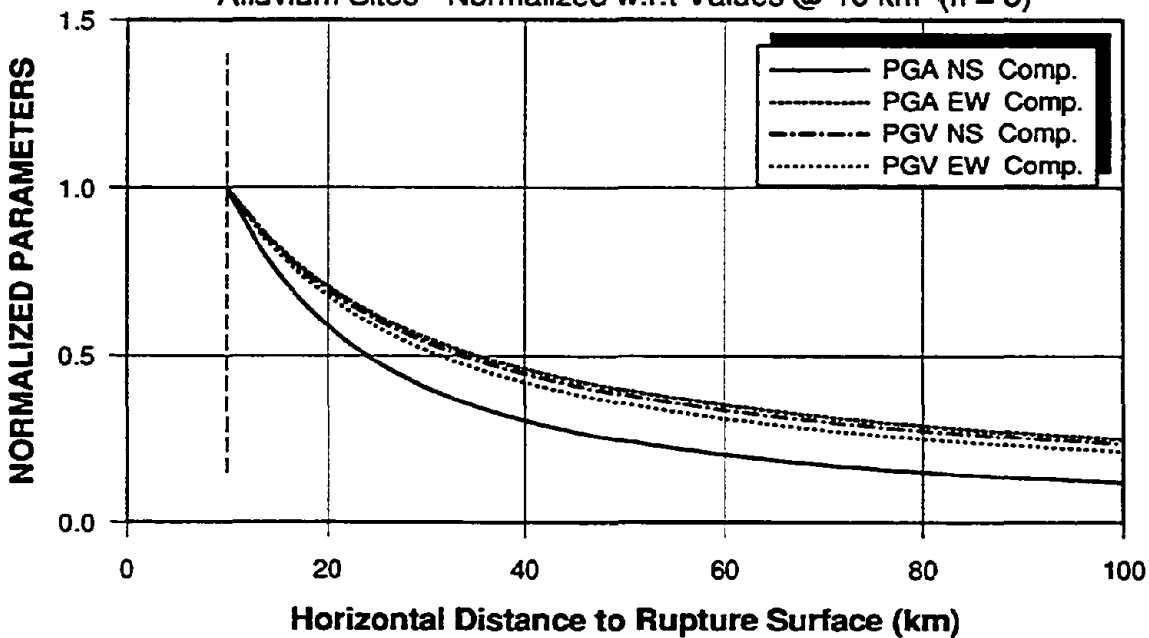
Rock Sites - Normalized w.r.t. Values @ 10 km (h = 8)



(a) Rock Sites

NORMALIZED REGRESSION CURVES

Alluvium Sites - Normalized w.r.t. Values @ 10 km (h = 8)

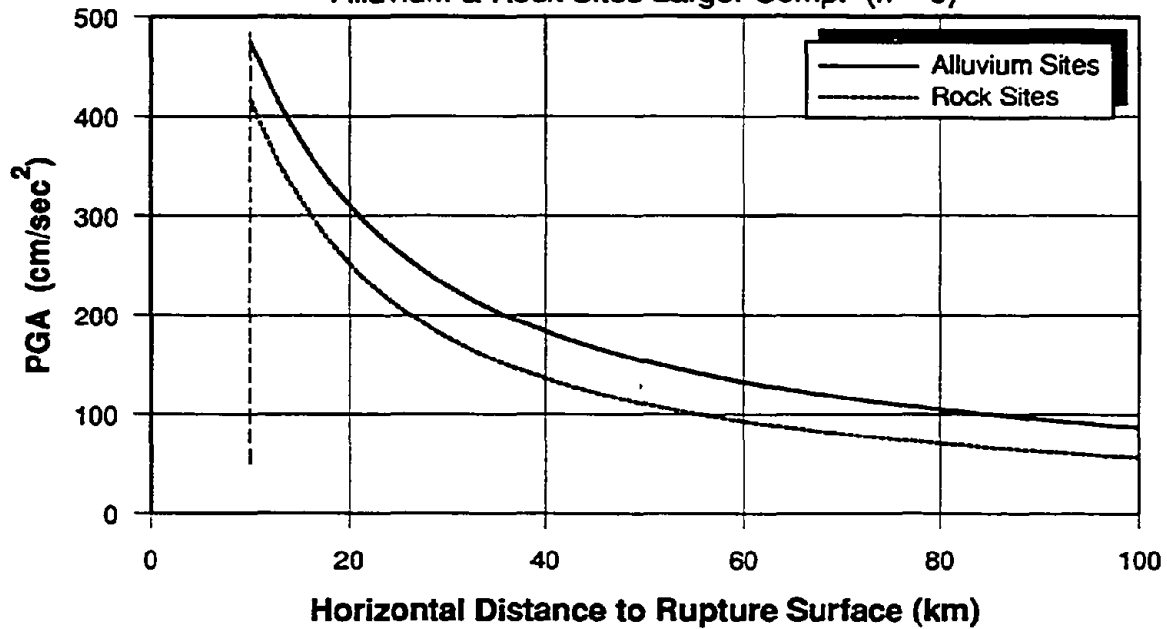


(b) Alluvium

Fig. 4.4 Normalized Regression Curves for PGA and PGV (NS & EW Components)

ATTENUATION OF PGA

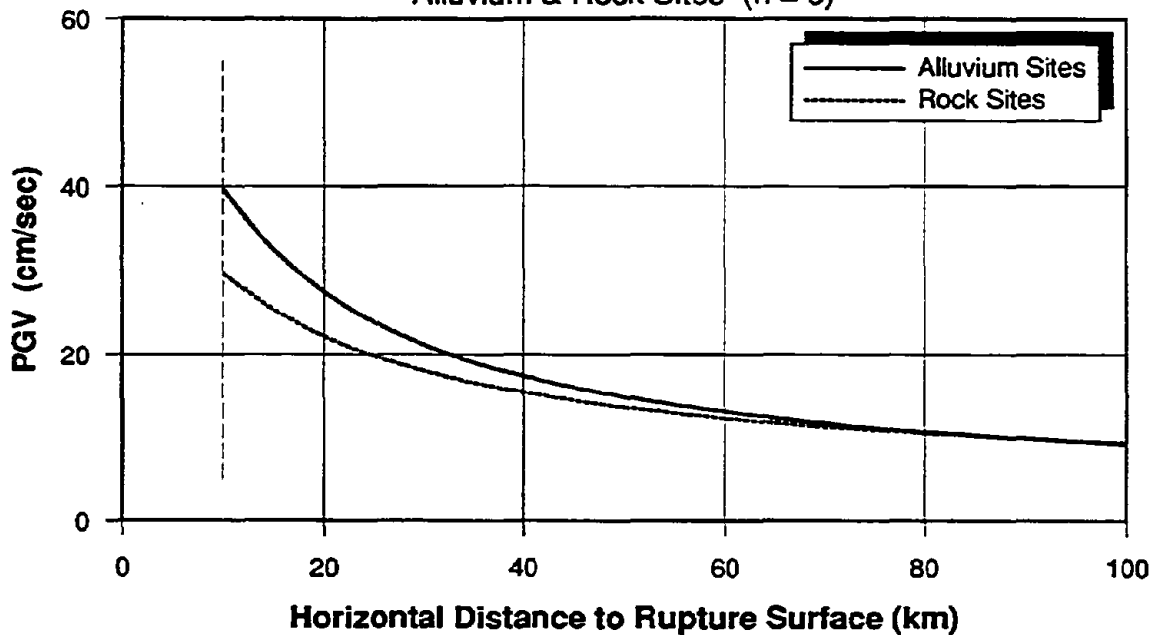
Alluvium & Rock Sites Larger Comp. ($h = 8$)



(a) PGA of Larger Component

ATTENUATION OF PGV

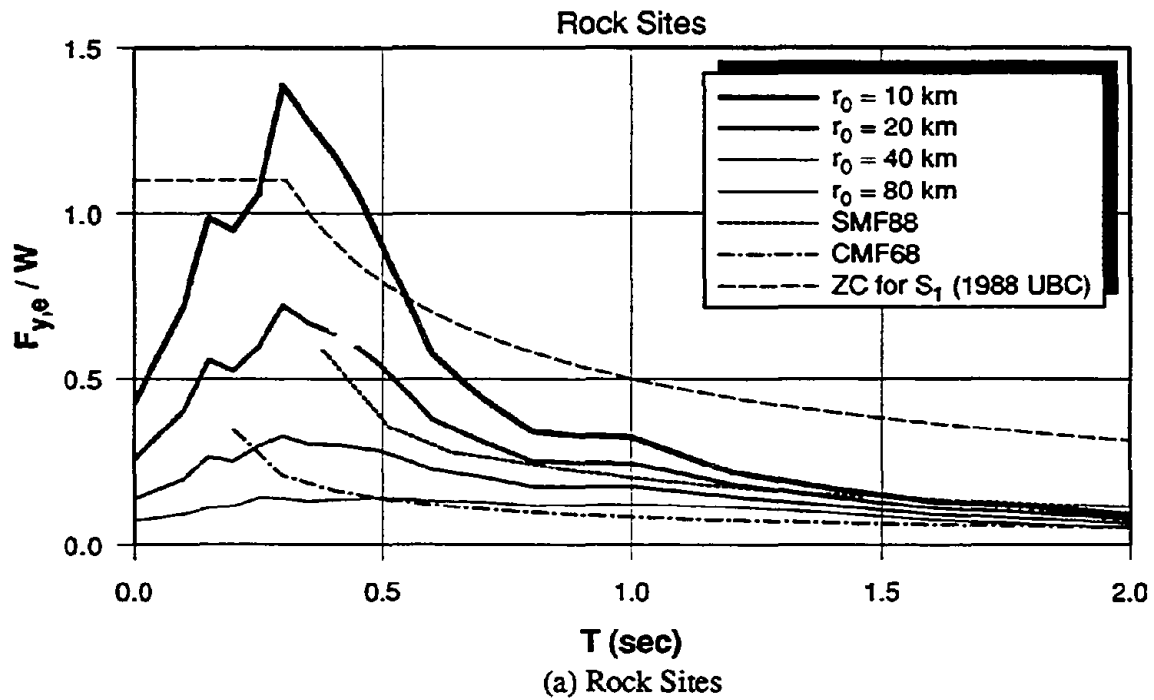
Alluvium & Rock Sites ($h = 8$)



(b) PGV of Larger Component

Fig. 4.5 Attenuation of PGA and PGV for Rock and Alluvium Sites (Larger Comp.)

ATTENUATION OF ELASTIC STRENGTH DEMAND SPECTRA



ATTENUATION OF ELASTIC STRENGTH DEMAND SPECTRA

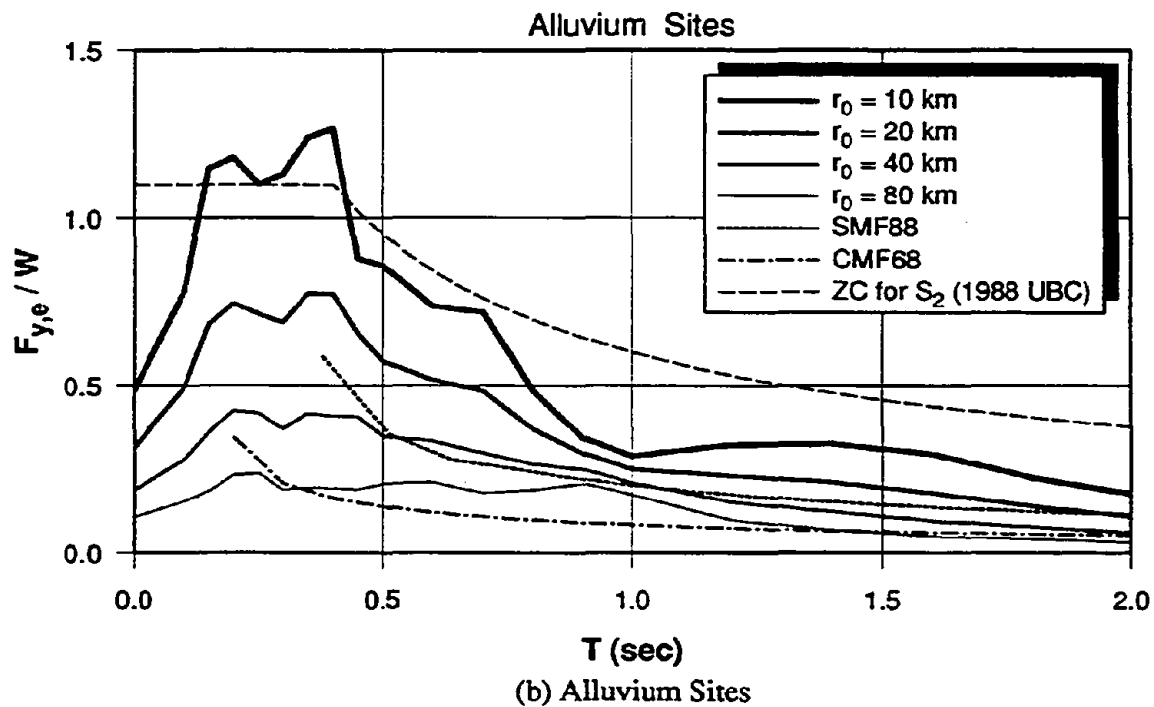
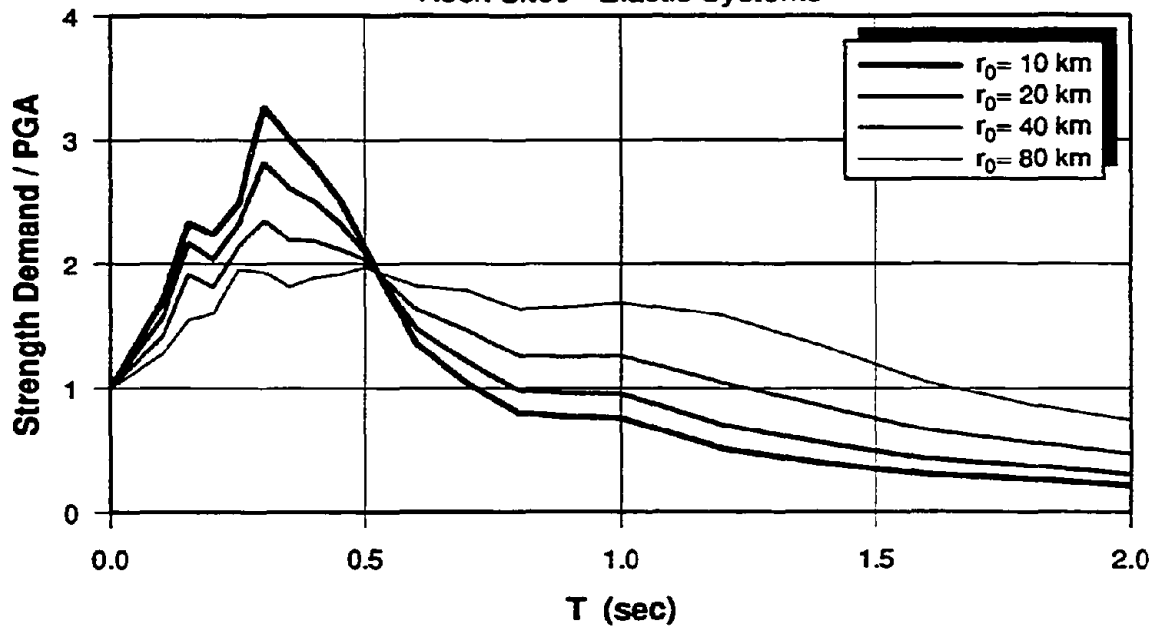


Fig. 4.6 Attenuation of Elastic Strength Demand Spectra

VARIATION OF SHAPE OF ELASTIC SPECTRA

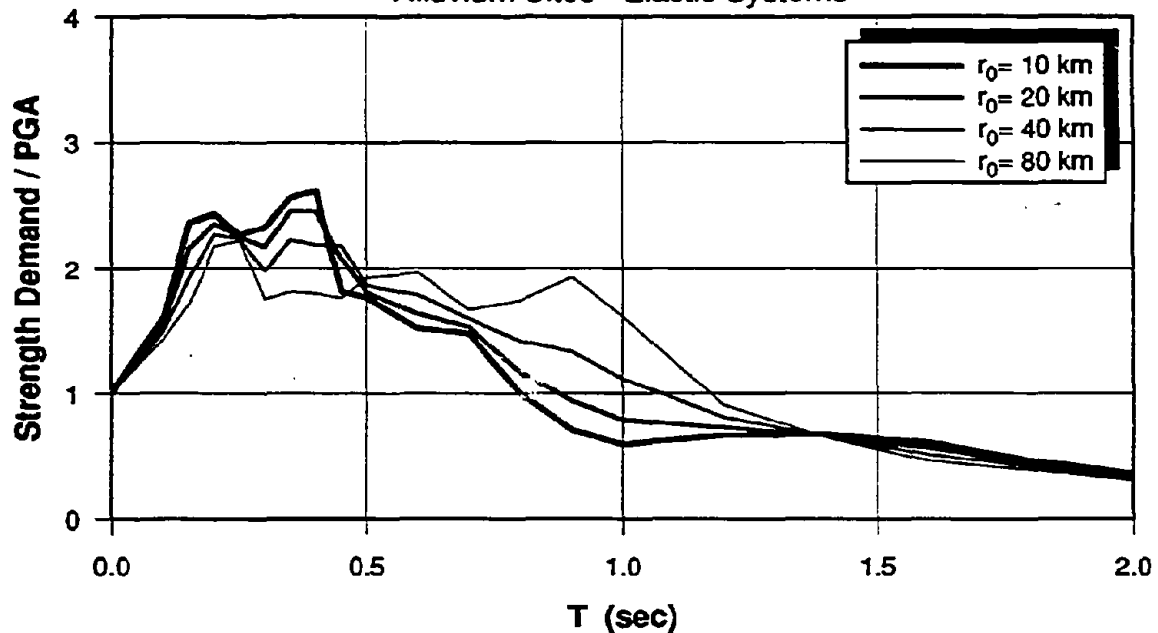
Rock Sites - Elastic Systems



(a) Rock Site Records

VARIATION OF SHAPE OF ELASTIC SPECTRA

Alluvium Sites - Elastic Systems

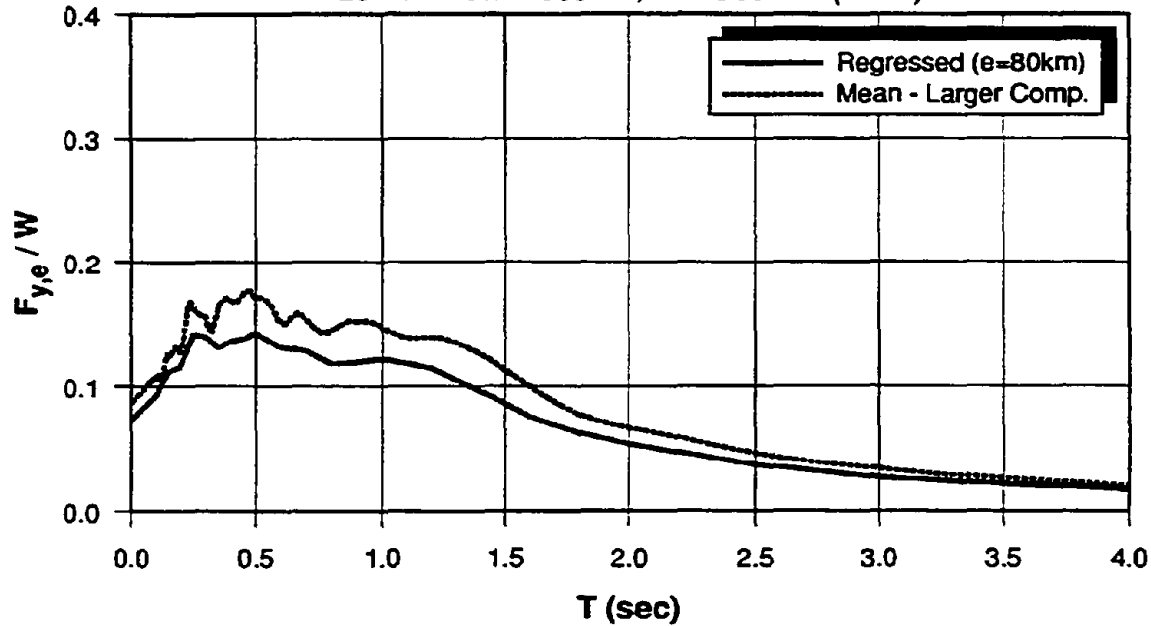


(b) Alluvium Site Records

Fig. 4.7 Variation of Shapes of Elastic Strength Demand Spectra with Distance

ELASTIC RESPONSE SPECTRA

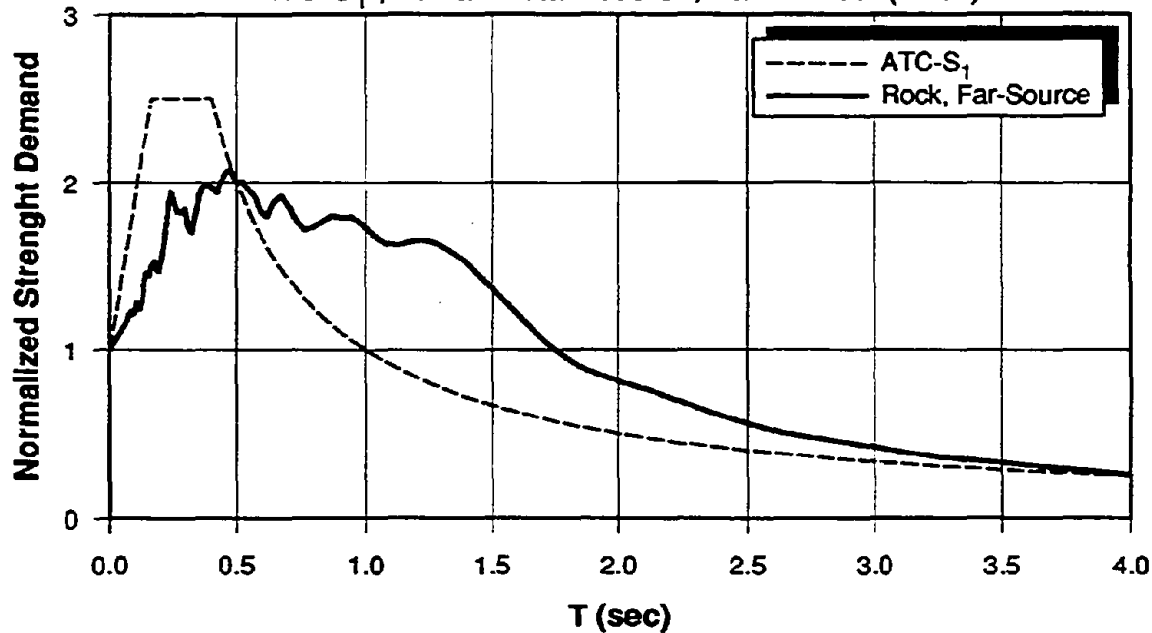
Loma Prieta Records, Far-Source (Rock)



(a) Comparison of Regressed and Mean Spectra (Rock)

NORMALIZED ELASTIC STRENGTH DEMAND SPECTRA - MEAN

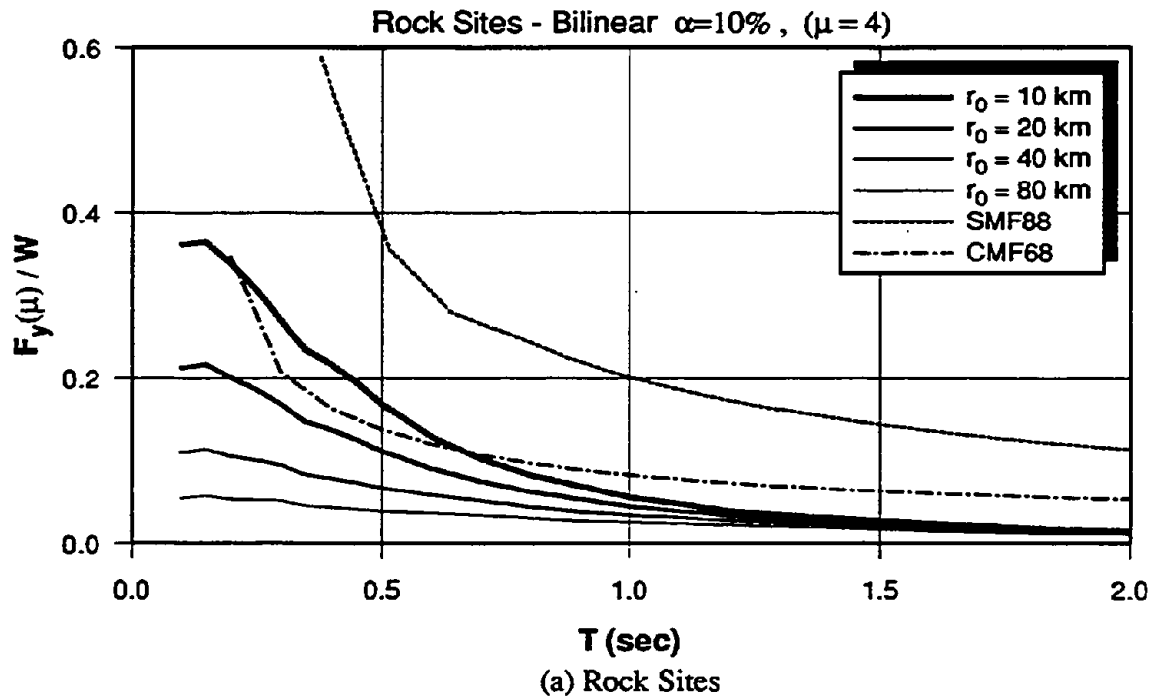
ATC-S₁, Loma Prieta Records, Far-Source (Rock)



(b) Mean Normalized Spectra of Far-Source Motions

Fig. 4.8 Mean of Elastic Strength Demand Spectra for San Francisco Area (Rock)

ATTENUATION OF INELASTIC STRENGTH DEMAND SPECTRA



ATTENUATION OF INELASTIC STRENGTH DEMAND SPECTRA

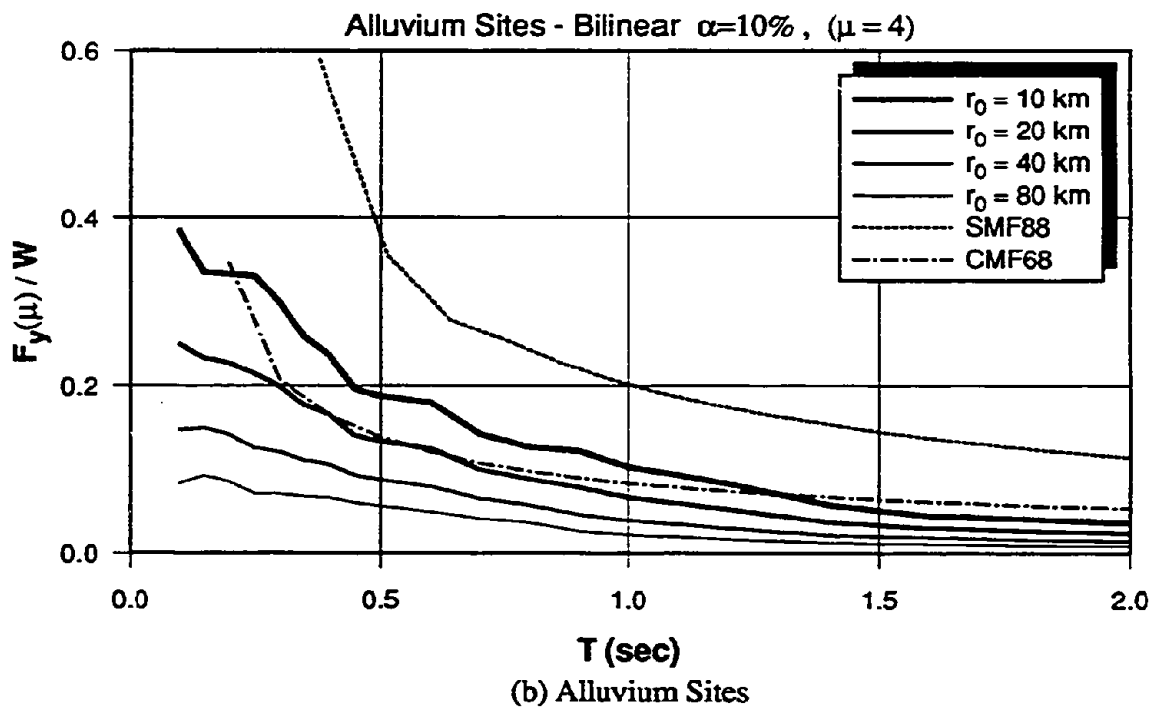
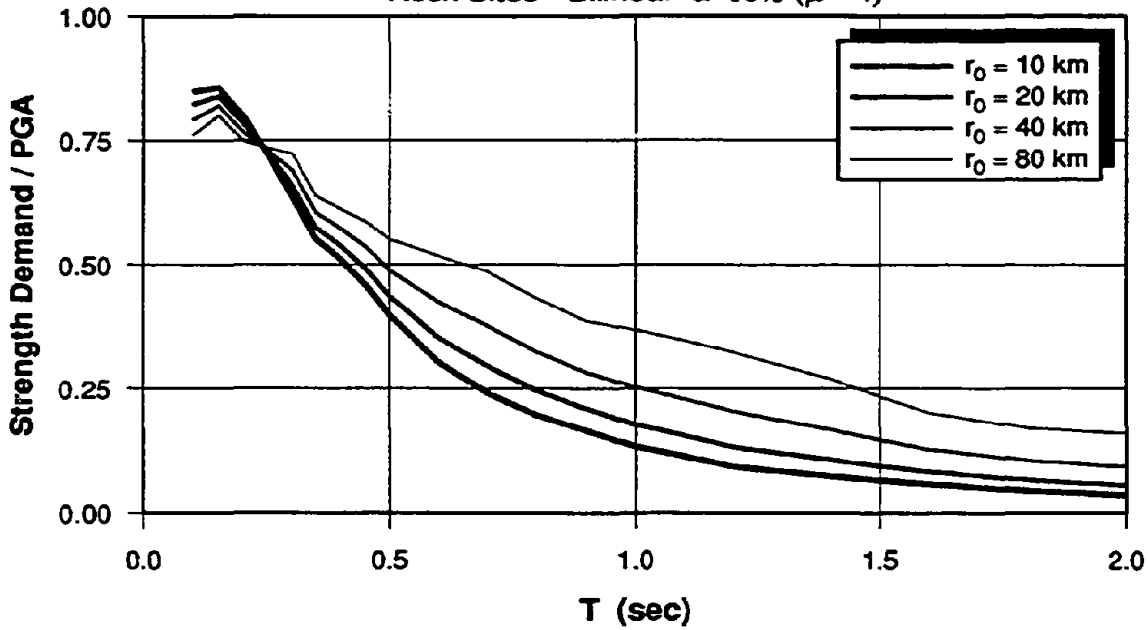


Fig 4.9 Attenuation of Inelastic Strength Demand Spectra for $\mu = 4$

VARIATION OF NORMALIZED STRENGTH DEMAND SPECTRA

Rock Sites - Bilinear $\alpha=10\%$ ($\mu = 4$)



VARIATION OF NORMALIZED STRENGTH DEMAND SPECTRA

Alluvium Sites - Bilinear $\alpha=10\%$ ($\mu = 4$)

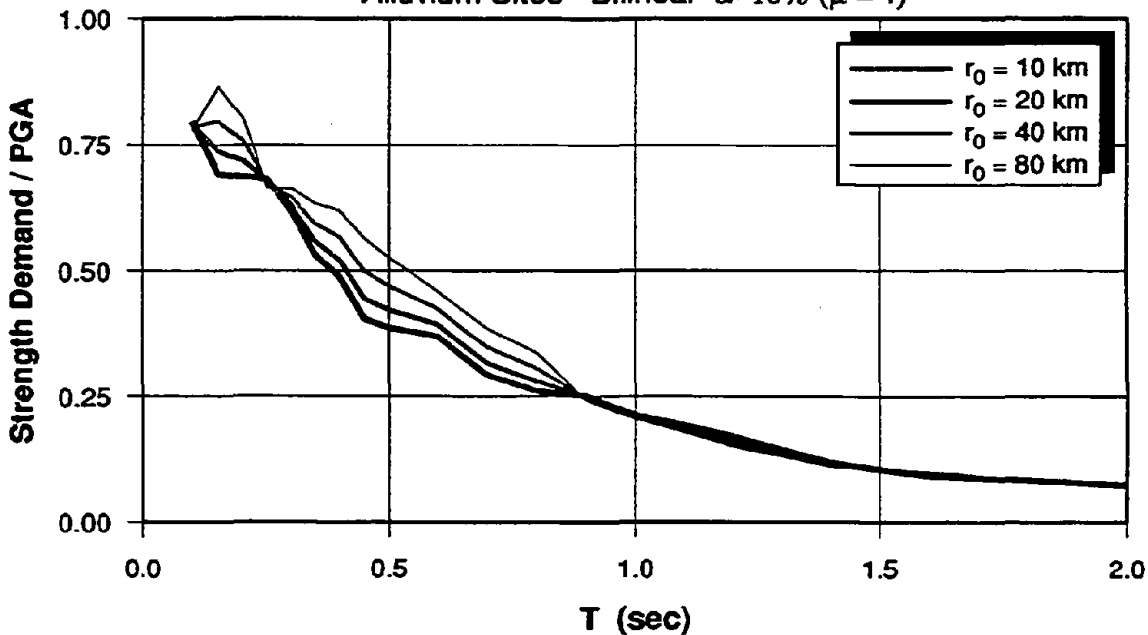
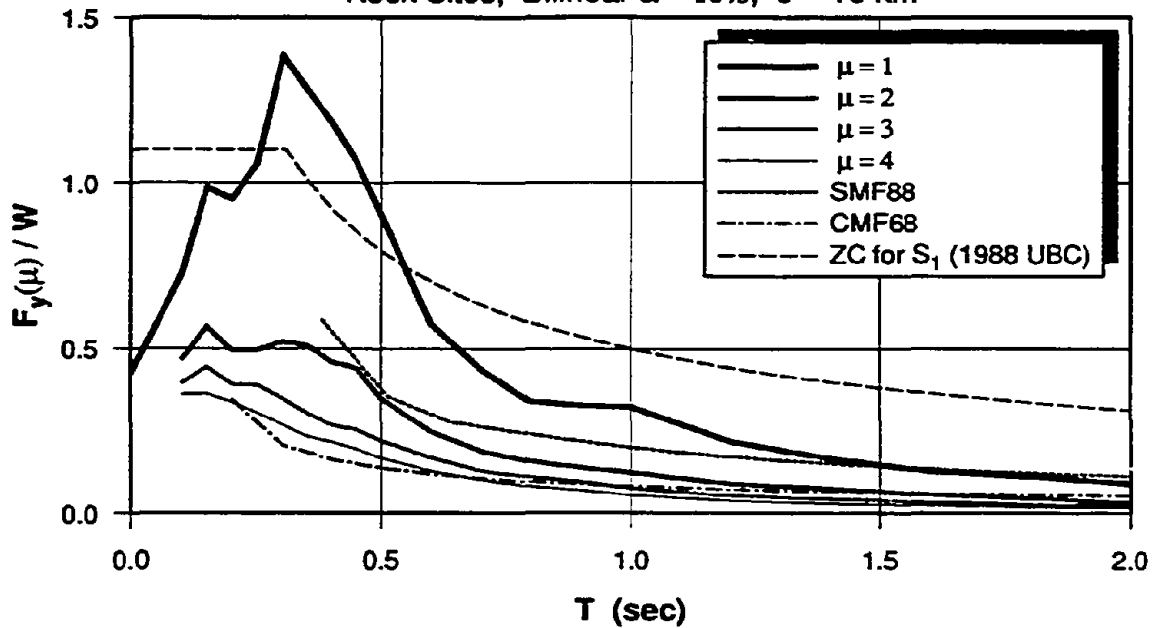


Fig. 4.10 Variation of Shapes of Inelastic Strength Demand Spectra with Distance ($\mu = 4$)

REGRESSED ELASTIC AND INELASTIC STRENGTH DEMANDS

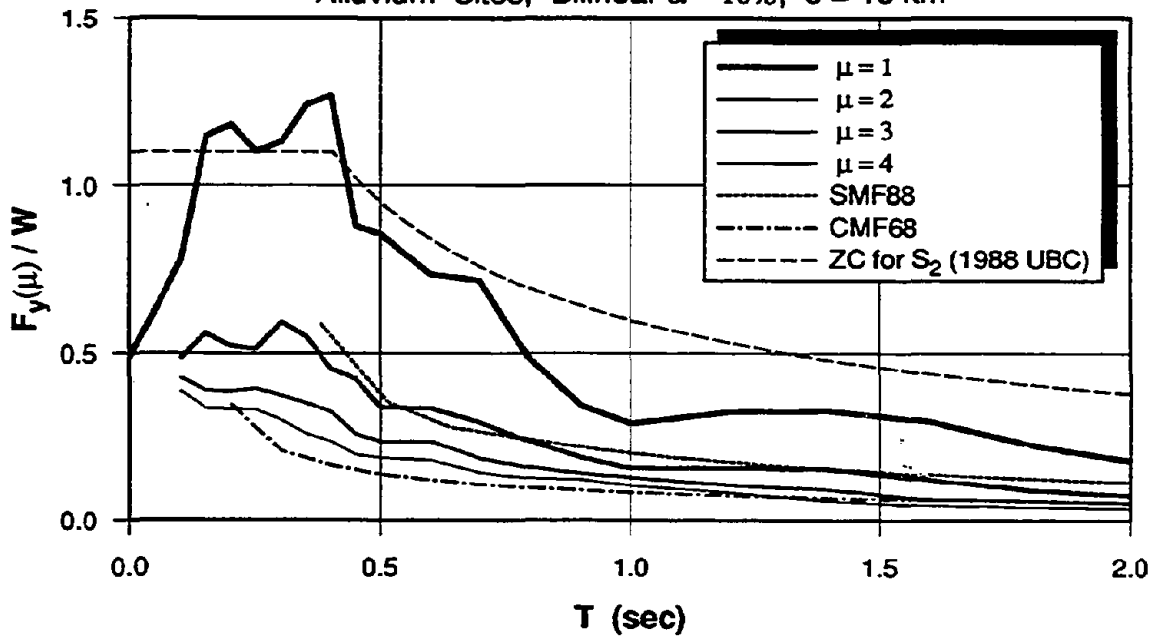
Rock Sites, Bilinear $\alpha = 10\%$, $e = 10$ km



(a) Rock Site Records

REGRESSED ELASTIC AND INELASTIC STRENGTH DEMANDS

Alluvium Sites, Bilinear $\alpha = 10\%$, $e = 10$ km

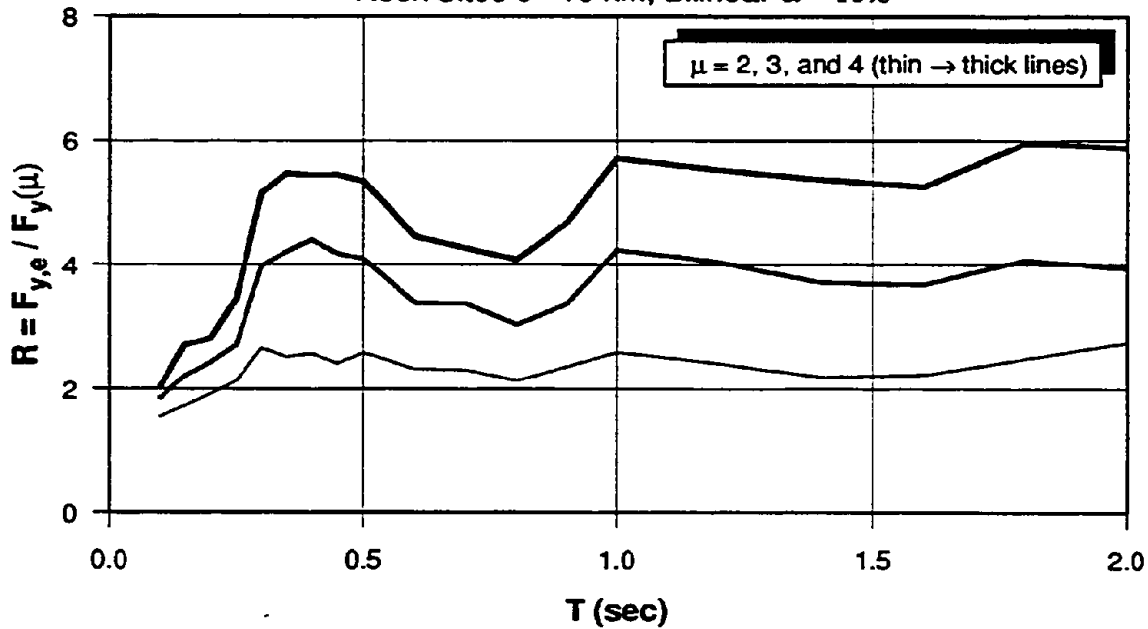


(b) Alluvium Site Records

Fig. 4.11 Regressed Elastic and Inelastic Strength Demand Spectra at $r_0 = 10$ km

REGRESSED STRENGTH REDUCTION FACTORS $-\mu=2,3,4$

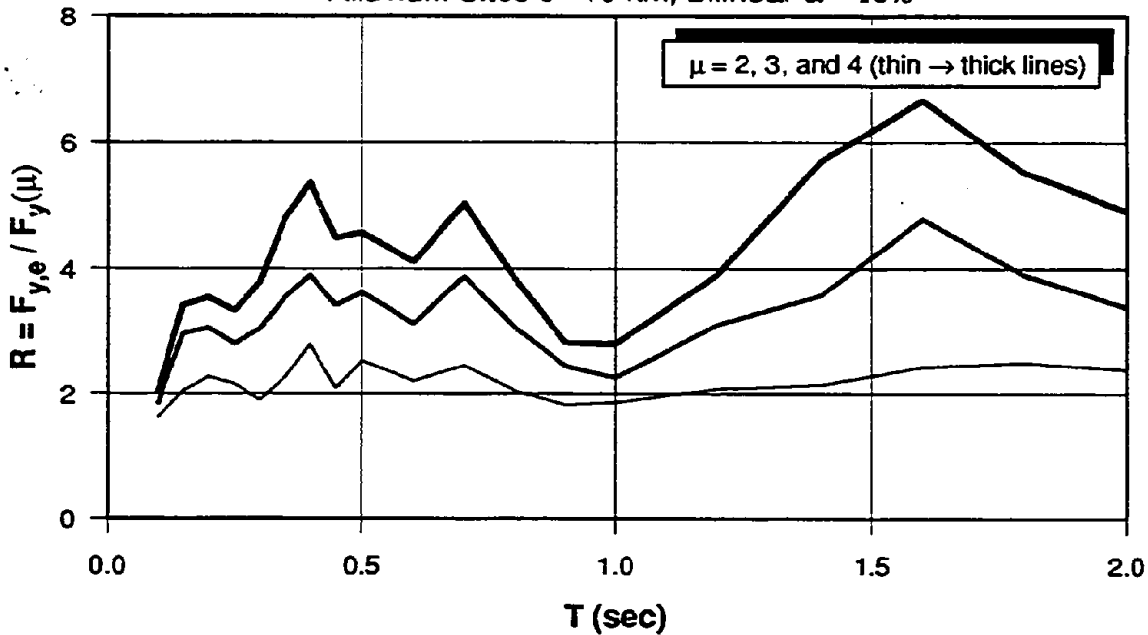
Rock Sites $e=10$ km, Bilinear $\alpha=10\%$



(a) Rock Sites

REGRESSED STRENGTH REDUCTION FACTORS $-\mu=2,3,4$

Alluvium Sites $e=10$ km, Bilinear $\alpha=10\%$



(b) Alluvium Sites

Fig. 4.12 Attenuation of Strength Reduction Factors

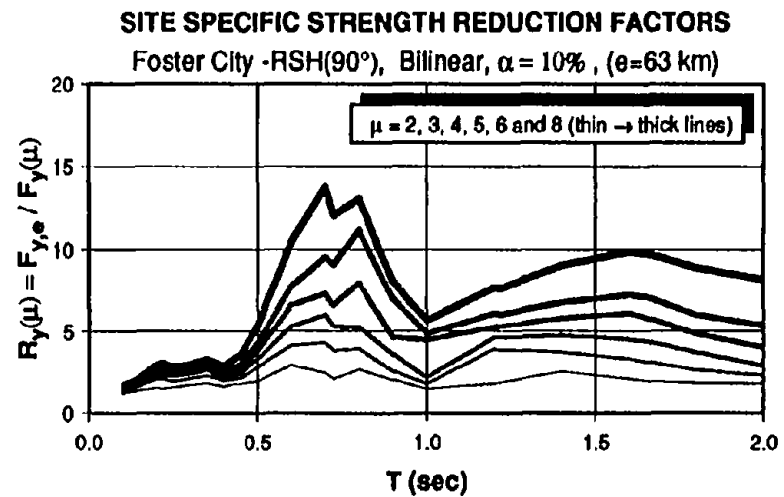
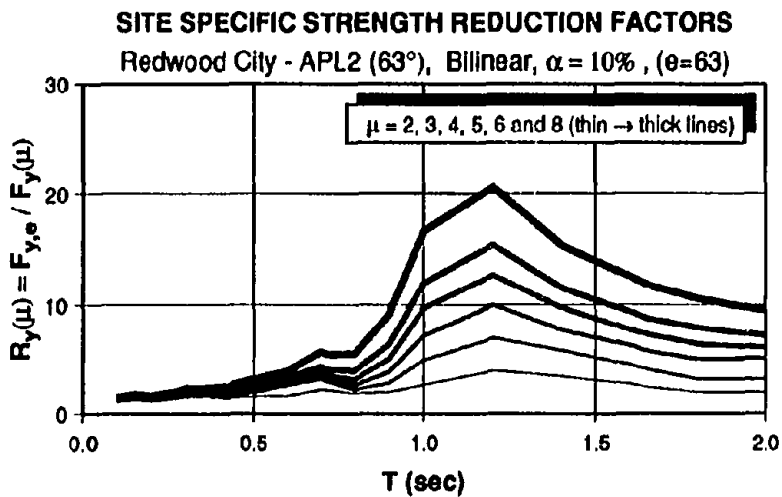
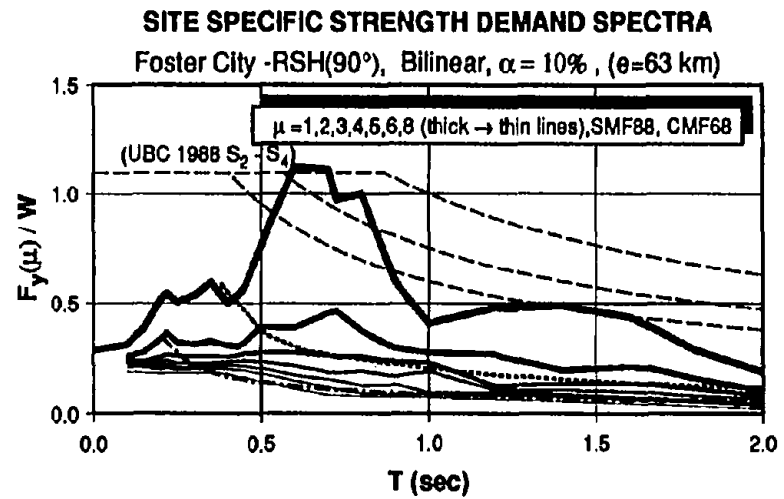
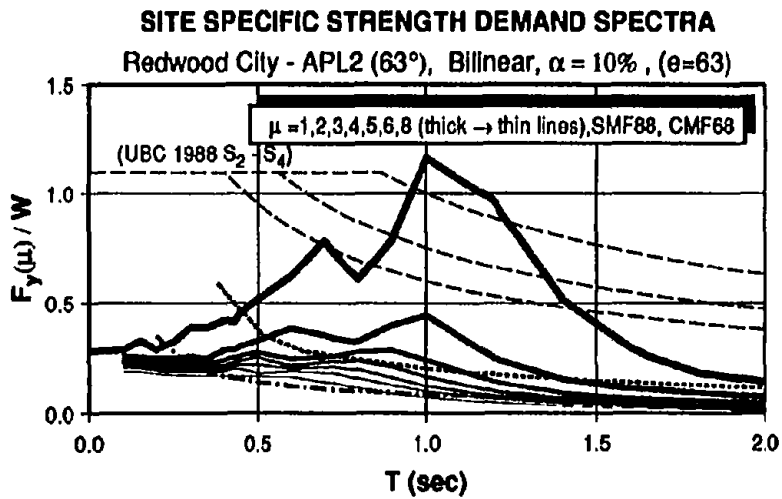


Fig. 4.13 Site Specific Strength Demand Spectra and Reduction Factors for Soft Soil Records

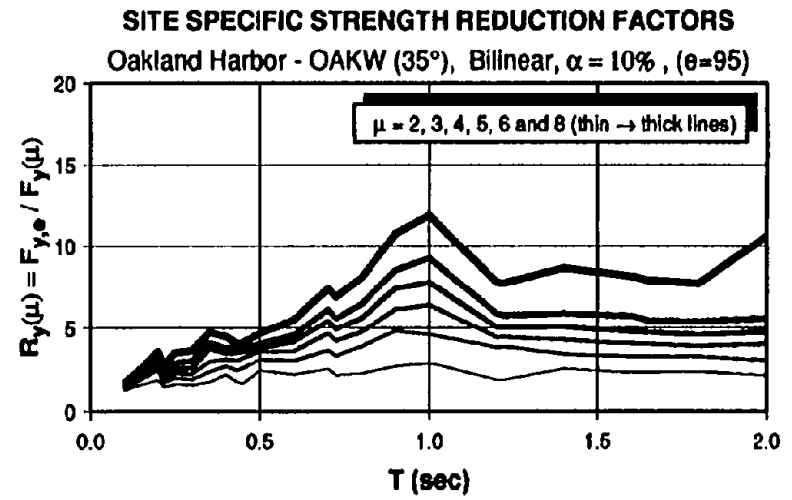
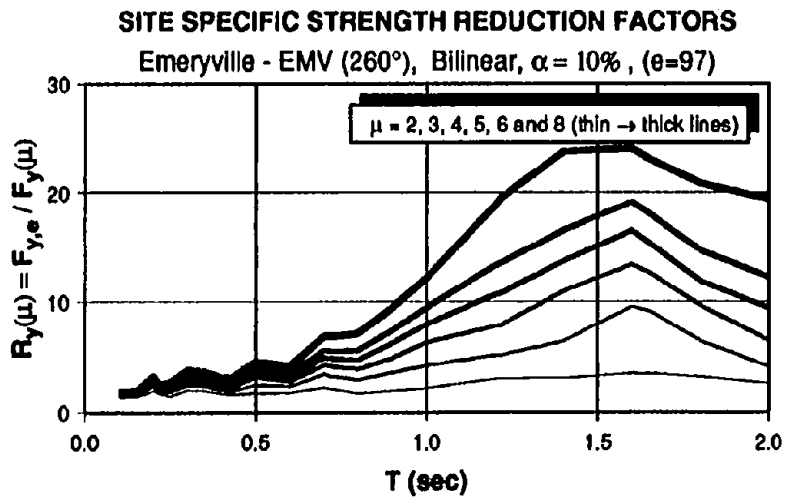
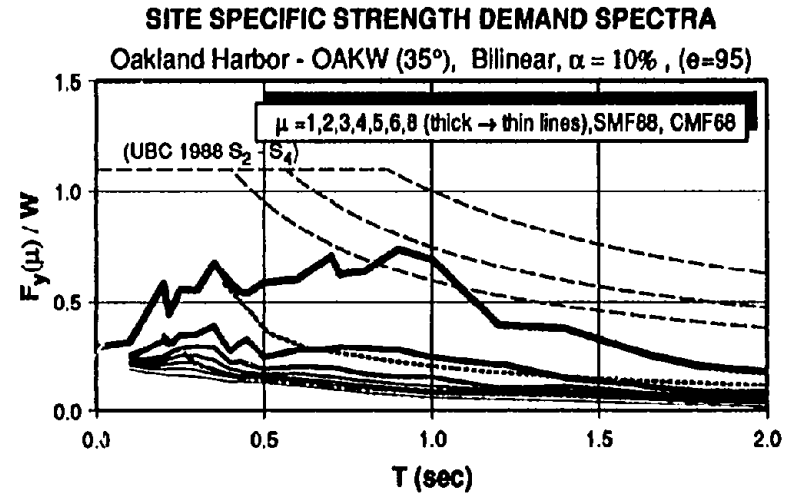
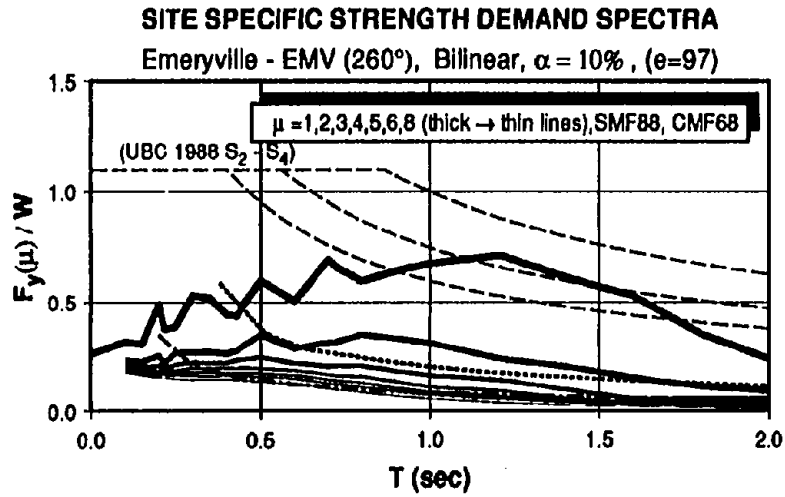


Fig. 4.13 (cont'd) Site Specific Strength Demand Spectra and Reduction Factors for Soft Soil Records

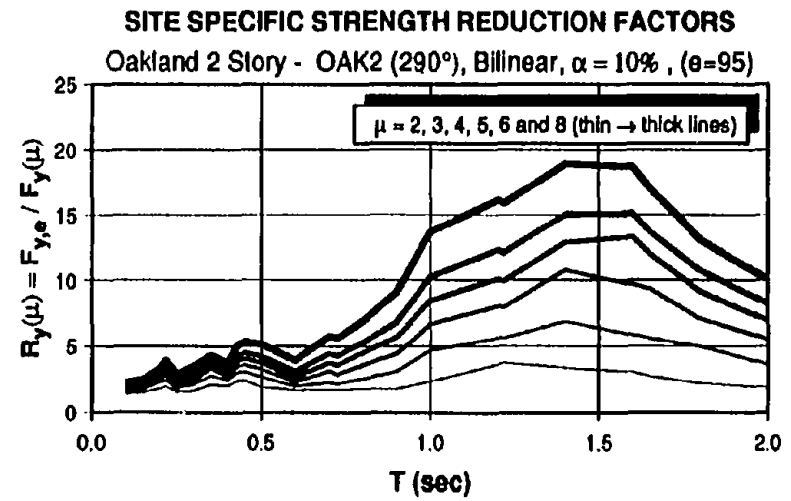
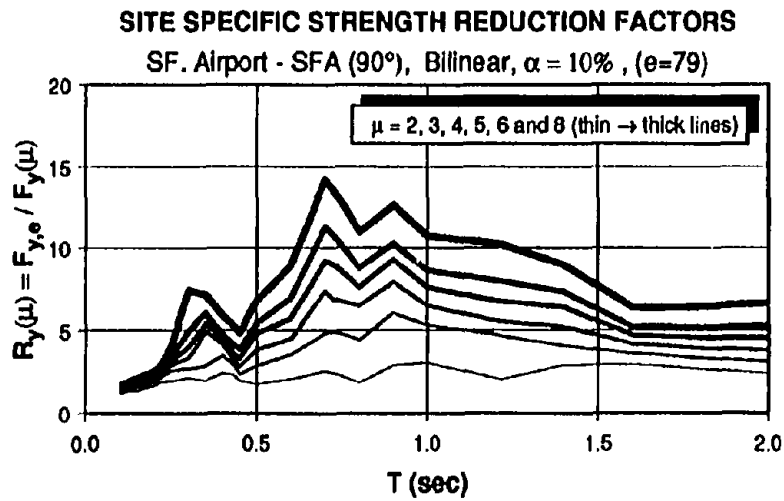
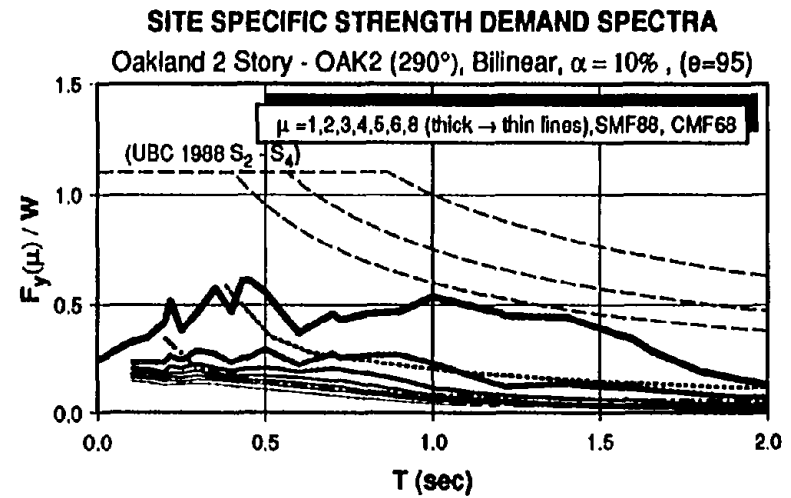
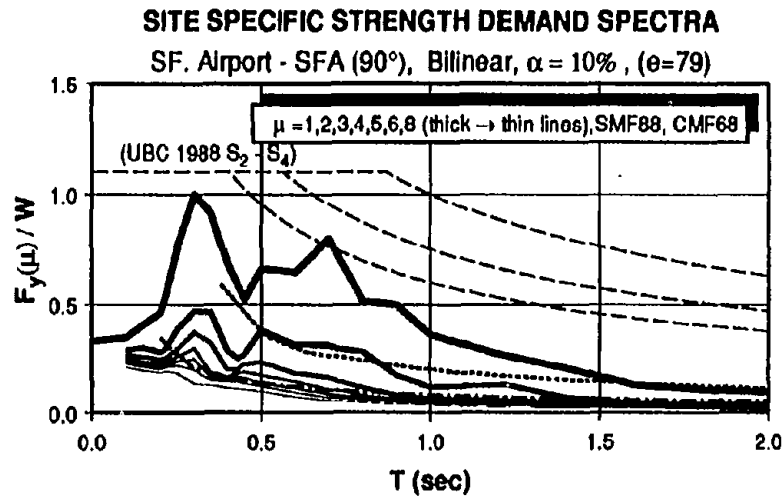
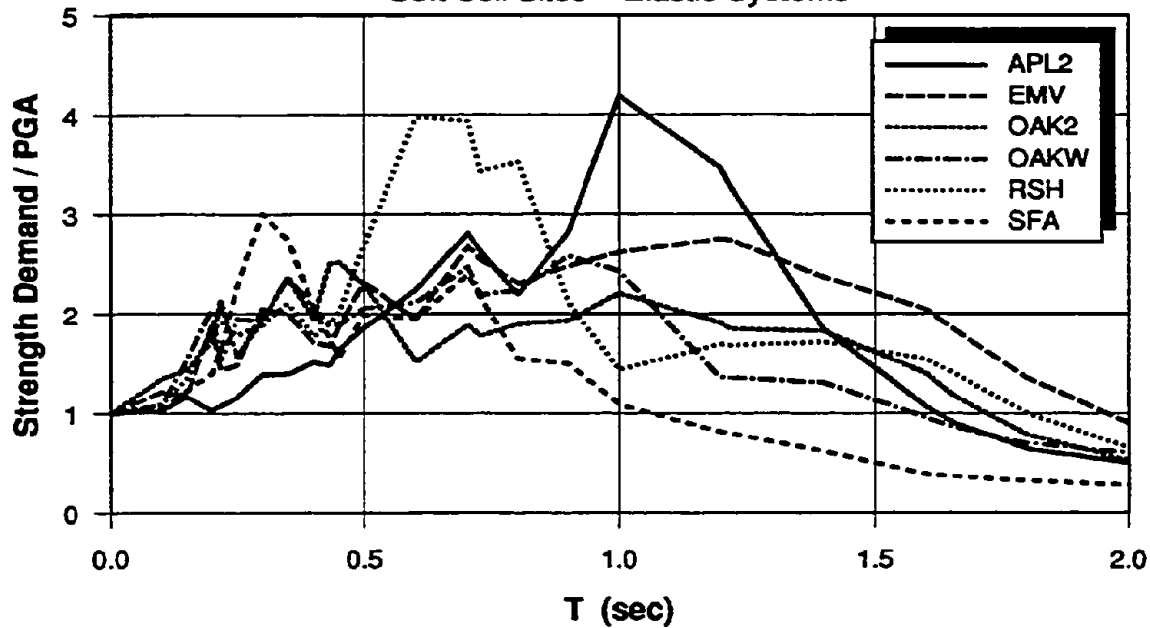


Fig. 4.13 (cont'd) Site Specific Strength Demand Spectra and Reduction Factors for Soft Soil Records

VARIATION OF SHAPE OF ELASTIC SPECTRA

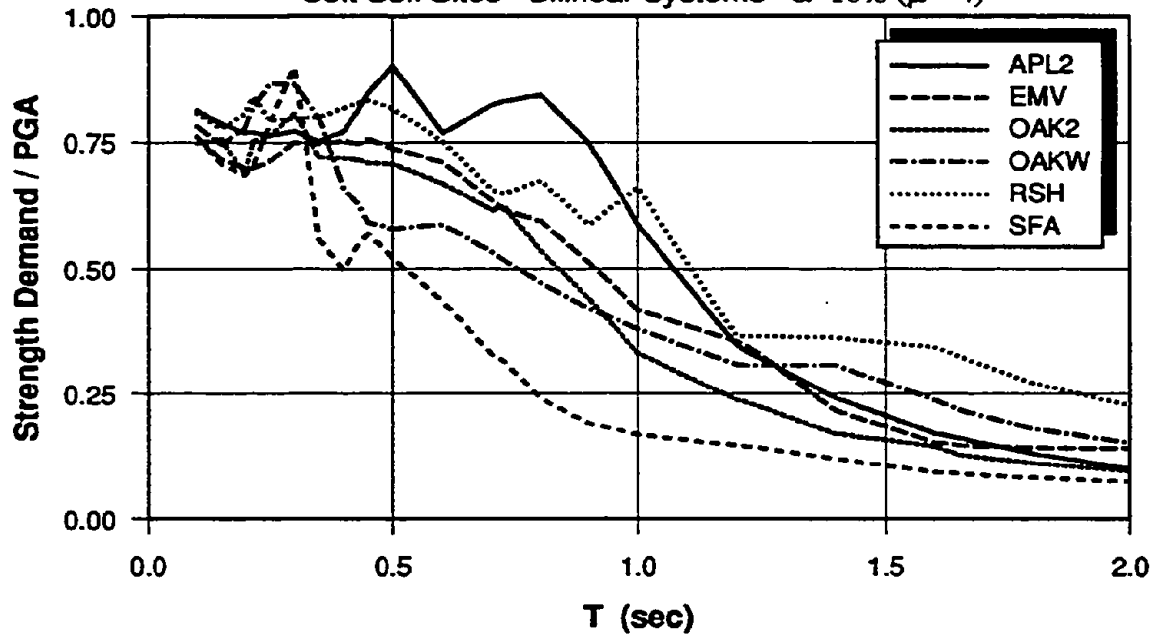
Soft Soil Sites - Elastic Systems



(a) Normalized Elastic Strength Demand Spectra

VARIATION OF SHAPE OF INELASTIC SPECTRA

Soft Soil Sites - Bilinear Systems $\alpha=10\%$ ($\mu=4$)

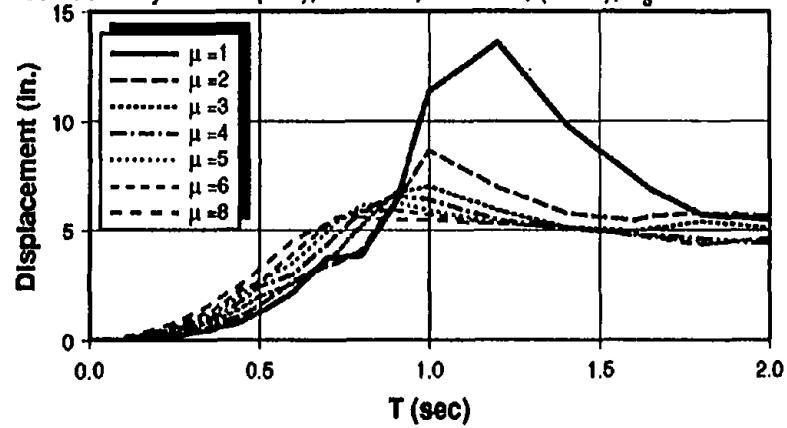


(b) Normalized Inelastic Strength Demand Spectra for $\mu=4$

Fig. 4.14 Variation of Shape of Elastic and Inelastic Strength Demand Spectra

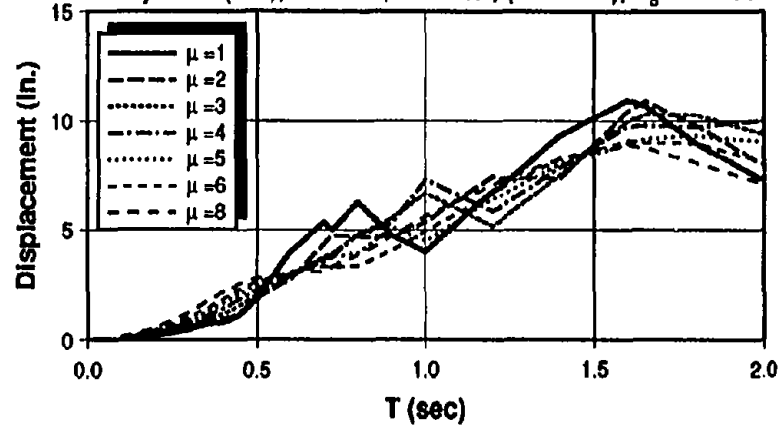
SITE SPECIFIC DISPLACEMENT DEMAND SPECTRA

Redwood City - APL2 (63°), Bilinear, $\alpha = 10\%$, ($\theta=63$), $T_g = 1.10$ sec.



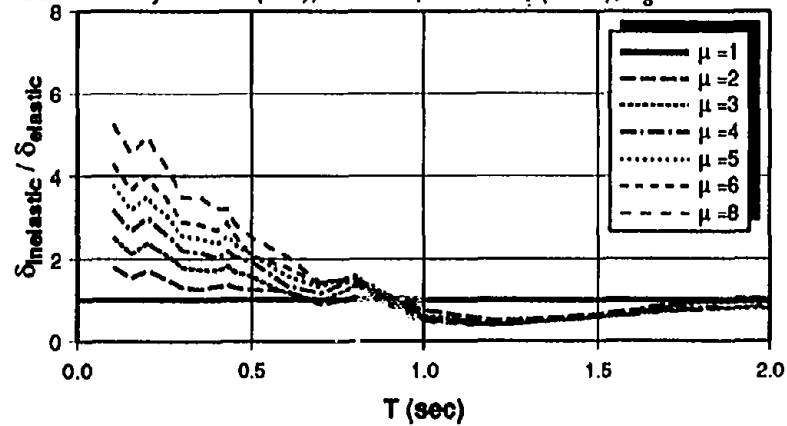
SITE SPECIFIC DISPLACEMENT DEMAND SPECTRA

Foster City - RSH(90°), Bilinear, $\alpha = 10\%$, ($\theta=63$ km), $T_g = 1.4$ sec.



SITE SPECIFIC NORMALIZED DISPLACEMENT DEMAND SPECTRA

Redwood City - APL2 (63°), Bilinear, $\alpha = 10\%$, ($\theta=63$), $T_g = 1.10$ sec.



SITE SPECIFIC NORMALIZED DISPLACEMENT DEMAND SPECTRA

Foster City - RSH(90°), Bilinear, $\alpha = 10\%$, ($\theta=63$ km), $T_g = 1.4$ sec.

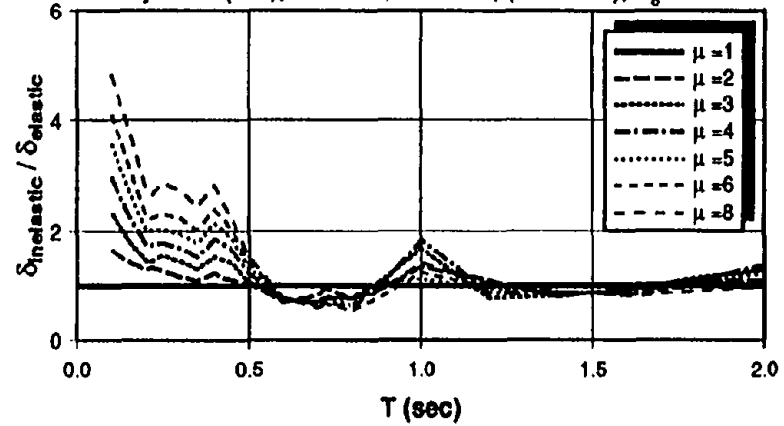


Fig. 4.15 Site Specific Displacement and Normalized Displacement Demands for Soft Soil Records

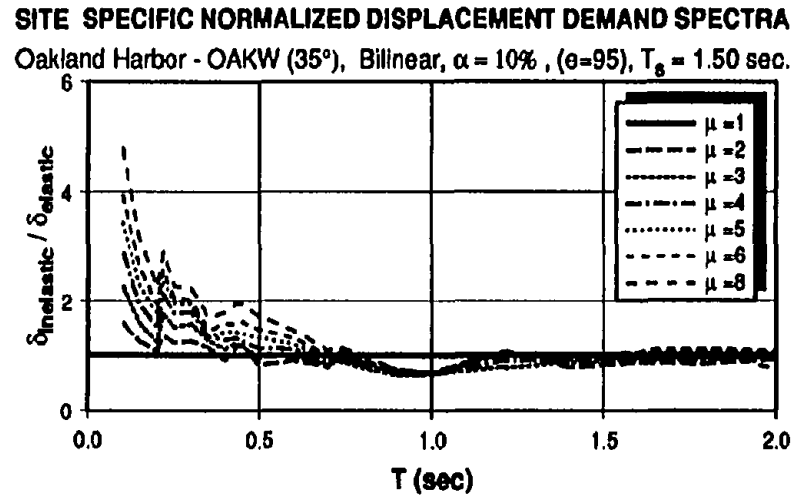
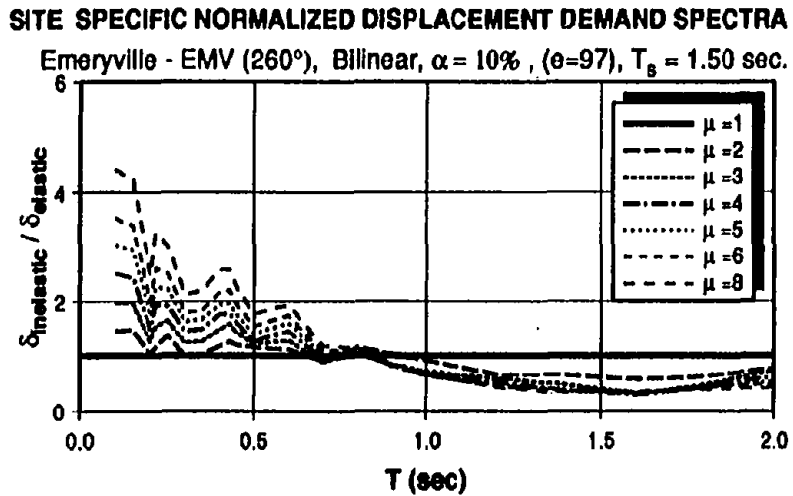
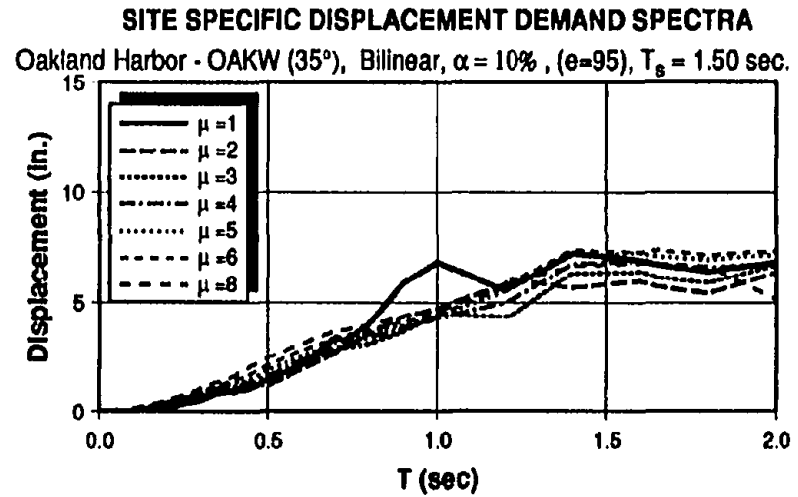
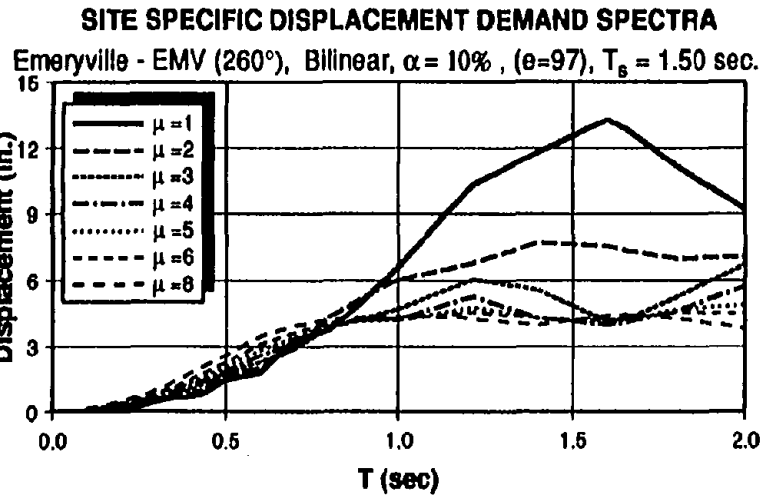
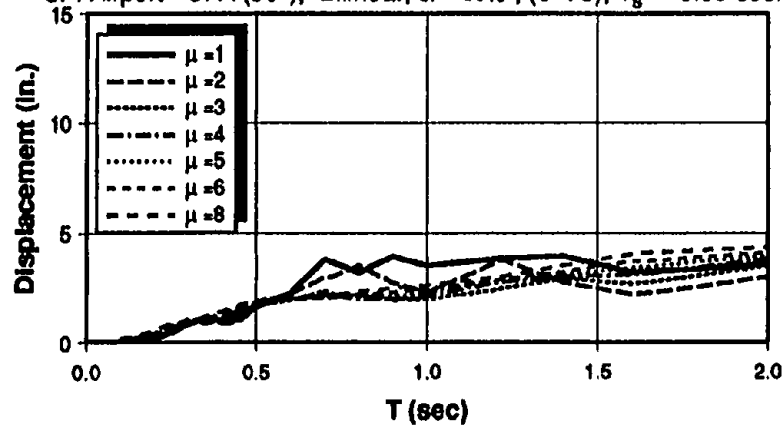


Fig. 4.15 (cont'd) Site Specific Displacement and Normalized Displacement Demands for Soft Soil Records

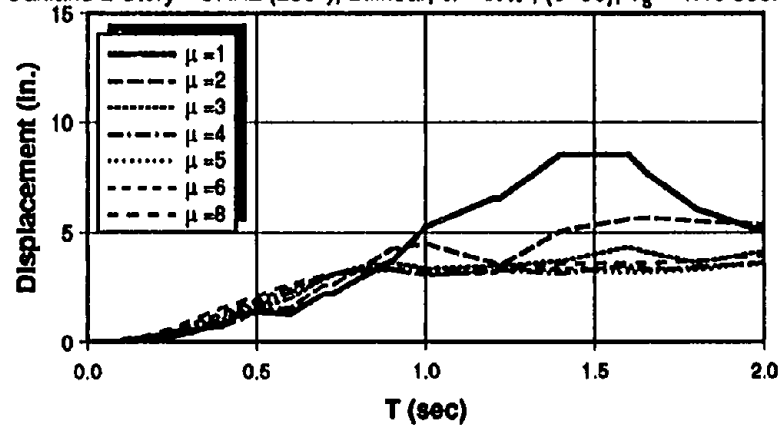
SITE SPECIFIC DISPLACEMENT DEMAND SPECTRA

SF. Airport - SFA (90°), Bilinear, $\alpha = 10\%$, ($\rho=79$), $T_g = 0.95$ sec.



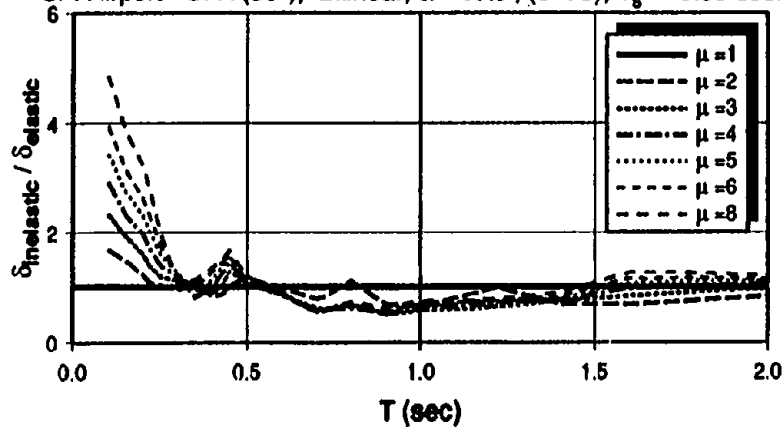
SITE SPECIFIC DISPLACEMENT DEMAND SPECTRA

Oakland 2 Story - OAK2 (290°), Bilinear, $\alpha = 10\%$, ($\rho=95$), $T_g = 1.15$ sec.



SITE SPECIFIC NORMALIZED DISPLACEMENT DEMAND SPECTRA

SF. Airport - SFA (90°), Bilinear, $\alpha = 10\%$, ($\rho=79$), $T_g = 0.95$ sec.



SITE SPECIFIC NORMALIZED DISPLACEMENT DEMAND SPECTRA

Oakland 2 Story - OAK2 (290°), Bilinear, $\alpha = 10\%$, ($\rho=95$), $T_g = 1.15$ sec.

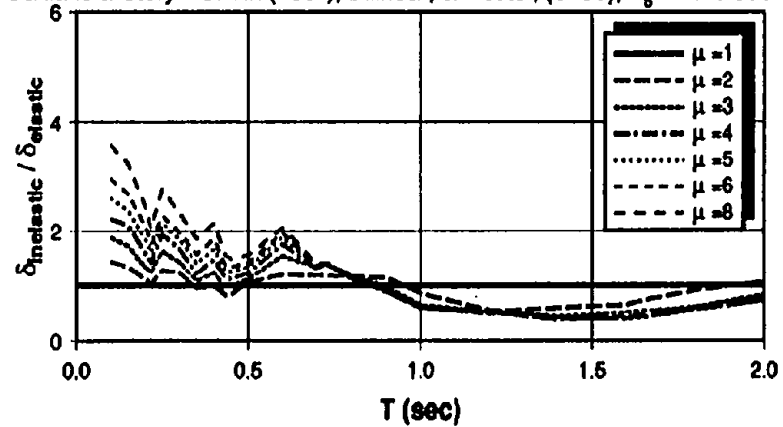
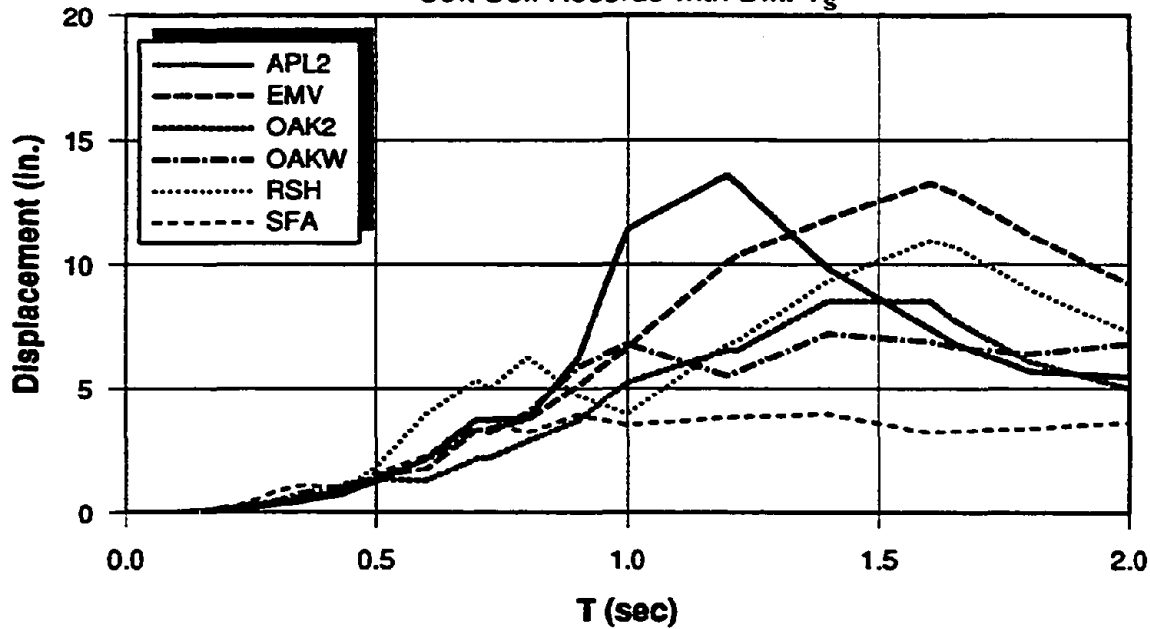


Fig. 4.15 (cont'd) Site Specific Displacement and Normalized Displacement Demands for Soft Soil Records

SITE SPECIFIC ELASTIC DISPLACEMENT DEMANDS

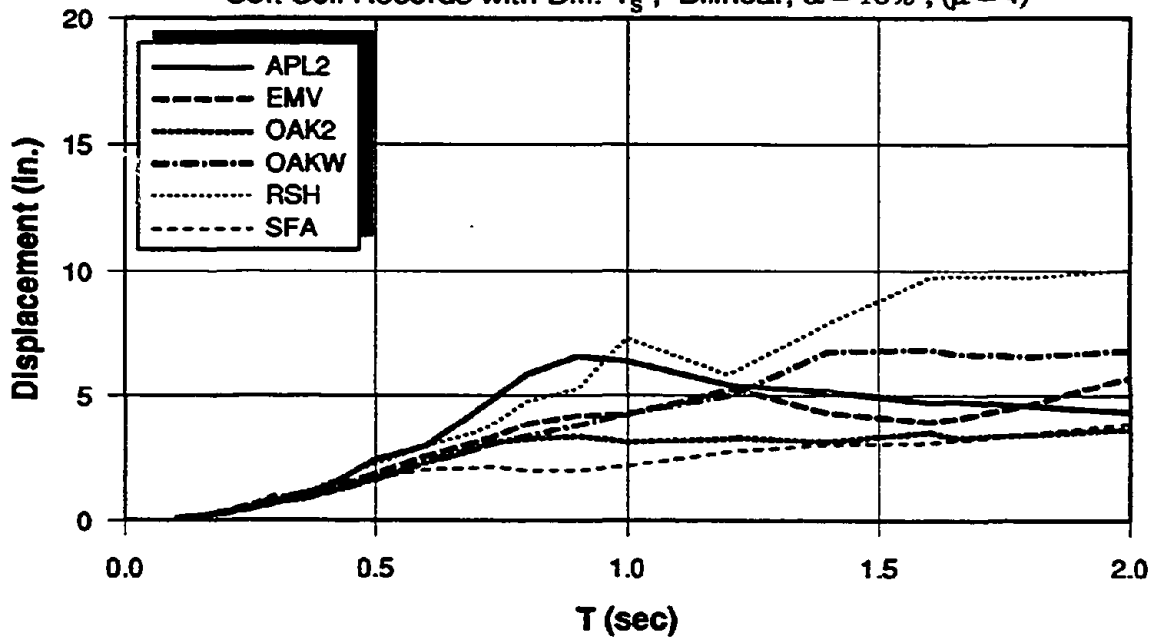
Soft Soil Records with Diff. T_s



(a) Elastic Displacement Demands

SITE SPECIFIC INELASTIC DISPLACEMENT DEMANDS

Soft Soil Records with Diff. T_s , Bilinear, $\alpha = 10\%$, ($\mu = 4$)



(b) Inelastic Displacement Demands

Fig. 4.16 Elastic and Inelastic Displacement Demands for Soft Soil Records

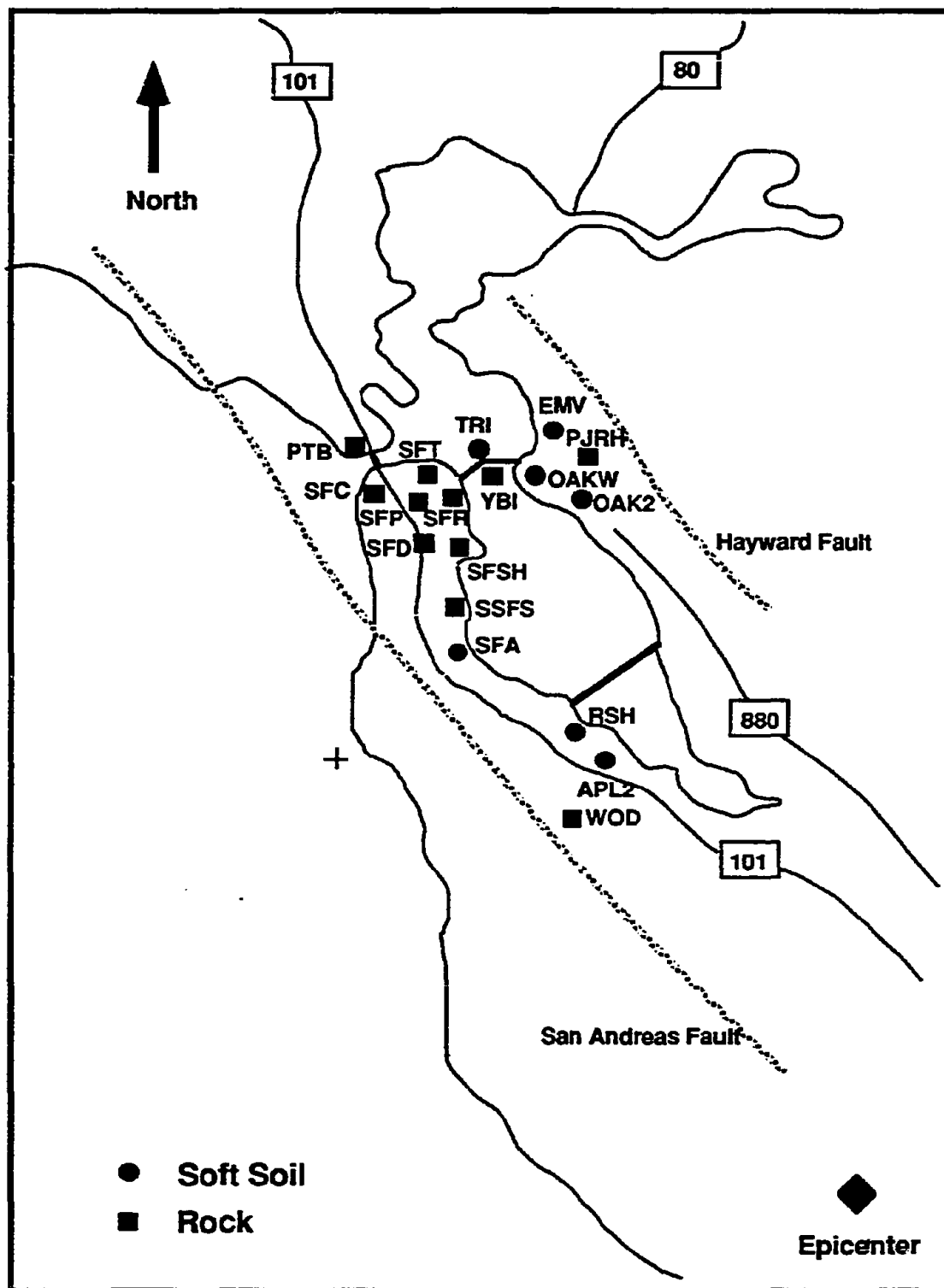
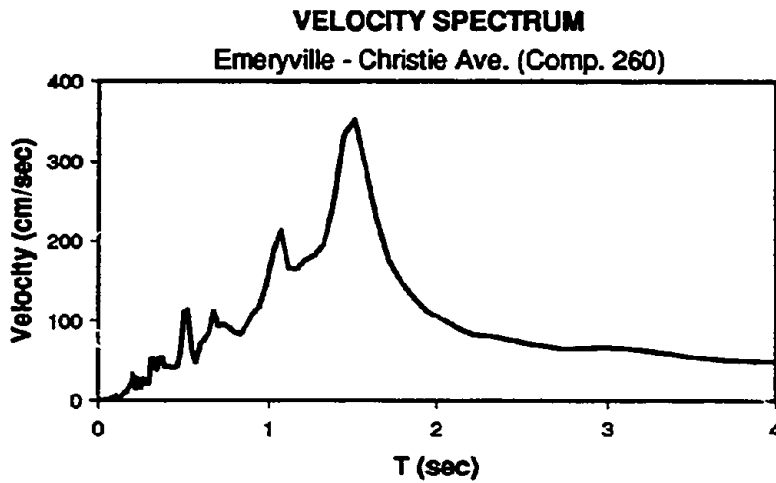
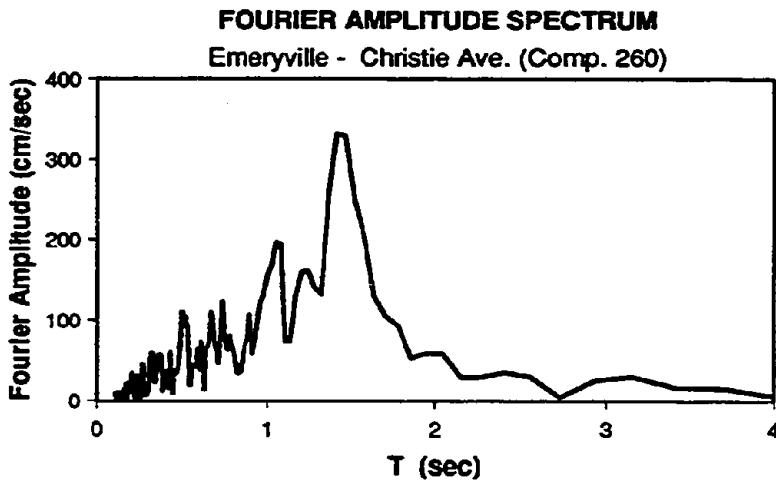


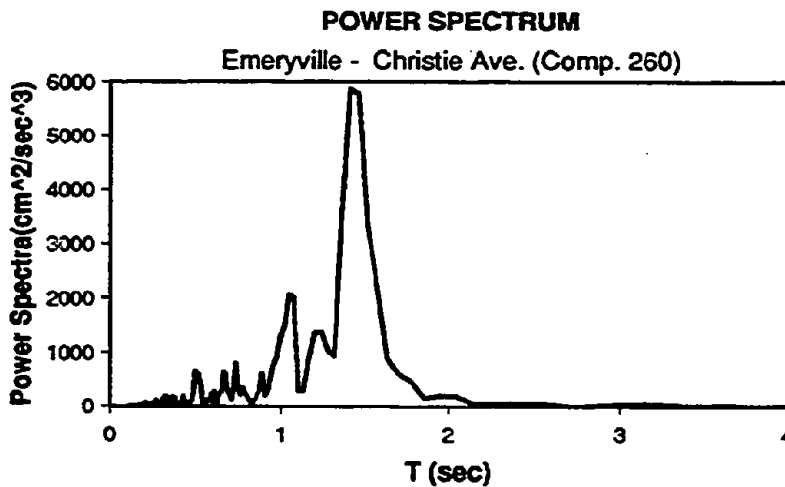
Fig. 4.17 Locations of Loma Prieta Ground Motion Stations Used in this Study



(a) Velocity Spectrum



(b) Fourier Amplitude Spectrum



(c) Power Spectrum

Fig 4.18 Estimation of Fundamental Period of Emeryville Site

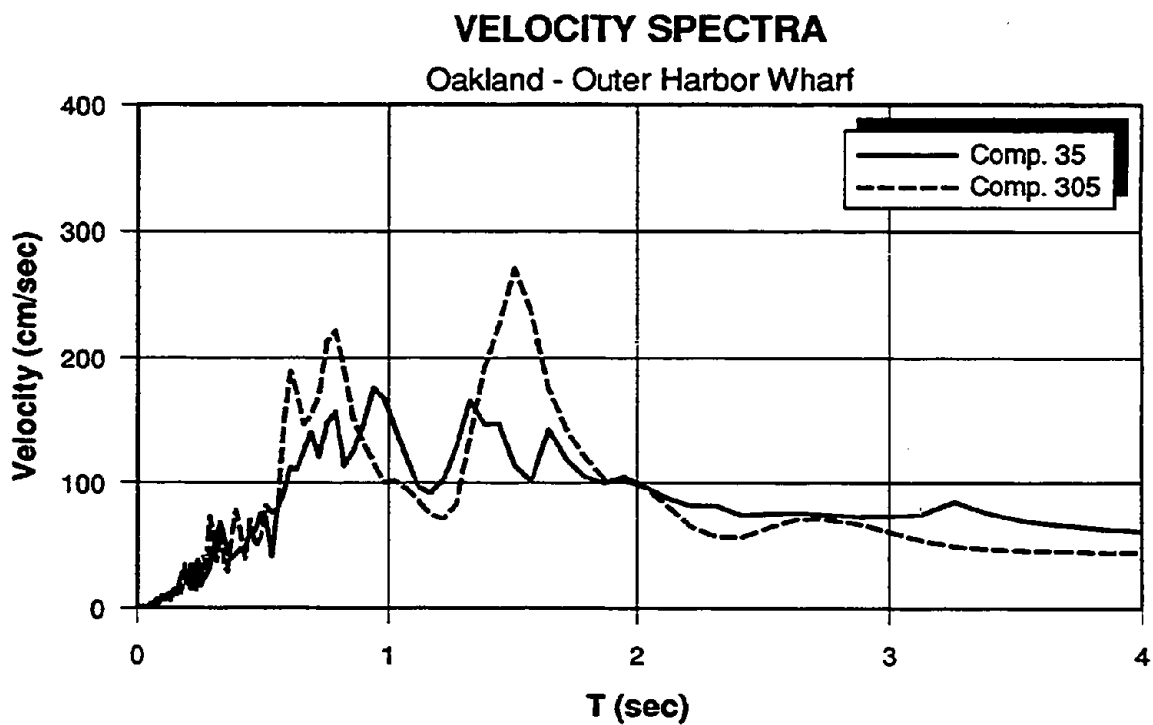
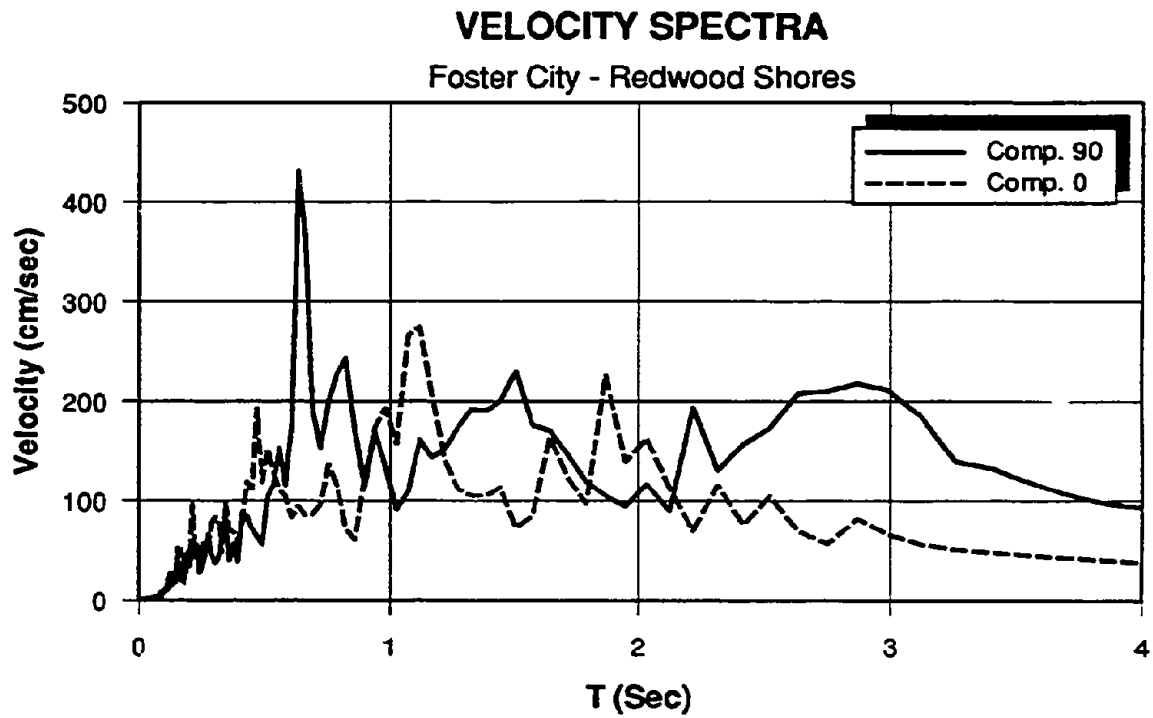


Fig. 4.19 Velocity Spectra of Recorded Horizontal Components of Two Soft Soil Motions

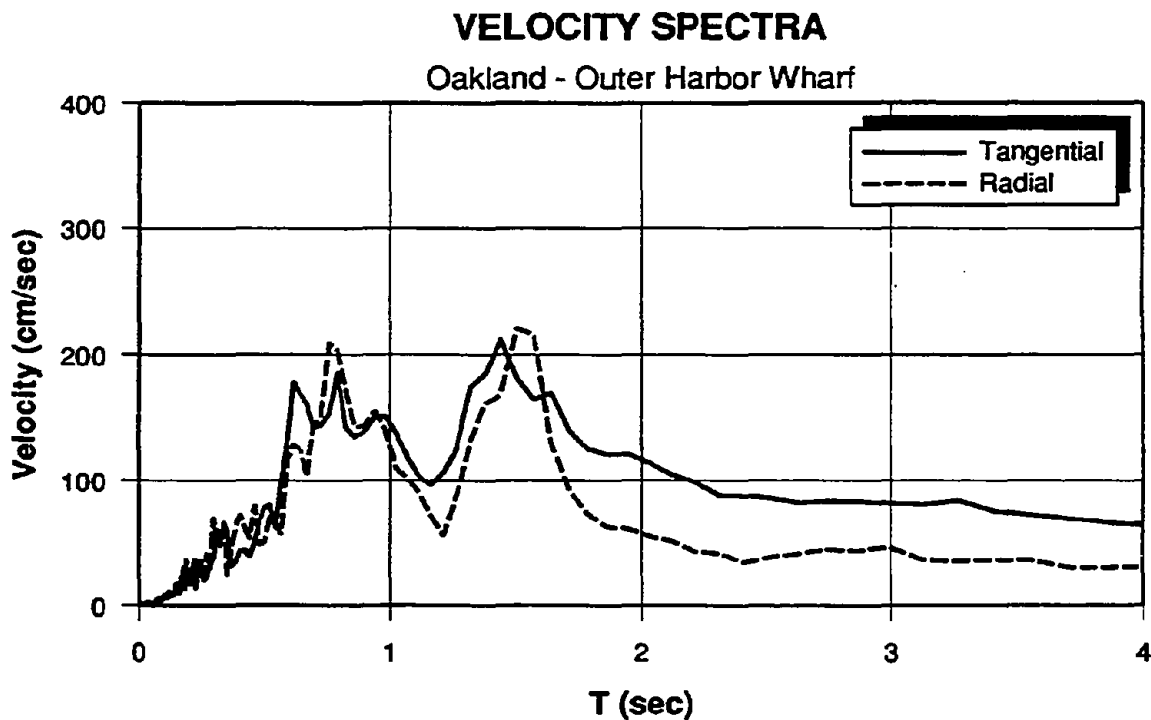
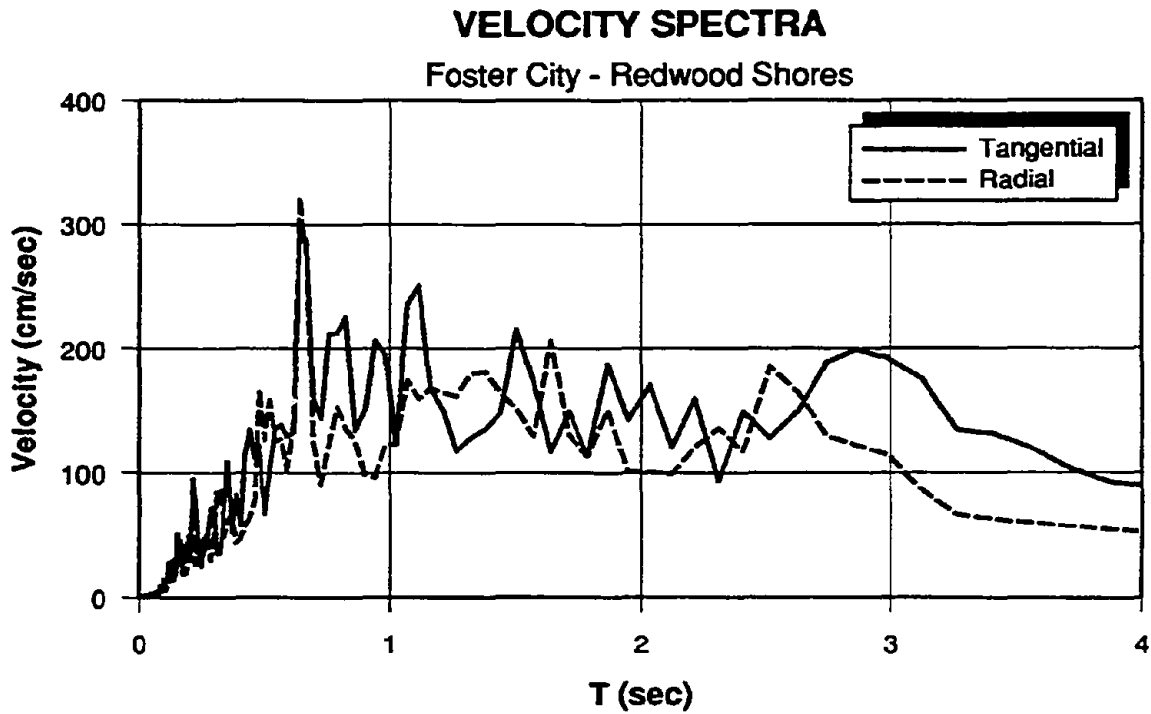
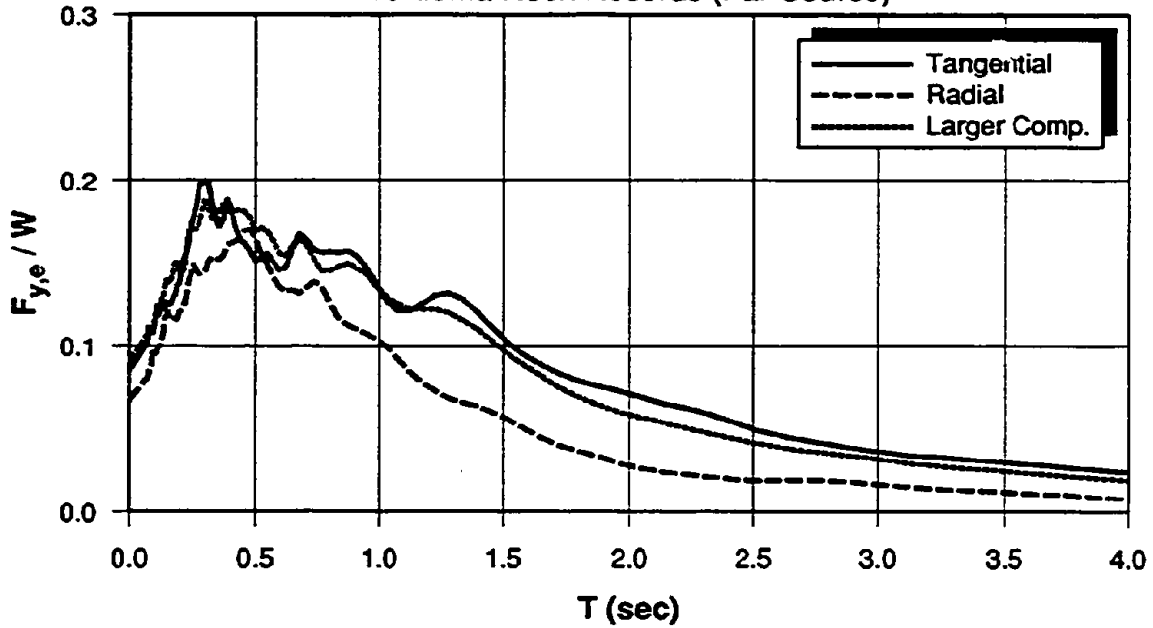


Fig. 4.20 Velocity Spectra of Tangential and Radial Components of Two Soft Soil Motions

ELASTIC STRENGTH DEMAND SPECTRA - MEAN

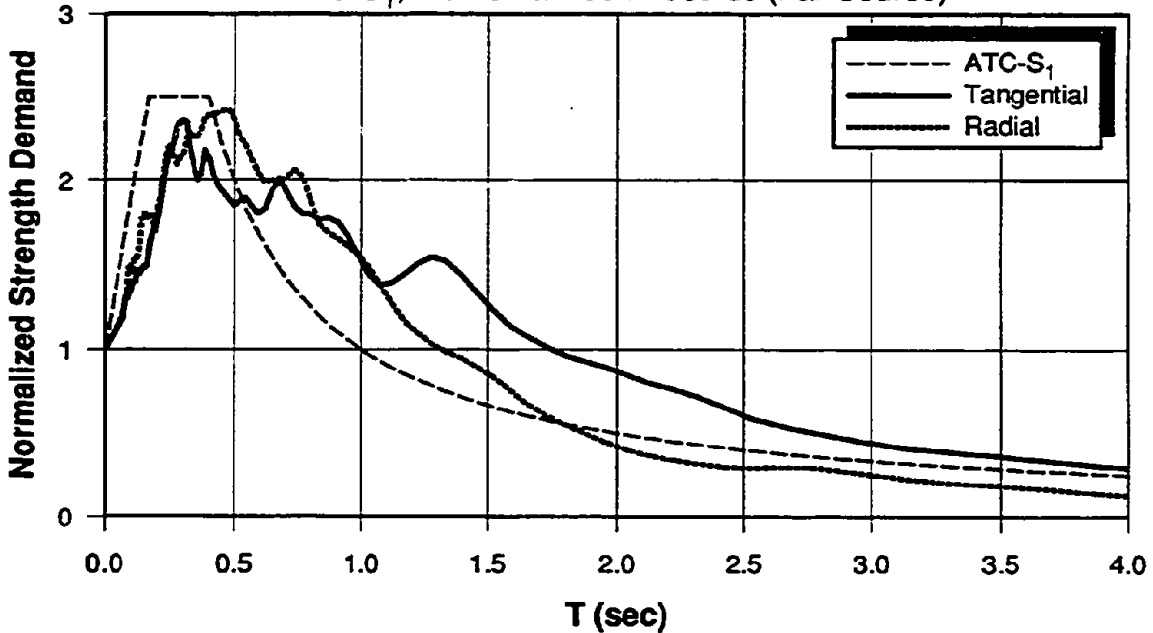
10-Loma Rock Records (Far-Source)



(a) Elastic Strength Demand

NORMALIZED ELASTIC STRENGTH DEMAND SPECTRA - MEAN

ATC-S₁, 10-Loma Rock Records (Far-Source)

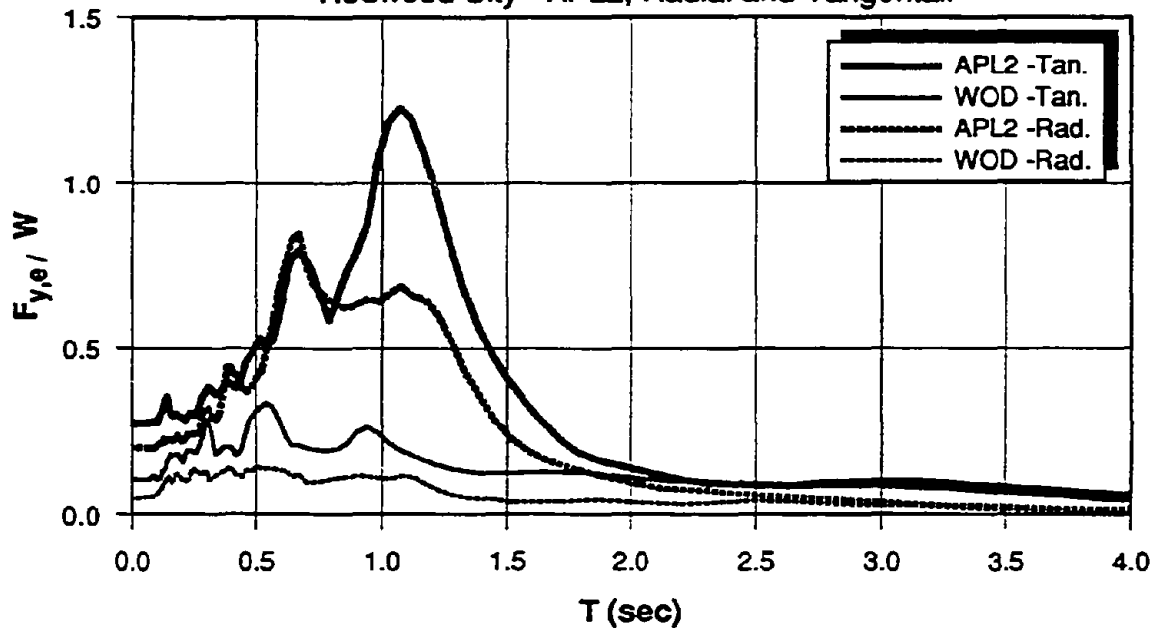


(b) Normalized Elastic Strength Demand

Fig. 4.21 Variation of Elastic Strength Demands for Rock Motions in Tangential and Radial Directions

ELASTIC STRENGTH DEMAND SPECTRA - SOFT SOIL & ROCK

Redwood City - APL2, Radial and Tangential



AMPLIFICATION OF ELASTIC STRENGTH DEMAND - APL2 / WOD

APL2 / WOD , Radial and Tangential

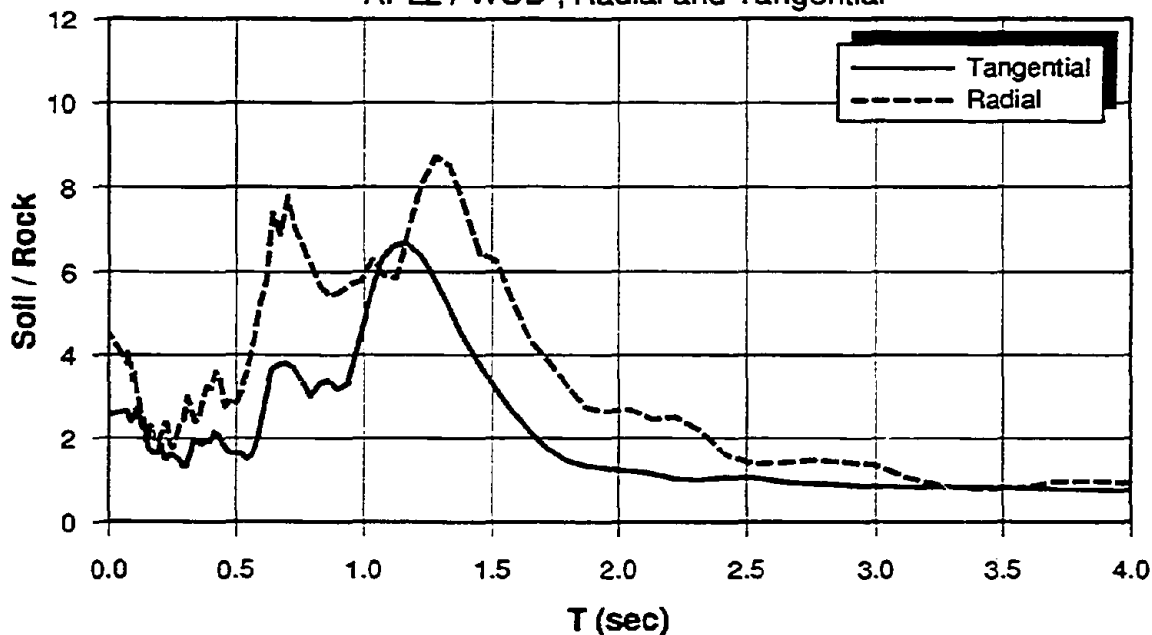


Fig. 4.22 Variation of Elastic Strength Demands in Tangential and Radial Directions

STRENGTH CAPACITY E_g FOR GENERIC STRUCTURES

Concrete and Steel Structures

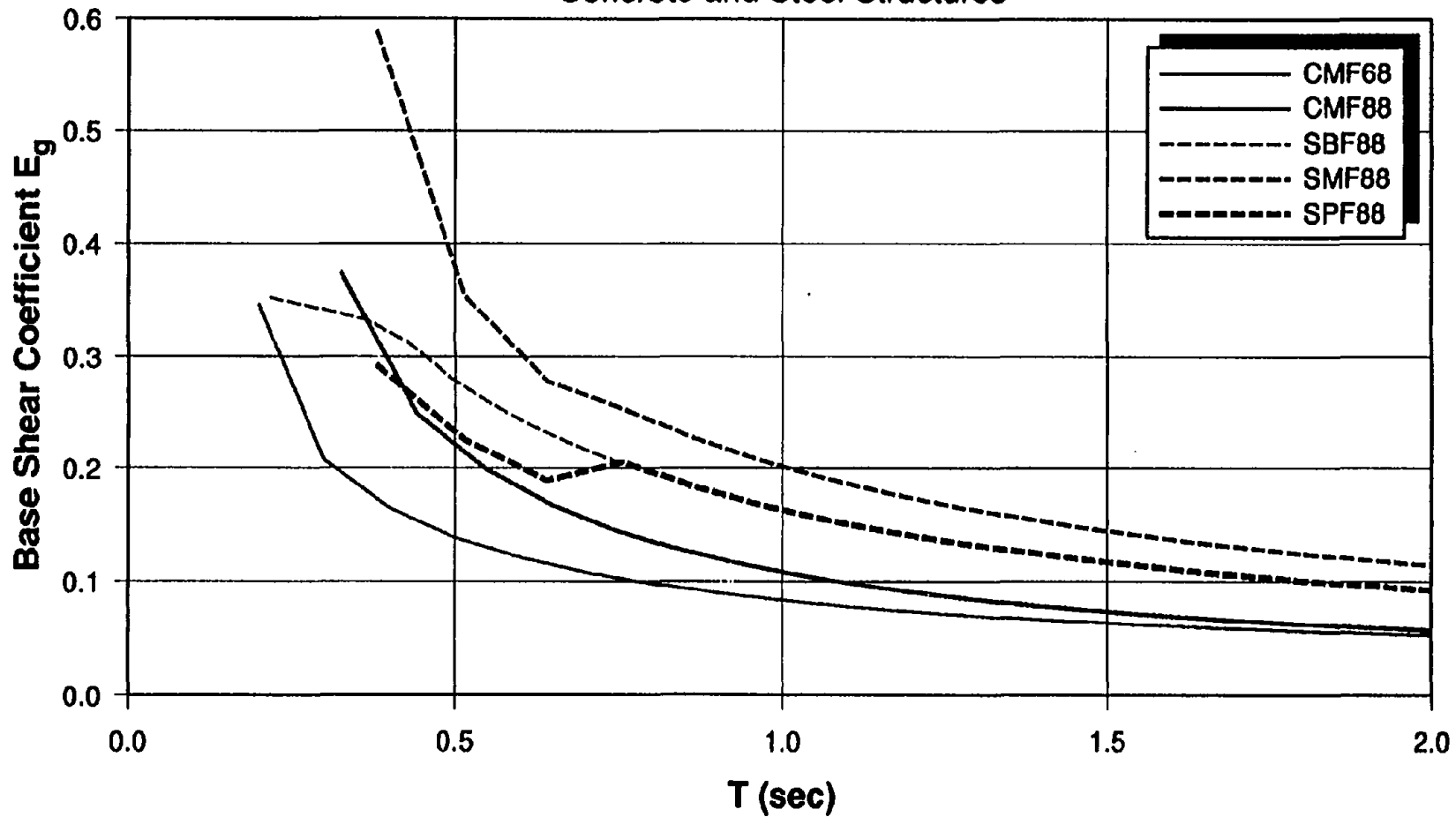


Fig 4.23 Strength Capacities of Five Types of Generic Structures (Nassar A. 1991)

CHAPTER 5

ANALYTICAL STUDY OF SOFT SOIL AMPLIFICATION

5.1 Introduction

The study summarized in this chapter is concerned with ground motions on soft soil sites and the representation of their effects in the design of structures. The site specific peak ground accelerations (or velocities) alone, or even site specific elastic response spectra, are inadequate to assess seismic demands for design. Structures respond inelastically to severe ground motions, and elastic response spectra may provide a very distorted picture of the inelastic demands. This has been observed in the 1985 Mexico earthquake (Osteraas and Krawinkler, 1990) and has been demonstrated in Chapter 4 for the Loma Prieta earthquake.

Most present seismic codes include procedures that account for soil site effects, but in an empirical and nontransparent manner that does not reflect the physical phenomena that occur when a structure, which is expected to respond *inelastically* in severe earthquakes, is subjected to soft soil ground motions. As a consequence, presently employed design procedures, which are probably adequate in most cases, cannot provide a consistent level of protection and may be overly conservative in some cases and unconservative in others.

As is documented in Chapter 4, not only the peak ground motion values but also the shapes of the elastic and inelastic strength and displacement demand spectra are greatly modified as rock motions travel through a soft soil medium. Typical elastic and inelastic strength demand spectra for a recorded soft soil ground motion (Redwood City, Apeel Array 2) are shown in Fig. 5.1(a), and the corresponding *R*-factors (ratios of elastic to

inelastic strength demands) are illustrated in Fig. 5.1(b). The elastic spectrum ($\mu = 1$) contains a clear signature of the soft soil on which the motion was recorded, as is evident in the large hump around a period of 1.1 seconds. It is important to note that this hump diminishes in the inelastic strength demand spectra and even disappears at large ductility ratios. Similar observation can be made from Fig. 5.2(a), which shows the elastic and inelastic strength demands from the Emeryville record. The wide hump in the elastic strength demand spectrum that extends beyond a period 1.5 seconds disappears in the inelastic strength demand spectra. As a consequence, the strength reduction factor R is strongly period dependent; it is much smaller than μ for periods of low elastic strength demands *preceding* the range of high elastic strength demands (hump in the elastic spectrum), and much larger than μ in the period range in which the elastic strength demand spectrum exhibits a large soil amplification. This is clearly demonstrated in Fig. 5.1(b) around the period of 1.0 second and in Fig. 5.2(b) around the period of 1.50 seconds.

The reason for this phenomenon is that the effective period of an inelastic system lengthens and shifts either into or out of the period range of high elastic strength demands. As a consequence the inelastic spectra become dissimilar to and much smoother than the elastic ones, the predominance of the site soil amplification decreases, and the R -factor becomes a period sensitive and highly nonlinear quantity.

This observation has significant implications for design. For structures with small ductility capacity the elastic strength demand spectrum will be an important design parameter and the required strength will be high and very sensitive to the predominant soil period. For structures with large ductility capacity the inelastic strength demand spectra, which are very different from the elastic ones, will control the design. This implies that it would be misleading to tune the structure strength to site-specific elastic response spectra and conventional R -factors, and that more knowledge needs to be acquired on the magnitudes and shapes of inelastic strength demand spectra. This conclusion is reinforced in Fig. 5.3, which shows strength demand spectra derived from two different records. The elastic spectra are very different whereas the inelastic spectra for $\mu = 4$ are similar in the range of the predominant soil periods.

This chapter focuses on analytical predictions of the effects of soft soils on seismic demands for elastic and inelastic *SDOF* systems. In this work the rock motions underlying the soft soil layers are used as the reference to estimate soft soil effects. Since

at this time no pairs of records exist for soft soil motions and corresponding bedrock motions, analytical means are utilized to predict soft soil motions from recorded rock motions. The analytical model used for this purpose and model calibration studies are discussed in Sections 5.3 and 5.4. Section 5.5 presents a parameter study that provides statistical information relating strength and displacement demands of analytically predicted soft soil motions to those of the underlying rock motions. In this study the soft soil is treated as a linear medium with 10% damping. In Section 5.6 a pilot study of the effects of soil nonlinearities on seismic demands is summarized. Up front, in Section 5.2, a short discussion is presented of an approach that permits an explicit incorporation of soft soil effects in the design process.

5.2 Soft Soil Consideration in Seismic Design

Seismic design, as proposed in Chapter 2, may be based on *SDOF* strength and displacement demands and appropriate *MDOF* modifications. Thus, fundamental information for design is derived from elastic and inelastic demand spectra for predetermined target ductility ratios, regardless whether a structure is built on rock or a soft soil site. Soft soils amplify these demand spectra over a large range of periods, particularly in the vicinity of the predominant soil period. In this work we have always avoided to address elastic demand spectra since their shapes and magnitudes are a function of many parameters that need to be considered in seismic hazard analysis. Since a hazard analysis is not part of this study, we have focused on relative seismic demands, which for rock and alluvium motions can be described by *R*-factors. For soft soil motions the *R*-factors follow a much different pattern and the elastic spectra have vastly different shapes and magnitudes than for rock motions. Since we are only concerned with relative shapes and magnitudes of demand spectra, the logical approach to be taken is to describe the soft soil effects in terms of spectral ratios that always relate the soft soil spectrum to the corresponding rock spectrum. These spectral ratios are defined here as soil modification functions.

With this definition in mind, the following approach is proposed for consideration of soft soil effects in *SDOF* strength demand spectra. For ground motions in rock and stiff soil sites the inelastic strength demand $F_y(\mu)$ can be related to the elastic one with reasonable accuracy by a strength reduction factor $R = F_{y,e} / F_y(\mu)$. As shown in Chapter 2, equations (2.5) and (2.6) together with mean or smoothed elastic response spectra can be employed in many cases to evaluate the inelastic strength demands. This can be done

with confidence for S_1 soil types, on which equations (2.5) and (2.6) are based, and probably also for S_2 soil types since the R -factors were found to be insensitive to relatively small variations in average response spectra shapes.

If soft soil effects are present, and assuming that the elastic spectrum for the rock motion underlying the soil is known, the use of the aforementioned soil amplification function permits a definition of soft soil strength demands in the following form:

$$F_y^s(\mu) = F_y^r(\mu)S(T_s, \mu) = \frac{F_{y,e}^r}{R} S(T_s, \mu) \quad (5.1)$$

In this equation the following definitions are used:

- $F_y^s(\mu)$ = Elastic ($\mu = 1$) or inelastic strength demand at soft soil site
- $F_y^r(\mu)$ = Elastic ($\mu = 1$) or inelastic strength demand for bedrock motion below soft soil site
- $F_{y,e}^r$ = Elastic strength demand for bedrock motion below soft soil site
- $S(T_s, \mu)$ = Soft soil modification function

This expression implies that the strength demand at a soft soil site can be expressed by the corresponding strength demand at a rock site and a modification function $S(T_s, \mu)$ that accounts for all soft soil effects. The process expressed in equation (5.1) is illustrated in Fig. 5.4.

The emphasis in this chapter is on the evaluation of this soil modification function. If the soft soil motion and the rock motion at the base of the soil layers were known, this function could be obtained directly as the ratio of the strength demands of soft soil to rock motions. To this date no recordings are available that permit a direct assessment of this amplification of strength demands. However, during the Loma Prieta earthquake several soft soil motions as well as nearby rock surface motions were recorded. The ratios of strength demands derived from these recordings are used in this study to provide basic information on soft soil amplification, even though it is recognized that rock surface motions differ somewhat from bedrock motions and may vary even within short distances.

Typical results for amplification functions obtained from a pair of recorded nearby motions are shown in Figs. 5.5(a) and 5.5(b). Fig. 5.5(a) shows the amplification of

elastic and inelastic strength demands for soft soil motion recorded at the Redwood City Apeel Array 2 station with respect to the nearby rock motion at Woodside. The time axis is normalized by the soil period $T_s = 1.10$ seconds estimated at the *APL2* site. The results show a clear pattern, with the largest amplification evident for the elastic strength demand at $T/T_s = 1.0$, and a decrease in amplification and shifting in maximum amplification to $T/T_s < 1.0$ evident for inelastic strength demands.

Figure 5.5(b) shows similar results for the soft soil motion recorded at the Emeryville station with respect to the nearby rock motion at the Piedmont (Jr. High School) station. The estimated soil period at Emeryville is around 1.50 seconds. The amplifications of elastic and inelastic strength demands have the same pattern as shown in Fig. 5.5(a) for the *APL2* record. This pattern was consistent for almost all the pairs of records analyzed, even though the magnitude of the amplification factor varied between record pairs.

These results led to the conclusion that the soil amplification function follows regular patterns and can be used as a basic measure to evaluate soil site effects. This function may depend on many parameters, including source-site distance (if needed, see later discussion), soil period T_s , soil nonlinearity, and target ductility ratio μ . Because of the lack of available rock / soft soil record pairs, a parameter study on the soil modification function necessitated the analytical prediction of soft soil records from recorded rock motions. Analytical procedures available for this purpose are summarized in the next section.

5.3 Methods of Ground Response Analysis

A number of sophisticated mathematical techniques and computer programs are available to predict the surface motion at the top of a soil deposit using the bedrock motions as input. Three-dimensional wave propagation analysis that accounts for most of the relevant material, geometric, and topographical characteristics of the soil/rock formation is a feasible process. However, within the objective of evaluating general site and structure response characteristics it is believed that simple one-dimensional wave propagation analysis can provide reasonable results that reflect the most important response patterns. With this simplification, the ground motions developed at the surface of a soil deposit during an earthquake can be viewed as the result of vertically propagating shear waves from an underlying rock formation and, therefore, the soil

deposit may be considered as a one-dimensional shear beam system. Alternatively, the soil profile can be represented by a multi-degree of freedom (*MDOF*) lumped mass system. This method is intuitively more appealing to structural engineers compared to wave propagation methods.

The following paragraphs summarize briefly the basic concepts of one-dimensional wave propagation analysis using equivalent linear systems and elastic *MDOF* lumped mass systems. Nonlinear methods of analysis are addressed in Section 5.6. In order to evaluate the equivalent linear and elastic *MDOF* lumped mass methods, a ground response analysis is carried out for selected soft soil sites and spectral accelerations of the computed surface motions are compared to the spectral acceleration of the recorded motions. This analysis is summarized in Section 5.4.

5.3.1 Equivalent Linear Method

The one-dimensional equivalent linear ground response method is widely used for evaluating the effect of local soil conditions on ground motions. The program *SHAKE*, developed by Schnabel et al. (1972), is used extensively for this purpose. This program takes into account the nonlinear effect of the soil by using an equivalent linear model in which a strain-compatible shear modulus and equivalent damping ratios are used to approximate the nonlinear behavior. The nonlinear problem is solved iteratively with each iteration involving a linear solution based on properties chosen to be consistent with the level of strain computed in the previous iteration. The characteristics of surface motions computed by this method are strongly depended on the level of shear strain, shear modulus and damping.

The dynamic characteristics of the soil depend upon many factors, such as the degree of compaction, the level of strain in the soil, and the nature of dynamic loading. In order to obtain surface motions that accurately represent the site condition, the selection of proper relationships between shear strains, shear modulus and damping is very important. In this method of analysis the shear modulus is defined as the slope of the line connecting the origin to the maximum point of the hysteresis loop, and the damping ratio is assumed proportional to the ratio of the area of the hysteresis loop to the total energy. Information on the shear wave velocity, shear modulus and damping ratio for different soils and detailed discussions on the effects of different parameters on the dynamic properties of soil are available in the literature (e.g., Seed, 1970, 1984, 1988).

5.3.2 Linear *MDOF* Lumped Mass Model

In this method of ground response analysis the soil column is represented by a *MDOF* lumped mass system. The appropriate number of degrees of freedom of the system depends on the characteristics of the soil profile and the depth of the soil column. The shear modulus (G) of a soil layer can be defined as

$$G = \rho V_s^2 \quad (5.2)$$

where ρ is the mass density of the soil and V_s is the shear wave velocity of the soil layer. Thus, for a soil layer of thickness H and unit area the stiffness can be defined as

$$K = \frac{G}{H} \quad (5.3)$$

The lumped mass model can be viewed as a multi-story structural model. The masses are lumped at the interfaces of adjacent soil layers, which defines the story heights. The amount of mass lumped at each story is determined by integrating the soil masses between the mid heights of adjacent stories (layers). The so determined stiffness and mass of each story are used to construct the mass and stiffness matrices of the *MDOF* system that represents the soil profile. In this method of analysis it is assumed that material behavior is linear and the structure responds elastically to the input rock motion. Any viscous damping value may be assigned to the system. The damping, which may be tuned to the expected soil nonlinearity, is assumed to be constant for each mode of vibration. The damping matrix is computed from the mode shapes and frequencies as follows:

$$c = m \left[\sum_1^n \frac{2\xi_n \omega_n}{M_n} \phi_n \phi_n^T \right] m \quad (5.4)$$

where

$$M_n = \phi_n^T m \phi_n$$

c, m = damping and mass matrices

ω_n, ξ_n, ϕ_n = frequency, damping ratio and mode shape of the n^{th} mode, respectively.

This method of site response analysis is utilized in the parameter study discussed in Section 5.5. A nonlinear approach utilizing a lumped *MDOF* system is discussed in Section 5.6.

5.4 Ground Response Analysis of Selected Soft Soil Sites

The Loma Prieta earthquake has provided several pairs of records (soft soil and nearby rock) that can be used for an evaluation of the site response analysis methods summarized in the previous section and for a preliminary assessment of the effects of soft soils on seismic demand spectra.

Figure 4.17 shows the selected soft soil and nearby rock sites that were used for this purpose. The characteristics of these records are presented in Tables 4.4 and 4.5. A ground response analysis of some of these sites has been carried out by several other researchers. The Treasure Island and Yerba Buena Island record pair was used by Idriss (1991), Seed (1990, 1992), and Hryciw (1991) to evaluate the ground response of the Treasure Island site. In these studies the equivalent linear method (*SHAKE* program) was used to perform the ground response analysis. The comparison of spectra of computed motions with those of recorded motions show a good agreement at periods less than one second. However, for periods greater than one second the spectra of computed motions underestimate the spectra of recorded motions. The difference between these spectra in the long period range could be the result of using one-dimensional wave propagation to represent a 3-D problem.

The study conducted by Hryciw (1991) pointed out that the characteristics of computed surface motion are not very sensitive to the shear wave velocity of the older bay deposit. The variation of *PGA* with depth was found to be small in the layers of old bay deposit and young bay mud. However, significant amplification of *PGA* was reported near the surface within the top sand fill material. For this site the contribution of fill material to the amplification of *PGA* was much greater than that of the young bay mud.

Seed (1992) performed nonlinear ground response analysis of ten Loma Prieta soft soil sites. The nonlinear analysis was performed using the modified program *DESRA-2* (Lee and Finn, 1978), which incorporates the Martin-Davidenkow model to represent the soil nonlinearity. The acceleration spectra of surface motions predicted from nonlinear and equivalent linear methods of analyses were similar and in good agreement with the spectra of recorded motions. In this reference it is recommended to perform nonlinear ground response analysis at higher level of shaking.

In our study the emphasis is on modeling the soil columns by linear *MDOF* lumped mass systems. The number of degrees of freedom are based on the variation of shear wave velocity and the depth of layers of the soil profile. These *MDOF* systems, with an assumed 10% damping in each mode, are subjected to the nearby rock motions. In order to compare the ground motions predicted from linear lumped mass systems and equivalent linear analyses, the program *SHAKE* was employed also to compute the surface motion for selected soft soil sites.

Figure 5.6 shows the soil columns at the Treasure Island, Okaland Harbor, Apeel Array 2, and San Francisco Airport sites. The estimated shear wave velocities of each soil profile and the information on the depth of soil layers and the depth to bedrock are taken from Seed (1992, 1990) and Fumal (1990). Salient results obtained from the ground response analysis of these four soft soil sites are presented in the following sections.

5.4.1 Evaluation of Site Response at Treasure Island

The two nearby ground motion records at Treasure Island and Yerba Buena Island are a very useful pair of records that can be used to examine the influence of local soil condition on ground surface response. Treasure Island is a fill compacted island that is located in the San Francisco Bay. Yerba Buena Island is a nearby rocky island. The ground motion recorded on this island was applied as input motion to the soil model. The E-W components recorded at both locations, which have the higher *PGAs*, were used for ground response analysis.

The soil profile for Treasure Island, shown in Fig. 5.7, consists of five layers with different height. For the elastic ground response analyses the soil profile was modeled by a six degrees-of-freedom lumped mass system. The 145 ft silty clay layer adjacent to the

bed rock is represented by two stories with each story height equal to approximately one half of the soil layer. The four remaining soil layers are each represented by an individual story whose height equals the thickness of the corresponding layer. The Yerba Buena Island E-W component was applied at the base of the soil model. The elastic time history response at the top of the *MDOF* system was assumed to represent the surface ground motion. For the equivalent linear *SHAKE* analysis the dynamic properties of the soil materials were assumed to be represented by the relationships between shear strain, damping, and shear modulus suggested by Seed et al. (1984) for sand and Seed and Sun (1988) for cohesive soils.

The fundamental period at the Treasure Island site is estimated as about 1.30 seconds. This estimate is based on the given soil properties of the site and is similar to the period reported by Seed R.B. (1990). The predominant period of the recorded motion at Treasure Island based on the velocity spectrum of the recorded motion (E-W component) is about 0.65 second, which is very close to the second mode period of the soil deposit.

The strength demand spectra of the computed and recorded soft soil motions were calculated for *SDOF* systems with 5% damping. The elastic spectra of these motions and of the Yerba Buena Island rock record are shown in Fig 5.8(a). As can be seen, the results from predicted and recorded motions match rather well around the predominant period of 0.65 seconds. For periods greater than 1.50 second the spectral response values based on the *MDOF* lumped mass model underestimate the results from the recorded motion, but they provide a closer match than those computed by the *SHAKE* program. The large differences between the response spectra of computed and recorded ground motions in the long period range must be attributed to the shortcomings of the simple one-dimensional wave propagation model. For periods not exceeding the fundamental soil period the one-dimensional equivalent linear and elastic *MDOF* ground response analysis methods give comparable predictions that capture most of the main features of the actual response spectrum.

Figure 5.8(b) shows a comparison of the inelastic strength demand spectra of the computed and recorded motions for bilinear systems with a ductility ratio of 4. Also for these spectra the *MDOF* lumped mass model with 10% damping appears to give better predictions than the *SHAKE* analysis.

5.4.2 Evaluation of Site Response at APL2, SFA, OAKW Sites

The soil layering and shear velocities used in the response analysis for the Redwood City Apeel Array 2 (*APL2*), San Francisco International Airport (*SFA*), and Oakland Outer Harbor Wharf (*OAKW*) sites are presented in Fig. 5.6. For the ground response analysis the closest available rock motions to these sites were selected as input rock motions. In order to have a consistent direction for analysis, the tangential components of the soft soil records and nearby rock records were used.

The soil profile of the *APL2* site consists of six layers with a total depth of 250 ft. to the bedrock. The top 10 ft of this site is a sandy fill with an average shear wave velocity of 575 ft/sec. This soil profile was modeled as a 6DOF lumped mass system. The Woodside Fire Station record was used as the rock input for response analysis at the *APL2* site.

The *SFA* soil profile consists of several thin layers of sand fill and soft bay mud on top of a stiff to hard clay layer and dense sand layers. This soil profile was modeled as a 6DOF lumped mass system and was subjected to the South San Francisco Sierra Point (*SSFS*) rock motion.

The *OKAW* site was subjected to a higher level of shaking than the other soft soil sites in the Oakland area. The soil profile of this site consists of several layers of sandy silt fill and soft bay mud on top of several dense sand and stiff old bay mud layers. The top 25 feet at this site is sand fill with an average shear velocity of 575 ft/sec. It is underlain by 5 feet of soft bay mud which lies on top of a stiff clay layer. The closest rock motion to this site, the Yerba Buena Island record, was used as the rock input motion. Since the *OKAW* site was subjected to higher level of shaking than the other soft soil sites in the Oakland area, the input rock record is scaled to the *PGA* of 0.12g for ground response analysis.

The elastic strength demand spectra of computed and recorded motions for *SDOF* systems with 5% damping are presented in Fig. 5.9. As can be observed, the responses of the computed and recorded motions are in good agreement.

This calibration study is intended to demonstrate that one-dimensional wave propagation modeling captures the most important features of soft soil ground motions

and their effects on structural response. The study also indicates that at this level of ground shaking an elastic *MDOF* lumped mass model with 10% damping gives prediction that are similar to those obtained from a *SHAKE* analysis.

5.4.3 Validity of One-Dimensional Soil Column Model

Simple one-dimensional soil column models are used widely by researchers and engineers for ground response analysis in order to evaluate soil amplification effects. Most researchers agree that such a model is a gross oversimplification of a complex three-dimensional problem in which wave form, direction, reflection and refraction, impedance contrast, as well as 3-D topographical effects play a major role. For instance, the observations made in Section 4.5.2 regarding directivity effects clearly show that a one-dimensional model, which will not distinguish between radial and tangential directions, cannot account for the difference in soil amplification in these two directions.

In support of one-dimensional soil column models it can be said that they capture most of the global soil amplification characteristics important for design in a quantitative (but not always accurate) manner. This is illustrated in the comparison of elastic strength demand spectra obtained from recorded and predicted soft soil motions (see Figs. 5.8 and 5.9). However, in several cases the spectral amplitudes for periods exceeding the predominant soil period were severely underestimated. Thus, it must be concluded that spectra derived from soil motions generated with 1-D soil column models may lead to poor predictions of the elastic and inelastic strength demands for periods exceeding the fundamental soil period.

5.5 Linear Ground Response Analysis Using *MDOF* Lumped Mass Models

Because of the lack of data on pairs of soft soil and underlying rock motions, a parametric evaluation of soft soil effects necessitates the generation of soft soil motions from available soil data and rock records. Despite the previously discussed shortcomings of one-dimensional wave propagation models, simple 1-D soil column models are used in this study to generate soft soil motions and acquire a basic understanding of the effects of soil amplification on seismic demands. The reasons are that a *simple* model is needed to evaluate these effects and that no realistic and more complex models of general validity are available at this time.

Even within the constraint of one-dimensional wave propagation it is evident that the results will strongly depend on the properties of the individual soil layers placed on bedrock. Also, the depth to bedrock and the rock properties, which may vary greatly, are not known in many cases. Recognizing these limitations, it is understood that the following study is conceptual and may lead to results that are not applicable to cases for which the assumptions made here are unrealistic. In a parametric study the focus needs to be on a small number of parameters that have the largest effect on the phenomena to be studied. We are assuming that the shear wave velocity follows certain patterns throughout the depth and that, correspondingly, the soil periods follow well established patterns. Furthermore, we are assuming in this section that the soil is only lightly nonlinear and that the effects of soil nonlinearity can be represented by a viscous damping of 10 percent. With these assumptions it turns out that the fundamental soil period T_s becomes the predominant parameter for assessing soft soil effects.

In this parameter study the soil column is modeled as a five layer system with increasing shear wave velocities as shown in Fig. 5.10. For all soil column models the top layer is of constant thickness of 30 ft, whereas the thickness H of all other layers is varied in a manner that results in first mode soil periods of $T_s = 0.5, 0.75, 1.0, 1.25, 1.5, 2.0, 3.0,$ and 4.0 seconds. For the eight soil systems so generated, the ratios of the first three modal periods are close to 1:0.5:0.33. These soil column models are converted to elastic *5DOF* lumped mass models with 10% damping in each mode. These structural models are subjected to bedrock motions, and the computed response histories at the top level are designated as soft soil motions for which soil amplification can be evaluated.

Two sets of bedrock motions are used in order to evaluate the sensitivity of soil amplification to the characteristics of the input rock motions. One is the *15-S₁* record set representing typical *S₁* records whose response spectra resemble in average the *ATC-S₁* ground motion spectrum. Information on this record set was presented in Table 3.2. The other is the *10-Loma* record set representing far-source rock motions obtained from the Loma Prieta earthquake. From this record set the tangential (w.r.t. epicenter) components of the records are used to establish a consistent directivity pattern. Data on this record set were presented in Table 4.4. Figure 5.11 shows the mean values of normalized elastic strength demands (dynamic amplification factors) for these two record sets. Figure 5.12 presents the mean *R-factors* (strength reduction factors) for *SDOF* bilinear systems with 5% strain hardening and 5% damping subjected to these two sets of rock ground motions. As can be seen from Figs. 5.11 and 5.12, the characteristics of these two sets of input

ground motions are very different. For the far-source rock records (*10-Loma*) the normalized elastic strength demand spectra show the slow attenuation of long period components of motion. The results from these two record sets, which have significantly different mean elastic spectra, are evaluated separately in order to assess the effects of rock spectral shapes on soil amplification.

All 25 rock records are used as input to the 8 soil column models, resulting in 200 soft soil records. For these 200 soft soil records and the 25 rock records nonlinear dynamic time history analyses are performed using bilinear *SDOF* systems with 5% strain hardening and 5% damping. The analyses are conducted for 38 discrete periods ranging from $T = 0.10$ to 4.0 seconds and for target ductility ratios $\mu = 1$ (elastic), 2, 3, 4, 5, 6, and 8. Strength and displacement demand spectra are computed, and the soft soil amplifications are obtained from the ratios of soft soil to rock spectra. Statistical averaging is performed on the amplification of strength and displacement demand parameters to evaluate patterns and variations of these seismic demand parameters for different soft soil sites. The mean and mean plus standard deviation ($\text{mean} + \sigma$) of the results are computed.

5.5.1 Amplification of Strength Demands

Typical results obtained from this parameter study on the amplification of strength demands are presented in Figs. 5.13 to 5.25. Figure 5.13 shows for both records sets the mean elastic strength demand spectra for the 8 soil column models together with the mean spectrum of the corresponding rock motions. Figure 5.14 shows results for inelastic strength demand spectra for $\mu = 4$. These figures, and similar ones not shown here, form the basis for the following figures that present the same information but in a normalized domain, using the rock spectra values and the fundamental period of the soil column models as normalizing factors. Thus, the following figures are graphical representations of the soft soil amplification of spectral values (soft soil value / rock value) plotted against the ratio of structure period T over soil column period T_s .

Figures 5.15 to 5.17 present results for the mean amplification of elastic and inelastic strength demands (for $\mu = 2, 3, 4, 5, 6,$ and 8) for three discrete soil periods ($T_s = 0.5, 1.0,$ and 1.5 seconds), using both record sets. It can be observed that the shapes of the amplification curves are similar to those obtained from recorded soft soil motions (see Fig. 5.5). Figure 5.18 shows the mean amplifications of elastic strength demands

(acceleration response spectra) for the eight soil column models. These are the same results as presented in Fig. 5.13, but in the normalized domain. Figures 5.19 to 5.21 present amplification curves for inelastic *SDOF* systems with $\mu = 2, 4,$ and $6,$ again for all 8 soil column models and using both record sets. Figures 5.22 and 5.23 provide the mean+ σ data for the amplification of strength demands whose means are shown in Figs. 5.18 and 5.20 (elastic and $\mu = 4$).

The maxima of the mean amplification values are presented in Figs. 5.24 and 5.25. These values represent the peak points of the previously presented amplification curves, regardless of the value of T/T_s . Figure 5.24 shows the dependence of these maximum values on the target ductility ratio $\mu,$ and Fig. 5.25 illustrates the dependence of the maximum amplification of elastic strength demands on the soil period $T_s,$ using near and far source rock input motions.

From these figures, and others not shown here, the following observations can be made on the soft soil amplifications of elastic and inelastic strength demands:

- The elastic strength demand spectra of the soft soil motions exhibit clear humps in the vicinity of the fundamental soil period and noticeable humps in the vicinity of the second mode soil period. The width of the humps increases with an increase in soil period T_s (see Fig. 5.13).
- The shapes of inelastic strength demand spectra of soft soil motions are much smoother than those of the corresponding elastic spectra, and the peaks of these spectra no longer occur at the soil column periods. The humps of the inelastic spectra (if they exist at all) are much wider than those of the elastic spectra. Except for soil columns with a very long fundamental period, the maximum inelastic strength demands occur at very short structural periods (see Fig. 5.14).
- The amplifications of strength demands for elastic and inelastic *SDOF* systems follow a consistent pattern (see Figs. 5.15 to 5.17). The amplification is largest for elastic systems and occurs at $T/T_s = 1.0$. For inelastic systems the amplification decreases with an increase in $\mu,$ and the peaks of the amplification curves occur at values of $T/T_s < 1.0$. The larger the target ductility ratio, the smaller is the T/T_s ratio at which maximum amplification occurs.

- In the normalized domain the amplification curves for elastic and inelastic strength demands follow a systematic pattern, regardless of soil column period T_s (see Figs. 5.18 to 5.21).
- The mean+ σ amplification curves are similar in shape to the mean amplification curves (see Fig. 5.18 vs. Fig. 5.22, and Fig. 5.20 vs. Fig. 5.23). The coefficient of variation of the maximum amplification is in the order of 0.15.
- The maximum soft soil amplifications are larger for elastic systems than inelastic ones. They decrease with an increase in ductility, but only at a low rate (see Fig. 5.24).
- The maximum soft soil amplifications of elastic (and inelastic) strength demands are only weakly dependent on the period of the soil column (see Fig. 5.25).
- The soft soil amplifications of elastic and inelastic strength demands do not depend strongly on the rock motion spectral shape. In general, the results obtained from the *15-S₁* record set are close to those obtained from the *10-Loma* record set. This does not apply, however, to the amplification of ground motion parameters (*PGA*, *PGV*, and *PGD*) as will be discussed later.

The amplification curves presented in Figs. 5.15 to 5.23 provide baseline data from which the soft soil modification functions discussed in Section 5.2 could be derived. It is not the objective of this study to derive such functions since many other design issues would have to be considered, such as uncertainties in determining structure and soil periods, soil properties, and degree of nonlinearity in the soil which will be a function of the severity of the ground motion. Just for illustration, the results presented in Figs. 5.18 and 5.20 are plotted again in Figs. 5.26 and 5.27 together with envelopes that may represent a range for mean modification functions. Clearly, this range is only meaningful for soil columns that can be represented by the model used in this parameter study (e.g., soils whose nonlinearity can be represented by 10% viscous damping).

5.5.2 Amplification of Displacement Demands

For elastic ($\mu = 1$) and inelastic *SDOF* systems the displacement demand spectra can be derived directly from the corresponding strength demand spectra using equation (4.4), which is repeated here:

$$\delta_{\max} = \frac{T^2}{4\pi^2} \mu F_y(\mu) \quad (5.5)$$

Since the amplification of displacements ($\delta_{\max}^s/\delta_{\max}^e$) for a given period T and ductility μ depends only on the ratio of strength demands $F_y^s(\mu)/F_y^e(\mu)$, it is concluded that the spectral displacement amplification is the same as the amplification of strength demands. Thus, all the conclusions drawn in the previous section on strength demand amplification apply to displacement demand amplification as well.

Specific data on displacement demand spectra and ratios of inelastic to elastic spectra (δ_{in}/δ_{el}) for soft soil motions are presented in Figs. 5.28 to 5.32. Results from recorded as well as predicted motions are shown. For the latter case the mean values obtained for soft soil motions computed from the *10-Loma* record set are used.

Figure 5.28(a) shows the mean of elastic displacement demands derived from the *10-Loma* record set for different soil period T_s . Figure 5.28(b) shows the elastic displacement demands for seven soft soil motions recorded at sites whose soil periods are in the range of 0.90 to 1.5 seconds. A comparison of these displacement demands with those of predicted motions ($T_s = 1.0, 1.25, 1.5$ sec.) indicates good agreement. Similarly, good agreement is evident in the comparison of ratios of inelastic to elastic spectra for $\mu = 6$ presented in Fig. 5.29. Figures 5.30 and 5.31 illustrate the elastic and inelastic displacement demand spectra together with the normalized inelastic displacement demands for a recorded motion and predicted motions in a soil with similar period ($T_s = 1.25$ sec.). Figure 5.32 shows displacement demands for predicted motions in a soil with $T_s = 1.5$ seconds.

From these figures and others not shown here the following observations can be made:

- Elastic displacement demand spectra show a peak around the fundamental soil period. The spectra rise rapidly to this peak as T/T_s approaches 1.0 and decay slowly (if at all) for $T/T_s > 1.0$.
- Inelastic displacement demand spectra rise to a plateau value at $T/T_s < 1.0$ and either maintain this plateau value or increase further for $T/T_s > 1.0$.
- The ratio of inelastic to elastic displacement demands shows very consistent patterns. It has a low point at $T/T_s = 1.0$, is usually less than 1.0 for $T/T_s > 0.75$, and increases rapidly for short period structures.
- The ratio of inelastic to elastic displacement demands for $T/T_s < 0.75$ is strongly dependent on the ductility ratio and the period ratio T/T_s .

5.5.3 Amplification of Input Energy

Figure 5.33 shows mean values of the amplification of the input energy (using elastic *SDOF* systems) for soft soil motions computed from the 10-Loma record set as well as the amplification for one recorded ground motion. The input energy is used in many studies as a measure of the damage potential of ground motions. The amplification curves are similar in shape to those of the elastic strength demands (Fig. 5.18), but with greatly increased values, particularly around $T/T_s = 1.0$. Around this value the amplification of energy is approximately 1.3 to 1.6 times the square of the amplification of strength demand, which indicates concentration of energy at $T/T_s = 1.0$ due to the harmonic nature of the soft soil motion at that period and due to an increase in strong motion duration from rock to soft soil. Since the relationship between input energy and hysteretic energy dissipation is rather stable (Nassar and Krawinkler, 1992) it must be concluded that the hysteretic energy dissipation demand around $T/T_s = 1.0$ is also very large, which demonstrates the greatly amplified damage potential of soft soil ground motions. However, this does not hold true for small ratios of T/T_s , for which little amplification of input energy is observed.

5.5.4 Amplification of Ground Motion Parameters

An interesting side result was obtained from the study of spectral amplifications. The Soft Soil / Rock ratios shown in Fig. 5.18 for $T/T_s = 0$ are means of soil amplification

factors for peak ground accelerations, *PGA*. Values of these factors, plotted against the soil period T_s , are shown in Fig. 5.34(a) for both the *15-S₁* and *10-Loma* record sets. These plots show a significant dependence of *PGA* amplification on both the soil column period and the rock record set. For the *15-S₁* set the *PGA* gets amplified for motions in soft soils with a period smaller than 2.0 seconds, whereas for the far-source *10-Loma* records amplification of *PGA* occurs in soft soils with periods smaller than 3.2 seconds. It must be emphasized that these results are obtained from studies with simple one-dimensional soil models with all the shortcomings discussed previously. Nevertheless, *PGA* amplification factors obtained from pairs of nearby soil and rock motions recorded during the Loma Prieta earthquake (individual data points shown in Fig. 5.34) fall rather close to the predicted curve for the *10-Loma* record set. The information shown in this figure indicates that it may be misleading to use *PGA* amplification as a reliable measure for soft soil amplification. For soils with very long periods the *PGA* amplification decreases significantly, however spectral amplifications around $T/T_s = 1.0$ are approximately equal for all soft soil periods, as shown in Fig. 5.18.

Figures 5.34(b) and (c) show the mean and mean+ σ amplifications of *PGV* and *PGD* for predicted soft soil motions obtained from the *10-Loma* record set. The curves of Fig. 5.34(b) indicate that the amplification of *PGV* is rather insensitive to the soil column period T_s , whereas the amplification of *PGD* increases with T_s . The predicted values of *PGD* amplifications and their increase with T_s are likely too low, as is indicated by the data points obtained from pairs of nearby soil and rock records. The low predictions of *PGDs* can be attributed to the shortcomings of the one-dimensional soil column model that does not account for impedance contrast and the contributions of waves with a period exceeding the fundamental soil period.

5.6 Ground Response Analysis with Nonlinear Soil Layer

Available data on the amplification of ground motions in soft soils at high levels of ground shaking are limited. As the severity of motion in the bedrock increases, high shear strains will be generated in the soil and the behavior of soil will become increasingly nonlinear. In such cases the simple elastic model with 10% viscous damping, which was used in the parameter study discussed in Section 5.5, will provide unrealistic results. This section summarizes a pilot study in which soil nonlinearity in the top soil layer is modeled explicitly. In this pilot study the same soil column profile and 5DOF lumped mass model as in the parameter study are used, but the top layer is

modeled as a nonlinear "story" as shown in Fig. 5.35. It is assumed that the upper 30 feet of the soil profile consist of soft Bay Mud with a low shear wave velocity.

The nonlinear dynamic response of soil subjected to earthquake loads depends to a large extent on the cyclic stress-strain characteristics of the soil in shear. The shear stress vs. shear strain relationship exhibits nonlinear behavior from the initial stage of loading as shown in Fig. 5.36. For the purpose of application in soil response analyses this behavior may be represented by mathematical models of stress-strain curves obtained from experimental investigations. Several mathematical models are proposed in the literature, such as the hyperbolic model by Hardin and Drnevich (1972), and the Ramberg-Osgood formulation for soil by Idriss (1978). Seed (1968) used a bilinear model to represent the nonlinear behavior of soil for ground response analysis. In the following sections the hyperbolic and Ramberg-Osgood models will be reviewed and a simple bilinear model will be derived that has been used in this pilot study to represent the nonlinear soil behavior. The three parameters of this bilinear model (initial stiffness, yield level and strain hardening) are defined using the properties of top 30 feet soil layer.

5.6.1 Hyperbolic Backbone Curve

The behavior of soil during cyclic loading is represented by an initial stress-strain curve, known as a backbone curve. Hardin and Drnevich (1972) proposed the following hyperbolic relationship between shear stress τ and shear strain γ :

$$\tau = \frac{\gamma}{\frac{1}{G_{\max}} + \frac{\gamma}{\tau_{\max}}} \quad (5-6)$$

The parameters used to define this relation are shown in Fig. 5.36. This stress-strain curve is characterized by an initial shear modulus G_{\max} corresponding to low-strains (10^{-4}). The hyperbolic curve is asymptotic to the horizontal line that identifies the shear stress at the failure, τ_{\max} . The reference strain γ_r is defined as the strain corresponding to the intersection of the maximum shear modulus line (G_{\max}) and maximum shear stress (τ_{\max}). Therefore,

$$\gamma_r = \frac{\tau_{\max}}{G_{\max}} \quad (5-7)$$

These parameters of soil cannot be determined with a great degree of accuracy. The initial shear modulus G_{max} may be defined by using the mass density and the shear wave velocity of the soil layer. The value of τ_{max} depends on the initial state of stress in the soil; it is the maximum shear stress that is developed at large strains (greater than 1.0 percent). The young Bay Mud in the San Francisco Bay area is mostly normally consolidated. The undrained shear strength of soil, τ_{max} , for normally consolidated soils under static conditions is approximately $0.3\sigma_v'$, where σ_v' is the effective overburden stress. To account for the effect of dynamic loading in the estimation of undrained shear strength of soils, Idriss (1991) has suggested to increase the shear strength under static conditions by a factor of 1.30 to 1.5, and by an additional factor of 1.4 if the soil is overconsolidated. A value of $\tau_{max} = 0.55\sigma_v'$, which is suggested by Idriss (1991), is used in this study.

Cycles of repeated loading will cause degradation of the stress-strain relationship. In order to account for the effects of degradation in the nonlinear analysis of soil, Hardin and Drnevich (1972) proposed the incorporation of a hyperbolic strain, γ_h , into equation (5.10), as follow:

$$\tau = \frac{\gamma}{\frac{1}{G_{max}} + \frac{\gamma_h}{G_{max}}} \quad (5-8)$$

where

$$\gamma_h = \frac{\gamma}{\gamma_r} [1 + a \exp^{-b(\frac{\gamma}{\gamma_r})}] \quad (5-9)$$

In this equation, a and b are soil constants that are defined based on experimental investigations. In our study deterioration was not considered.

5.6.2 Ramberg-Osgood Model

Initially the Ramberg-Osgood (*R-O*) formulation was used to model the stress-strain relationship for steels. The same model may be employed in nonlinear ground response

analysis to reproduce the behavior of soils under cyclic loading. The model calculates strains as a function of stress by using the following equation for the backbone curve:

$$\gamma_c = \gamma_y \left(\frac{\tau_c}{G_{\max} \gamma_y} \right) \left(1 + \alpha \left| \frac{\tau_c}{G_{\max} \gamma_y} \right|^{R-1} \right) \quad (5-10)$$

In this equation γ_y is a reference strain, α and R are constants of the R - O model, γ_c and τ_c are the coordinates of the tips of the loops. The model parameters are defined by fitting the backbone curve to data points obtain from experimental investigations. For Bay Mud, based on the data from first cycle tests, the values of $R = 3.5$, $\alpha = 0.5$, and $\gamma_y = 0.02\%$ were suggested by Idriss (1978). In order to account for degradation of soil properties due to dynamic loading, a degradation index δ was introduced by Idriss into equation (5.10) in the form of

$$\gamma_c = \gamma_y \left(\frac{\tau_c}{\delta G_{\max} \gamma_y} \right) \left(1 + \alpha \left| \frac{\tau_c}{\delta G_{\max} \gamma_y} \right|^{R-1} \right) \quad (5-11)$$

Figure 5.37(a) shows a typical R - O stress-strain relationship, defined by the aforementioned R - O parameters and equation (5.10).

5.6.3 Method of Analysis and Discussion of Results of Nonlinear Ground Response Analyses

For the purpose of our study a hyperbolic stress-strain relationship was selected as the basis for modeling the top 30 feet soil layer. The initial shear modulus G_{\max} is defined using a shear wave velocity of 400 ft/sec and a unit weight equal to 130 pcf. The maximum shear stress, τ_{\max} , is taken as $0.55\sigma_v'$, where σ_v' is the effective overburden stress. The maximum shear stress at the mid-depth of the 30 feet soil layer is used to represent the average shear strength of the top layer in the ground response analysis, resulting in the hyperbolic model presented in Fig. 5.37(b). This model is converted into the simple bilinear stress-strain model shown in Fig. 5.37(b), which is then used to develop the nonlinear story force vs. story displacement structural model. In the bilinear stress-strain model the initial stiffness is maintained as G_{\max} , and the strain hardening stiffness is defined as $0.01G_{\max}$. The yield level of the bilinear model is obtained by judgment, placing the strain hardening stiffness in a manner that intersects the hyperbolic

analysis to reproduce the behavior of soils under cyclic loading. The model calculates strains as a function of stress by using the following equation for the backbone curve:

$$\gamma_c = \gamma_y \left(\frac{\tau_c}{G_{\max} \gamma_y} \right) \left(1 + \alpha \left| \frac{\tau_c}{G_{\max} \gamma_y} \right|^{R-1} \right) \quad (5-10)$$

In this equation γ_y is a reference strain, α and R are constants of the $R-O$ model, γ_c and τ_c are the coordinates of the tips of the loops. The model parameters are defined by fitting the backbone curve to data points obtain from experimental investigations. For Bay Mud, based on the data from first cycle tests, the values of $R = 3.5$, $\alpha = 0.5$, and $\gamma_y = 0.02\%$ were suggested by Idriss (1978). In order to account for degradation of soil properties due to dynamic loading, a degradation index δ was introduced by Idriss into equation (5.10) in the form of

$$\gamma_c = \gamma_y \left(\frac{\tau_c}{\delta G_{\max} \gamma_y} \right) \left(1 + \alpha \left| \frac{\tau_c}{\delta G_{\max} \gamma_y} \right|^{R-1} \right) \quad (5-11)$$

Figure 5.37(a) shows a typical $R-O$ stress-strain relationship, defined by the aforementioned $R-O$ parameters and equation (5.10).

5.6.3 Method of Analysis and Discussion of Results of Nonlinear Ground Response Analyses

For the purpose of our study a hyperbolic stress-strain relationship was selected as the basis for modeling the top 30 feet soil layer. The initial shear modulus G_{\max} is defined using a shear wave velocity of 400 ft/sec and a unit weight equal to 130 pcf. The maximum shear stress, τ_{\max} , is taken as $0.55\sigma_v'$, where σ_v' is the effective overburden stress. The maximum shear stress at the mid-depth of the 30 feet soil layer is used to represent the average shear strength of the top layer in the ground response analysis, resulting in the hyperbolic model presented in Fig. 5.37(b). This model is converted into the simple bilinear stress-strain model shown in Fig. 5.37(b), which is then used to develop the nonlinear story force vs. story displacement structural model. In the bilinear stress-strain model the initial stiffness is maintained as G_{\max} , and the strain hardening stiffness is defined as $0.01G_{\max}$. The yield level of the bilinear model is obtained by judgment, placing the strain hardening stiffness in a manner that intersects the hyperbolic

stress-strain curve at a value of approximately 4% strain and trying to achieve also equal area under the hyperbolic and bilinear stress-strain curves.

In this pilot study only soil columns with periods of $T_s = 1.0$ and 1.5 seconds are used to investigate the effects of soil nonlinearity of the top layer on the amplification of ground motions. Dynamic analyses are conducted on these soil models using a modified version of the Drain-2D program. A viscous damping coefficient of 10% is assumed. The 10-Loma rock motions are used as input to the *SDOF* lumped mass model to generate soft soil surface motions. The baseline severity of each of the 10 rock motions is that level of motion that causes first yielding on top of the *SDOF* model. In order to investigate the effect of higher levels of ground motion, each record is then increased in severity by factors of 1.5, 2.0, 2.5 and 3.0, causing increasing degrees of nonlinearity in the top soil layer. These factors, designated by *SL* (severity level), are scaling factors of rock ground motions. Thus, a total of 50 scaled rock records are used as input to the two soil models, resulting in 100 soft soil surface motions. For these 100 soft soil records and the 50 scaled rock input motions the elastic strength demand spectra (for *SDOF* systems with 5% damping) are computed and the spectral ratios of strength demands (soft soil / rock, i.e., amplification factors) are evaluated.

Figure 5.38 shows the mean values of the amplification of elastic strength demands for the soil columns with fundamental periods of 1.0 and 1.5 seconds, subjected to the different levels of input rock motions. The solid curves (for $SL = 1.0$) are identical to the curves shown in Fig. 5.18 for elastic soils with $T_s = 1.0$ and 1.5 seconds. For inelastic soils ($SL > 1.0$) the spectral amplification decreases as the severity of motion (i.e., soil nonlinearity) increases. However, the decrease around $T/T_s = 1.0$ is not as large as anticipated, and the spectral amplifications are large even at ground motions three times as severe as those causing first soil yielding. Thus, soil nonlinearity may greatly reduce the amplification of *PGA* (see $T/T_s = 0.00$) but does not have an overpowering effect on spectral amplifications.

The *PGA* amplifications for these two soil periods is plotted against the severity level of the input rock motion in Fig. 5.39. As expected, the amplification of *PGA* decreases significantly as the rock motion severity increases since the limited shear strength of the soil prevents the soil column from transferring high levels of acceleration to the ground surface. However, also the decrease in *PGA* amplification is not nearly as large as the increase in severity. For instance, for the severity level of 3.0 the *PGA*

amplification is about half of that for a severity level of 1.0. Thus, for $SL = 3.0$ the PGA is about 1.5 times as large as that for $SL = 1.0$, the severity level associated with first "yielding" in the top layer. This amounts to a 50% increase in PGA from $SL = 1.0$ to $SL = 3.0$. Most of this increase can be attributed to the 1% strain hardening assumed in the bilinear soil constitutive model. For instance, for the soil column with $T_s = 1.5$ sec. the mean of the maximum "ductility" ratio in the top story (soil layer) at $SL = 3.0$ is 42, which corresponds to a 41% increase in maximum shear stress compared to first yielding. Figure 5.40 shows the means of the maximum "ductility" ratios at the different severity levels. The ductility ratio of 1.0 corresponds to a shear strain of 0.126%.

The amplification of peak ground displacement (PGD) for the different severity levels of input rock motion is presented in Fig. 5.41. The figure shows that the mean amplification of PGD is almost constant for all levels of input motion. This indicates that the PGD is only weakly dependent on the extent of nonlinearity in the top soil layer. Considering that the PGA amplification decreases with increasing severity, whereas the PGD amplification stays constant, it is concluded that the PGD/PGA ratio of the soft soil motion increases significantly with the ground motion severity. In this pilot study this ratio increases by a factor of approximately 2 when the ground motion severity is increased from $SL = 1.0$ to $SL = 3.0$.

Figures 5.42 and 5.43 are used here to illustrate the effects of nonlinearity in the top soil layer on the predicted ground motions at higher levels of ground shaking. Figure 5.42 shows the elastic strength demand spectra for predicted motions at the top and bottom of the top soil layer, using a soil column with $T_s = 1.0$ sec. and the San Francisco Rincon Hill rock record with a severity level of 3.0 as input. Due to the limited shear strength of the top layer, the PGA of the surface motion as well as the spectral accelerations for periods less than 1.5 seconds are significantly smaller than those at the bottom of the top layer. The maximum displacement, however, is somewhat larger as can be seen from the displacement time histories presented in Fig. 5.43.

The nonlinear behavior of soil can be taken into account approximately by assigning an appropriate viscous damping ratio for the ground response analysis. In order to investigate the effects of damping on the amplification of surface motions, the elastic $SDOF$ soil models for two soil periods, $T_s = 1.0$ and 1.5 seconds, were subjected to the *10-Loma* set of rock records using damping ratios of 5, 10 and 20% for each mode of vibration. Figure 5.44 shows the mean amplification of elastic strength demands for

these cases. As indicated in this figure, the amplifications are very sensitive to the damping ratios, and a damping of 20% results in amplifications that are smaller than those in the nonlinear analysis for $SL = 3.0$. However, the results of the two analyses cannot be compared directly since the viscous damping in the linear analysis is assigned to all modes whereas nonlinearity in the nonlinear analysis is confined to the top soil layer.

The conclusions drawn from the nonlinear ground response analysis, using a 5DOF soil model with nonlinear behavior in the top layer, can be summarized as follows:

- The presence of a nonlinear soil layer decreases the elastic strength demands. However, this decrease is not very large around the critical period ratio of $T/T_s = 1.0$. For ground motions causing very large inelastic deformations (i.e., $SL = 3.0$) this decrease is only about 25%, even though the *PGA* amplification is reduced by about 50%.
- The *PGA* amplification decreases significantly as the level of ground shaking increases. The highly nonlinear behavior of soils at higher level of ground shaking prevents the input ground acceleration from being fully transmitted to the ground surface. Similar results for amplification of *PGA* at the higher level of ground shaking are reported by other researchers. Idriss (1991) estimates that at rock *PGAs* exceeding 0.40g no soft soil *PGA* amplification occurs. Seed et. al. (1992) conducted a fully nonlinear ground response analysis using an idealized soil profile subjected to different levels of ground acceleration. The results of their study also show a large decrease in the *PGA* amplification for soft soil sites when high levels of input accelerations are applied.
- The *PGD* amplification is not very sensitive to the level of ground shaking, but the ratio of *PGD/PGA* increases significantly with an increase in nonlinearity in the top soil layer.

It must be emphasized that the results presented in this section are not final answers in many cases. They are based on a simplified one-dimensional soil model with nonlinear behavior in the top 30 ft., and assuming a 10% damping ratio in all modes. A fully nonlinear soil model and different soil damping ratios will lead to somewhat different results. However, most important is the recognition that soft soils, when

subjected to high acceleration, will respond in a highly nonlinear fashion and will not be capable of transmitting accelerations larger than those associated with the soil shear strength. Thus, *PGA* amplifications and amplifications of strength demands depend on the severity of input (rock) ground motions and need to be adjusted accordingly. This limited pilot study indicates that the adjustments are quite different for amplifications of *PGA* and amplifications of strength demands.

5.7 Implications for Seismic Design

The study summarized here has shown that soft soil effects cannot be lumped into a soil factor that is independent of structure period and target ductility ratio, and ground motion severity (such as S_3 and S_4 in the 1991 UBC). Rather, it appears to be feasible to relate the strength demand (elastic or inelastic) for a soft soil motion to that of the motion in the underlying rock by a modification function $S(T_s, \mu)$ as shown in Eq. 5.1. This function can be derived from the type of information presented in the previous sections, which provide quantitative values for amplification factors in soils with small nonlinearity (represented by 10% viscous damping), and preliminary results for soils with large nonlinearity in the top layer.

Considering that soil and structure periods cannot be determined with certainty, some enveloping of amplification of strength demands is recommended. This enveloping can be based on either a narrow band of estimated T_s or a broad band that places more emphasis on the uncertainties in the determination of soil periods and the shortcomings of the data derived from one-dimensional wave propagation models. The suggested process of modifying the *SDOF* strength demands is illustrated in Fig. 5.4. As in design for structures located on rock, the need exists to modify *SDOF* strength demands for *MDOF* effects. This issue is not addressed here.

The inelastic strength demand spectra provide basic design information needed to control ductility ratios. Perhaps equally important, the maximum displacement of a structure needs also be controlled in order to limit structural and non-structural damage and provide protection against incremental collapse due to P-delta effects. Because of the relationship that exist between strength and displacement demands, the displacement demand for a soft soil motion can be related to the strength demand of the motion in the

underlying rock by the same modification function $S(T_s, \mu)$, as is illustrated next. The displacement demand for rock motions can be obtained from the following relation:

$$\delta^r(\mu) = \frac{\mu}{R} \frac{F_{y,e}^r}{\omega^2} \quad (5.12)$$

where $\delta^r(\mu)$ is the maximum displacement of the *SDOF* system with a ductility of μ on rock sites, ω is the circular frequency, and $F_{y,e}^r$ is the elastic strength demand for the bedrock motion below soft soil sites.

The elastic and inelastic displacement demands for a structure located on soft soil can therefore be written in the following form:

$$\delta_e^s = \frac{F_{y,e}^r}{\omega^2} S(T_s, \mu = 1) \quad (5.13)$$

$$\delta_{in}^s(\mu) = \frac{\mu}{R} \frac{F_{y,e}^r}{\omega^2} S(T_s, \mu) \quad (5.14)$$

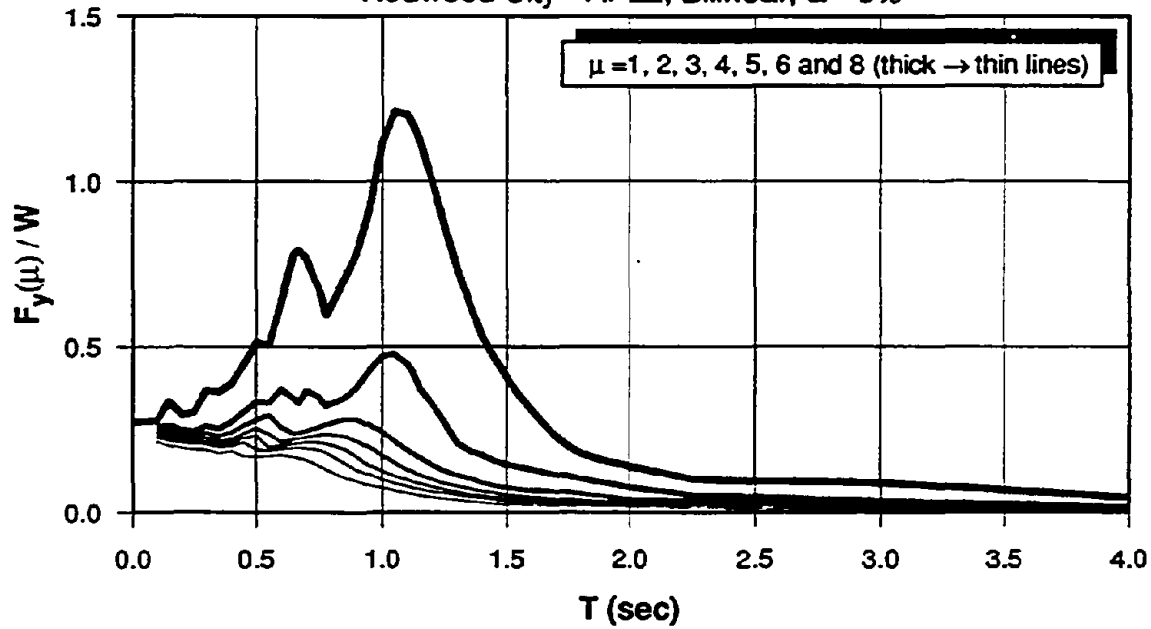
where δ_e^s and $\delta_{in}^s(\mu)$ are the elastic and inelastic displacement demands for the soft soil motion. The above equations can be used to define the ratio of elastic to inelastic displacement demand spectra in soft soils (Eq. 5.15), examples of which are shown in Figs 5.29 to 5.32.

$$\frac{\delta_{in}^s(\mu)}{\delta_e^s} = \frac{\mu}{R} \frac{S(T_s, \mu)}{S(T_s, \mu = 1)} \quad (5.15)$$

Information of this type is needed to provide drift control in structural design.

SITE SPECIFIC STRENGTH DEMAND SPECTRA

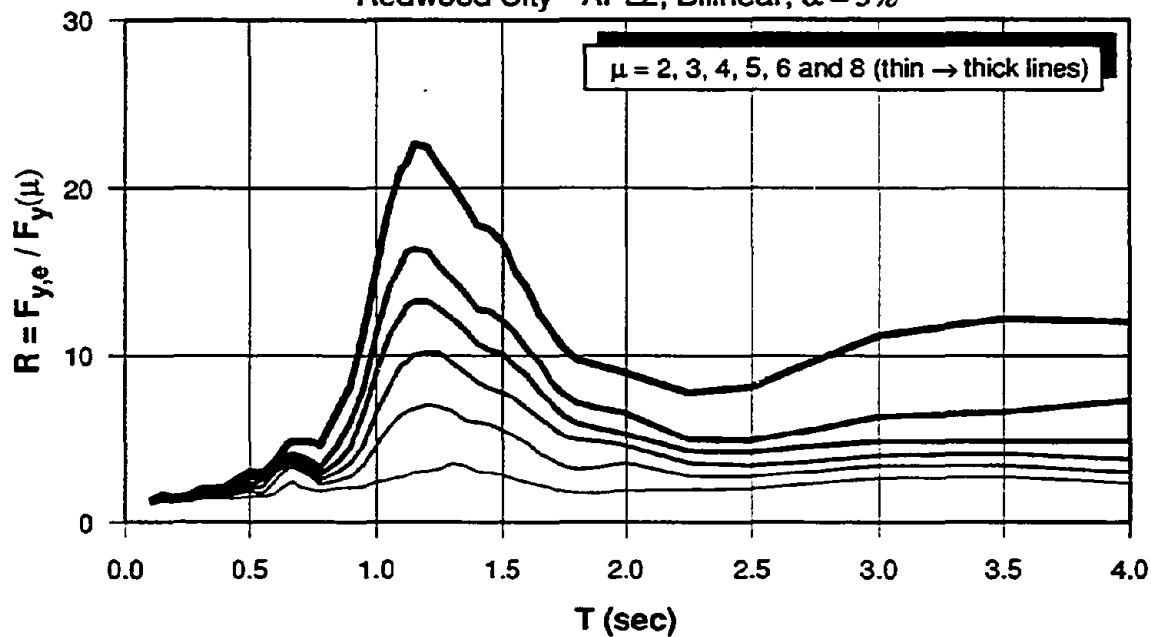
Redwood City - APL2, Bilinear, $\alpha = 5\%$



(a) Elastic & Inelastic Strength Demand Spectra

SITE SPECIFIC STRENGTH REDUCTION FACTORS

Redwood City - APL2, Bilinear, $\alpha = 5\%$

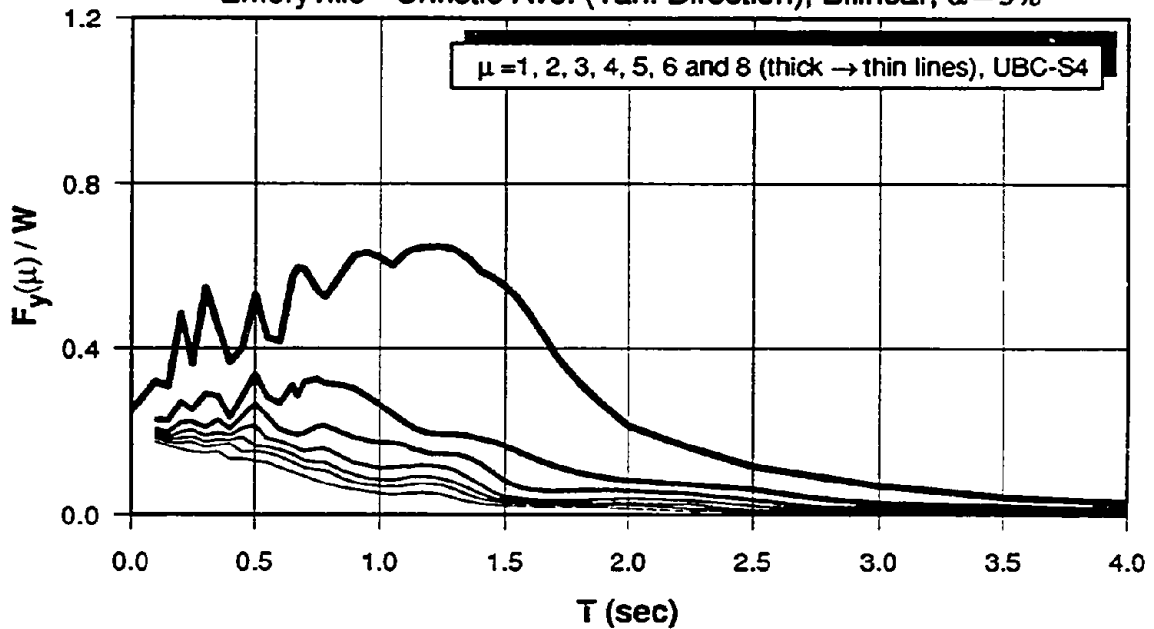


(b) Strength Reduction Factors

Fig. 5.1 Site Specific Strength Demands - Apeel Array 2 Soft Soil Site

SITE SPECIFIC STRENGTH DEMAND SPECTRA

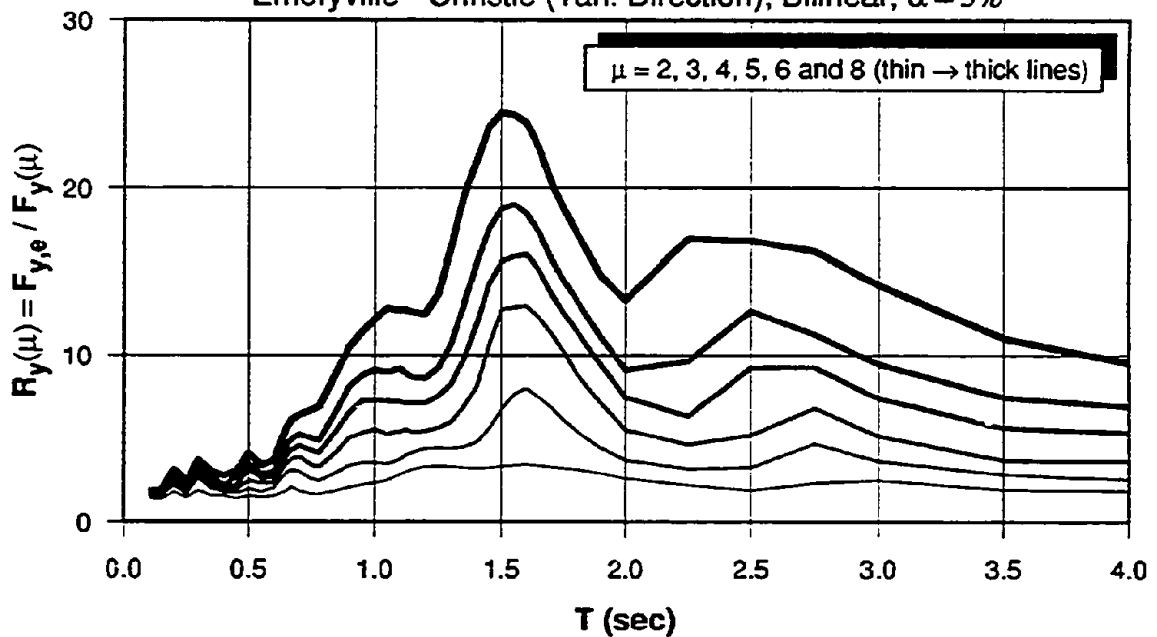
Emeryville - Christie Ave. (Tan. Direction), Bilinear, $\alpha = 5\%$



(a) Elastic & Inelastic Strength Demand Spectra

SITE SPECIFIC STRENGTH REDUCTION FACTORS

Emeryville - Christie (Tan. Direction), Bilinear, $\alpha = 5\%$



(b) Strength Reduction Factors

Fig. 5.2 Site Specific Strength Demands - Emeryville Soft Soil Site

ELASTIC & INELASTIC STRENGTH DEMAND SPECTRA

Redwood Shore & Apeel Array 2, $\mu = 1,4$

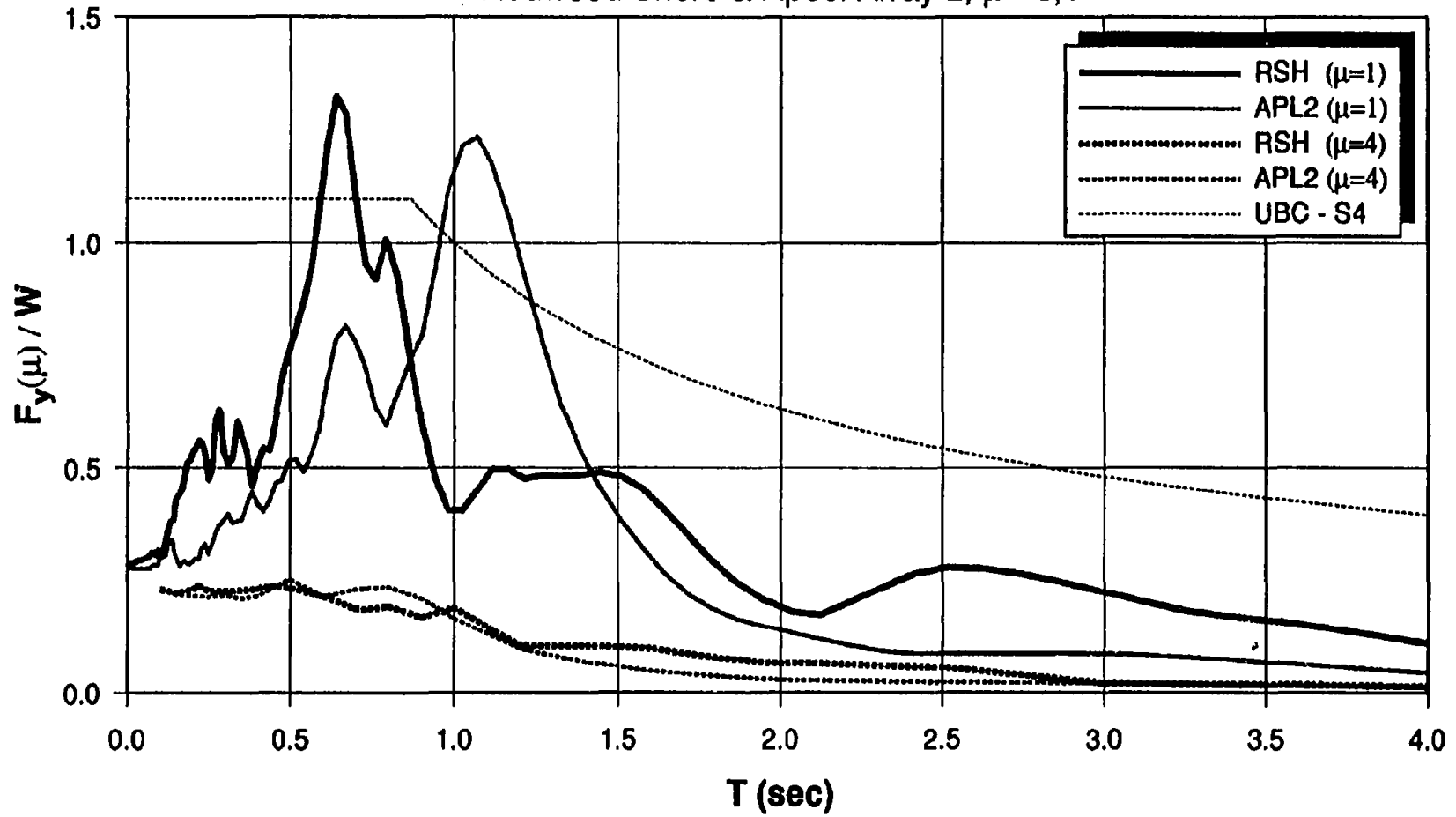


Fig. 5.3 Elastic and Inelastic Strength Demand Spectra for Two Recorded Soft Soil Motions

DESIGN STRENGTH DEMAND

On Rock and Stiff Soils

$$F_y^r(\mu) = \frac{F_{y,e}^r}{R}$$

On Soft Soils

$$F_y^s(\mu) = F_y^r(\mu)S(T_s, \mu) = \frac{F_{y,e}^r}{R}S(T_s, \mu)$$

$F_y^s(\mu)$ = Inelastic Strength Demand at Soft Soil Site

$F_y^r(\mu)$ = Inelastic Strength Demand for bedrock motion below soft soil site

$F_{y,e}^r$ = Elastic Strength Demand for bedrock motion below soft soil site

$S(T_s, \mu)$ = Soft Soil Modification Function

MODIFICATION OF STRENGTH DEMAND SPECTRA FOR SOFT SOIL EFFECTS

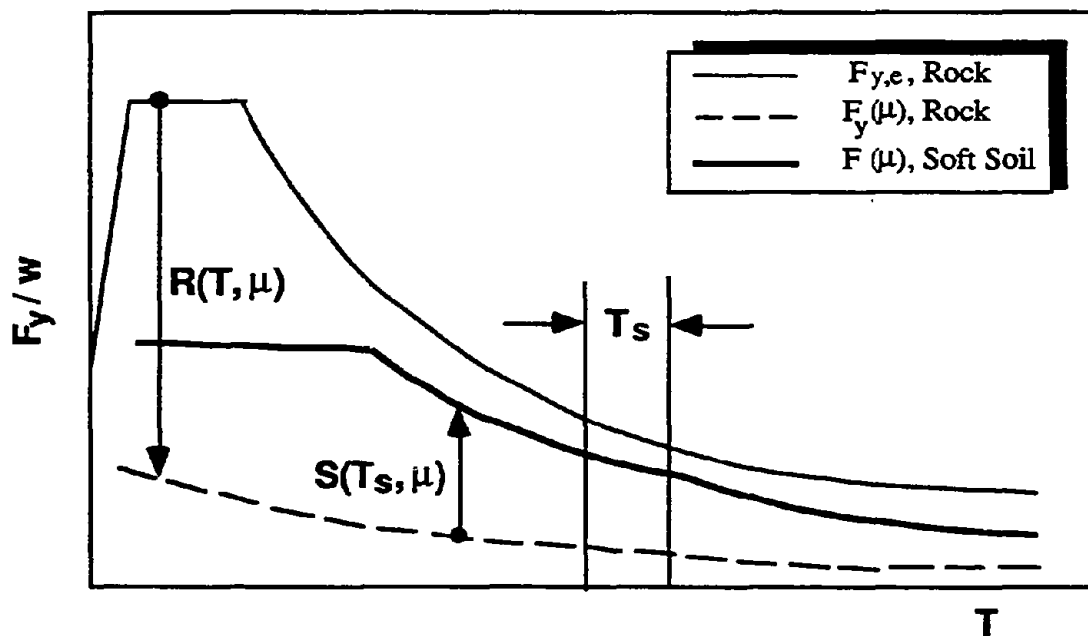
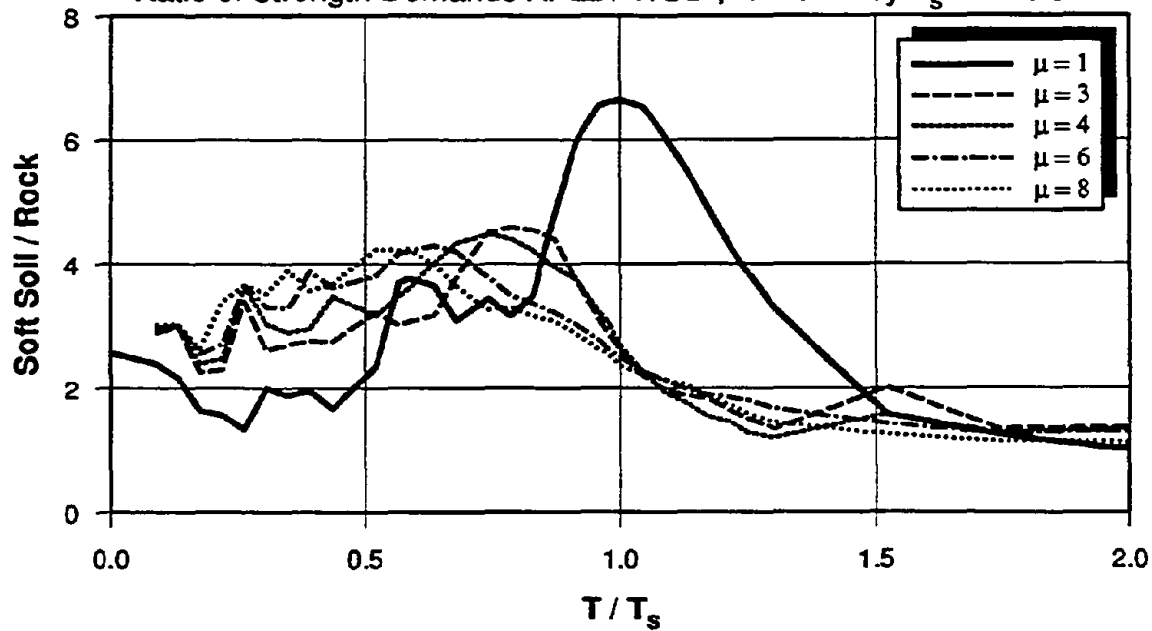


Fig. 5.4 Suggested Process for Modification of SDOF Strength Demands for Soft Soil Effects

AMPLIFICATION OF STRENGTH DEMANDS

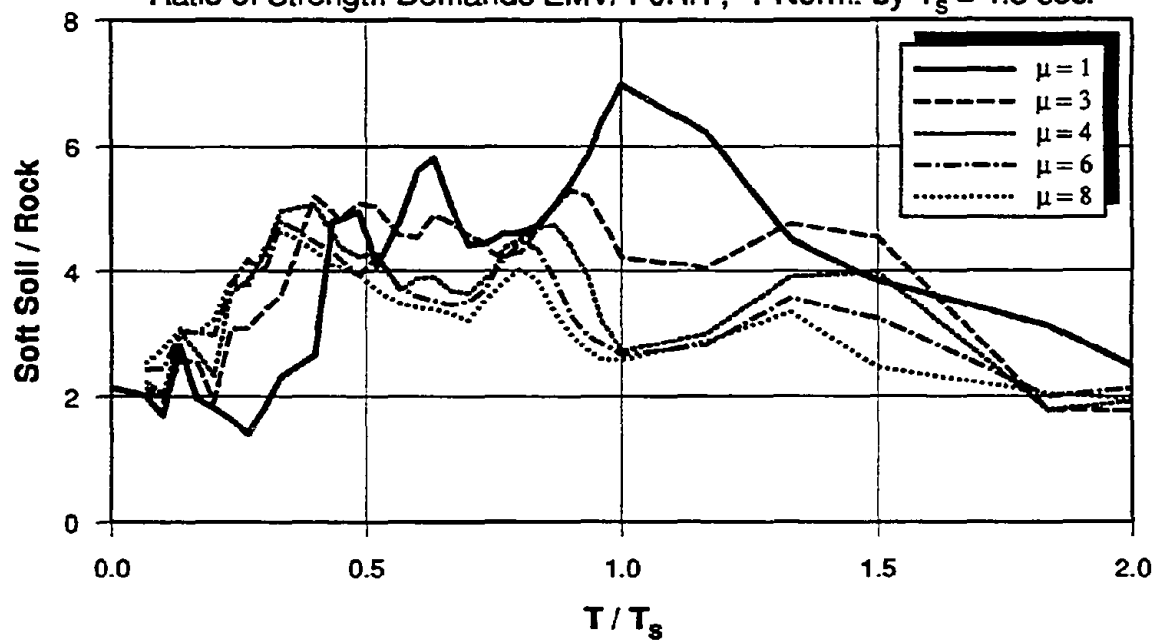
Ratio of Strength Demands APL2 / WOD , T Norm. by $T_s = 1.10$ sec.



(a) Apeel Array 2

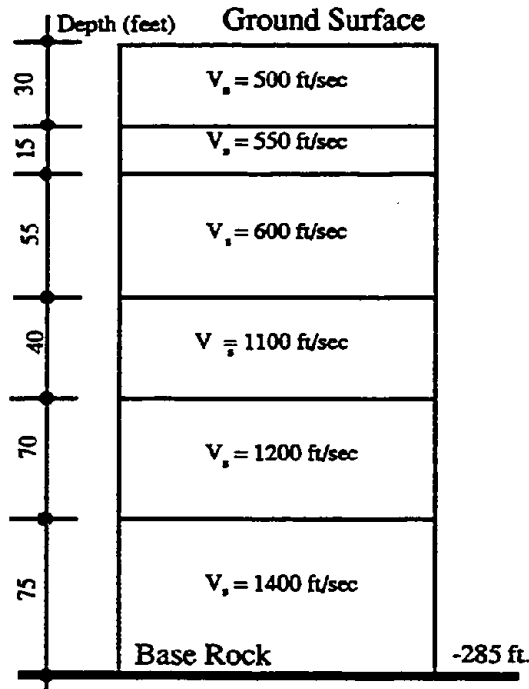
AMPLIFICATION OF STRENGTH DEMANDS

Ratio of Strength Demands EMV/ PJRH , T Norm. by $T_s = 1.5$ sec.

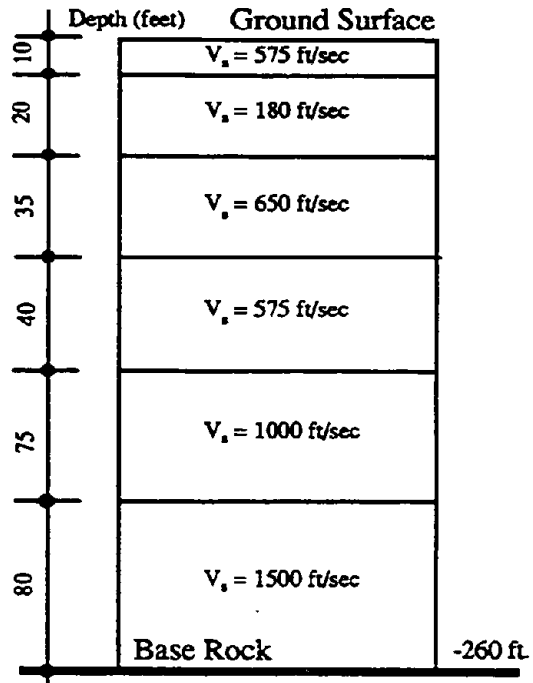


(b) Emeryville

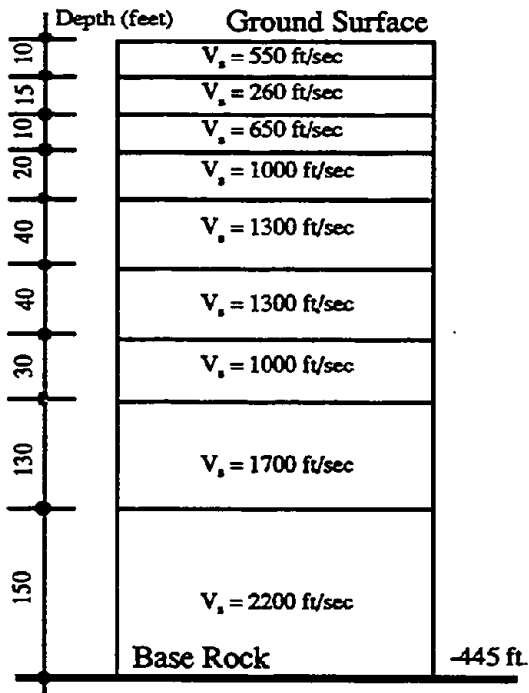
Fig. 5.5 Amplification of Strength Demands for Two Selected Soft Soil Sites



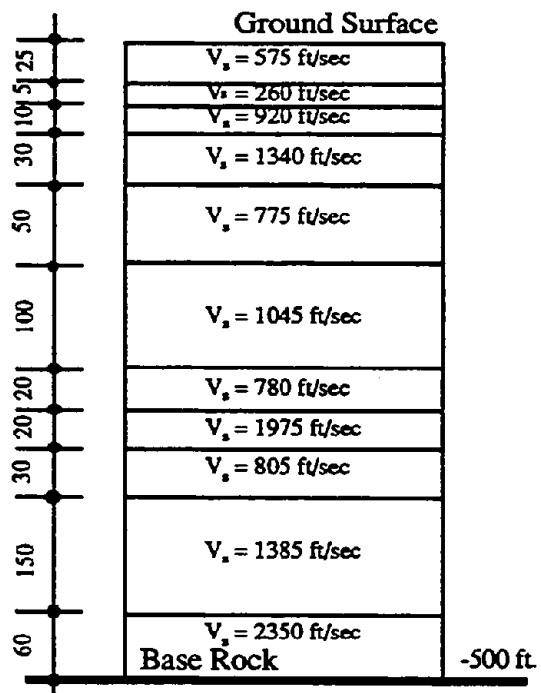
TREASURE ISLAND (TRI)



APEEL ARRAY -2 (APL2)



SF. AIRPORT (SFA)



OAKLAND HARBOR (OAKW)

Fig. 5.6 Shear Wave Velocity Profile for Selected Soft Soil Sites

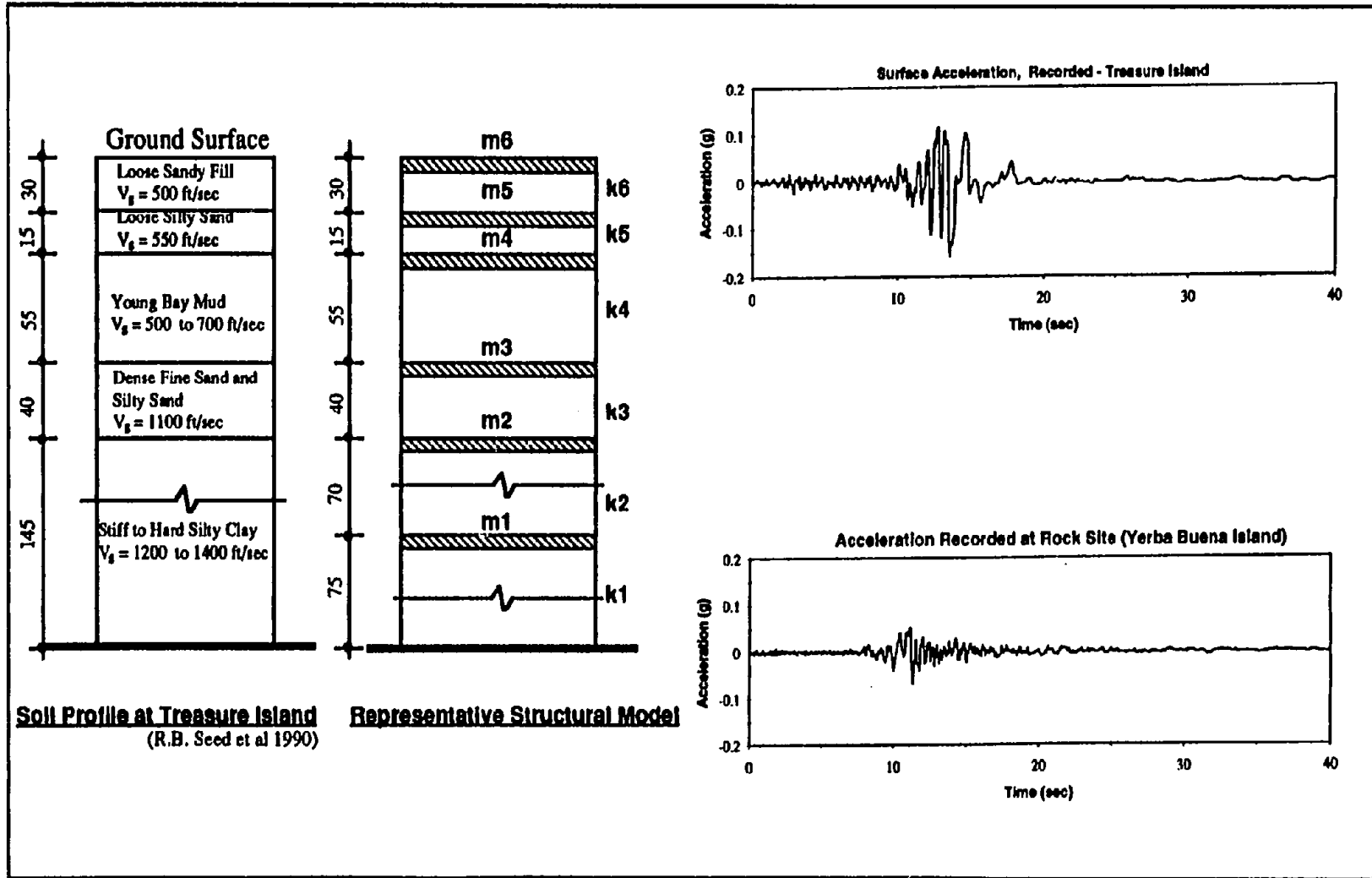
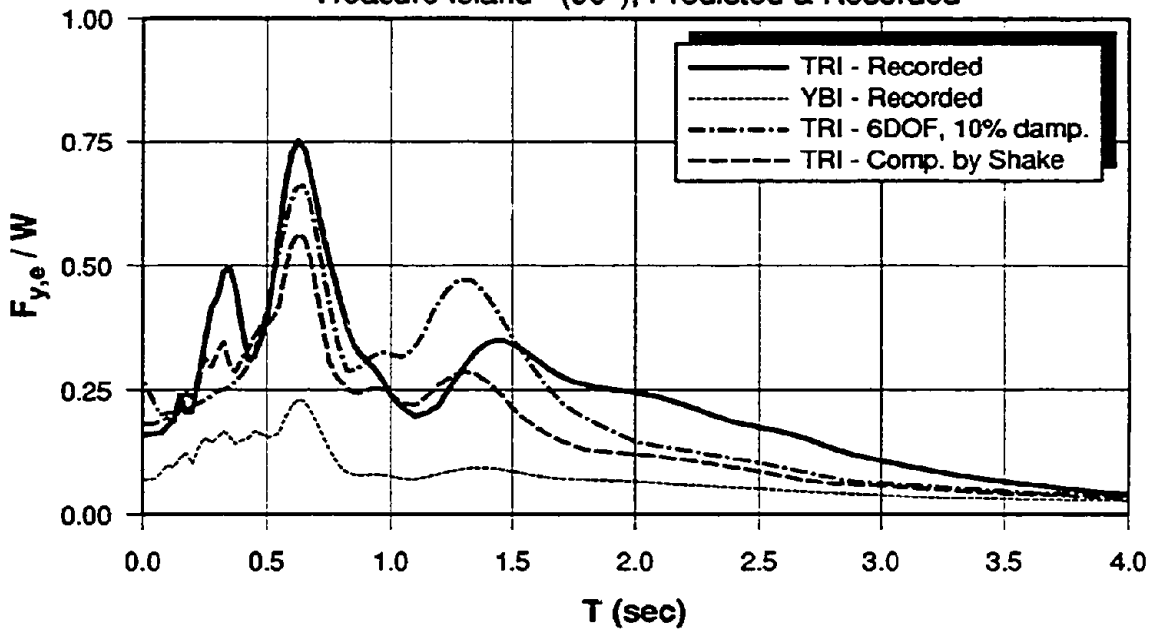


Fig. 5.7 Soil Profile at Treasure Island and Representative MDOF Lumped Mass Model

SITE SPECIFIC ELASTIC STRENGTH DEMAND SPECTRA

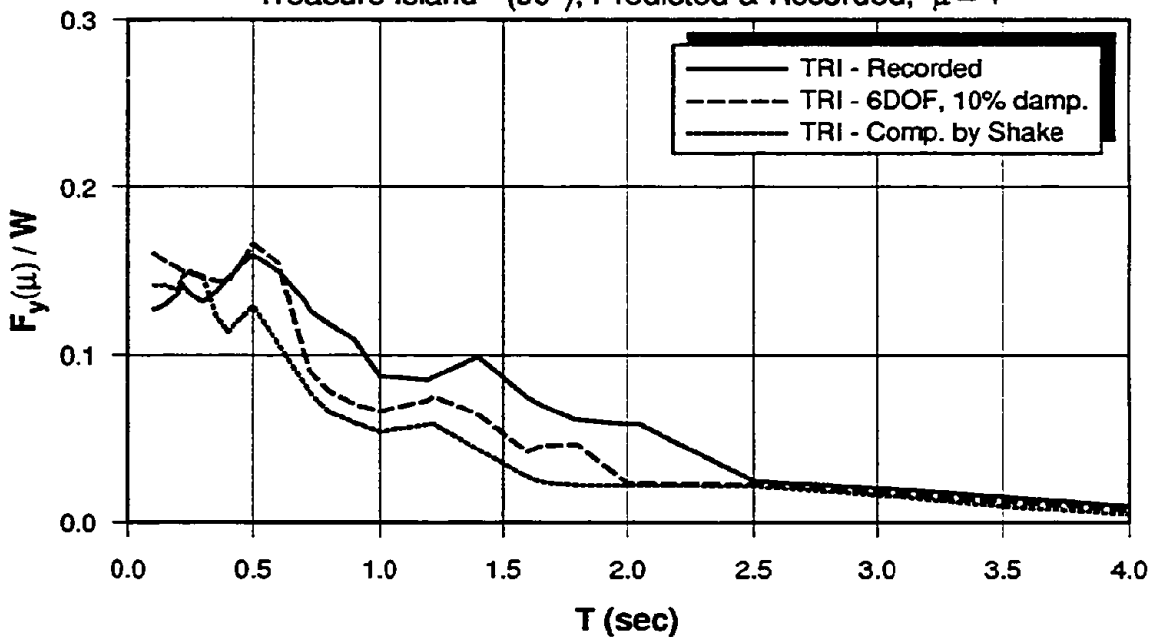
Treasure Island - (90°), Predicted & Recorded



(a) Elastic Strength Demand Spectra

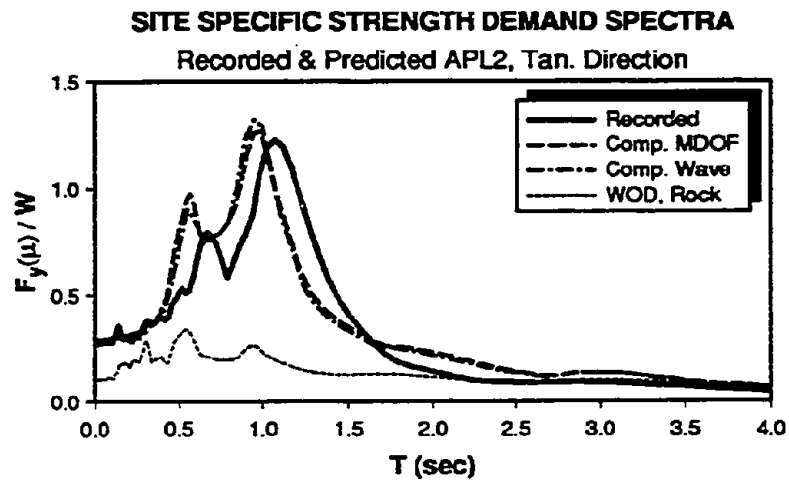
SITE SPECIFIC INELASTIC STRENGTH DEMAND SPECTRA

Treasure Island - (90°), Predicted & Recorded, $\mu = 4$

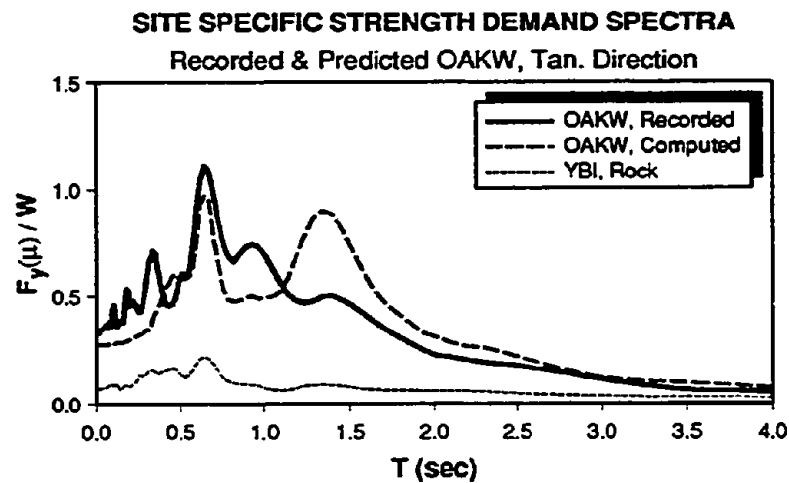


(b) Inelastic Strength Demand Spectra, $\mu = 4$

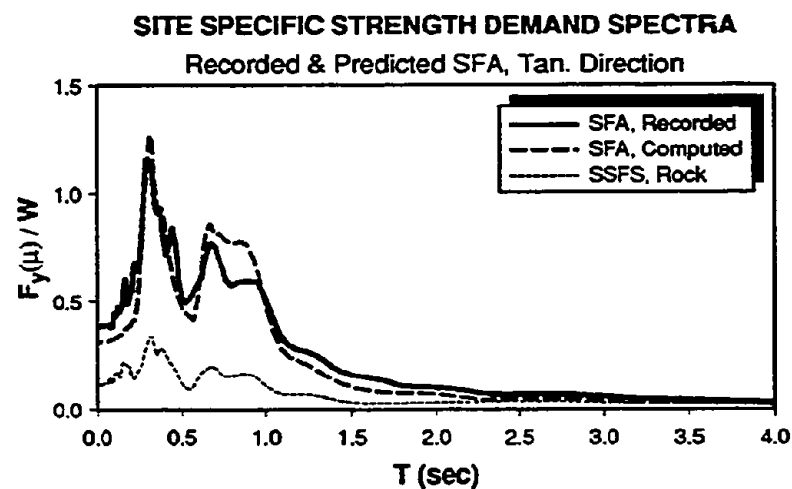
Fig. 5.8 Comparison of Strength Demands of Predicted and Recorded Motions for Treasure Island



(a) Redwood City Apeel Array 2



(b) Oakland - Outer Harbor Wharf



(c) San Francisco International Airport

Fig. 5.9 Comparison of Strength Demands of Predicted and Recorded Soft Soil Motions

SOIL PROFILE AND MDOF SOIL MODEL

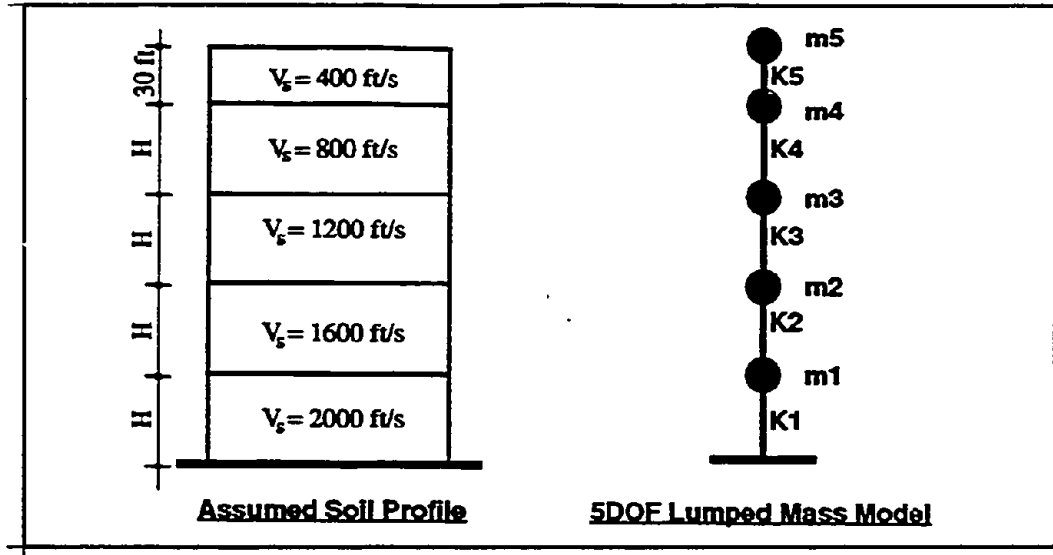


Fig. 5.10 Soil Column Models Used in Parameter Study

NORMALIZED ELASTIC STRENGTH DEMAND SPECTRA - MEAN

ATC-S₁, 15-S₁, 10-Loma (Rock)

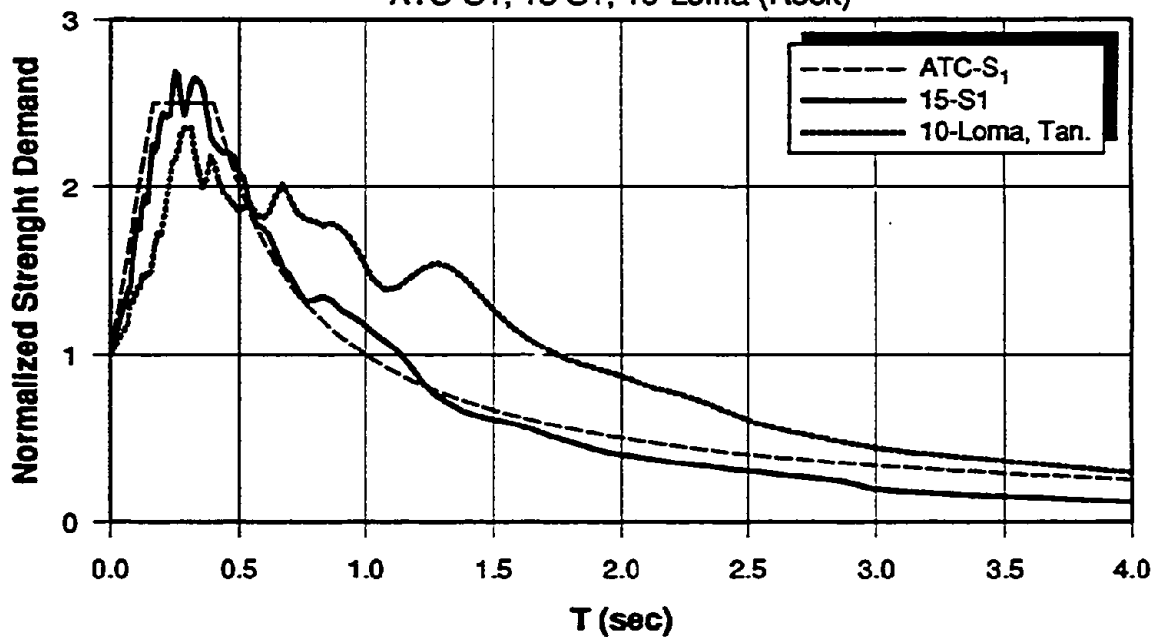
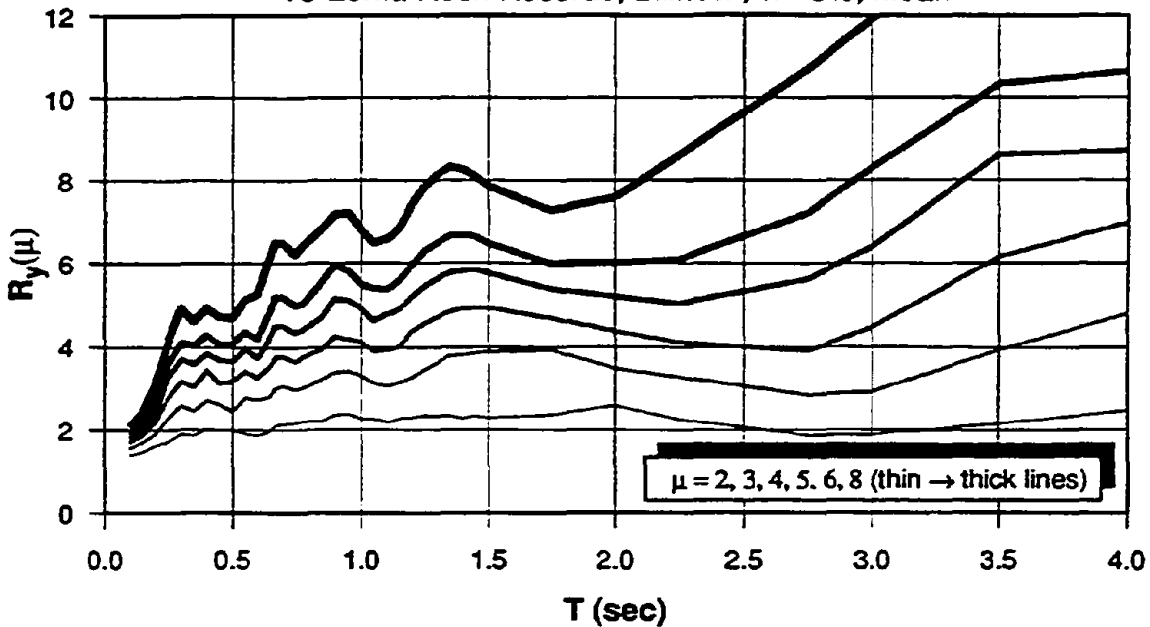


Fig. 5.11 Mean of Normalized Elastic Spectra of 15-S₁ and 10-Loma Rock Record Sets

STRENGTH REDUCTION FACTOR, $R_y(\mu)$ – (10-Loma.bi-5)

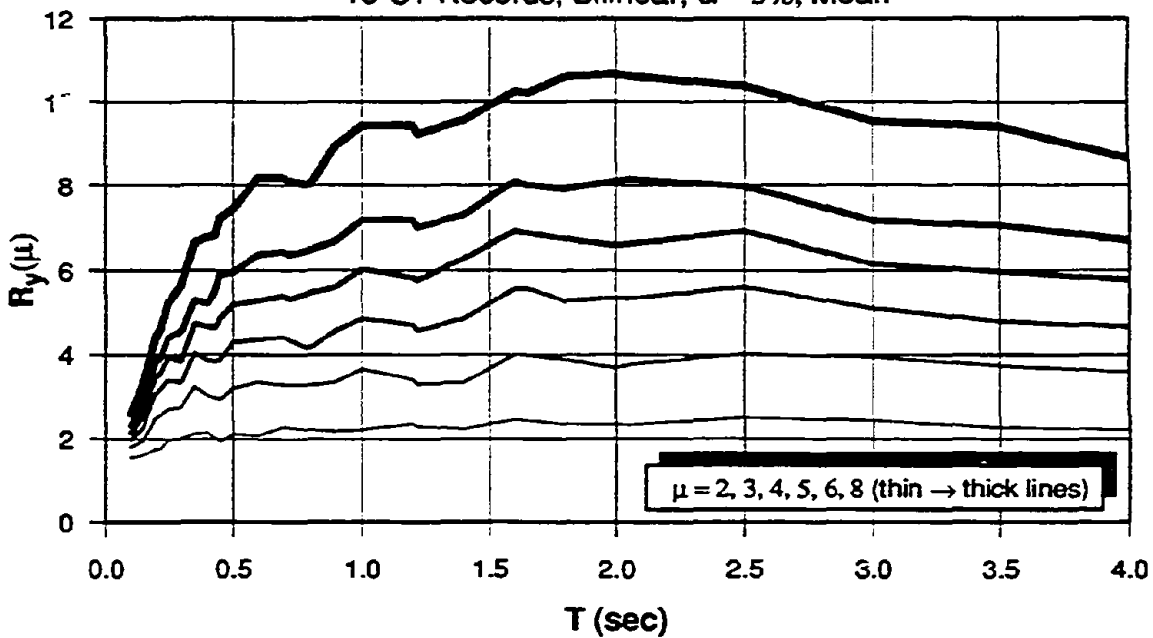
10 Loma Rock Records, Bilinear, $\alpha = 5\%$, Mean



(a) 10-Loma Record Set

STRENGTH REDUCTION FACTOR, $R_y(\mu)$ – (15-S1.bi-5)

15-S1 Records, Bilinear, $\alpha = 5\%$, Mean

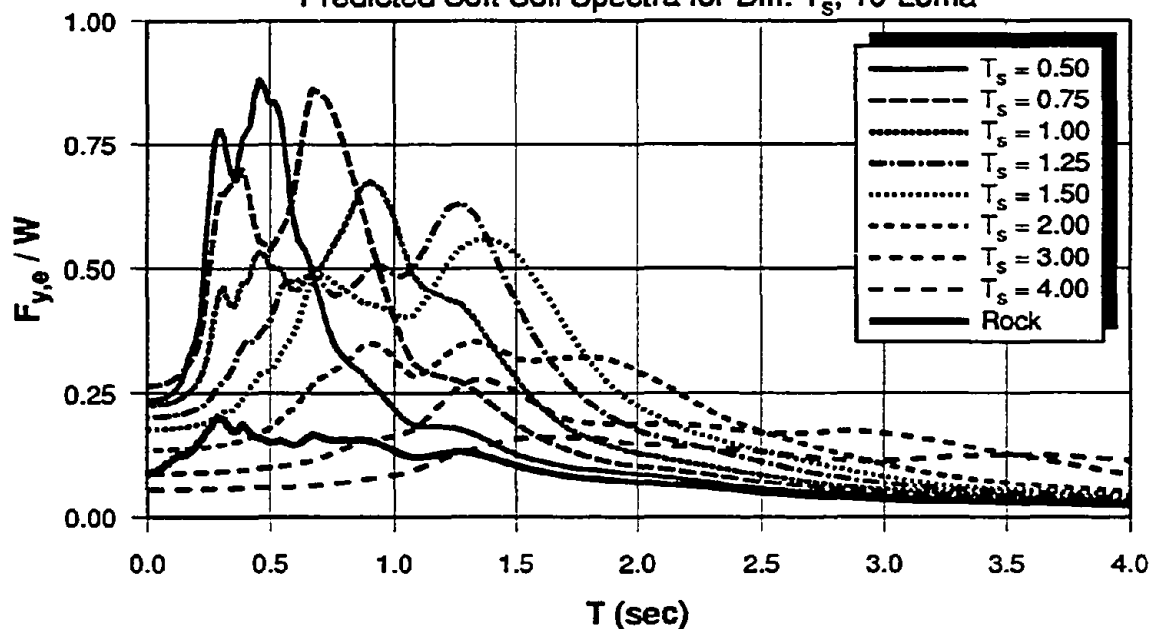


(b) 15-S₁ Record Set

Fig. 5.12 Mean Strength Reduction Factors of 15-S₁ and 10-Loma Rock Record Sets

MEAN ELASTIC STRENGTH DEMANDS

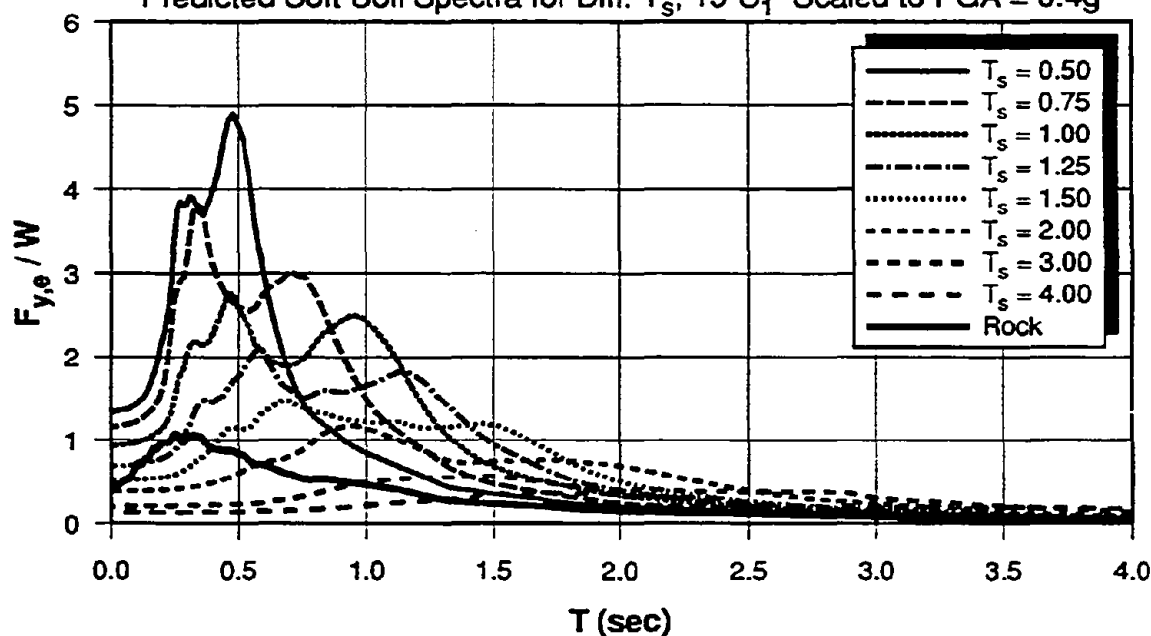
Predicted Soft Soil Spectra for Diff. T_s , 10-Loma



(a) 10-Loma Record Set

MEAN ELASTIC STRENGTH DEMANDS

Predicted Soft Soil Spectra for Diff. T_s , 15-S₁ Scaled to PGA = 0.4g

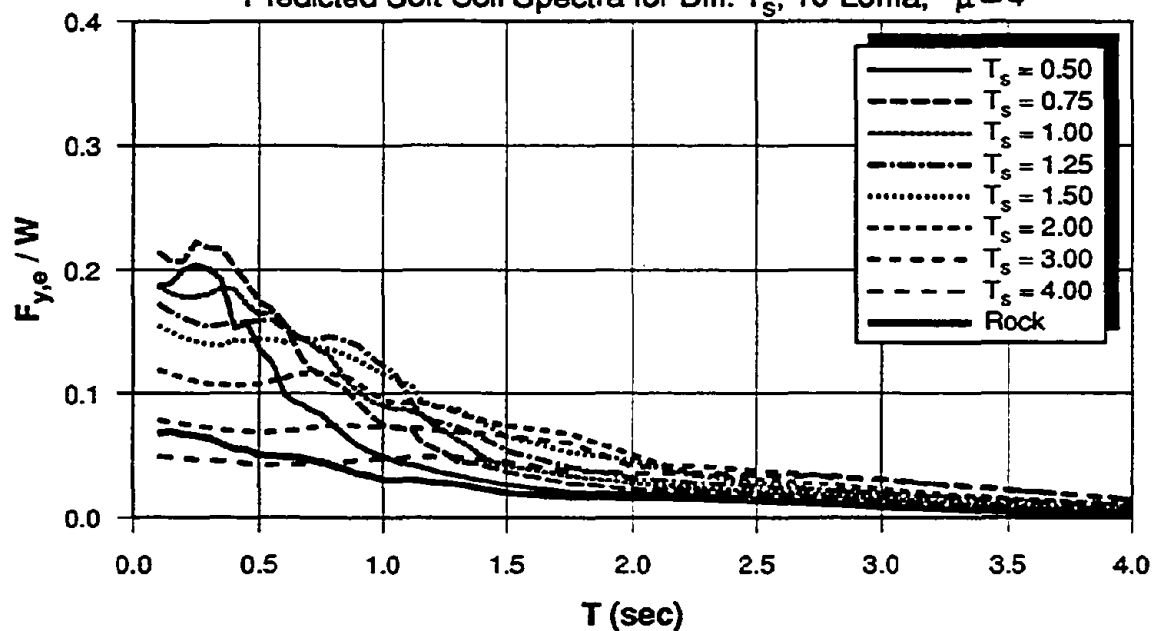


(b) 15-S₁ Record Set

Fig. 5.13 Mean of Elastic Strength Demands Using 10-Loma and 15-S₁ Record Sets

MEAN INELASTIC STRENGTH DEMANDS

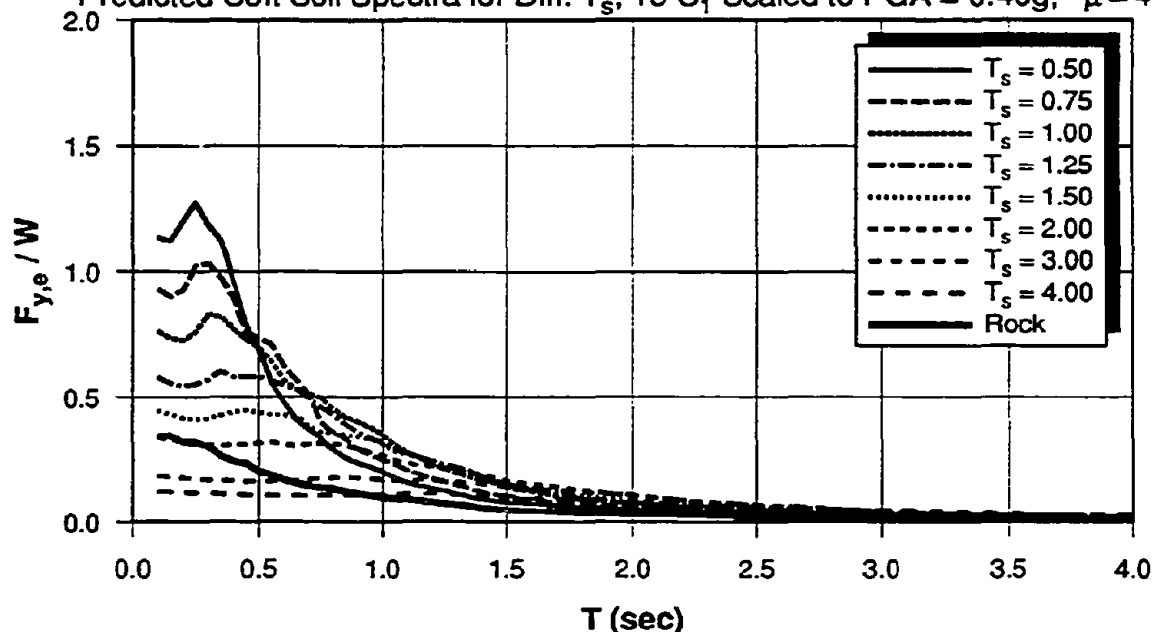
Predicted Soft Soil Spectra for Diff. T_s , 10-Loma, $\mu = 4$



(a) 10-Loma Record Set

MEAN INELASTIC STRENGTH DEMANDS

Predicted Soft Soil Spectra for Diff. T_s , 15- S_1 Scaled to PGA = 0.40g, $\mu = 4$

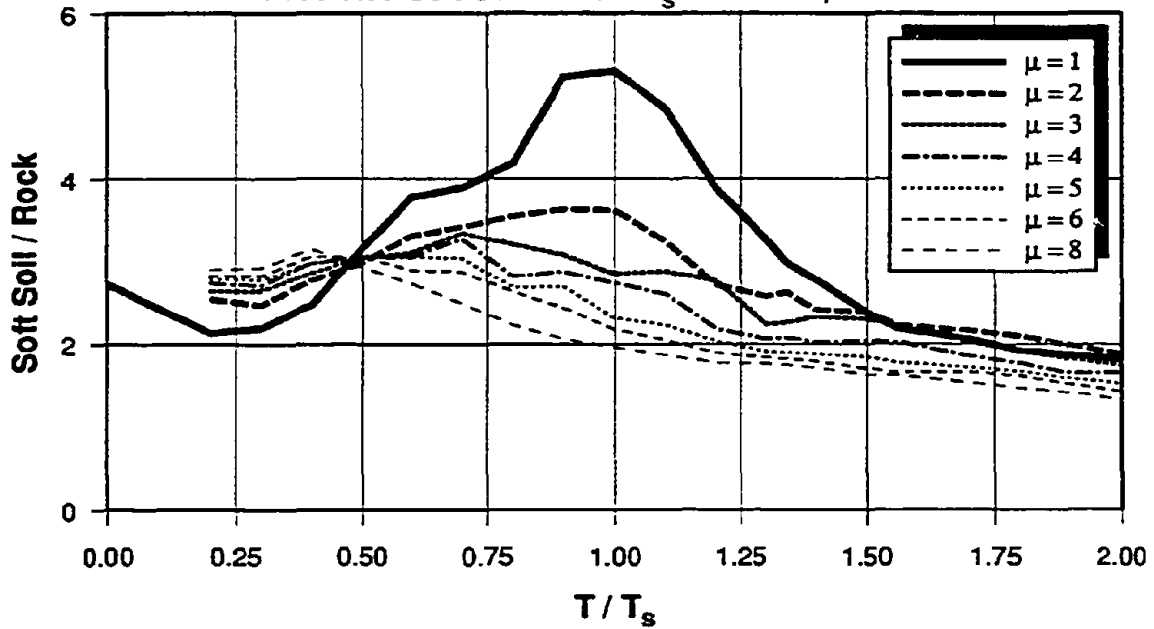


(b) 15- S_1 Record Set

Fig. 5.14 Mean of Inelastic Strength Demands Using 10-Loma and 15- S_1 Record Sets

AMPLIFICATION OF STRENGTH DEMANDS - MEAN

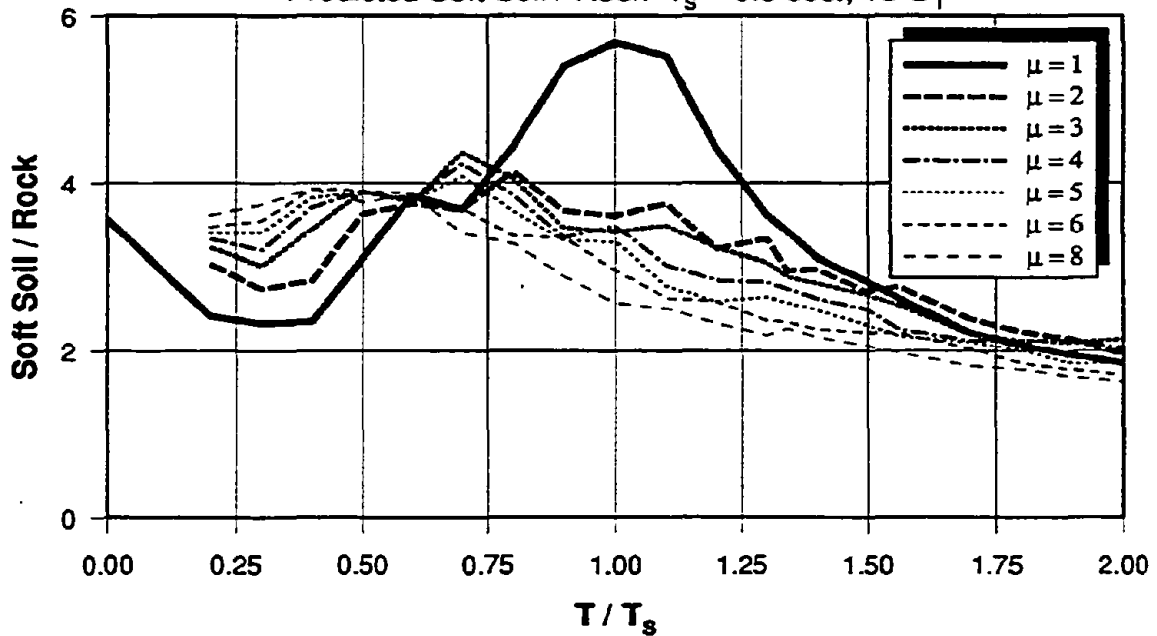
Predicted Soft Soil / Rock $T_s = 0.5$ sec., 10-Loma



(a) 10-Loma Record Set

AMPLIFICATION OF STRENGTH DEMANDS - MEAN

Predicted Soft Soil / Rock $T_s = 0.5$ sec., 15-S₁

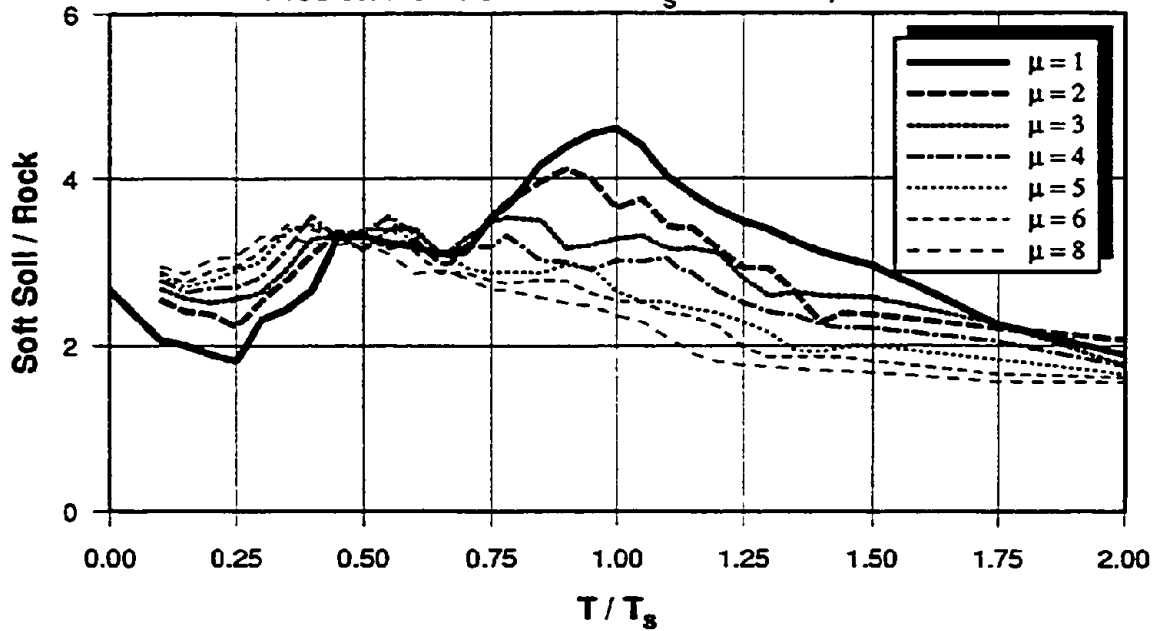


(b) 15-S₁ Record Set

Fig. 5.15 Amplification of Strength Demands for Predicted Soft Soil Motions - $T_s = 0.5$ (sec)

AMPLIFICATION OF STRENGTH DEMANDS - MEAN

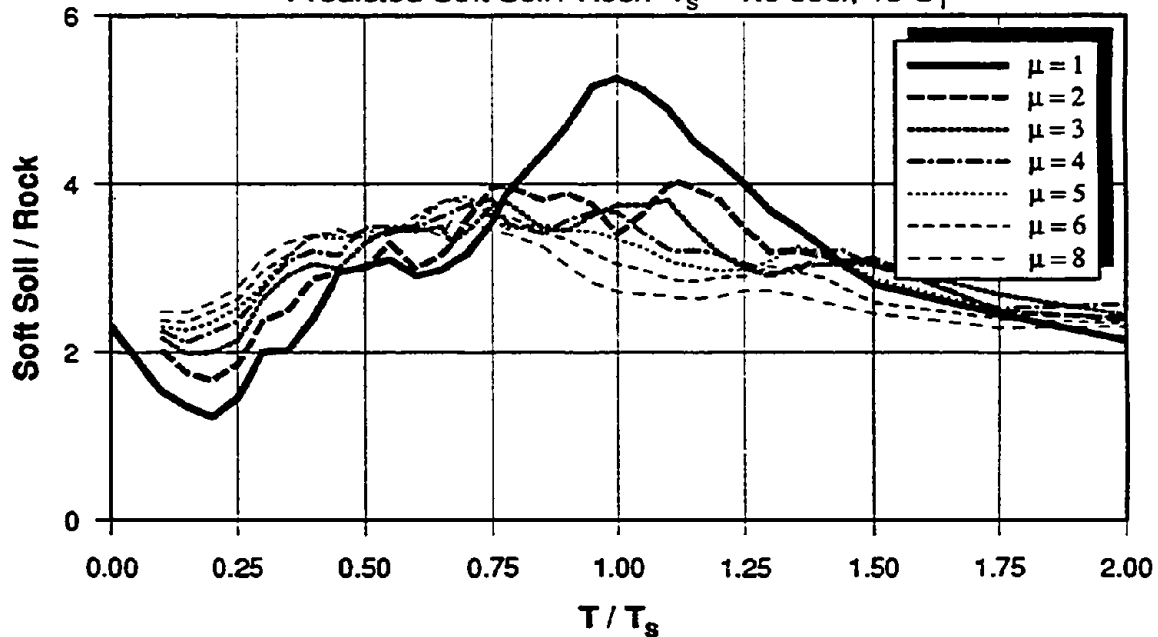
Predicted Soft Soil / Rock $T_s = 1.0$ sec., 10-Loma



(a) 10-Loma Record Set

AMPLIFICATION OF STRENGTH DEMANDS - MEAN

Predicted Soft Soil / Rock $T_s = 1.0$ sec., 15-S₁

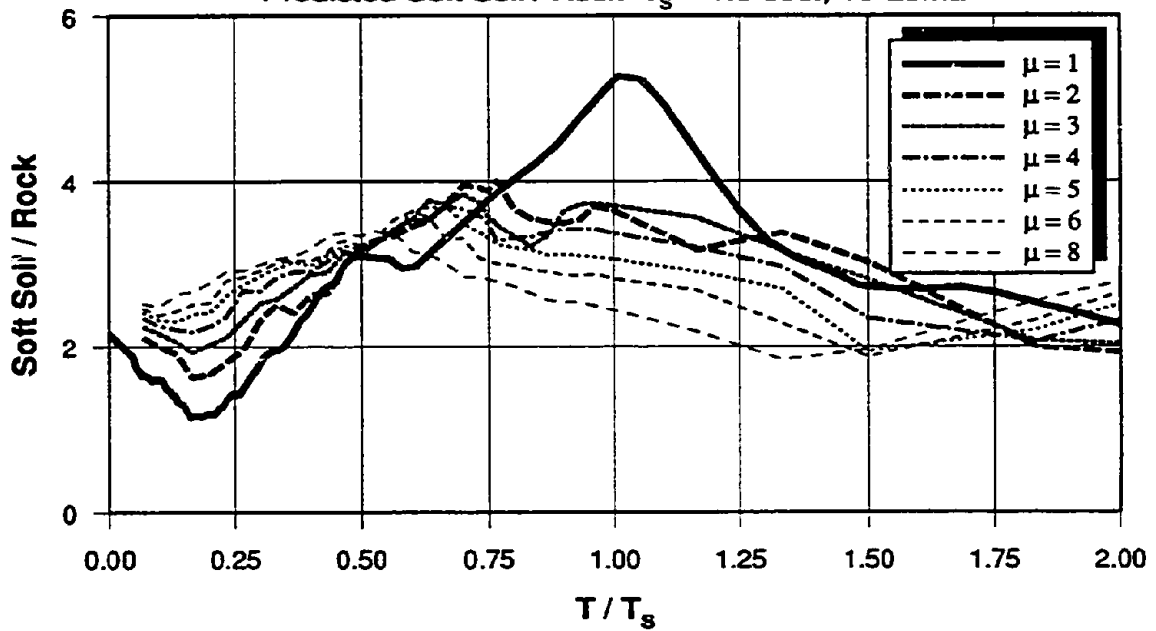


(b) 15-S₁ Record Set

Fig. 5.16 Amplification of Strength Demands for Predicted Soft Soil Motions - $T_s = 1.0$ (sec)

AMPLIFICATION OF STRENGTH DEMANDS - MEAN

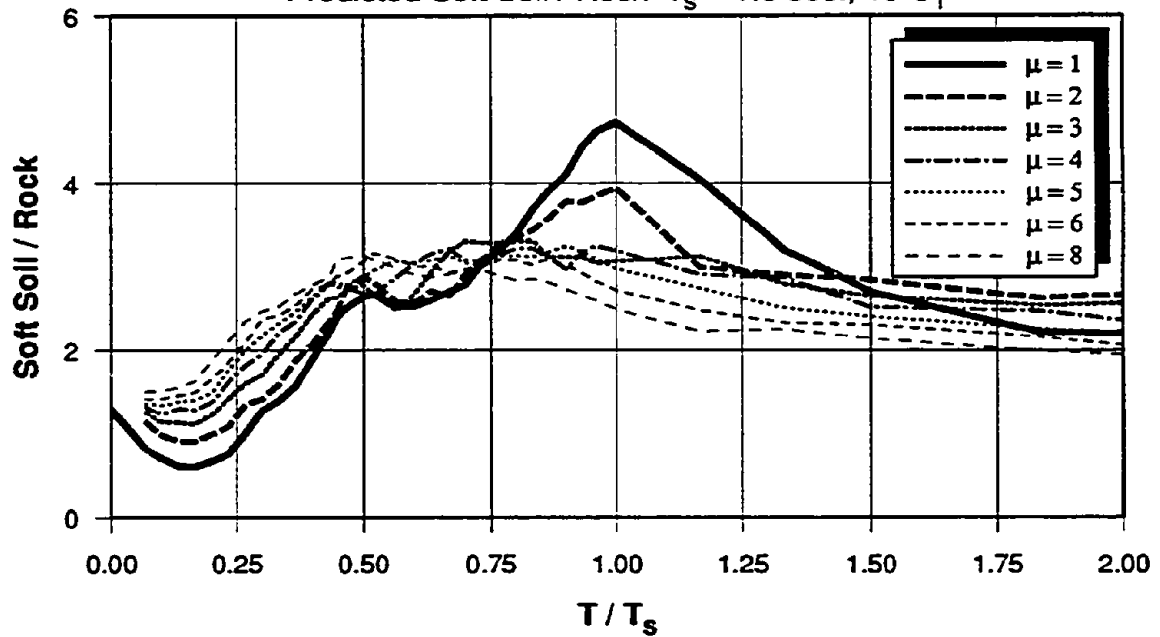
Predicted Soft Soil / Rock $T_s = 1.5$ sec., 10-Loma



(a) 10-Loma Record Set

AMPLIFICATION OF STRENGTH DEMANDS - MEAN

Predicted Soft Soil / Rock $T_s = 1.5$ sec., 15-S₁

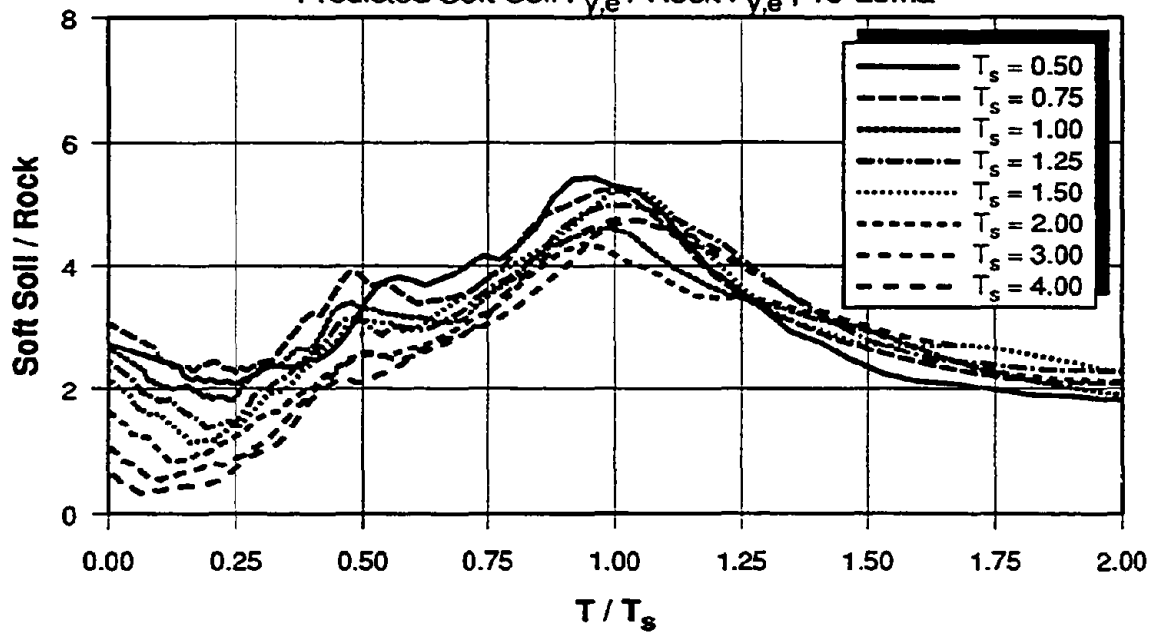


(b) 15-S₁ Record Set

Fig. 5.17 Amplification of Strength Demands for Predicted Soft Soil Motions - $T_s = 1.5$ (sec)

AMPLIFICATION OF ELASTIC STRENGTH DEMANDS - MEAN

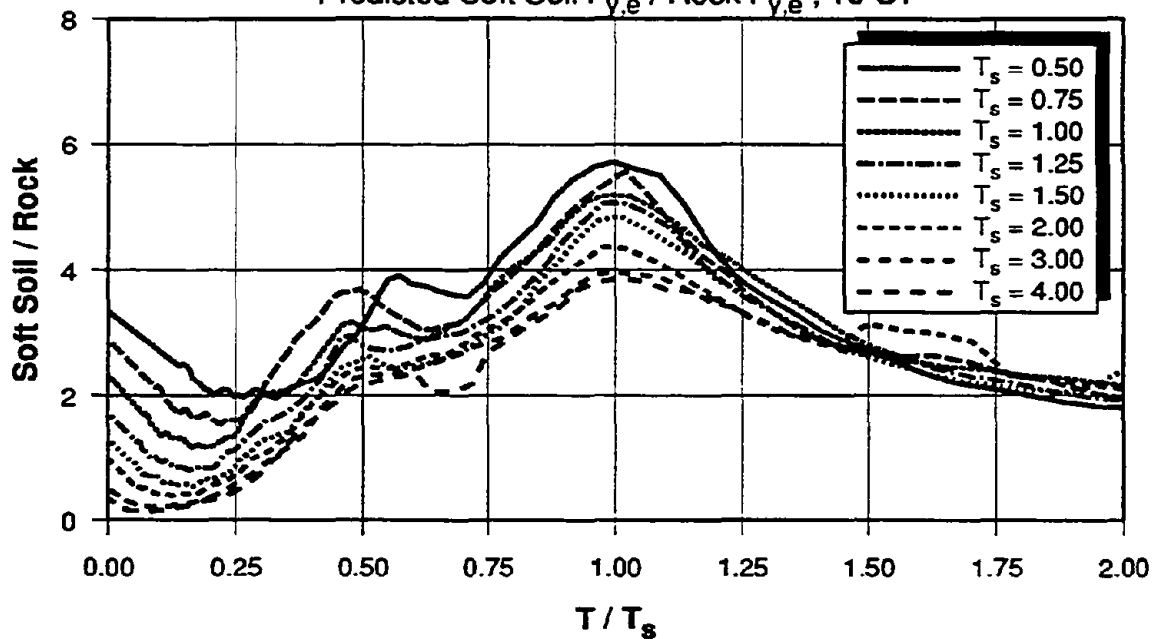
Predicted Soft Soil $F_{y,e}$ / Rock $F_{y,e}$, 10-Loma



(a) 10-Loma Record Set

AMPLIFICATION OF ELASTIC STRENGTH DEMANDS - MEAN

Predicted Soft Soil $F_{y,e}$ / Rock $F_{y,e}$, 15-S1

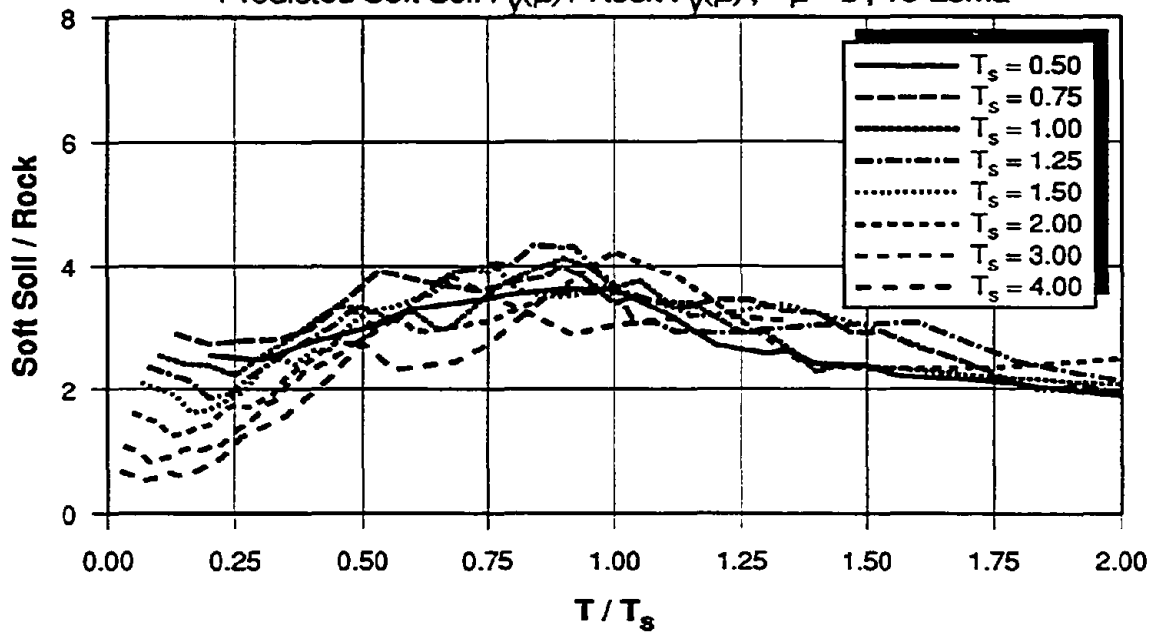


(b) 15-S₁ Record Set

Fig. 5.18 Amplification of Elastic Strength Demands Using 10-Loma and 15-S₁ Record Sets

AMPLIFICATION OF INELASTIC STRENGTH DEMANDS - MEAN

Predicted Soft Soil $F_y(\mu)$ / Rock $F_y(\mu)$, $\mu = 2$, 10-Loma



AMPLIFICATION OF INELASTIC STRENGTH DEMANDS - MEAN

Predicted Soft Soil $F_y(\mu)$ / Rock $F_y(\mu)$, $\mu = 2$, 15-S₁

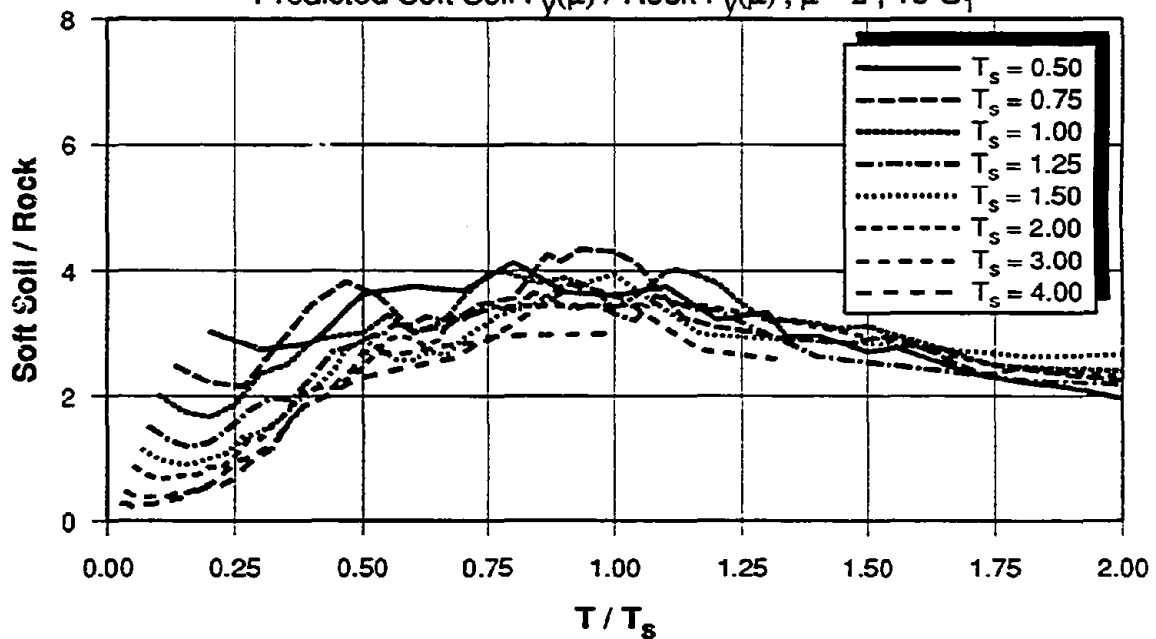
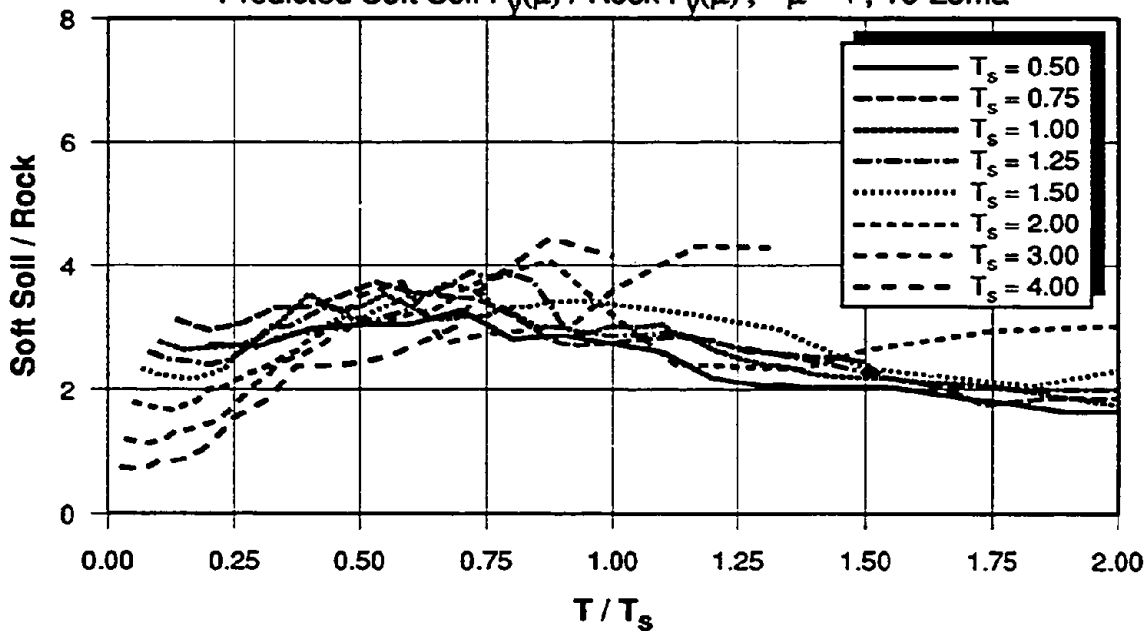


Fig. 5.19 Amplification of Inelastic Strength Demands Using 10-Loma and 15-S₁ Record Sets, $\mu = 2$

AMPLIFICATION OF INELASTIC STRENGTH DEMANDS - MEAN

Predicted Soft Soil $F_y(\mu)$ / Rock $F_y(\mu)$, $\mu = 4$, 10-Loma



AMPLIFICATION OF INELASTIC STRENGTH DEMANDS - MEAN

Predicted Soft Soil $F_y(\mu)$ / Rock $F_y(\mu)$, $\mu = 4$, 15-S₁

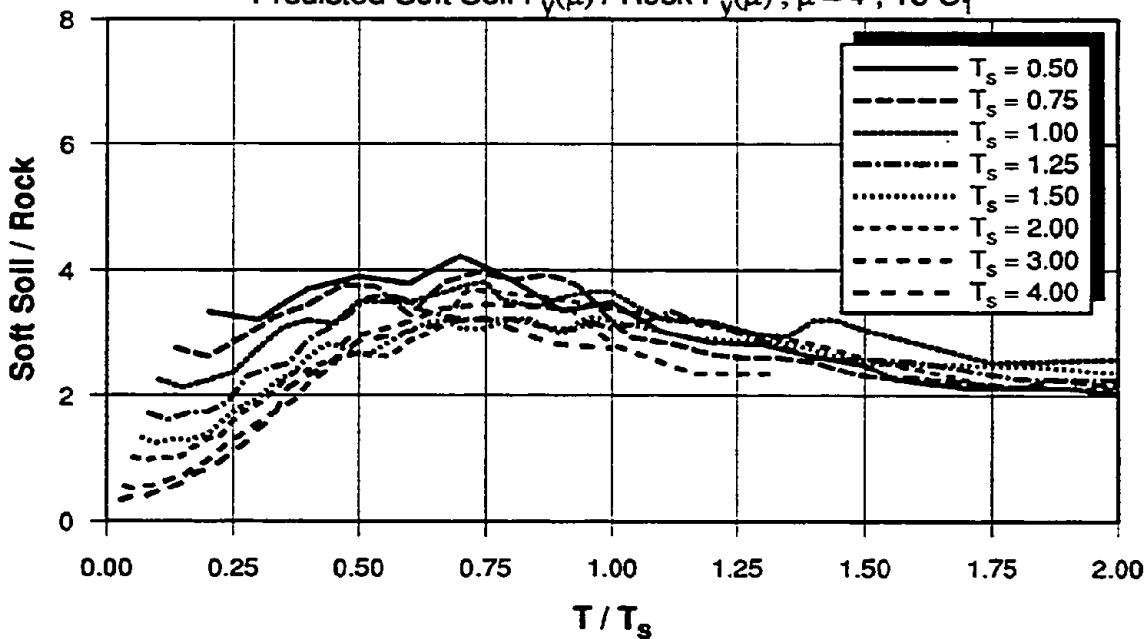
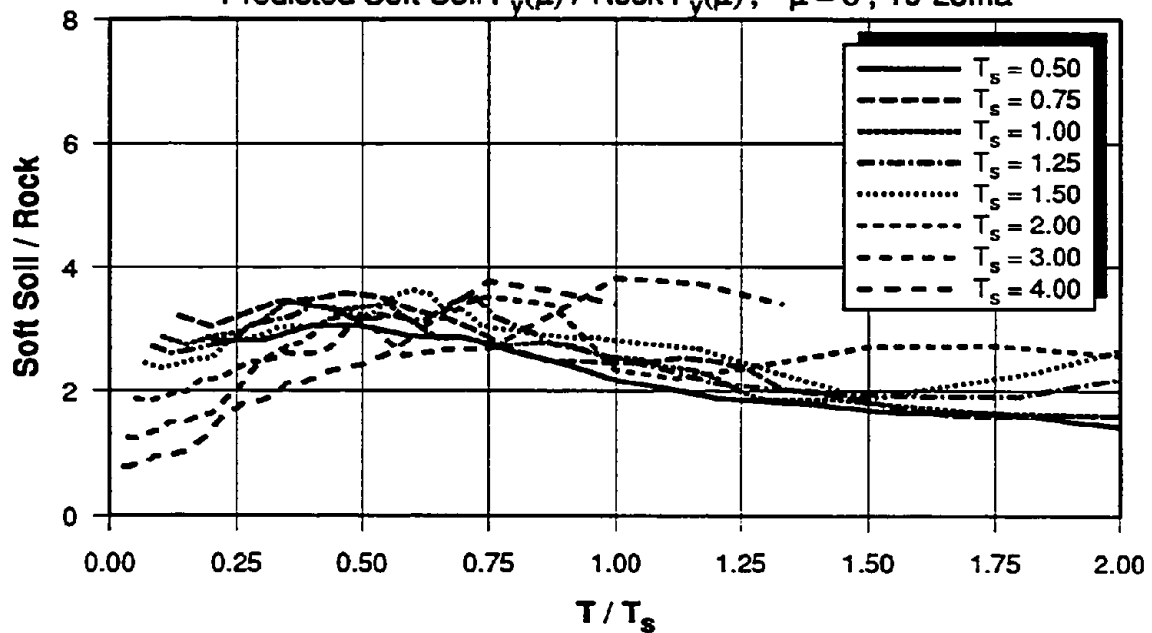


Fig. 5.20 Amplification of Inelastic Strength Demands Using 10-Loma and 15-S₁ Record Sets, $\mu = 4$

AMPLIFICATION OF INELASTIC STRENGTH DEMANDS - MEAN

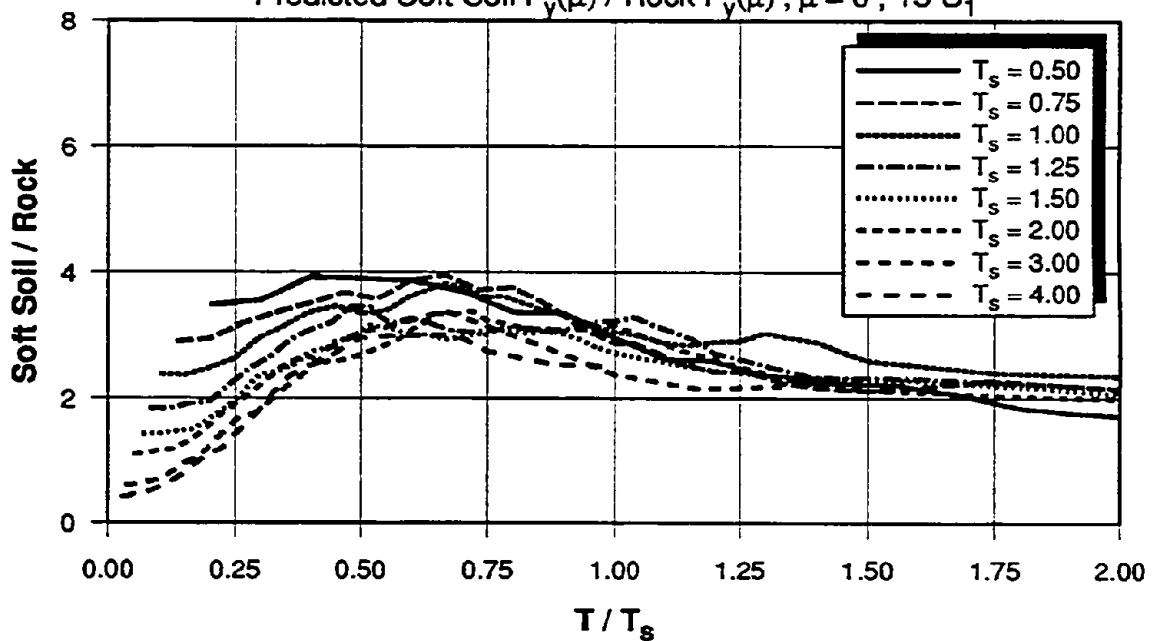
Predicted Soft Soil $F_y(\mu)$ / Rock $F_y(\mu)$, $\mu = 6$, 10-Loma



(a) 10-Loma Record Set

AMPLIFICATION OF INELASTIC STRENGTH DEMANDS - MEAN

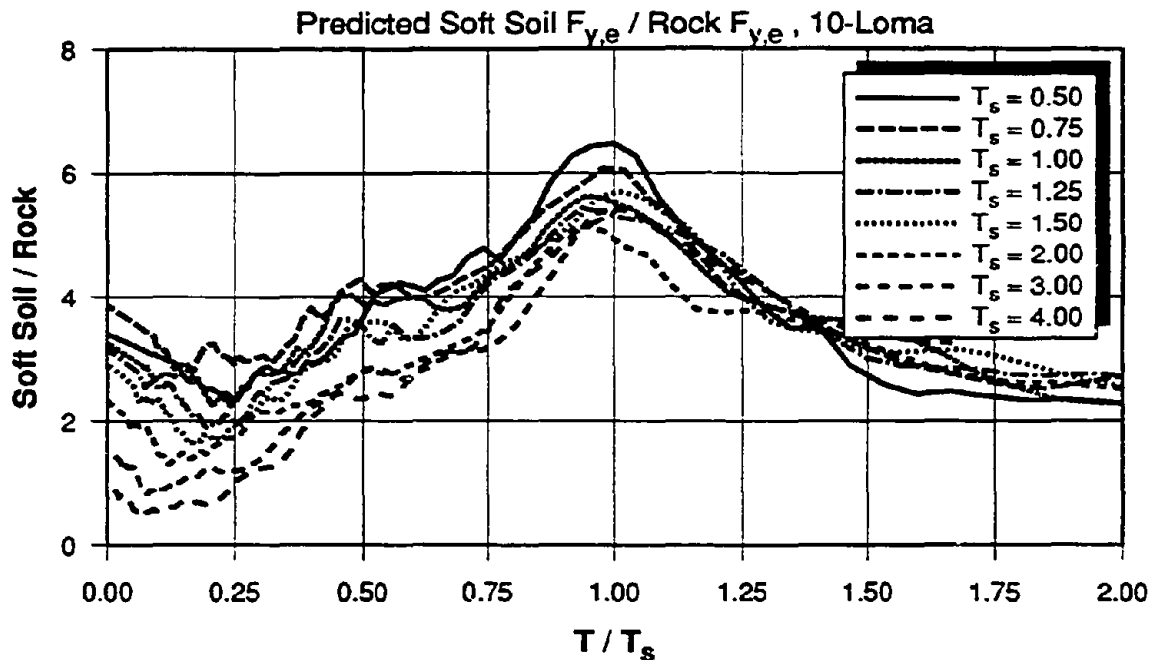
Predicted Soft Soil $F_y(\mu)$ / Rock $F_y(\mu)$, $\mu = 6$, 15-S₁



(b) 15-S₁ Record Set

Fig. 5.21 Amplification of Inelastic Strength Demands Using 10-Loma and 15-S₁ Record Sets, $\mu = 6$

AMPLIFICATION OF ELASTIC STRENGTH DEMANDS - MEAN + σ



AMPLIFICATION OF ELASTIC STRENGTH DEMANDS - MEAN + σ

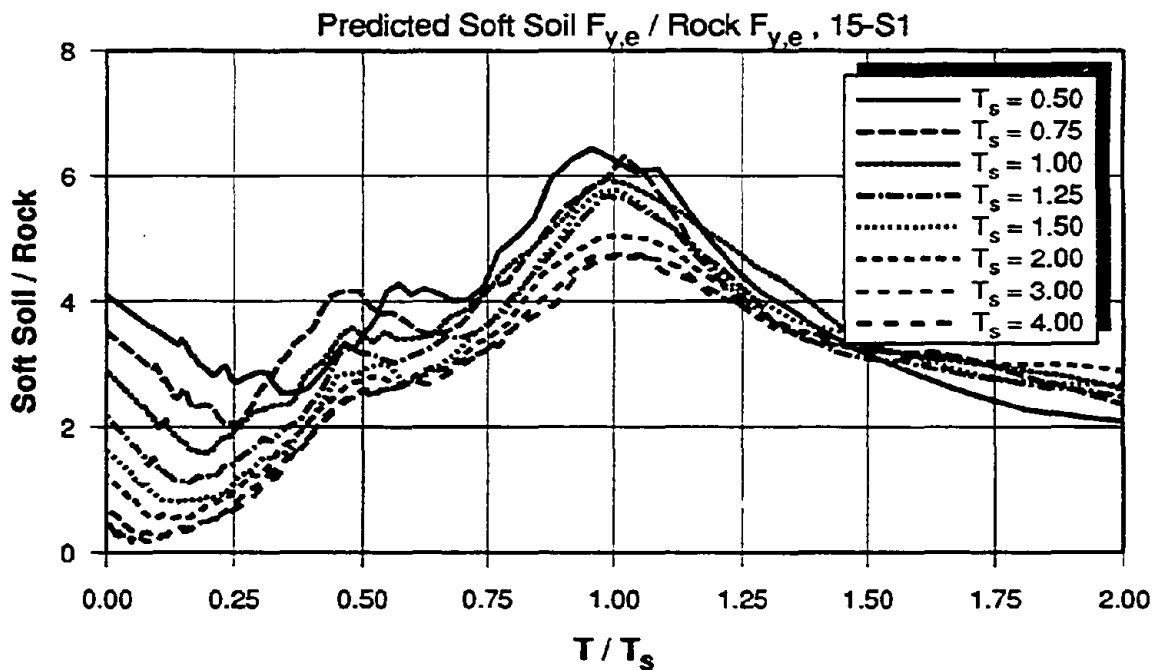
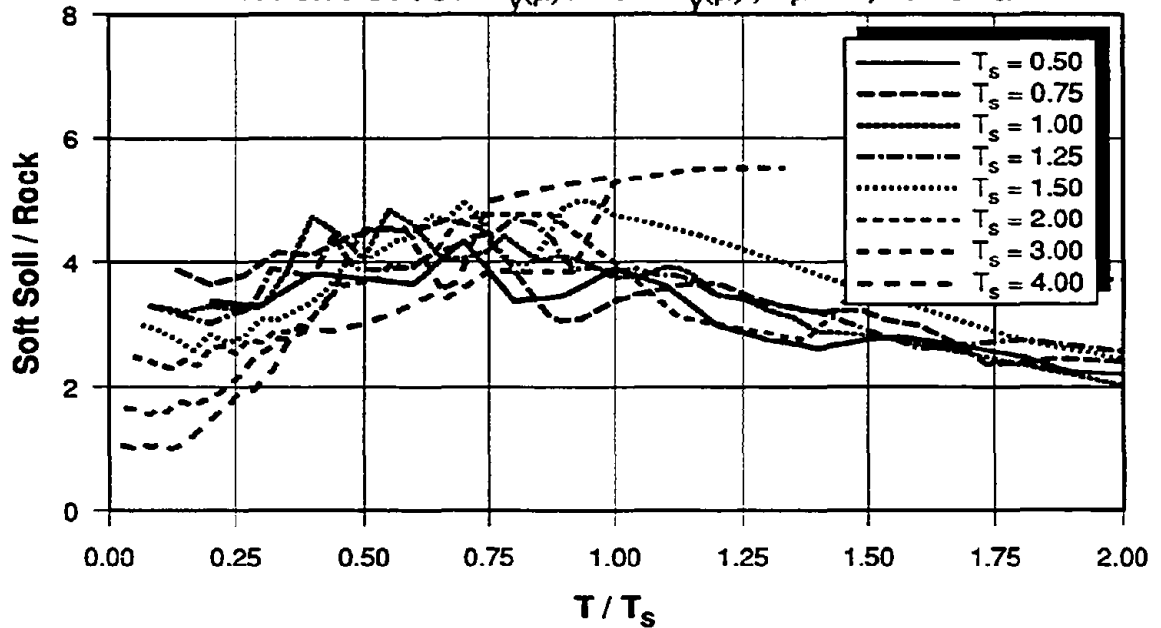


Fig. 5.22 Amplification of Elastic Strength Demands Using 10-Loma and 15-S₁ Record Sets, Mean + σ

AMPLIFICATION OF INELASTIC STRENGTH DEMANDS - MEAN + σ

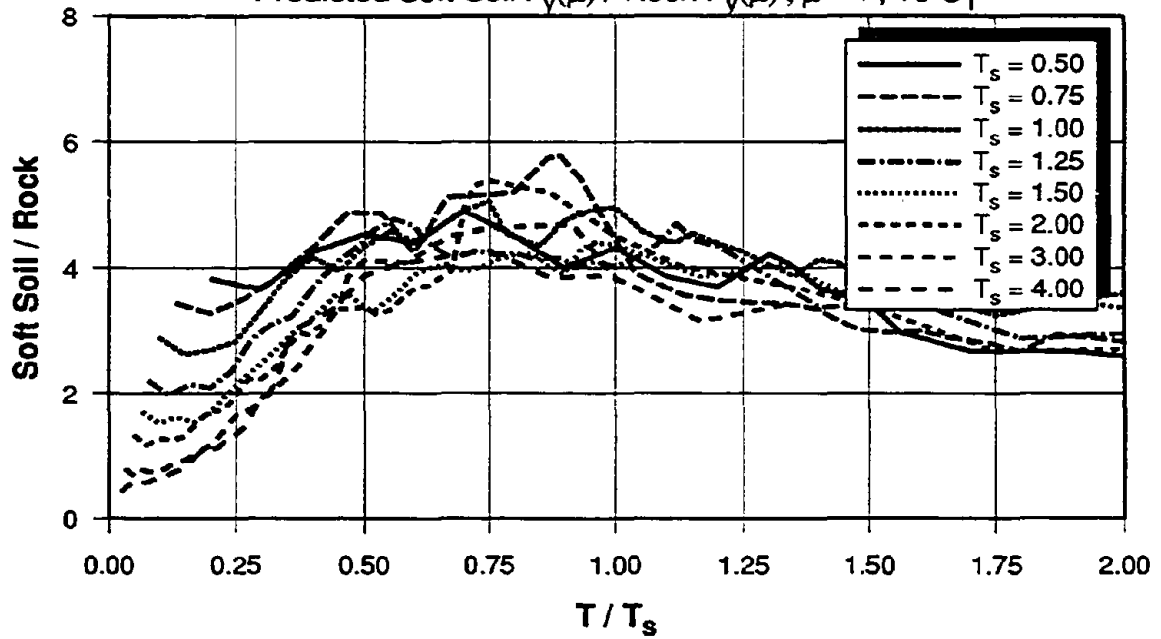
Predicted Soft Soil $F_v(\mu)$ / Rock $F_v(\mu)$, $\mu = 4$, 10-Loma



(a) 10-Loma Record Set

AMPLIFICATION OF INELASTIC STRENGTH DEMANDS - MEAN + σ

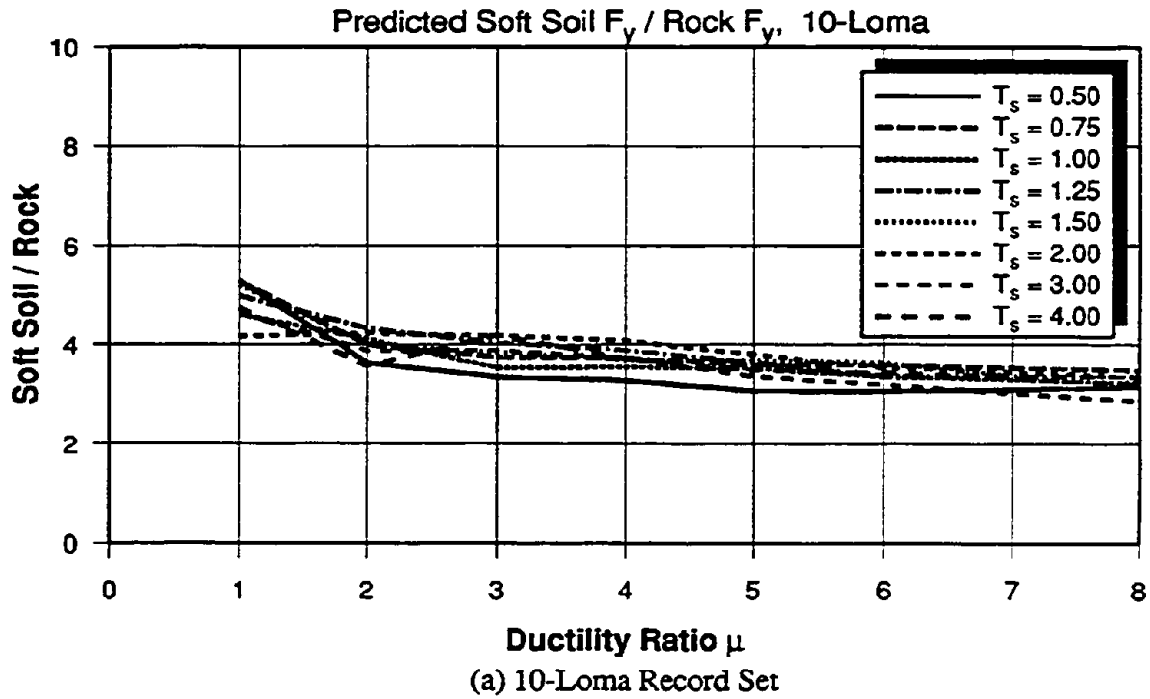
Predicted Soft Soil $F_v(\mu)$ / Rock $F_v(\mu)$, $\mu = 4$, 15-S₁



(b) 15-S₁ Record Set

Fig. 5.23 Amplification of Inelastic Strength Demands Using 10-Loma and 15-S₁ Record Sets, Mean + σ

EFFECT OF μ ON MAX. AMPLIFICATION OF STRENGTH DEMANDS



EFFECT OF μ ON MAX. AMPLIFICATION OF STRENGTH DEMANDS

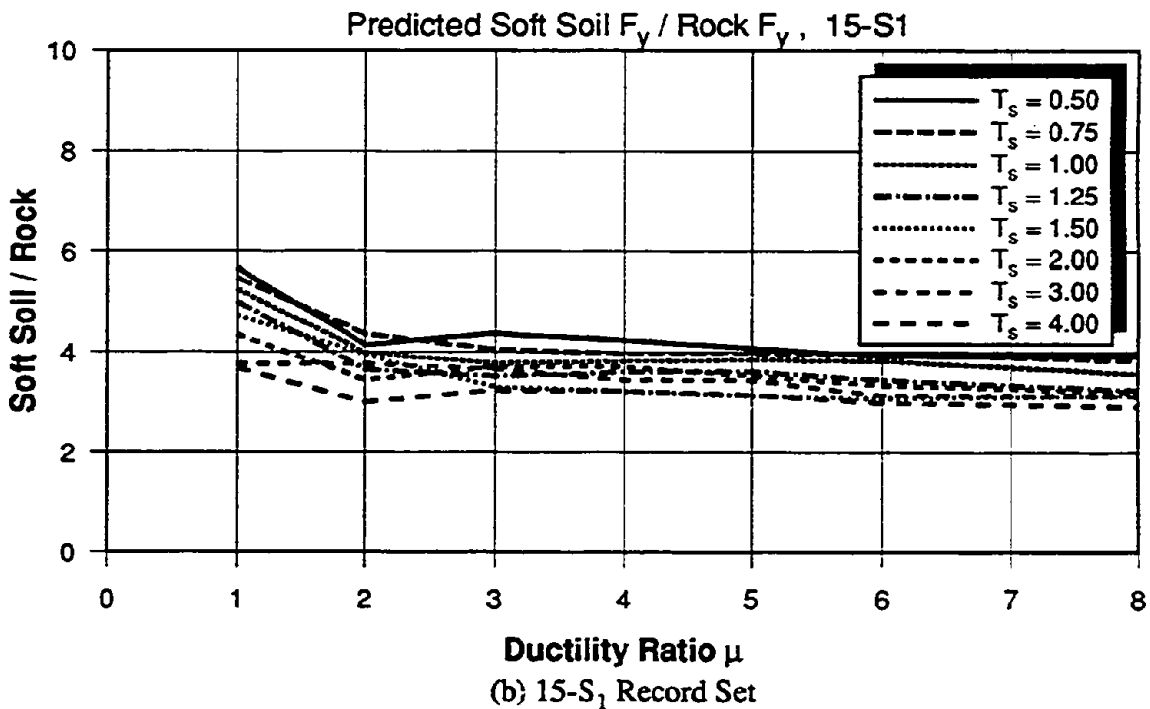


Fig 5.24 Effect of Ductility on Maximum Amplification of Strength Demands, Mean

MAX. AMPLIFICATION OF ELASTIC STRENGTH DEMANDS - MEAN

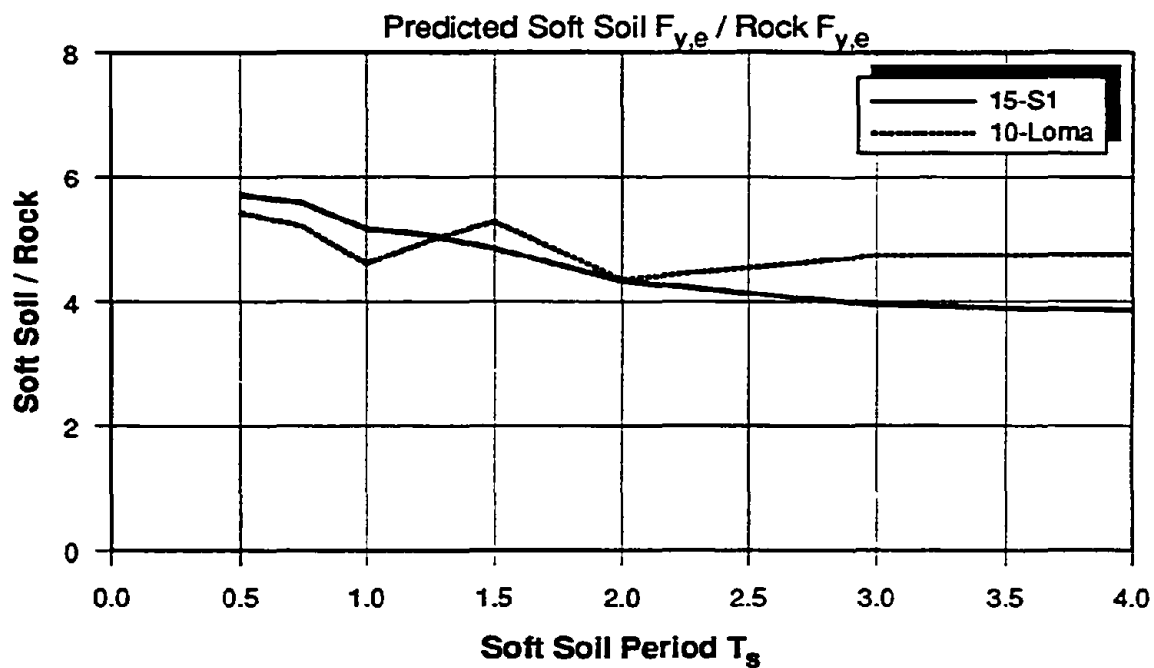
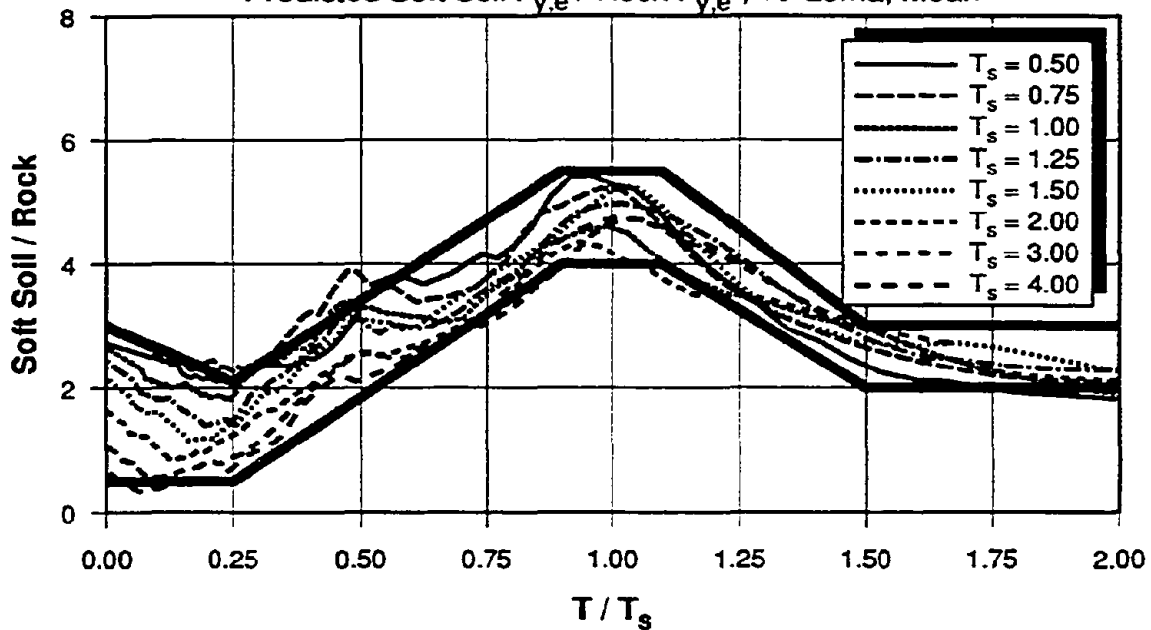


Fig. 5.25 Variation of Maximum Amplification of Elastic Strength Demand with T_s

ENVELOPE FOR ELASTIC SOIL MODIFICATION FUNCTION

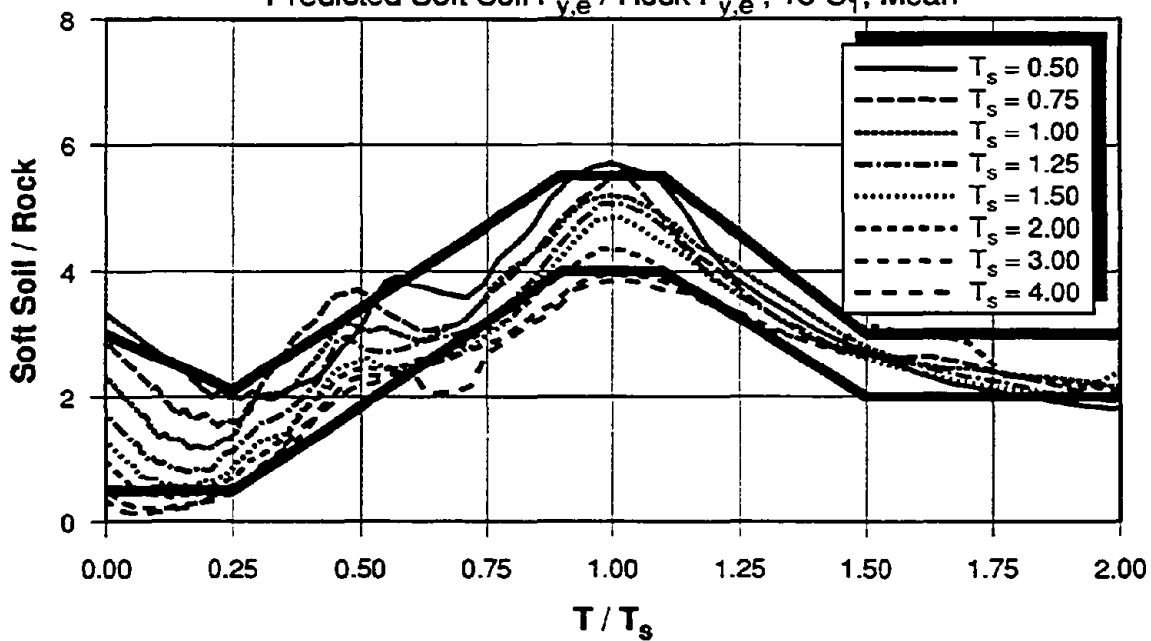
Predicted Soft Soil $F_{y,e}$ / Rock $F_{y,e}$, 10-Loma, Mean



(a) 10-Loma Record Set

ENVELOPE FOR ELASTIC SOIL MODIFICATION FUNCTION

Predicted Soft Soil $F_{y,e}$ / Rock $F_{y,e}$, 15-S₁, Mean

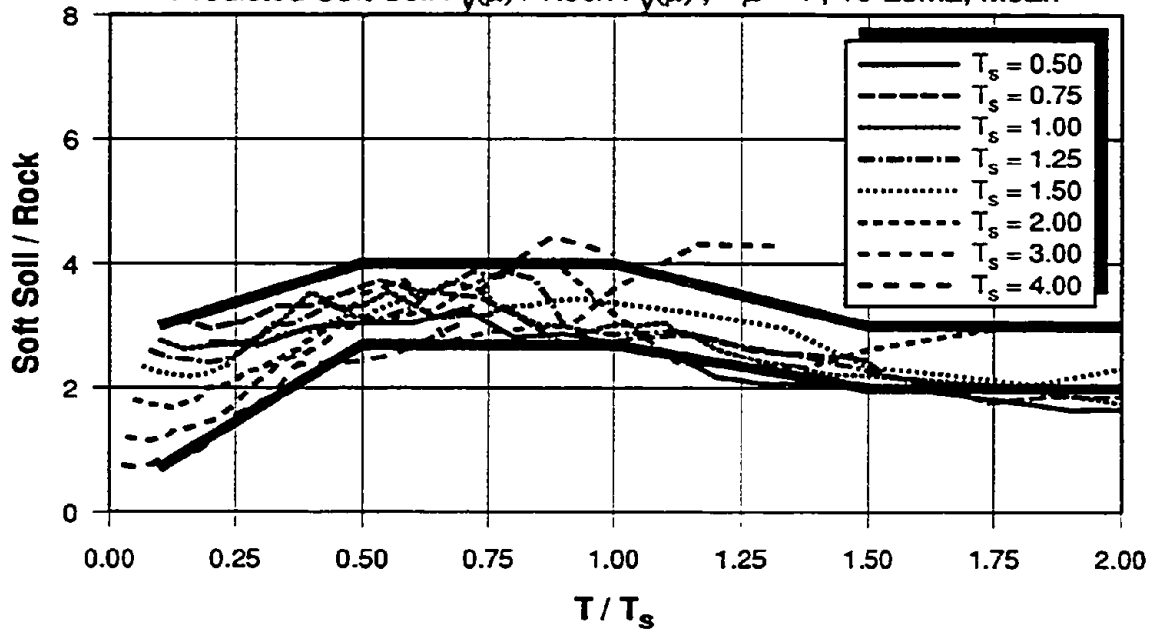


(b) 15-S₁ Record Set

Fig. 5.26 Envelope for Elastic Soil Modification Function Using 10-Loma and 15-S₁ Record Sets

ENVELOPE FOR INELASTIC SOIL MODIFICATION FUNCTION

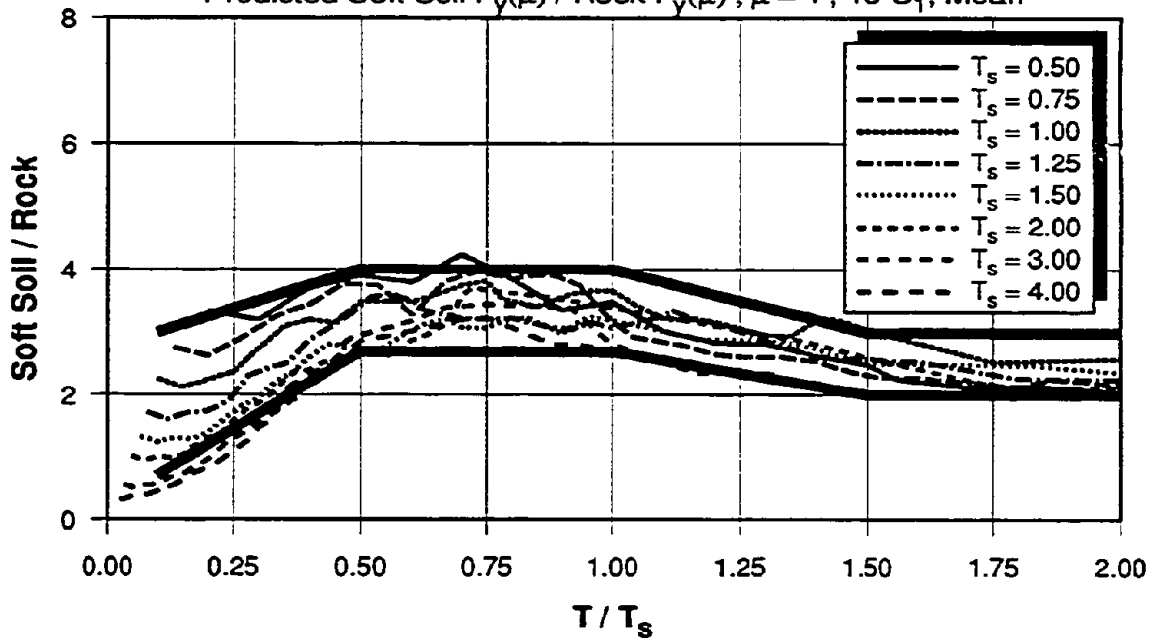
Predicted Soft Soil $F_v(\mu)$ / Rock $F_v(\mu)$, $\mu = 4$, 10-Loma, Mean



(a) 10-Loma Record Set

ENVELOPE FOR INELASTIC SOIL MODIFICATION FUNCTION

Predicted Soft Soil $F_v(\mu)$ / Rock $F_v(\mu)$, $\mu = 4$, 15-S₁, Mean

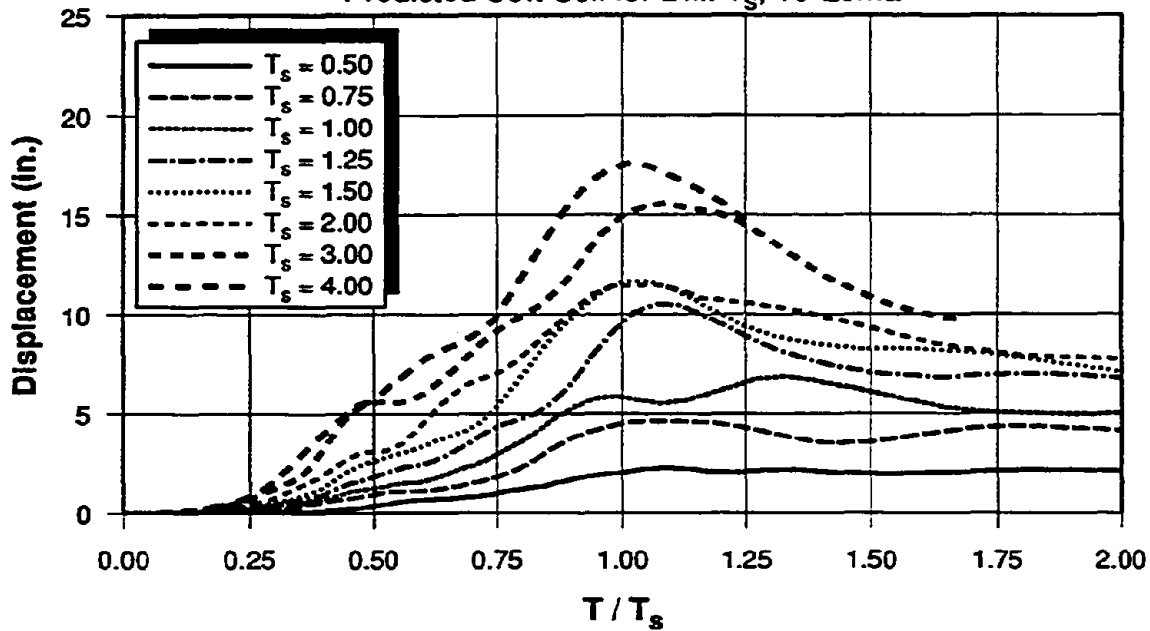


(b) 15-S₁ Record Set

Fig. 5.27 Envelope for Inelastic Soil Modification Function for $\mu = 4$ Using 10-Loma and 15-S₁ Record Sets

MEAN ELASTIC DISPLACEMENT DEMAND SPECTRA

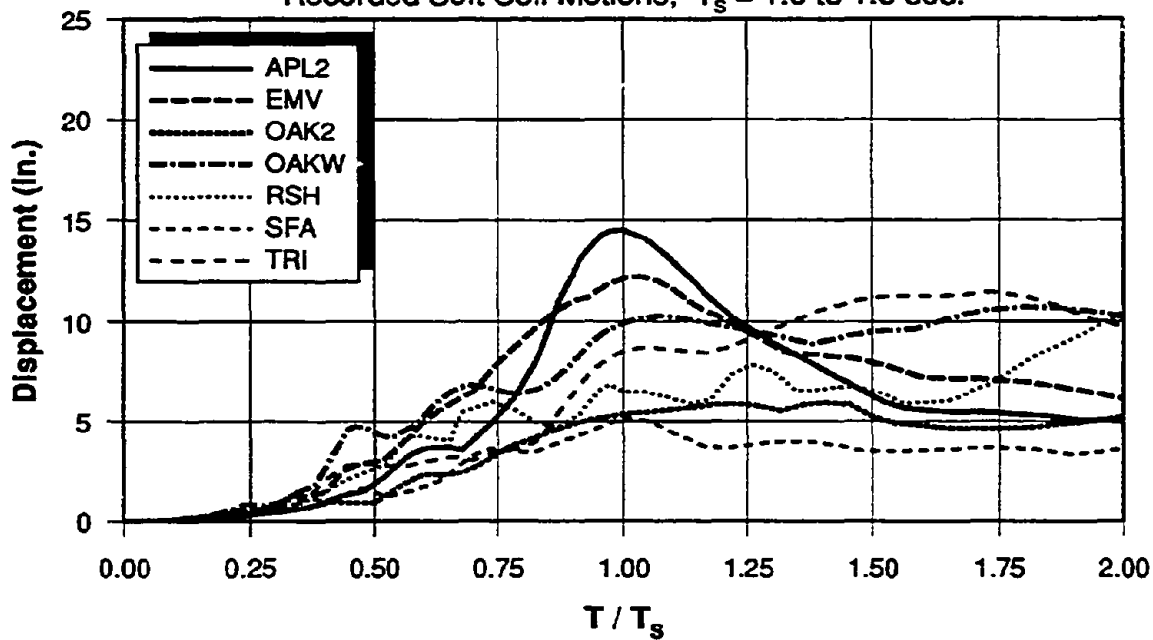
Predicted Soft Soil for Diff. T_s , 10-Loma



(a) Predicted Soft Soil Motions

SITE SPECIFIC ELASTIC DISPLACEMENT DEMAND SPECTRA

Recorded Soft Soil Motions, $T_s = 1.0$ to 1.5 sec.

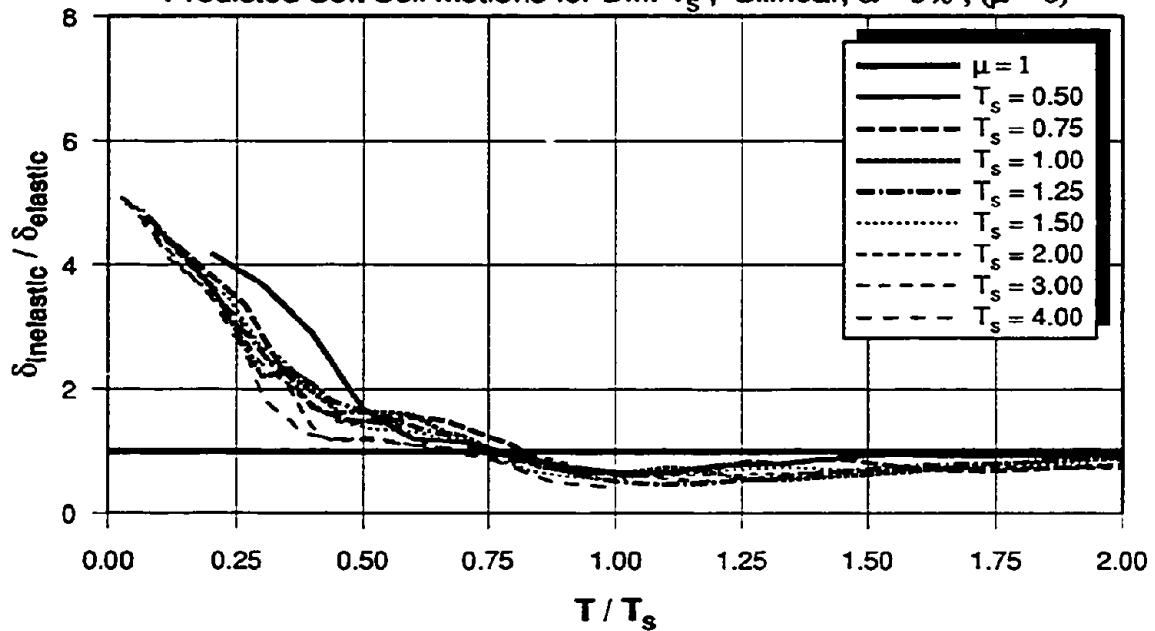


(b) Recorded Soft Soil Motions

Fig. 5.28 Elastic Displacement Demands - Recorded and Predicted Soft Soil Motions

NORMALIZED INELASTIC DISPLACEMENT DEMANDS

Predicted Soft Soil Motions for Diff. T_s , Bilinear, $\alpha = 5\%$, ($\mu = 6$)



NORMALIZED INELASTIC DISPLACEMENT DEMANDS

Recorded Soft Soil Motions, $T_s = 1.0$ to 1.5 , Bilinear, $\alpha = 5\%$, ($\mu = 6$)

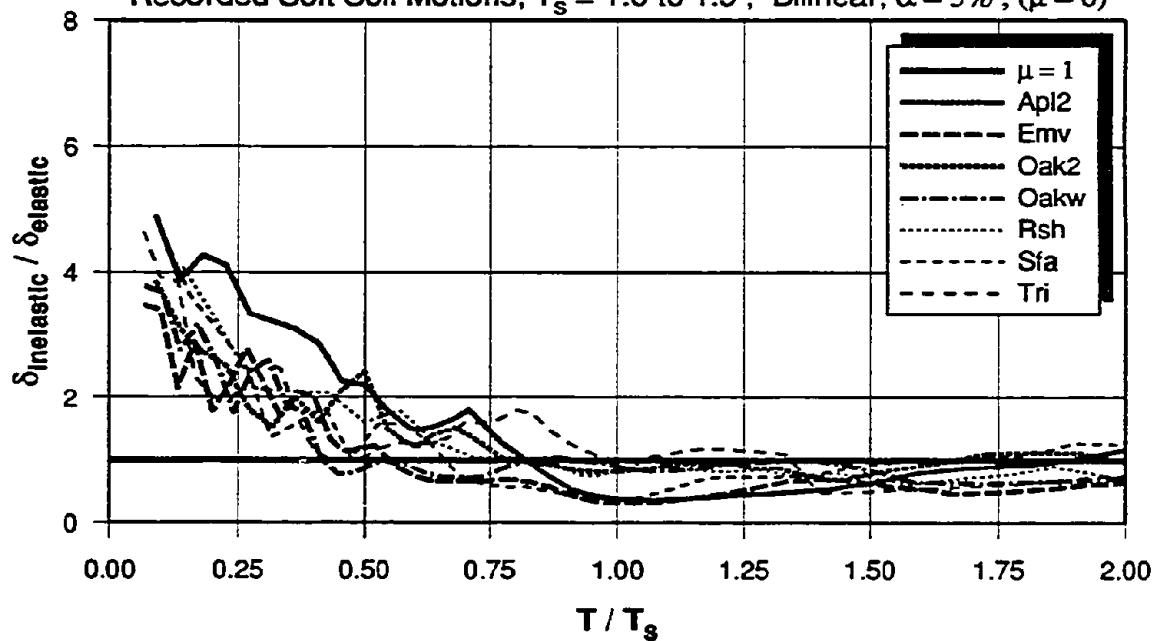
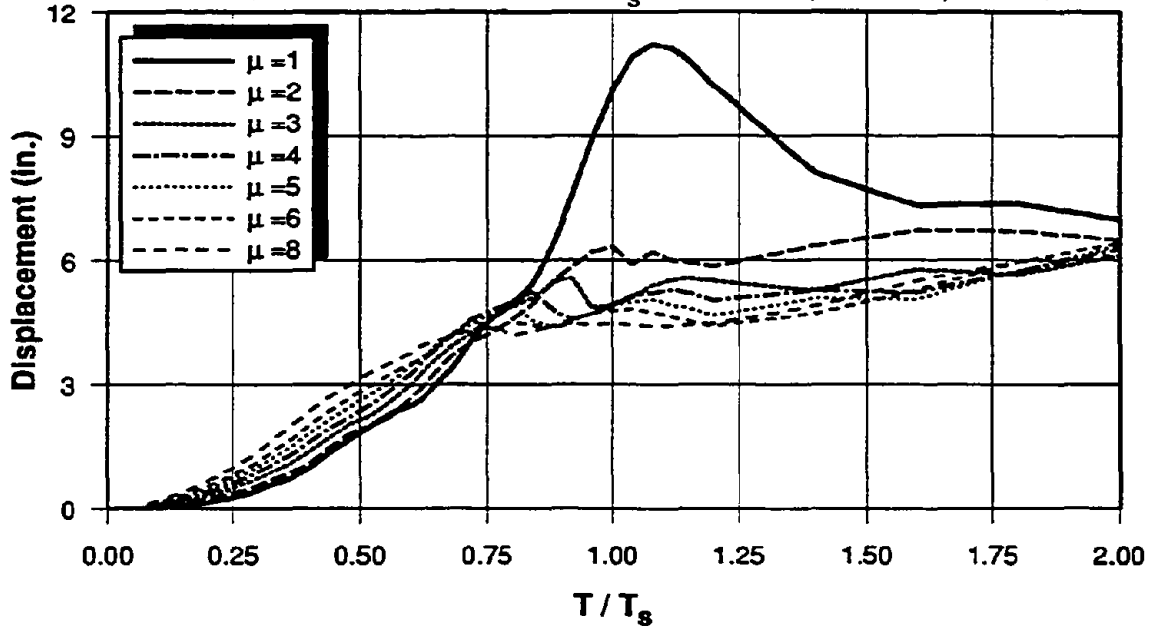


Fig. 5.29 Normalized Inelastic Displacement Demands for $\mu = 6$, Recorded and Predicted Soft Soil Motions

MEAN DISPLACEMENT DEMAND SPECTRA

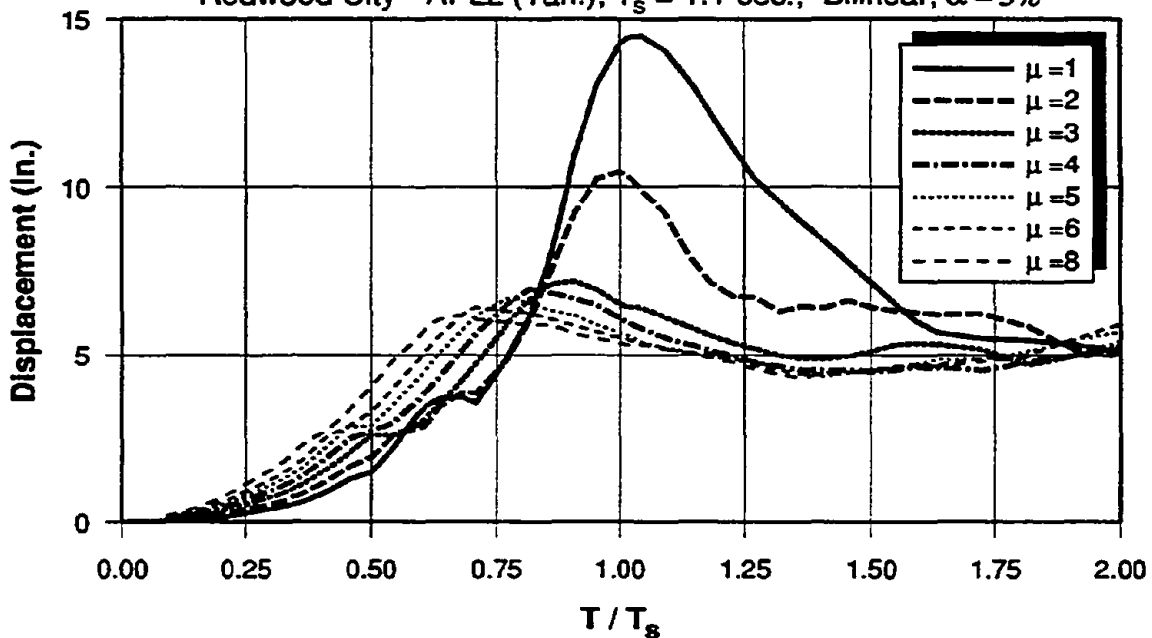
Predicted Soft Soil Motions for $T_s = 1.25$ sec., Bilinear, $\alpha = 5\%$



(a) Predicted Soft Soil Motions, $T_s = 1.25$ sec.

SITE SPECIFIC DISPLACEMENT DEMAND SPECTRA

Redwood City - APL2 (Tan.), $T_s = 1.1$ sec., Bilinear, $\alpha = 5\%$

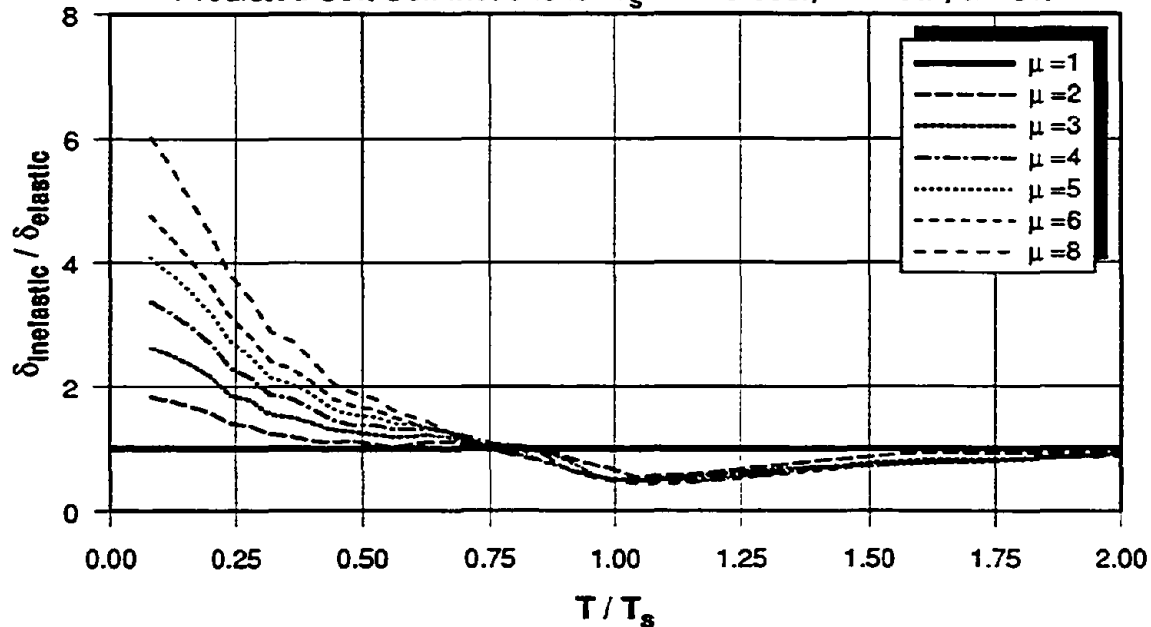


(b) Recorded Soft Soil Motion (APL2)

Fig. 5.30 Elastic and Inelastic Displacement Demands - Recorded and Predicted Soft Soil Motions

NORMALIZED INELASTIC DISPLACEMENT DEMANDS

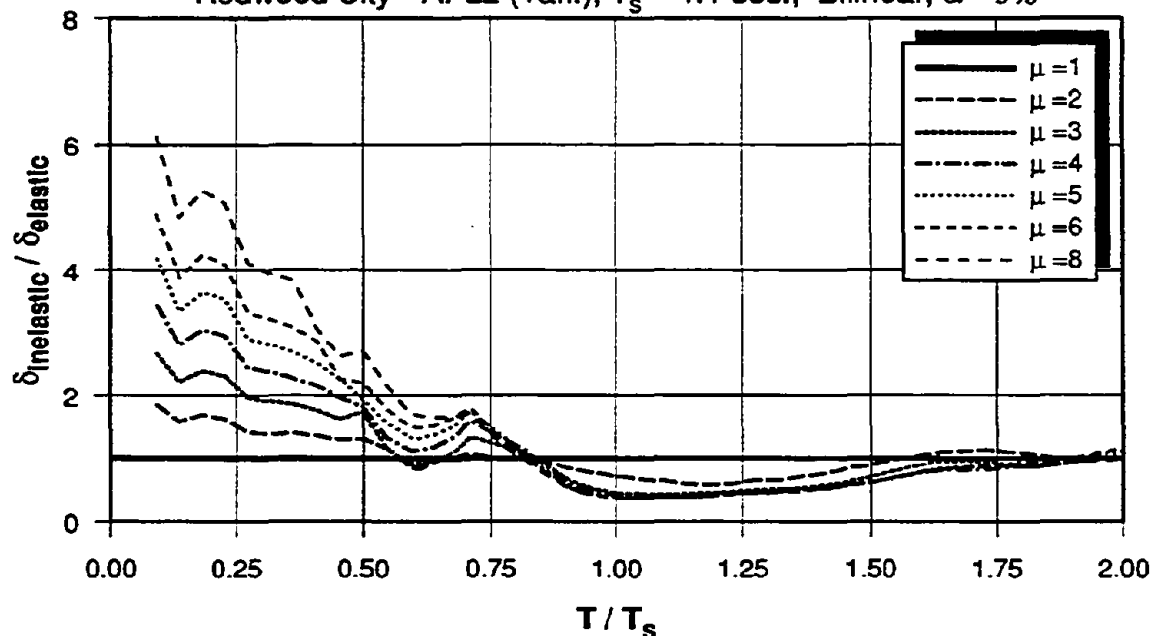
Predicted Soft Soil Motions for $T_s = 1.25$ sec., Bilinear, $\alpha = 5\%$



(a) Predicted Soft Soil Motions, $T_s = 1.25$ sec.

SITE SPECIFIC NORMALIZED INELASTIC DISPLACEMENT DEMANDS

Redwood City - APL2 (Tan.), $T_s = 1.1$ sec., Bilinear, $\alpha = 5\%$

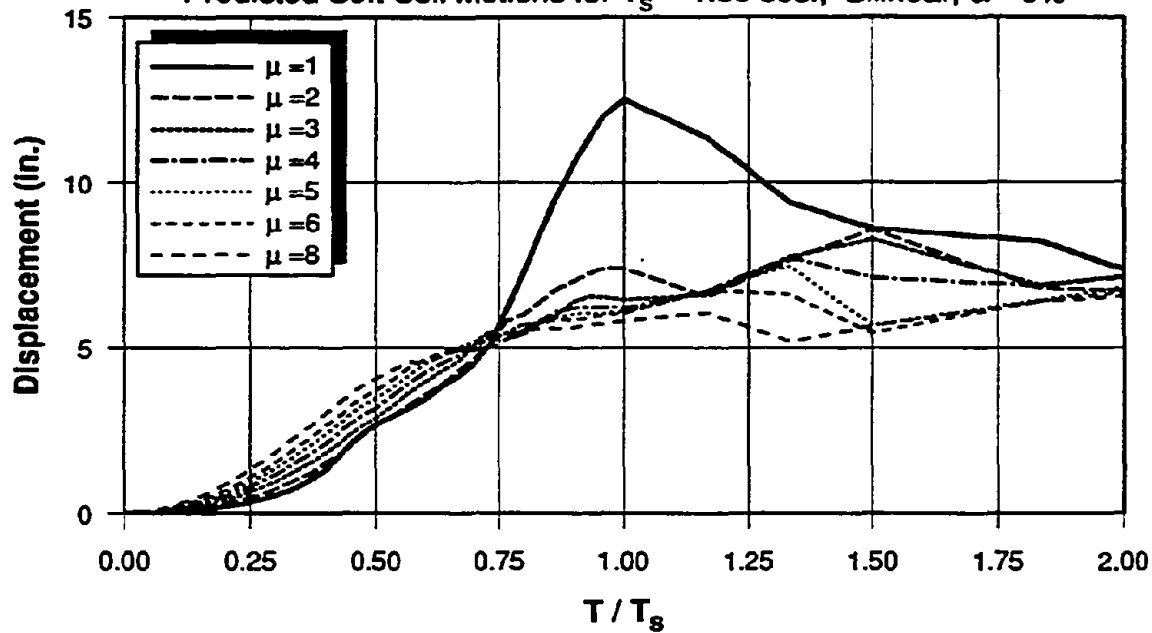


(b) Recorded Soft Soil Motion (APL2)

Fig. 5.31 Normalized Inelastic Displacement Demands - Recorded and Predicted Soft Soil Motions

MEAN DISPLACEMENT DEMAND SPECTRA

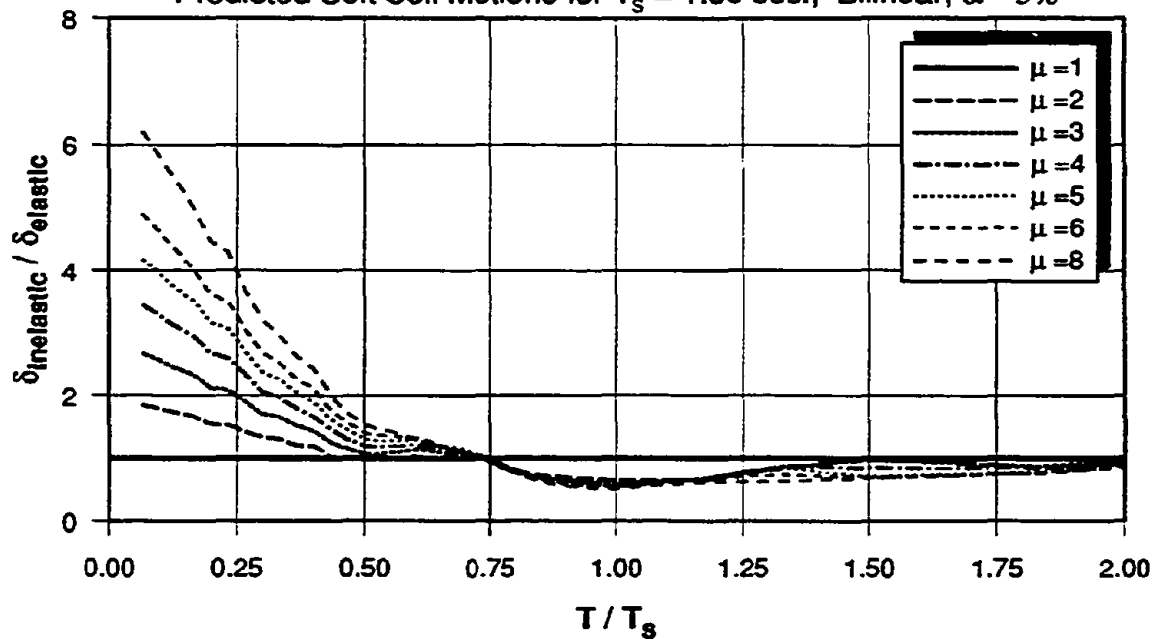
Predicted Soft Soil Motions for $T_s = 1.50$ sec., Bilinear, $\alpha = 5\%$



(a) Elastic and Inelastic Displacement Demand Spectra

NORMALIZED INELASTIC DISPLACEMENT DEMANDS

Predicted Soft Soil Motions for $T_s = 1.50$ sec., Bilinear, $\alpha = 5\%$

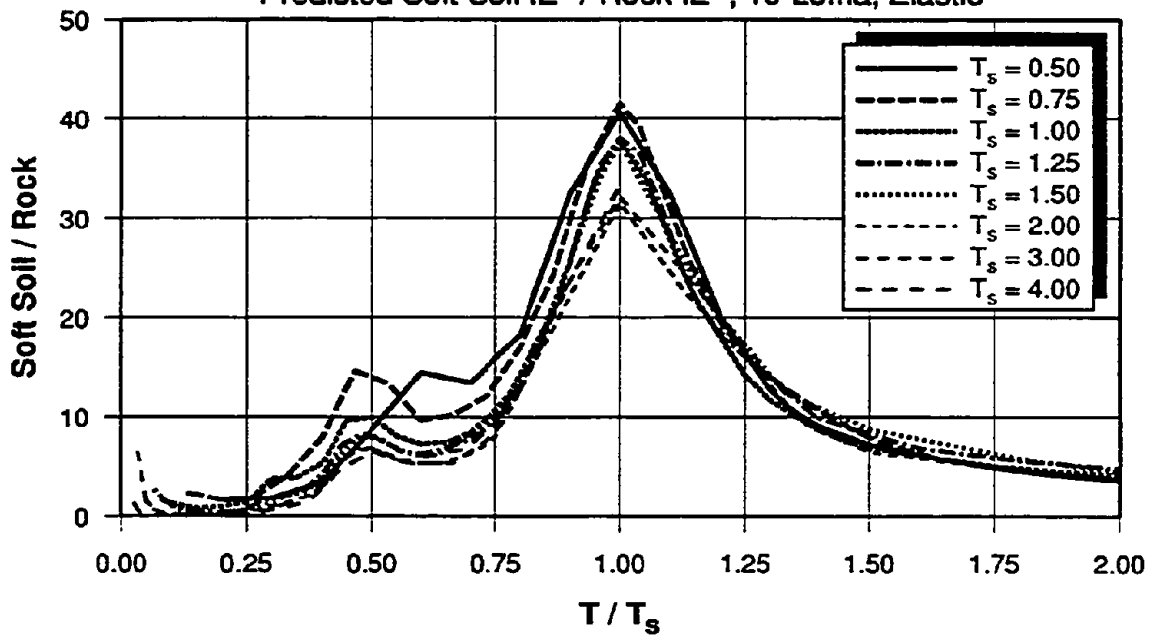


(b) Normalized Inelastic Displacement Demands

Fig. 5.32 Elastic and Inelastic Displacement Demands - Predicted Soft Soil Motions, $T_s = 1.5$ sec.

AMPLIFICATION OF INPUT ENERGY - MEAN

Predicted Soft Soil IE^S / Rock IE^R , 10-Loma, Elastic



AMPLIFICATION OF INPUT ENERGY

Recorded Soft Soil A_{pl2} / Recorded Rock W_{od} , IE^S / IE^R

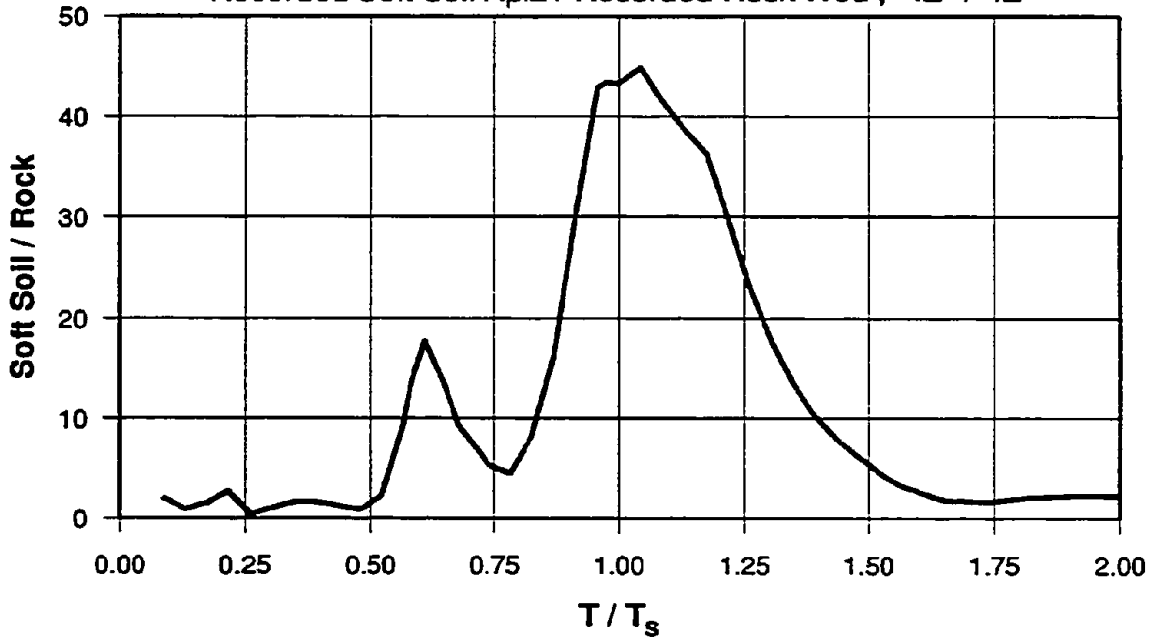
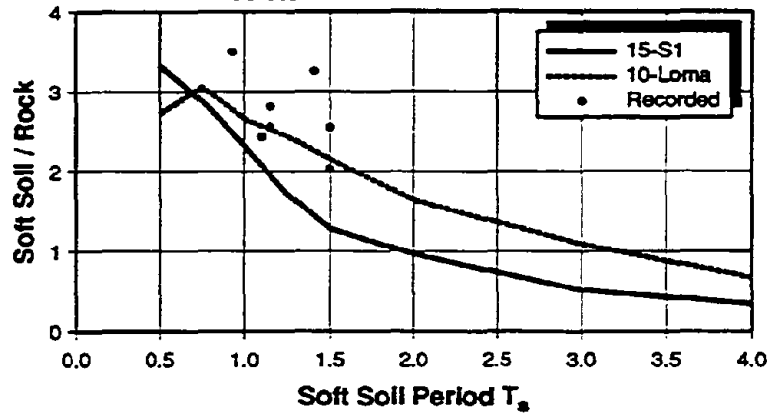


Fig. 5.33 Amplification of Input Energy - Recorded and Predicted Soft Soil Motions

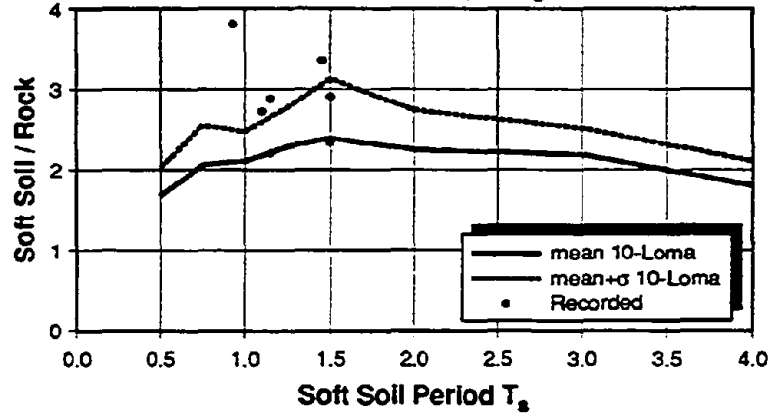
AMPLIFICATION OF PGA - MEAN
 Predicted Soft Soil PGA / Rock PGA



(a) Amplification of Peak Ground Acceleration

AMPLIFICATION OF PGV

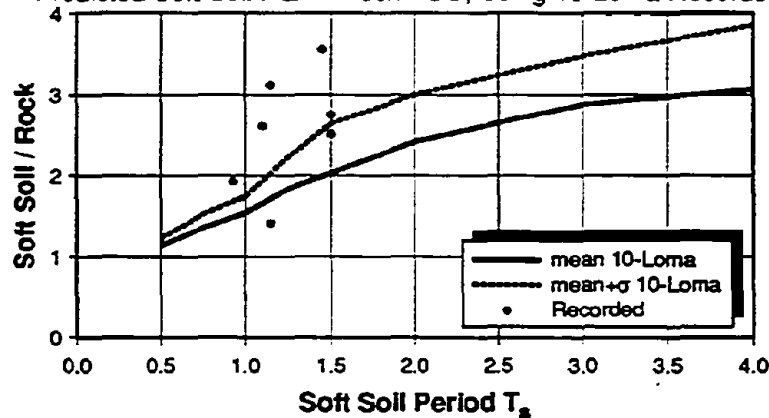
Predicted Soft Soil PGV / Rock PGV, Using 10-Loma Records



(b) Amplification of Peak Ground Velocity

AMPLIFICATION OF PGD

Predicted Soft Soil PGD / Rock PGD, Using 10-Loma Records



(c) Amplification of Peak Ground Displacement

Fig. 5.34 Amplification of PGA, PGV, and PGD

IDEALIZATION OF ASSUMED SOIL PROFILE

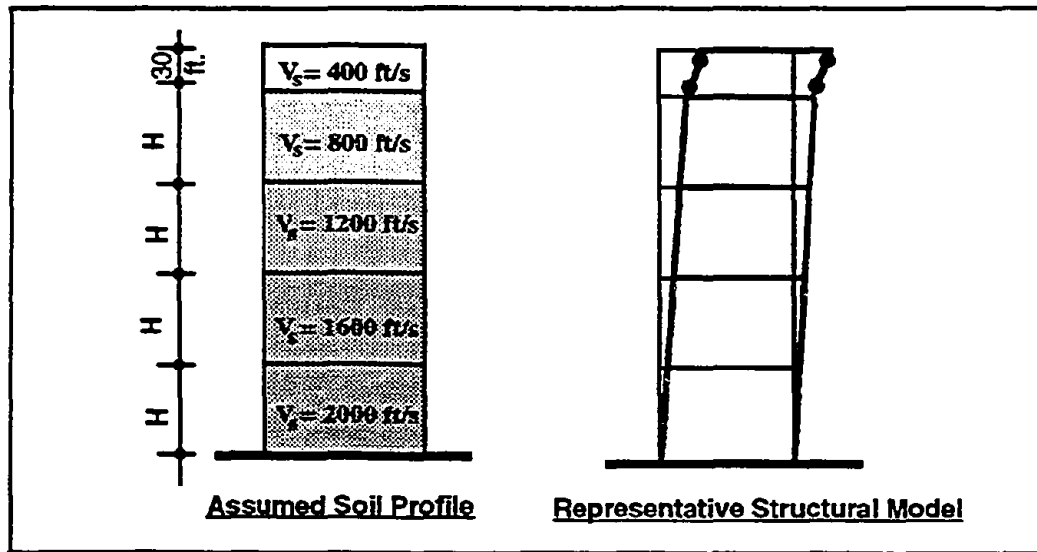


Fig. 5.35 Idealization Adopted for Nonlinear Ground Response Analysis

HYPERBOLIC STRESS-STRAIN RELATION

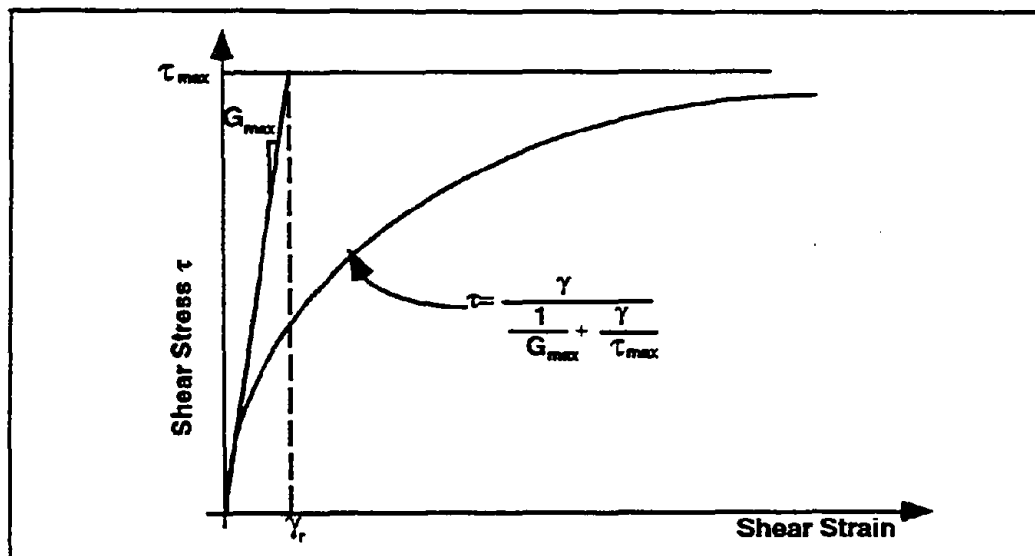
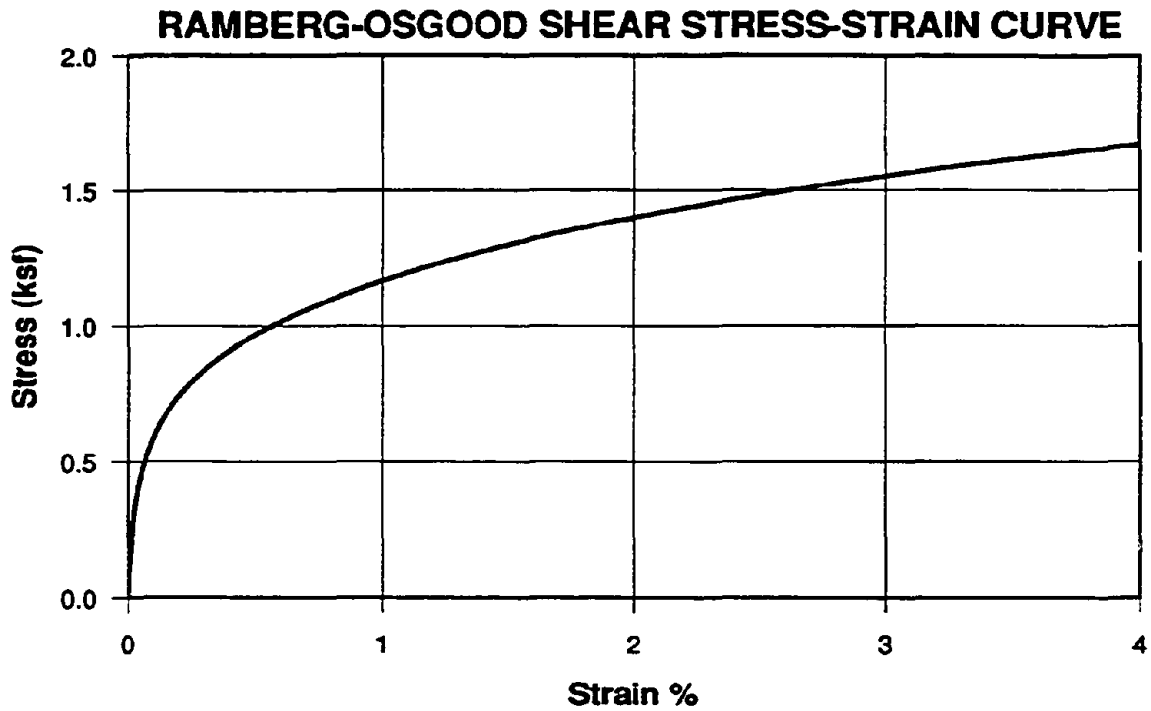
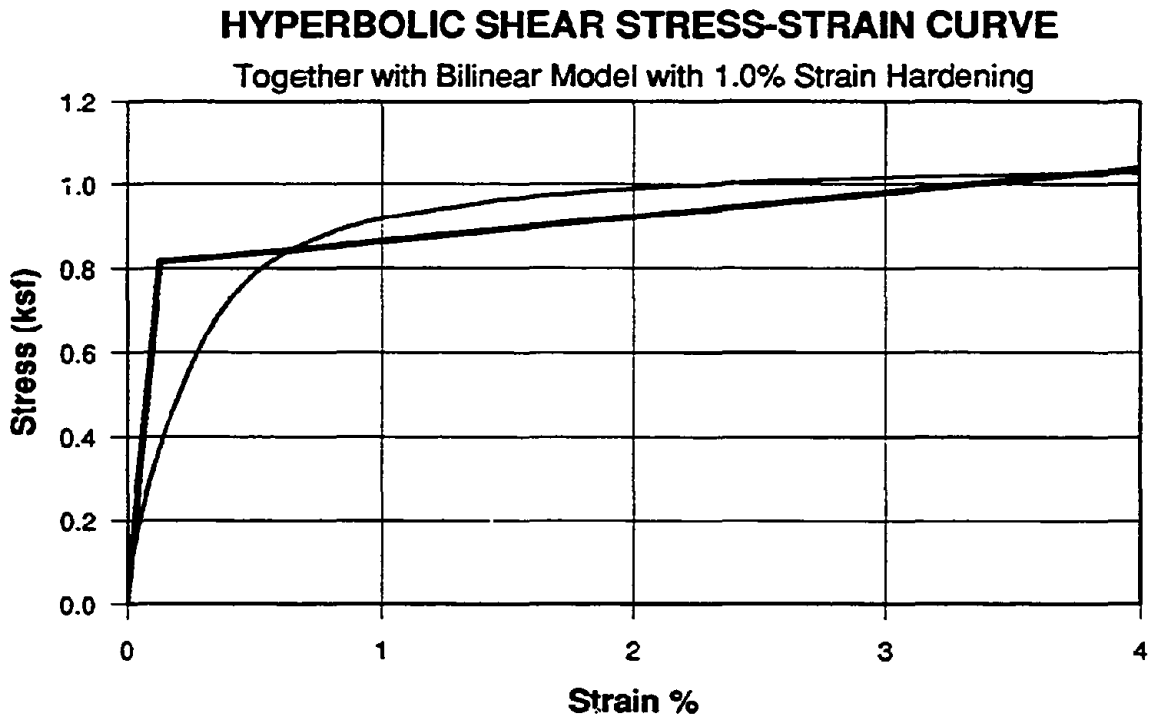


Fig. 5.36 Hyperbolic Stress Strain Relation (Hardin and Drnevich 1972)



(a) Ramberg-Osgood Model

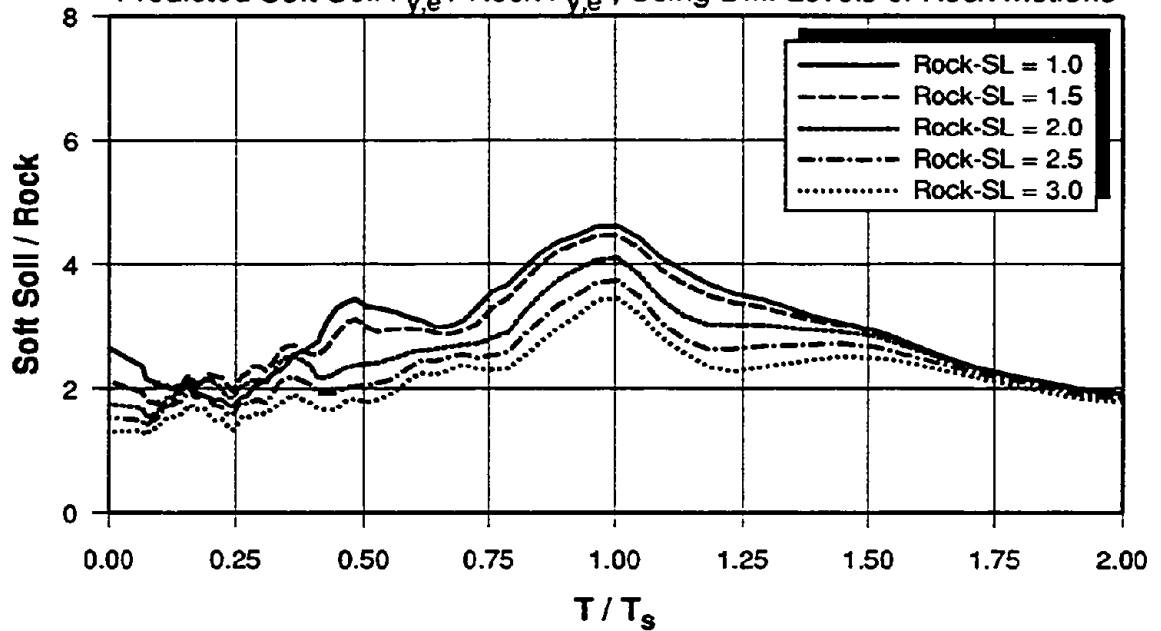


(b) Hyperbolic Model with Idealized Bilinear Model

Fig. 5.37 Typical Stress Strain Relationships Used to Model the Nonlinear Behavior of Soil

AMPLIFICATION OF ELASTIC STRENGTH DEMANDS - MEAN

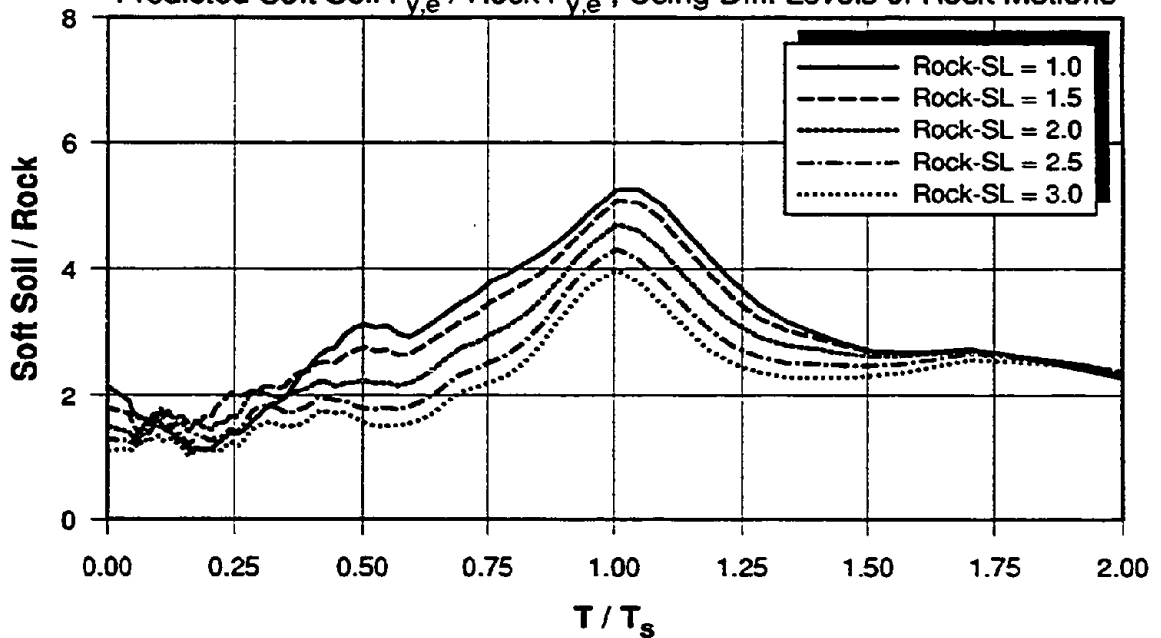
Predicted Soft Soil $F_{y,e}$ / Rock $F_{y,e}$, Using Diff. Levels of Rock Motions



(a) Site Period $T_s = 1.0$ sec.

AMPLIFICATION OF ELASTIC STRENGTH DEMANDS - MEAN

Predicted Soft Soil $F_{y,e}$ / Rock $F_{y,e}$, Using Diff. Levels of Rock Motions



(b) Site Period $T_s = 1.5$ sec.

Fig. 5.38 Mean Amplification of Elastic Strength Demands for Diff. Levels of Rock Motions

AMPLIFICATION OF PGA AT HIGHER LEVELS OF GROUND SHAKING

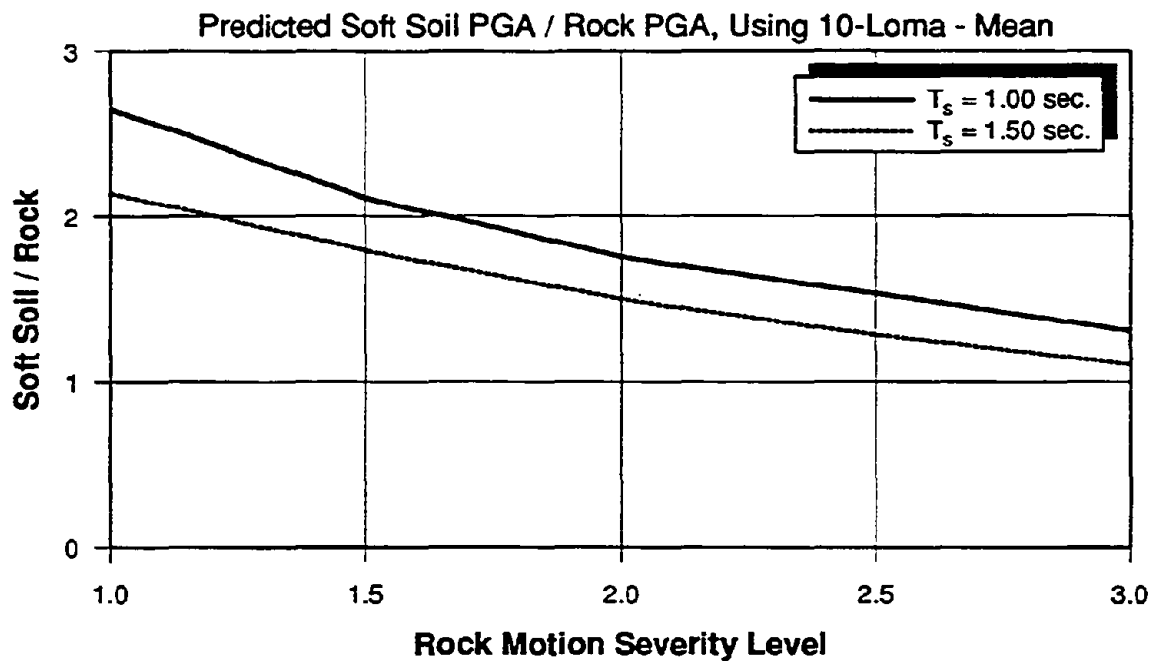


Fig. 5.39 Mean Amplification of PGA at Higher Levels of Ground Shaking

VARIATION OF STRAIN RATIO IN TOP SOIL LAYER

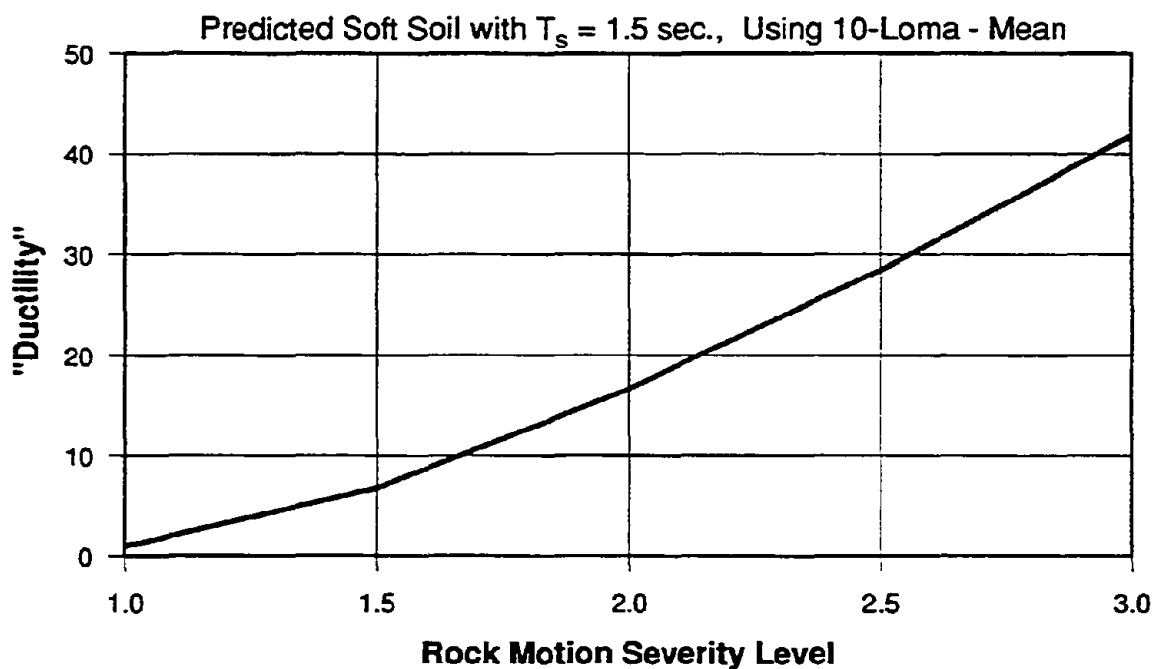


Fig. 5.40 Increase in "Ductility" Ratio with Level of Ground Shaking

AMPLIFICATION OF PGD AT HIGHER LEVELS OF GROUND SHAKING

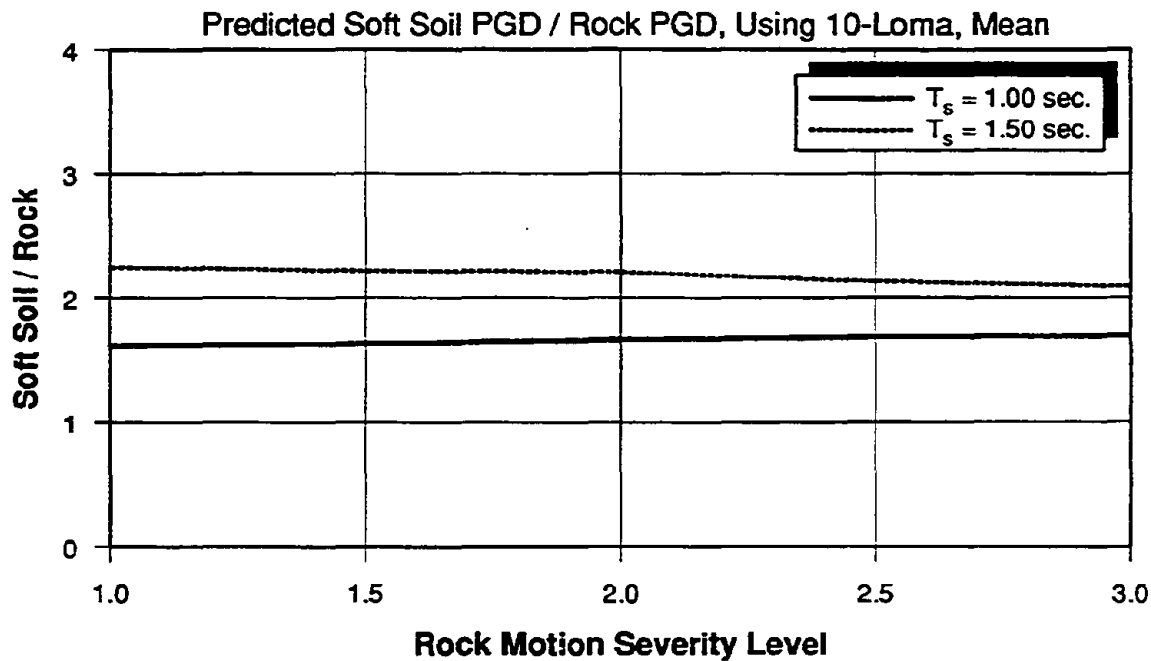


Fig. 5.41 Amplification of PGD at Higher Levels of Ground Shaking

SITE SPECIFIC ELASTIC STRENGTH DEMAND SPECTRA

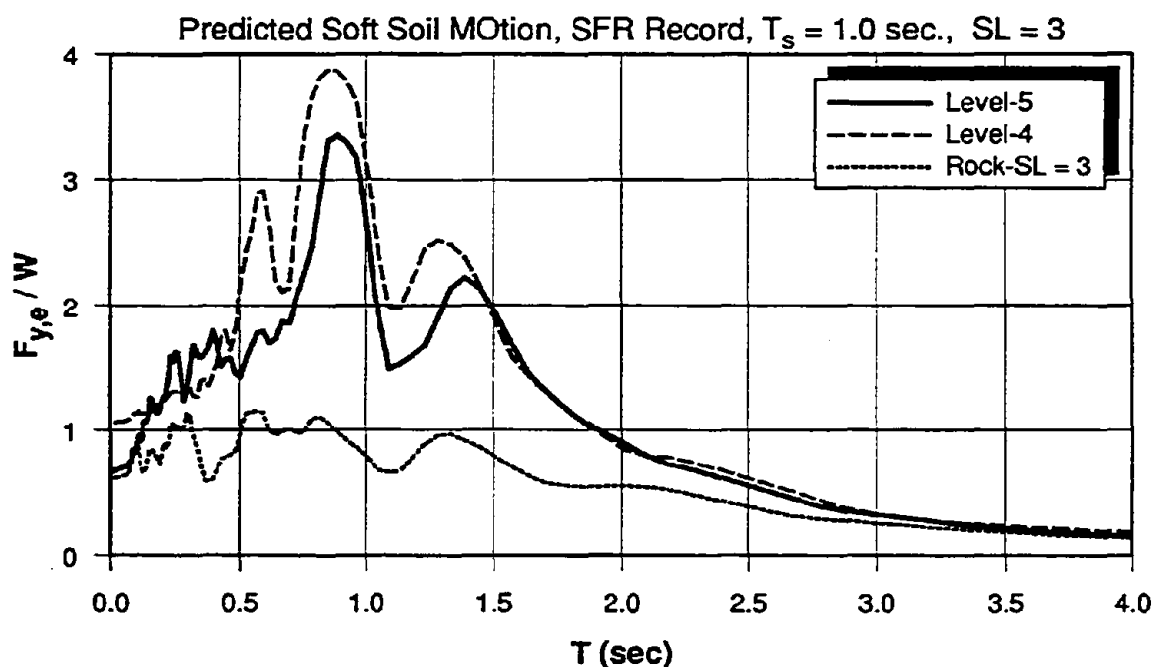
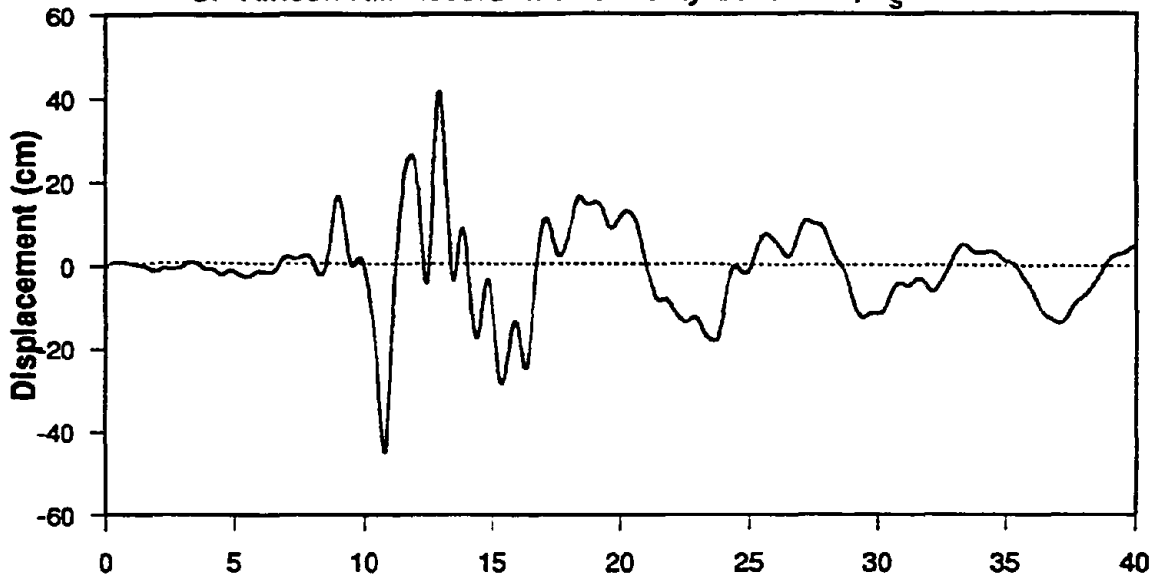


Fig. 5.42 Site Specific Elastic Strength Demands at Higher Levels of Ground Shaking

DISPLACEMENT TIME HISTORY

SF Rincon Hill Record with Severity Level of 3, $T_s = 1.0$ sec.

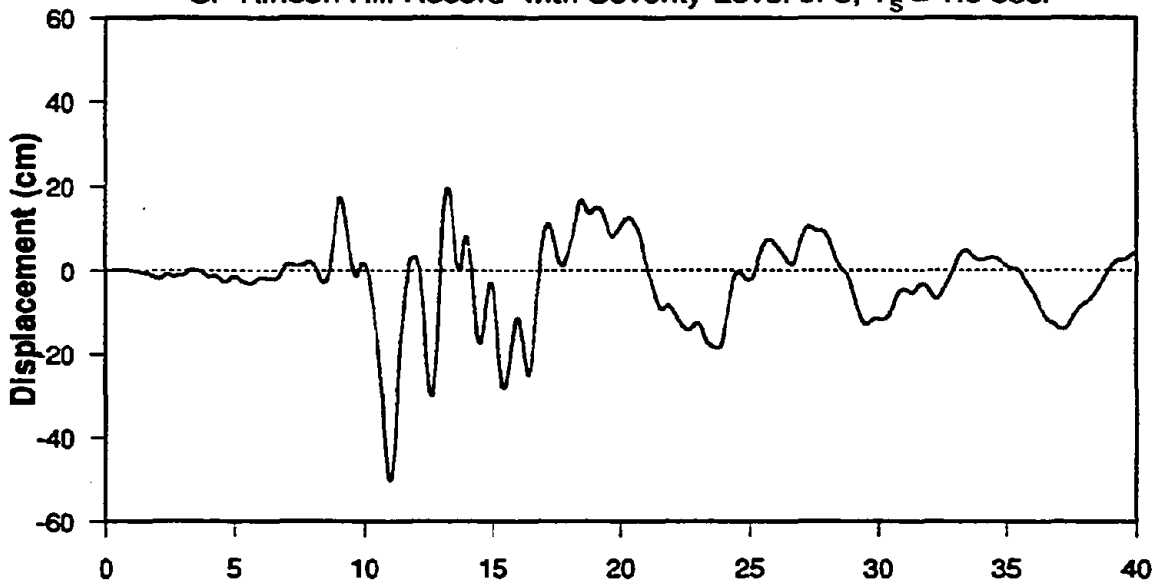


Time (sec)

(a) Level - 4

DISPLACEMENT TIME HISTORY

SF Rincon Hill Record with Severity Level of 3, $T_s = 1.0$ sec.



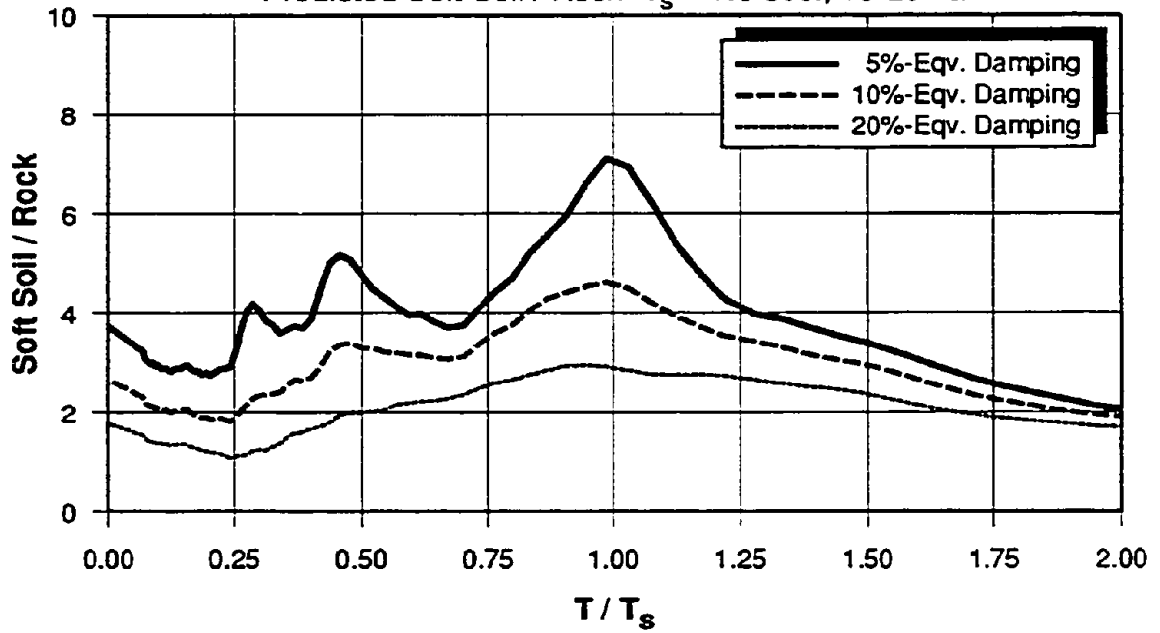
Time (sec)

(b) Level - 5

Fig. 5.43 Displacement Time History of Predicted Soft Soil Motion at Higher Levels of Ground Shaking

AMPLIFICATION OF ELASTIC STRENGTH DEMANDS - MEAN

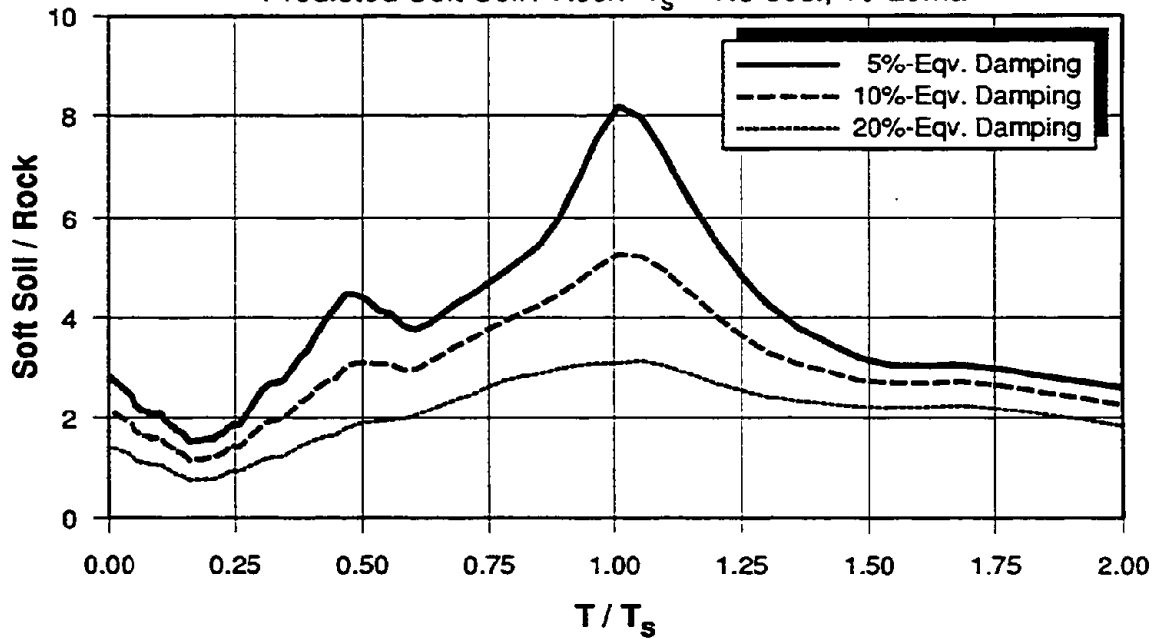
Predicted Soft Soil / Rock $T_s = 1.0$ sec., 10-Loma



(a) Site Period - $T_s = 1.0$ sec.

AMPLIFICATION OF ELASTIC STRENGTH DEMANDS - MEAN

Predicted Soft Soil / Rock $T_s = 1.5$ sec., 10-Loma



(b) Site Period - $T_s = 1.50$ sec.

Fig 5.44 Effect of Damping of Soil Model on the Amplification of Elastic Strength Demands

CHAPTER 6

SUMMARY AND CONCLUSIONS

The objective of the research discussed in this dissertation is to develop fundamental information needed to implement a demand/capacity based inelastic seismic design approach. In this approach the design objective is to provide a structure with sufficient strength and stiffness so that the deformation or ductility demands imposed by a design earthquake do not exceed the available capacities. Thus, design is based on an evaluation of demands and capacities, considering the inelastic response characteristics of structures.

This research is concerned with the evaluation of seismic demands derived from statistical studies on nonlinear *SDOF* systems on a rigid foundation. The emphasis is on the evaluation of strength demands for specified target ductility ratios. Recognizing the need to relate interstory displacements to ductility ratios, and the effect of cumulative damage on ductility capacities, the issues of inelastic displacement demands and energy demands are also addressed. The demands derived for *SDOF* systems form the basis for design, but need to be modified to account for *MDOF* effects in order to be implemented in the proposed design approach. These *MDOF* modifications are not addressed in this study.

A consistent evaluation of inelastic seismic demands (strength, displacement, and energy demands) can be achieved from statistical studies of the ground motion response of hysteresis systems in which the strength of each system is tuned to a predefined target ductility ratio. In this manner all seismic demands can be derived for specified ductility ratios and can be represented in terms of inelastic demand spectra for discrete ductility ratios.

In the process of deriving seismic demands due consideration must be given to the severity and frequency characteristics of the expected ground motions, effects of local soil conditions, the hysteretic characteristics of the structure's load-deformation response, secondary effects such as P-delta effects, cumulative damage issues, energy input and dissipation, strength and stiffness distribution over the height of the structure, torsional effects, and soil-structure interaction effects. This research focuses on the following two specific aspects of seismic demand evaluation: (a) the sensitivity of important seismic demand parameters to the type of hysteresis model, including P-delta effects, and (b) the effect of soft soil amplification on these demand parameters.

In order to evaluate the sensitivity of seismic demand parameters to the type of hysteresis model, a general hysteresis model is developed in which hysteretic energy dissipation is used as a measure of cumulative damage and deterioration. Deterioration in strength and stiffness properties is described by a history dependent deterioration parameter which is used to modify the characteristics of the hysteresis model during each inelastic excursion. The effects of strength deterioration and stiffness degradation on inelastic seismic demands are evaluated statistically for *SDOF* systems with periods of 0.50 and 1.0 second, using a set of 15 recorded ground motions. The results are presented in terms of the ratios of seismic demands of deteriorated system over the undeteriorated system. This part of the study has led to the following conclusions:

- Systems with strength deterioration or unloading stiffness degradation undergo larger displacements, thus requiring higher strength capacities for the same target ductility ratio. However, the effects of unloading stiffness degradation are relatively small.
- Stiffness degradation of the type represented by the peak oriented model (Clough model) has very little detrimental effect on the seismic response.
- Strength deterioration may greatly affect the response of *SDOF* systems if the hysteretic energy demand approaches the hysteretic energy capacity of the structural system. The response is sensitive to the deterioration parameter that identifies the rate at which strength deterioration occurs.

P-delta effects are studied by varying the strain hardening ratio of the bilinear and stiffness degrading Clough models between values of +0.1 and -0.2 and evaluating the increase in strength required for strain softening systems (negative strain hardening) in order to maintain a specified target ductility ratio. The following conclusions are drawn from this study:

- Strain softening has a significant effect on seismic response. Bilinear hysteresis systems with a negative hardening stiffness drift significantly and their strength compared to hardening systems needs to be increased considerably in order to limit inelastic displacements to the same ductility ratio. This is reflected in a rapid decrease of the *R-factor* for systems with negative stiffness. The required strength of systems with negative hardening may be as large as twice that of elastic-plastic systems.
- Stiffness degrading systems behave similar to bilinear systems for positive hardening, but are clearly superior if P-delta effects lead to a negative hardening stiffness.
- The inelastic strength demand for a system with negative hardening stiffness is strongly dependent on the strain hardening ratio, the target ductility ratio, and the period of the *SDOF* system. The so-called "secondary" effects due to P-delta may become primary effects and may lead to a large increase in displacements and possibly to incremental collapse unless this problem is explicitly addressed in design.

The study on the effects of soft soils on seismic demands is performed in two parts. The first part is concerned with an evaluation of the soft soil amplifications of ground motions recorded during the 1989 Loma Prieta earthquake. Measured shear wave velocity data and recorded surface motions are used to estimate soil periods, and one-dimensional wave propagation concepts are employed to predict ground motions in soft soil from nearby rock motions. The elastic strength demand spectra of predicted and recorded soft soil motions are computed for *SDOF* system with 5% damping. The spectra obtained from predicted surface motions match reasonably well with the spectra obtained from the measured records. This indicates that one-dimensional wave propagation concepts provide reasonable predictions of soft-soil motions to an extent that

permits a conceptual assessment of soft soil effects on the demand spectra of interest for design.

This conclusions made it possible to embark on a more comprehensive statistical study in which soft-soil effects are evaluated for a wide range of one-dimensional soil column and for typical sets of near- and far-source ground motions. In this study the soil column is modeled as a five-degree-of-freedom lumped mass system whose properties are varied to cover a soil period range from 0.5 to 4.0 seconds. Fifteen near-source and ten far-source rock records are used as input to the soil columns to generate a comprehensive set of soft-soil records. The elastic and inelastic strength, displacement, and energy demand spectra of the rock and soft soil records are compared, and the amplifications of spectral values of soil versus rock motion are evaluated statistically. A comprehensive study is performed using a linear soil column model with 10% viscous damping in each mode, and a pilot study is performed in which the top soil layer is modeled as a bilinear system with 1% strain hardening.

The study on soft soil effects has led to the following conclusions, which must be interpreted within the context of the assumptions made in the soil response analysis.

- The elastic strength demand spectra of soft soil motions exhibit a clear hump in the vicinity of the fundamental soil period. The shapes of inelastic strength demand spectra are much smoother and the humps of the inelastic spectra are much wider than those of the elastic spectra.
- The maximum soft soil amplifications are larger for elastic systems than inelastic ones, but differ only little for systems with ductility ratios between 2 and 8. For soft soils without strong nonlinearities the amplification of strength and displacement demands in the vicinity of the soil period is approximately 5 for elastic strength demands, and between 3 and 4 for inelastic strength demands.
- The soft soil amplifications of elastic and inelastic strength demands do not depend strongly on the rock motion spectral shape. In general, the results obtained from near-source rock motions are close to those obtained from the far-source rock motions.

- The displacement demand spectra are amplified in the same manner as the strength demand spectra. The ratio of elastic to inelastic displacement demands shows very consistent patterns. It has a low point at $T/T_s = 1.0$, is usually less than 1.0 for $T/T_s > 0.75$ and increases rapidly for short period structures.
- The amplification of the input energy spectra is larger than the square of the amplification of the strength demand spectra. This shows that the strong motion duration of the soft soil motion increases compared to the rock motion.
- Soil nonlinearity in the top soil layer is important but not as dominant as anticipated. For instance, a ground motion that is three times as severe as that causing first "yielding" in the soil causes a reduction in the maximum spectral amplification from a value of 5.2 to a value of 4.0. The *PGA* amplification decreases at a much higher rate than the spectral amplification, whereas the *PGD* amplification is not very sensitive to the level of ground shaking.

In the context of seismic design the following conclusions can be drawn from this study of soft soil effects on elastic and inelastic seismic demand parameters:

- For motions that are greatly affected by soft soil conditions, the required strength for specified target ductilities is strongly site dependent. Elastic site-specific response spectra can provide misleading information on inelastic strength demands, since the shapes of the strength demand spectra change with the target ductility ratio.
- Soft soil effects cannot be lumped into a soil factor that is independent of structure period and target ductility ratio, and ground motion severity (such as S_3 and S_4 in the 1991 UBC). Rather, it appears to be feasible to relate the strength and displacement demands (elastic or inelastic) for a soft soil motion to that of the motion in the underlying rock by a modification function $S(T_s, \mu)$. This function can be derived from the type of information presented in this dissertation, which provides quantitative values for amplification factors in soils with small nonlinearity (represented by 10%

viscous damping), and preliminary results for soils with large nonlinearity in the top layer.

- The spectral amplifications in the vicinity of $T/T_s = 1.0$ are approximately the same for soil columns of all periods, whereas the amplification of *PGA* is soil period dependent. In fact, the *PGA* may get deamplified in soil columns with very long periods. Thus, the *PGA* of soft soil motions is a poor indicator of the spectral demands in the vicinity of the soil period and, consequently, an assessment of soft soil effects must be based on spectral amplifications and not on *PGA* amplification.

The research presented in this dissertation addressed only a few of the issues that are involved in implementing the proposed demand/capacity methodology. Much work remains to be done in order to make the proposed methodology feasible for practical design. Further research is needed particularly in the following areas:

1. Identification of acceptable risk levels and development of design ground motions for serviceability and collapse safety designs.
2. Development of performance criteria consistent with acceptable levels of risk
3. Consideration of uncertainties in the determination of demands and capacities and of reliability concept in the design process.
4. Development of more reliable damage models than those that exist at present for the assessment of ductility capacities as a function of cumulative damage.
5. Development of *MDOF* modifications that account for higher mode effects, overstrength, torsional effects, and strength and stiffness irregularities.
6. Development of procedures that permit a realistic incorporation of soil-structure interaction effects in the design process.

BIBLIOGRAPHY

ATC-3-06, (1978). "Tentative Provisions for the Development of Seismic Regulations for Buildings", Applied Technology Council, June 1978.

Aki, K., (1988). "Local Site Effects on Strong Ground Motion", in J. Lawrence Van Thun (Ed.), Earthquake Engineering and Soil Dynamic Recent Advance in Ground Motion Evaluation, ASCE Geotechnical Special Publication No. 20, pp. 103-155.

Bertero, V.V., Anderson, J.C., Krawinkler, K., Miranda, E., (1988). "Design Guidelines for Ductility and Drift Limits: Review of State-of-the-Art in Ductility and Drift-Based Earthquake-resistant Design of Buildings", UCB/EERC-91/15, Earthquake Engineering Research Center, University of California, Berkeley, July 1991.

Bertero, V.V. and Uang, C., (1992). "Issues and Future Directions in the Use of and Energy Approach for Seismic-Resistant Design of Structures", Nonlinear Seismic Analysis and Design of Reinforced Concrete Buildings (H. Krawinkler and P. Fajfar, eds.), Elsevier Science Publishing Co., New York, 1992.

Borcherdt, R.D., (1990). "Influence of Local Geology in the San Francisco Bay Region, California, on Ground Motion Generated by the Loma Prieta Earthquake of October 17, 1989", Proceeding International Symposium on Safety and Urban Life and Facilities, Tokyo Ins. Tech, Tokyo, Japan 1990.

Boatwright, J., Seekings, L.C., Fumal, T.E., Liu, H., and Mueller C.S., (1991). "Ground Motion Amplification in the Marina District", Bulletin of the Seismological Society of America, Vol. 81, No. 5, pp. 1980-1997, October, 1991.

Boor, D.M., Seekins, L., and Joyner, W.B., (1989). "Peak Acceleration from the 17 October 1989 Loma Prieta Earthquake", Seismological Society of America, Vol. 60, No. 4 pp 151-166 October-December 1989.

California Division of Mines and Geology, (1989). "CSMIP Strong Motion Records from the Santa Cruz Mountains (Loma-Prieta) Earthquake of 17 October 1989, California Department of Conservation, Division of Mines and Geology, Office of Strong Motion Studies, Report No. OSMS 89-06.

California Division of Mines and Geology, (1990). "CSMIP Strong Motion Records from the Santa Cruz Mountains (Loma-Prieta) Earthquake of 17 October 1989, California Department of Conservation, Division of Mines and Geology, Office of Strong Motion Studies, Report No. OSMS 90-05.

Campbell, K.W., (1991). "An Empirical Analysis of Peak Horizontal Acceleration for the Loma Prieta, California, Earthquake of 18 October 1989", Bulletin of the Seismological Society of America, Vol. 81, No. 5, pp. 1838-1858, October, 1991.

Chung, Y.S., Meyer, C., and Shinozuka, M., (1987). "Seismic Damage Assessment of Reinforced Concrete Members", Report NCEER-87-0022, National Center for Earthquake Engineering Research, State University of New York at Buffalo, October 1987.

Clough, R.W., (1966). "Effect of Stiffness Degradation on Earthquake Ductility Requirements", Report No. 66-16, Structures and Material Research University of California Berkeley October 1966.

Clough R.W., and Penzien, J., (1975). "Dynamics of Structures", McGraw-Hill, Inc. 1975.

Cosenza, E., and Manfredi, G., (1992). "Seismic Analysis of Degrading Models By Means of Damage Functions Concept", Nonlinear Seismic Analysis and Design of Reinforced Concrete Buildings (H. Krawinkler and P. Fajfar, eds.), Elsevier Science Publishing Co., New York, 1992.

Dobry R., Oweis I., and Urzua A., (1976). "Simplified Procedures for Estimating the Fundamental Period of a Soil Profile" Bulletin of the Seismological Society of America Vol. 66, No 4, May 1990.

Earthquake Spectra, (1990). "Loma Prieta Earthquake Reconnaissance Report", EERI, Vol. 4, No. 1, February 1988.

Fajfar, P., and Fischinger, M., (1988). "N2 - A Method For Non-Linear Seismic Analysis of Regular Buildings", Proceedings of 9WCEE, Vol. 5, Tokyo, Japan, August, 1988, pp. 111-116.

Fajfar, P., Vidic, T., and Fischinger, M., (1992). "On Energy Demand and Supply in SDOF Systems", Nonlinear Seismic Analysis and Design of Reinforced Concrete Buildings (H. Krawinkler and P. Fajfar, eds.), Elsevier Science Publishing Co., New York, 1992.

Finn, W.D.L., (1991). "Geotechnical Engineering Aspects of Microzonation", Forth International Conference on Seismic Zonation, Vol. 1, Stanford California August 1991.

Finn, W.D.L., and Martin, G.R., and Lee, M.K.W., (1978). "Comparison of Dynamic Analyses for Saturated Sands", Earthquake Engineering and Soil Dynamic ASCE, Vol. 1, 1978, PP. 472-491.

Fumal, T.E., "A Compilation of the Geology and Measured and Estimated Shear-Wave Velocity Profiles at Strong-Motion Stations that Recorded During the Loma Prieta, California Earthquake", Open-File Report 91-311, U.S. Department of the Interior U.S. Geological Survey, 1991.

Hadidi-Tamjed, H., (1993). "Seismic Response of SDOF systems including P-delta Effect and Stiffness Degradation" Engineer Thesis Stanford University, August 1983.

Hadidi-Tamjed, H., (1988). "Statistical Response of Inelastic SDOF Systems Subjected to Earthquakes", Ph.D. Dissertation submitted to the Department of Civil Engineering, Stanford University, December 1987.

Hardin, B.O., and Drnevich, V.P., (1972). "Shear Modulus and Damping in Soils: Measurement and Parameter Effects", Journal of the Soil Mechanics and Foundations Division ASCE, Vol. 98 no. SM6, June 1972.

Hardin, B.O., and Drnevich, V.P., (1972). "Shear Modulus and Damping in Soils: Design Equations and Curves", Journal of Soil Mechanics and Foundation Division ASCE, Vol. 98, No. SM7, July 1972.

Hart, J.D. and Wilson, E.L., (1989). "Simplified Earthquake Analysis of Buildings Including Site Effects", Report No. UCB/SEMM-89/23, University of California, Berkeley 1989.

Hryciw, R.D., Rollins, K.M., Homolka, M., Shewbridge, S.E. and Mchood, M., (1991). "Soil Amplification at Treasure Island During the Loma Prieta Earthquake", Proceedings, Second International Conference on Recent Advances in Geotechnical Earthquake Engineering and Soil Dynamics, St. Louis, Missouri, Vol. II, pp. 1679-1685.

Housner, G.W., Chairman., (1990). "Computing Against Time", Report to Governor George Deukmejian from the Governor's Board of Inquiry on the 1989 Loma Prieta Earthquake May 1990.

Idriss I.M., (1991). "Earthquake Ground Motions at Soft Soil Sites" Second International Conference on Recent Advances in Geotechnical Earthquake Engineering on Soil Dynamics" St. Louis Missouri March 1991

Idriss, M.I., (1990). "Response of Soft Soil Sites During Earthquakes", Proceeding a Memorial Symposium to Honor Professor H.B. Seed, University of California Berkeley, May 1990.

Idriss M.I., Dobry R., Singh R.D., (1978). "Nonlinear behavior of Soft Clays During Cyclic Loading" Journal of the Geotechnical Engineering Division ASCE, Vol. 104, No. GT12 December 1978.

Joyner, W.B., and Boore, D.M., (1988). "Measurement, Characterization, and Prediction of Strong Ground Motion," Proceedings of Earthquake Engineering & Soil Dynamics II, GT Div/ASCE, Park City, Utah, June 27-30, 1988.

Kanaan, A.E., Powell, G.H., (1973). "General Purpose Computer Program for Inelastic Dynamic Response of Plane Structures", UCB/EERC-73/6, Earthquake Engineering Research Center, University of California, Berkeley, 1973.

Krawinkler H., (1993). "Ideas on Inelastic Design Methods," Proceedings of the SEAOC Workshop on the Next Generation of Seismic Design Practices, Ixtapa, Mexico, Sept. 29, 1992 (to be published).

Krawinkler, H., and Nassar, A., (1992). " Seismic Design Based on Ductility and Cumulative Damage Demands and Capacities", Nonlinear Seismic Analysis and Design of Reinforced Concrete Buildings (H. Krawinkler and P. Fajfar, eds.), Elsevier Science Publishing Co., New York, 1992.

Krawinkler, H. Nassar, A., and Rahnama, M., (1991). "Damage Potential of Loma Prieta Ground Motions", Bulletin of the Seismological Society of America, Vol. 81, No. 5, pp. 2048-2069, October, 1991.

Krawinkler, H., Rahnama, M., and Nassar, A., (1991). "Zonation Based on Inelastic Strength Demand Spectra", International Conference on Seismic Zonation, Vol. 2, Stanford California August 1991.

Krawinkler, H., Rahnama, M., (1992). "Effects of Soft Soils on Design Spectra", Proceeding of the Tenth World Conference on Earthquake Engineering, Vol. 10, Madrid Spain 1992.

Krawinkler, H., Zohrei, M., Lashkari, B., Cofie, N., and Hadidi, H., (1983). "Recommendations for Experimental Studies on the Seismic Behavior of Steel Components and Materials," John A. Blume Earthquake Engineering Center, Report No. 61, Department of Civil Engineering, Stanford University, September 1983.

Mahin, S.A., and Bertero, V.V., (1975). "An Evaluation of Some Methods for Predicting the Seismic Behavior of Reinforced Concrete Buildings", UCB/EERC-75/5, Earthquake Engineering Research Center, University of California, Berkeley, 1975.

Mahin, S.A., Lin, J., (1983). "Construction of Inelastic Response Spectra for Single-Degree-of-Freedom Systems - Computer Program and Applications", UCB/EERC-83/17, Earthquake Engineering Research Center, University of California, Berkeley, June 1983.

Martin P.P., and Seed H.B. (1982). "One - Dimensional Dynamic Ground Response Analyses" Journal of the Geotechnical Engineering Division ASCE, Vol. 108, No. GT7 July 1982.

McCann, M.W., and Shah, H.C., (1979). "Determining Strong-Motion Duration of Earthquakes," Bulletin of the Seismological Society of America, Vol. 69, No. 4, August 1979.

Miranda, E., (1992). "Nolinear vResponse Spectra for Earthquake Resistance Design", Proceeding of the Tenth World Conference on Earthquake Engineering, Vol. 10, Madrid Spain 1992.

Nassar, A.A., and Krawinkler, H., (1991). " Seismic Demands for SDOF and MDOF Systems", Report No. 95, John A. Blume Earthquake Engineering Research Center, Department of Civil Engineering, Stanford University, September 1991.

Osteraas, J.D., and Krawinkler, H., (1990). "Strength and Ductility Considerations in Seismic Design," John A. Blume Earthquake Engineering Center, Report No. 90, Department of Civil Engineering, Stanford University, June 1990.

Park, Y.J., Reinhorn, A.M., and Kunnath, S.K., (1988). Seismic Damage Analysis of Reinforced Concrete Buildings", Proceedings of 9WCEE, Vol. 3, Tokyo, Japan, August, 1988, pp. 211-216.

Park, Y.J., Ang, A.H-S., and Wen, Y.K., (1984). "Seismic Damage Analysis and Damage-Limiting Design of R.C. Buildings", Structural Research Series No. 516, Civil Engineering Studies, University of Illinois at Urbana-Champaign, October, 1984.

Powell, G.H. and Allahabadi, R., (1987). "Seismic Damage Prediction By Deterministic Methods: Concepts and Procedures", Earthquake Engineering and Structural Dynamics, Vol. 116, Date, pp. 719-734.

Rahnama, M., and Krawinkler H., (1991). "Analysis of Damage Potential of Earthquake Ground Motions", First International Conference on Seismology and Earthquake Engineering, Tehran Iran, May 1991

Schnabel, P.B., Lysmer, J. and Seed, H.B., (1972). "SHAKE, A Computer Program for Earthquake Response Analysis of Horizontally Layered Sites." Report No. EERC 72-12, University of California, Berkeley, December 1972.

SEAOC, (1988). "Recommended Lateral Force Requirements and Commentary." Structural Engineers Association of California, 1988.

Seed, H.B., and Idriss, I.M., (1970). "Soil Moduli and Damping Factors for Dynamic Response Analyses" Report No. EERC 70-10, University of California, Berkeley, 1970.

Seed H.B., Ugas C., and Ysmer J., (1976-1). "Site-Dependent Spectra for Earthquake Resistant Design" Bulletin of the Seismological Society of America. Vol. 66, No. 1, February 1976.

Seed H.B., Murarka R., Lysmer J., and Idriss I.M., (1976-2). "Relationship of Maximum Acceleration, Maximum Velocity, Distance from Source, and Local Site Conditions for Moderately Strong Earthquakes" Bulletin of the Seismology Society of America Vol. 66, No. 4, August 1976

Seed, H.B., (1989). "Implications of Site Effects in the Mexico City Earthquake of September, 19, 1985 for Earthquake Resistant Design Criteria in the San Francisco Bay Area of California", Report No. UCB/EERC-89/03, University of California, Berkeley 1989.

Seed H.B., Sun J.I., (1989). "Implications of Site Effects in the Mexico City Earthquake of Sept. 1985 for Earthquake Resistance Design Criteria in the San Francisco Bay Area of California" UBC / EERC-89/03 , March 1989.

Seed, H.B., Wong, R.T., Idriss I.M., and Tokimatsu, k., (1984). "Moduli and Damping Factors for Dynamic Analyses of Cohesionless Soils", Report No UCB/EERC-84/14, Earthquake Engineering Research Center, University of California, Berkeley, September. 1984.

Seed, H.B., and Idriss, I.M., (1969). "Influence of Soil Conditions on Ground Motions During Earthquakes:", Journal of the Soil Mechanics and Foundation Division, ASCE, Vol. 95 No. SM1, Jan. 1969.

Seed, R.B., Dickenson S.E., Riemer M.F., Bary, J.D., Sitar N., Mitchell, J.K., Idriss, I.M., Kayen, R.E., Kropp, A., Harder, L.F., and Power M.S., (1990). "Preliminary Report on the Principal Geotechnical Aspects of the October 17, 1989 Loma Prieta Earthquake" Report No. UCB/EERC-90/05, University of California, Berkeley, 1990.

Seed, R.B., Dickenson, S.E., and Mok, C.M., (1992). "Seismic Response of Soft Clay Sites: Recent Lessons", EERI Forty-Fourth Annual Meeting, San Francisco, California, February 6-8, 1992.

Seed, R.B., Dickenson, S.E., Rau, G.A., White, R.K., and Mok, C.M., (1992). "Observations Regarding Seismic Response Analyses for Soft and Deep Clay Sites", NCEER/SEAOC/BSSC Workshop on Site Response During Earthquake and Seismic Code Provisions November 18-20, University of Southern California, 1992 (to be published).

Singh R.D., Dobry R., Doyle E.H., Idriss I.M., (1981). "Nonlinear Seismic Response of Soft Clay Sites" Journal of the Geotechnical Engineering Division ASCE, Vol. 107, No. GT9 September 1981.

Sun, J.I., Golesorki, R., and Seed H.B., (1988). "Dynamic Moduli and Damping Ratios for Cohesive Soils", Report No UCB/EERC-88/15, Earthquake Engineering Research Center, University of California, Berkeley, August 1988.

Taylor, P.W., and Larkin, T.J., (1978). "Seismic Response of Non-Linear Soil Media", Journal of the Geotechnical Engineering Division ASCE, Vol. 104, No. GT3, March 1978.

Trifunac, M.D., and Brady, A.G., (1975). "A Study of the Duration of Strong Earthquake Ground Motion," Bulletin of the Seismological Society of America, Vol. 65, 1975.

Uang, C., and Bertero, V.V., (1988). "Use of Energy as a Design Criterion in Earthquake-Resistant Design", UCB/EERC-88/18, Earthquake Engineering Research Center, University of California, Berkeley, Nov. 1988.

UBC, (1992). "Uniform Building Code", International Conference of Building Officials, Whittier, California 1992.

U.S. Geological Survey, (1989). "U.S. Geological Survey Strong Motion Records from the Northern California (Loma Prieta) Earthquake of October 17, 1989", U.S. Geol. Surv. Open-file Report 89-568.

U.S. Geological Survey, (1990). "U.S. Geological Survey Strong Motion Records from the Northern California (Loma Prieta) Earthquake of October 17, 1989", U.S. Geol. Surv. Open-file Report 90-247.

Vanmarcke, E.H., and Lai, S.P., (1977). "Strong Motion Duration of Earthquakes," Dept. of Civil Engineering, M.I.T., Publication No. R77-16.

Whitman, R.V., (1987). "Are the Soil Depositions in Mexico City Unique", The Mexico Earthquake 1985, Factor Involved and Lessons Learned, American Society of Civil Engineers ASCE 1987.